Molecular Dissection of Maize-*Sporisorium reilianum* Interactions:

Host Developmental Changes and Pathogen Effectors

DISSERTATION

zur
Erlangung des Doktorgrades
der Naturwissenschaften
(Dr. rer. nat.)

am Fachbereich Biologie
der Philipps-Universität Marburg
vorgelegt von

Hassan Ghareeb
aus Giza/Ägypten

Marburg/Lahn, 2011

Die Untersuchungen zur vorliegenden Arbeit wurden von Oktober 2007 bis März 2010 am Max-Planck-Institut für Terrestrische Mikrobiologie in der Abteilung Organismische Interaktionen und von April 2010 bis Mai 2011 an der Gerog-August-Universität Göttingen in der Abteilung Molekularbiologie der Pflanze-Mikroben-Interaktion unter der Leitung von Herrn Prof. Dr. Jan Schirawski durchgeführt.

Vom Fachbereich Biologie der Philipps-Universität Marburg als Dissertation angenommen am: 16.06.2011

Erstgutachter: Prof. Dr. Jan Schirawski
Zweitgutachter: Prof. Dr. Regine Kahmann

Tag der mündlichen Prüfung am: 30.06.2011

Ein Teil der während der Promotion erzielten Ergebnisse wurde in folgenden Originalpublikationen veröffentlicht:

Ghareeb H, Becker A, Iven T, Feussner I, Schirawski J (2011) *Sporisorium reilianum* Infection changes inflorescence and branching architectures of maize. Plant Physiology, in revision.

Schirawski J, Mannhaupt G, Münch K, Brefort T, Schipper K, Doehlemann G, Di Stasio M, Rössel N, Mendoza-Mendoza A, Pester D, Müller O, Winterberg B, Meyer E, Ghareeb H, Wollenberg T, Münsterkötter M, Wong P, Walter M, Stukenbrock E, Güldener U, Kahmann R (2010) Pathogenicity determinants in smut fungi revealed by genome comparison. Science 330: 1546-1548.

ERKLÄRUNG

Ich versichere, dass ich meine Dissertation mit dem Titel "Molecular Dissection of Maize-*Sporisorium reilianum* Interactions: Host Developmental Changes and Pathogen Effectors" selbstständig und ohne unerlaubte Hilfe angefertigt habe und mich dabei keiner anderen als der von mir ausdrücklich bezeichneten Quellen und Hilfsmittel bedient habe.

Diese Dissertation wurde in der jetztigen oder einer ähnlichen Form noch bei keiner anderen Hochschule eingereicht und hat noch keinen sonstigen Prüfungszwecken gedient.

Göttingen, Juni, 2011

Hassan Ghareeb

I dedicate my PhD dissertation to the people who sacrificed their life for the Egyptian revolution (25th January, 2011) seeking freedom, justice and a better future.

"*To exist is to change, to change is to mature, to mature is to go on creating oneself endlessly*"

Henri Bergson (1859-1941)

TABLE OF CONTENTS

LIST OF ABBREVIATIONS

Abbreviation	Description	Abbreviation	Description
Δ	Deletion	*CLV*	*CLAVATA* gene
µl	Microliter	C-terminal	Carboxy terminal
A	Aureobasidin A	DAB	3,3'-Diaminobenzidine
AD	Activation domain of Gal4 transcription factor	DDO	Double dropout
Ade	Adenin	DHR	double homologous recombination
ADE2	Adenine auxotrophy marker gene	DIC	Differential interference contrast
AG	*AGAMOUS* gene	DIG	Digoxigenin
amiRNA	Artifical miRNA	DMF	N,N dimethylformamide
Amp	Ampicillin	His	Histidin
AP1	*APETALA1*	*HIS3*	Histidin auxotrophy
AP2	*APETALA2*	hpi	Hour post inoculation
AUR1-C	Aureobasidin A resistance gene	HR	Hypersensitive response
avr	Avirulence gene	DNA	Deoxyribonucleic acid
BA1	*BARREN STALK1* gene	dNTPs	Desoxynucleotid triphosphate
BD	DNA-binding domain of Gal4 transcription factor	DP	Declustering potential
BD1	*BRANCHED SILKLESS1* gene	dpi	Day(s) post infection
BDE	*BEARDED EAR* gene	EDTA	Ethylene diamine tetraacetic acid
BIF2	*BARREN INFLORESCENCE2* gene	EP	Entrance potential
bp	Base pair	EST	Expressed sequence tag
BSA	Bovine serum albumin	FCF	Fast green
BSM	Branch spikelet meristem	FM	Floral meristem
ca	Carpel	GA	Gibberellin
CBE	Chlorazole black E	GFP	Green fluorescent protein
cbx	Carboxin	gl	Glume
cDNA	Complementary DNA	Hyg	Hygromycin
CE	Collision energy	IAA	Indole acetic acid
CK	Cytokinin	*ID1*	*INDETERMINATE1* gene

Abbreviation	Description	Abbreviation	Description
IDS1	*INDETERMINATE SPIKELET1* gene	PCD	Programmed cell death
IFA1	*INDETERMINATE FLORAL APEX1* gene	PCR	Polymerase chain reaction
IM	Inflorescence meristem	PD	Potato dextrose“
in planta	Within the plant	pl	Palea
IR	Inverted repeat	QDO	SD medium lacking tryptophan and leucin
Kan	Kanamycin	QDO/A	SD lacking tryptophan, leucin, adenine and histidin
kb	Kilo base pair	qRT-PCR	Quantitative real time RT-PCR
KDa	Kilo Dalton	QTL	Quantitative trait locus
le	Lemma	*R*	Resistance gene
Leu	Leucin	RT-PCR	Reverse transcription polymerase chain reaction
lf	lower floret	*ra1,ra2,ra3*	*ramosa* mutants
lo	Lodicule	RNA	Ribonucleic acid
LRR	Leucine rich repeat	RNAi	RNA interference
M	Molar (g/L)	ROS	Reactive oxygen species
MEL1	Galactosidase metabolizes α-X-GAL to produce blue color	*sad1*	*suppressor of apical dominance 1*
mig1	*maize induced gene 1*	SAD1-IP	SAD1 interaction partner
mM	Millimolar (mg/L)	*sad2*	*suppressor of apical dominance 2*
NCBI	National Center for Biotechnology Information	*sakA*	Stress-activated mitogen-activated protein kinase
NLS	Nuclear localisation sequence	SD/-Leu	SD medium lacking Leucine
N-terminal	Amino terminal	SDS	Sodium dodecyl sulphate
o	Ovule	*SEP*	*SEPALLATA* gene
OD_{600}	Optical Density at 600 nm	*SI1*	*SILKY1* gene
on planta	On the plant surface	*SID1*	*SISTER INDETERMINATE SPIKELET1* gene
PAGE	Polyacrylamide gel electrophoresis	SM	Spikelet meristem
PAT	Polar auxin transport	SPM	Spikelet pair meristem
PBS	Phosphate buffer saline	sr10077	*sad1* gene

Abbreviation	Description	Abbreviation	Description
sr10079	*vag1* gene	wpi	Weak(s) post infection
sr14220	*mig1*	wpi	Weak(s) post infection
sr16838	*dicer* gene	wt	Wild type
st	Stamen	wt-*gfp*	Wt expressing cytoplasmic GFP
TAE	Tris-Acetate + Na2-EDTA	*WUS*	*WUSCHEL* gene
TBE	Tris-Borate + Na2-EDTA	X	α-X-GAL
TEMED	N,N,N',N'-Tetramethylendiamine	wt	Wild type
tin1,2,3,4,5	*tumor inducing gene 1,2,3,4,5*	wt-*gfp*	Wt expressing cytoplasmic GFP
Trp	Tryptophan	*WUS*	*WUSCHEL* gene
uf	Upper floret	X	α-X-GAL
UV	Ultraviolet light	*ZAG1*	*Zea AGAMOUS1*
vag1	*virulence associated gene 1*	*ZAG2*	*Zea AGAMOUS2*
WGA-AF	Wheat germ agglutinin conjugated with Alexa Fluor	*ZAG3*	*Zea AGAMOUS3*

Note: The names of plant genes are formatted capital italic, whereas of fungal genes are formatted small italic.

ZUSAMMENFASSUNG

Sporisorium relianum ist ein Verursacher von Maiskopfbrand. Die Symptome werden sichtbar, wenn der Pilz Sporenbildung und Verlaubung (Phyllodie) im Blütenstand verursacht. In dieser Studie sollten Symptom- und Virulenzfaktoren des Pathogens identifiziert und charakterisiert werden, und herausgefunden werden, wie der Pilz das Entwicklungsprogramm von Mais verändert. Die Interaktion zwischen Mais und *S. reilianum* wurde von beiden Seiten untersucht. Auf der Seite der Maispflanze wurden die induzierten Veränderungen in Bezug auf Transkription, Hormongehalt und Konzentration der reaktiven Sauerstoffspezies (ROS) untersucht. Morphologische Studien zeigten, dass eine Infektion mit *S. reilianum* den subapikalen Auswuchs von Kolben förderte, welches darauf hindeutete, dass die Anwesenheit des Pilzes die Apikaldominanz unterdrückt. Eine Kolonisierung mit *S. reilianum* führte außerdem zu einem Anstieg der Zytokinin- und Auxingesamtkonzentrationen im Blütenstand und zu einer Akkumulation von ROS, was die Unterdrückung der Apikaldominanz erklären könnte. Ferner führte eine Infektion mit *S. reilianum* zum Verlust der Identität der Blütenorgane und des Meristems, sowie zum Verlust der Meristem-Determinanz. Microarray-Analysen zeigten, dass diese Entwicklungsveränderungen von einer transkriptionellen Regulation von Genen begleitet waren, die für bekannte oder postulierte Regulatoren der Identität der Blütenorgane und des Meristems sowie der Meristem-Determinanz kodieren.

Auf der Seite von *S. reilianum* wurden Genomvergleiche mit den eng verwandten Brandpilzen *Ustilago maydis* und *Ustilago hordei* durchgeführt, um potentielle Genkandidaten zu identifizieren die für die Symptomausbildung oder Virulenz auf Mais verantwortlich sind. Eine funktionelle Charakterisierung der Kandidaten zeigte, dass die Deletion von *dicer* nicht zu einer Veränderung der Virulenz oder der Stressresistenz führte. Weiterhin wurden Gene mit Avirulenz- (sr10057, sr10060, *sruni1* und *sruni2*) und mit Virulenzfunktion (clusters 19A, cluster 5-1uni und *sruni5*) identifiziert. Cluster 19A3 scheint Faktoren zur Unterdrückung der Blattalterung zu kodieren, da seine Deletion das verfrühte Sterben der Spitzen infizierter Blätter auslöste. Weiterhin erfüllte *vag1* Virulenzfunktionen in Blättern und Avirulenzfunktionen in Nodien. Zwei Gene, *sad1* und *sad2*, zeigten eine Beteiligung an der Unterdrückung der Apikaldominanz. SAD1 und VAG1 werden im Blatt proteolytisch abgebaut. Nach Expression in Pflanzenzellen lokalisierte SAD1 im Zellkern und im Zytoplasma und interagierte mit dem Effektor MIG1 sowie mit Pflanzenproteinen, welche vermutlich an der Ubiquitinierung, an Kernfunktionen und an Signalprozessen beteiligt sind. Diese Interaktionspartner könnten den Mechanismus des organspezifischen Abbaus von SAD1 und die Rolle von SAD1 in der Unterdrückung der Apikaldominanz erklären. Somit konnte eine molekulare Verbindung zwischen spezifischen Effektoren von *S. reilianum* und induzierten Entwicklungsveränderungen im Wirt etabliert werden.

SUMMARY

Sporisorium reilianum causes head smut disease on maize. Symptoms of *S. reilianum* become obvious when the fungus forms spores and induces phyllody in the inflorescences. This study aimed to provide an understanding of how *S. reilianum* changes the developmental program of maize, and to identify and characterize symptom and virulence determinants of the pathogen. The maize-*S. reilianum* interaction was approached from both sides. From the side of maize, the induced alterations on morphology, transcription, hormone level and concentration of reactive oxygen species (ROS) were investigated. Morphological analysis showed that *S. reilianum* infection promoted outgrowth of subapical ears suggesting that fungal presence suppressed apical dominance. *S. reilianum* colonization also led to an increase in the total cytokinin and auxin content of the inflorescence and an accumulation of ROS that could explain suppression of apical dominance. Furthermore, *S. reilianum* infection triggered loss of floral organ and meristem identities, and loss of meristem determinacy. Microarray analysis showed that these developmental changes were accompanied with transcriptional regulation of genes known or proposed to regulate floral organ and meristem identities, and meristem determinacy in maize.

From the side of *S. reilianum*, genome comparison with the closely related smuts *Ustilago maydis* and *Ustilago hordei* was performed to predict potential candidate genes with function in symptom formation or virulence on maize. Functional characterization of the candidates showed that deletion of *dicer* did not lead to changes in virulence or in the mutant behavior in response to different stresses. In addition, genes with avirulence functions (sr10057, sr10060, *sruni1* and *sruni2*) and those with virulence functions (clusters 19A, cluster 5-1uni and *sruni5*) were identified. Cluster 19A3 was suggested to encode leaf senescence inhibitors, since its deletion triggered leaf tip death. Additionally, *vag1* fulfilled avirulence and virulence functions in leaves and nodes, respectively. Two genes, *sad1* and *sad2* showed involvement in suppression of apical dominance. SAD1 and VAG1 were degraded in a leaf-specific manner. SAD1 localized to the nucleus and the cytoplasm when expressed in plant cells and, interacted with the effector MIG1 and plant proteins involved in ubiquitination, nuclear functions and signaling. These interaction partners could shape the mechanism of tissue-specific degradation of SAD1 and the role of SAD1 in suppression of apical dominance. Hence, a molecular link could be established between specific effectors of *S. reilianum* and induced developmental changes in the host.

1. INTRODUCTION

Corn is one of the most important crops on our planet. The land cultivated with corn covers 156.3 million hectares (USAD, 2010). The production of corn is threatened by several diseases, in particular smut diseases. Smut diseases are caused by a basidiomycete group of fungi, most of which belong to the order Ustilaginales (Agrios, 1997). The name of the disease represents the prominent symptom caused by the pathogen: masses of dark spores replacing a plant organ, i.e., the inflorescence. Two members of smut pathogens, *Sporisorium reilianum* (Kühn) and *Ustilago maydis* are able to infect maize leading to head smut or common smut symptoms, respectively.

S. reilianum was first described as *Ustilago reiliana* by Kühn in 1875 and then renamed *Sphacelotheca reiliana* (Kühn). The first isolate was from an infected sorghum specimen from Egypt (Reed et al., 1927; Edw, 1931). *S. reilianum* is a soil born pathogen, occurring world wide, and its host range covers maize, sorghum, teosinte and sudan grass. It causes considerable loses in temperate regions, in particular in combination with dry whether. The disease can spread through contaminated seeds, thereby represent a danger to seed production (Leslie, 2003). The incidence of head smut is increasing in France (Bernardo et al., 1992), and since 1993 the disease has been occurring in Germany (Dutzmann and Duben, 1993; Meinert, 1997). Studying the interaction between maize and *S. reilianum* will provide an understanding on how the pathogen modulates changes in the host and how the host responds to these changes.

1.1 The Life Cycle of *S. reilianum*

S. reilianum is a close relative of the intensively investigated smut pathogen, *U. maydis* (Begerow et al., 2006). Although both infect the same host, maize, they differ fundamentally in their behavior during proliferation *in planta* and site of symptom development. Using *U. maydis* as a model, several steps in the life cycle of *S. reilianum* could be resolved. The teliospores of *S. reilianum* germinate under favorable conditions to give rise to lemon-shaped haploid sporidia. Each haploid cell has two unlinked mating type loci, *a* and *b* (Schirawski et al., 2005). The *a* locus exists in three alleles containing genes encoding two active pheromone and one pheromone receptor needed for cell-cell recognition. The *b* locus exists in at least five alleles and encodes two subunits of a heterodimeric homeodomain transcription factor, a key regulator for pathogenicity (Feldbrügge et al., 2004; Schirawski et al., 2005).

When two sporidia with compatible mating type meet on the plant surface, they form conjugation tubes, which fuse to produce a filamentous dikaryon (Figure 1). The dikaryon develops a penetration structure, seen as swelling hyphal structure called appresorium, to invade the epidermal layer of the host tissue (Banuett and Herskowitz., 1994). The invading hyphae proliferate within the leaf and eventually spores replace the male and female inflorescences giving rise to the smut symptoms (Figure 1).

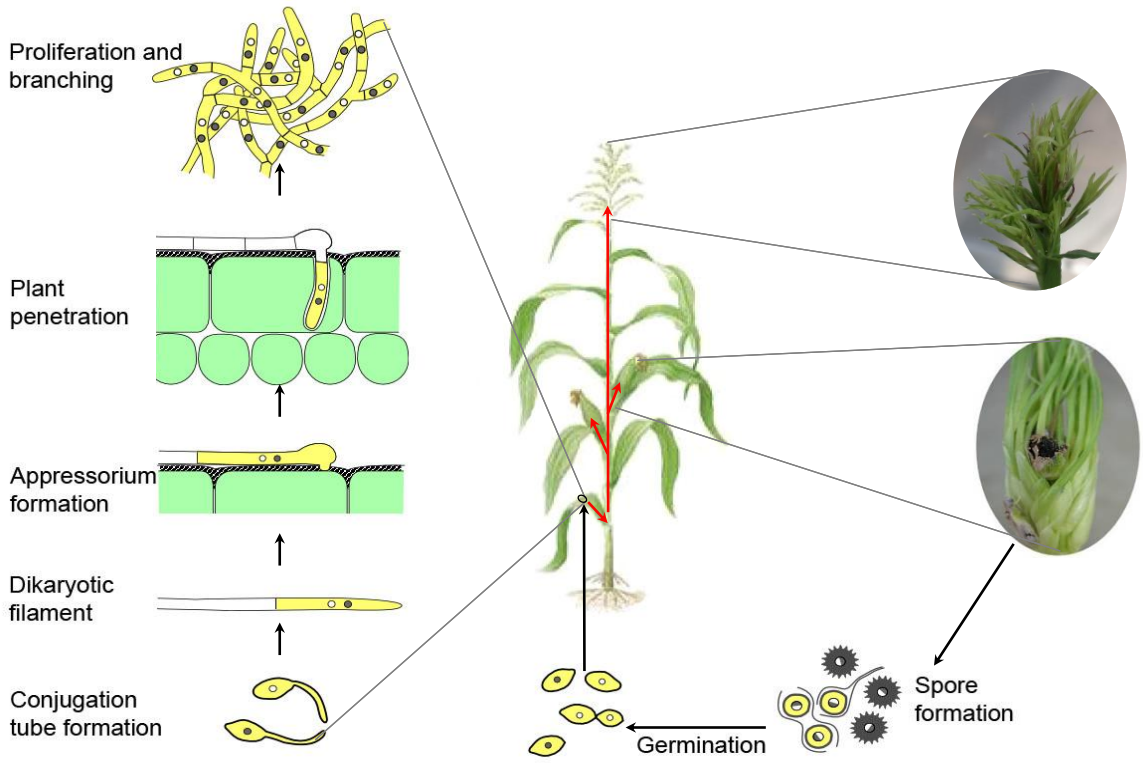

Figure 1. *Sporisorium reilianum* life cycle. Spores germinate under favorable conditions leading to haploid sporidia. Once two haploid sporidia with different mating type occur near to each other on the leaf, conjugation tubes form and fuse, leading to dikaryotic filaments. A penetration structure, appressorium, is formed at the proper site to invade the plant. After penetration of the epidermal layer, the invading hyphae proliferate filamentously within the leaf. Finally, at the flowering time, spores-filled sori replace the kernels. The figure is modified from a figure provided by Jan Schirawski.

1.2 Factors Influencing *S. reilianum* Development and Infection

The interaction balance between any host and its pathogen is affected by environmental conditions that could privilege any of the protagonists. In the maize-*S. reilianum* interaction, dry

and cool weather at the time of seedling growth favors the disease since seedling growth is slow. Later dry and warm (21-30°C) weather favors disease severity. The disease incidence is also increased under nitrogen deficiency conditions. Soil moisture content of 15-25% is optimal for seedling infection (Matyac and Kommedahl, 1985). Furthermore, it was found that low soil water potential (−1.2 MPa) has an effect on transition from lemon-shaped sporidia to hyphal growth facilitating the fusion of compatible mating strains leading to increased disease severity (Martinez et al., 2003).

On the other hand, as spore formation occurs exclusively in the inflorescence, it is likely that the host inflorescence harbors factors inducing *S. reilianum* morphogenesis. Experimentally it was shown that the floral meristem of sorghum is capable of inducing mycelial growth of *S. reilianum in vitro*. By fractionation of the floral meristem extract, it could be concluded that the factor triggering mycelial growth is heat stable and has glycoprotein nature (Bhaskaran et al., 1991). It was subsequently shown that the glycoprotein content changes following developmental transition from vegetative to floral growth (Oh et al., 1994). The changes included disappearance of galactosebinding glycoproteins and appearance of glucosebinding and mannosebinding glycoproteins in the floral meristem. Based on these findings it was suggested that certain components in the host primary cell wall containing glycoprotein bonds may act as inducers for enzymatic degradation and utilization of its components by *S. reilianum* to promote mycelial growth (Bhaskaran et al., 1991; Bhaskaran and Smith, 1993). Interestingly, it was also shown that two glycoproteins enriched in fucose were only expressed in floral meristems during incompatible interaction (Oh et al., 1994). Glycoprotein composition on plant cell wall varies between cell types, during development and in response to environmental conditions. It was suggested that availability of the proper glycoprotein on flower cell walls might be a factor determining fungal morphogenesis and/or interaction compatibility with the host (Bhaskaran and Smith, 1993).

1.3 Symptoms Caused by *S. reilianum*

S. reilianum typically generates masses of spores filling the inflorescences of the host. In maize, the symptoms occur on both inflorescences; tassel and ears. In maize and sorghum, the spores are formed within sori, white tissue enclosing spores. The sorus can replace individual flowers or a whole inflorescence (Bressman and Barss, 1933). Additionally, sorghum panicles, and maize

ears and tassels may develop phyllodied inflorescences with twisted leafy shoots (Figure 1, 2) (Reed et al., 1927; Stromberg et al., 1984; Njuguna, 2001). Morphological changes in inflorescences are usually linked to a partial or complete vegetative reversion of a floral meristem. Floral reversion can occur in response to biotic and abiotic stresses, in particular, upon attack by viruses, mycoplasma-like organisms or fungi (Meyer, 1966). Among the latter are smuts, downy mildews or bunts. They cause phyllodied inflorescences in cereals of major economic importance, e.g.; maize, sorghum, wheat, pearlmillet and ragi (Raghavendra and Safeeulla, 1979; Semisi and Ball, 1989).

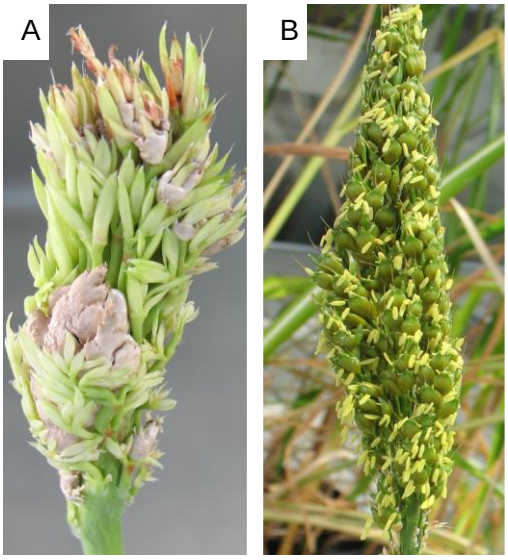

Figure 2. Symptoms of *S. reilianum* on sorghum. (A) Phyllodied inflorescence with white peridia carrying spores inside. (B) Healthy inflorescence of sorghum.

In addition to spore and phyllody formation, maize infected with *S. reilianum* develops multiple ears at the node, or sometimes shows a stunting phenotype (Reed et al., 1927; Stromberg et al., 1984). Likewise, sorghum infected with *S. reilianum* shows enhanced tillering and stunting (Casady, 1969; Bhaskaran et al., 1990; Matheussen et al., 1991). To identify factor responsible for symptom formation, the gibberellin GA3 was applied to floral primordia of sorghum *in vitro*, which led to reversion of the inflorescence to vegetative leafy growth and mimicked the developmental defect of *S. reilianum* infection (Bhaskaran et al., 1990). From phyllodied panicles complete plants could be generated (Bhaskaran et al., 1990). It was reported that *S. reilianum* sporidia are able to synthesize GA1 and GA3 (Matheussen et al., 1991). In contrast,

in vitro application of GA3 to maize inflorescences did not trigger phyllody formation (Touraud et al., 1997). Furthermore, quantitative analysis of the GAs in phyllodied panicles of infected sorghum revealed a decreased total GA content but an increase level of GA20. It was suggested that the fungus interferes with GA biosynthesis of the host leading to decreased GA content, which might be responsible for the increased tillering phenotype (Matheussen et al., 1991). Application of GA to sorghum led to inhibition of tillering supporting the involvement decreased GA concentrations in increased tillering caused by *S. reilianum* (Morgan et al., 1977; Isbell and Morgan, 1982).

The disease severity differs from one plant to another, i.e.; one to several inflorescences could show symptoms on the same plant. In infected plants all ears are usually smutted, if the tassel is smutted (Bressman and Barss, 1933). As all signs and symptoms of *S. reilianum* were not present in each infected plant, it was suggested that the systemic infection by *S. reilianum* hyphae depends on the stage of meristem differentiation at the time of the infection (Stromberg et al., 1984). Soil factors, moisture and temperature could also be important determining factors for symptom development (Stromberg et al., 1984). Apparently, there are no unambiguous pathogens or host factors known to be involved in symptom development of *S. reilianum*.

1.4 Host-*S. reilianum* Interaction

In maize, it was shown that *S. reilianum* is able to penetrate the epidermal cell layers of root and shoot (Lübberstedt et al., 1999; Martinez et al., 2000). It was suggested that *S. reilianum* enters the plant through the root and then grow into the rest of the plant (Martinez et al., 2000). In the leaf, *S. reilianum* caused chlorosis. In the chlorotic flecks, the hyphae were always collapsed and surrounded by a matrix (Martinez and Roux, 2002). Neither in root nor in vegetative apical meristems of maize did the fungus cause any cell damage or signs of host defense reactions like, thickening of the cell wall or accumulation of plant material (Martinez et al., 1999; Martinez et al., 2000). Based on these observations, *S. reilianum* was considered to be a biotrophic endophyte (Martinez et al., 1999; Martinez et al., 2000).

In node and floral tissue of infected sorghum the fungus proliferates mainly in the vascular bundles and the parenchyma cells (Matyac, 1985). As the sori mature, the hyphae grow intracellularly, and hyphae between the vascular tissues intertwine and form globose to

subglobose sporogenous hyphal masses. Later, each hyphal group forms a mass of spores, which is surrounded with nonsporogenous hyphae. The sori are enclosed with a peridium, a white cover around the spores, which consists of two to three cell layers of host tissue, sometimes having an inner layer of fungal hyphae. The presence of the hyphae in the axillary buds results in the development of a sorus in place of the normal ear. Likewise colonization of the shoot apex at the transition from vegetative to floral meristem results in the formation of a sorus in place of the tassel (Matyac, 1985).

In the floral tissue of maize four types of interaction between *S. reilianum* and the host cells were observed: (i) fungal hyphae and host cells appeared alive; (ii) the hyphae are collapsed and the host cell was alive; (iii) both the hyphae and the host cells were collapsed; (iv) the hyphae was alive and colonized the whole host cell, which consequently was collapsed (Martinez and Roux, 2002). It is unclear why there are different reactions between the same protagonists. Nevertheless it seems that *S. reilianum* is able to keep a high degree of compatibility with its host in order to survive within the host until flowering. During intracellular growth in the floral tissue of maize the hyphae were always surrounded with a matrix, which separated it from the plasmalemma. The latter observation was not noticed in infected root. The matrix was suggested to be an exchange zone between the plant and the fungus (Martinez et al., 1999). Vesicle-like structures were observed to be endocytosed from the hyphae-surrounded-plasma membrane toward the host cytoplasm (Martinez et al., 1999). The vesicles might transport virulence effectors to mediate compatibility with the host.

Different maize cultivars show different degrees of susceptibility to infection with *S. reilianum* (Fuyao et al., 2010; Magill et al., 2011). Several quantitative trait loci (QTLs) were identified to be associated with resistance to *S. reilianum* (Bernardo et al., 1992; Njuguna, 2001). Resistance to *S. reilianum* is an additive treat, which varies according to the experimental conditions used (Bernardo et al., 1992; Wisser et al., 2006; Chen et al., 2008). Additionally, only few QTLs showed resistance association to both *S. reilianum* and *U. maydis* (Bernardo et al., 1992; Njuguna, 2001). This could be due to difference in the infection style of both pathogens: *S. reilianum* causes systemic infection, whereas *U. maydis* causes local infection (Lübberstedt et al., 1999). Alternatively, this could reflect that *S. reilianum* evoloved the capacity to infect maize indepenetely of *U. maydis*. In spite of the identification of resistence associated QTLs, so far no gene-for-gene resistance has been described for the maize-*S. reilianum* interaction.

1.5 Identification of Pathogenic Determinants by Genome Comparison

Based on phylogenetic analysis *S. reilianum*, *U. maydis* and *Ustilago hordei* are closely related smuts (Begerow et al., 2006), nevertheless they differ in the symptoms caused and their mode of colonization. Whereas *S. reilianum* causes smutted and phyllodied inflorescences on maize, *U. maydis* causes tumors on the leaf and inflorescence of maize (Figures 1, 3), and *U. hordei* causes smut on barely inflorescences (Figure 3). Regarding the mode of colonization, *S. reilianum* and *U. hordei* grow systemically to reach the inflorescence, whereas *U. maydis* causes symptoms locally where it infects (Lübberstedt et al., 1999; Singh and Mathur, 2004). Evolutionary studies suggested that a large number of Ustilaginomycetes taxa including the three smut fungi were evolved by jumps of the ancestors to new hosts (Bauer et al., 2001; Munkacsi et al., 2007).

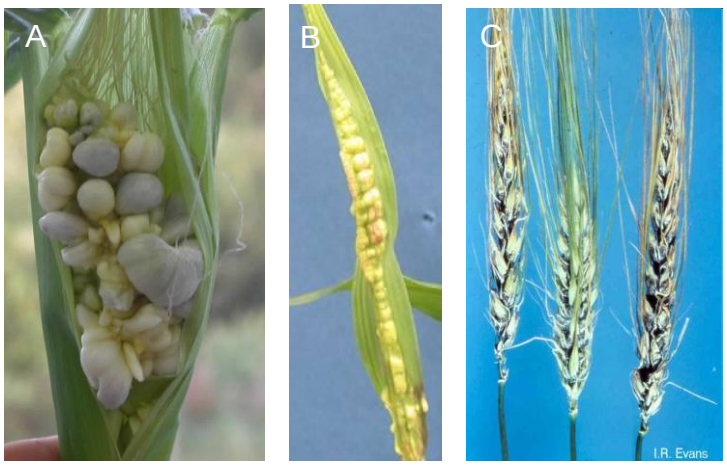

Figure 3. Symptoms of *U. maydis* and *U. hordei*. (A) Tumors caused by *U. maydis* on ear (A) and on leaf (B). (C) The smut symptoms caused by *U. hordei* on barley, black spores fill the grains. Pictures A and C were kindly provided by J. Schirawski and I. R. Evans, respectively.

Sequencing of complete fungal genomes facilitates investigation of genes involved in plant-pathogen interaction. One prominent example is the identification of effector loci in *U. maydis* by identification of gene clusters coding for secreted proteins (Kämper et al., 2006). Genome comparison of *S. reilianum* and *U. maydis* led to identification of new effector loci in both *S. reilianum* and *U. maydis*. Whereas the approach has been functionally proven to be promising for identification of effectors in *U. maydis*, it is still to be proven in *S. reilianum*. So far there are no functionally characterized effectors known in *S. reilianum*. However, since tools for genetic

manipulation of *S. reilianum* are available (Schirawski et al., 2010), this system can be used for the identification of factors that communicate with and functuanly modulate the host pathogenicity and symptom specificities. Recently, the *U. hordei* genome has been sequenced and is currently being annotated (J. Schirawski, R. Kahmann, personal communication). Genome comparison of *S. reilianum* and *U. maydis* with *U. hordei* may help to reveal the genetic basis of the biological differences among these smut pathogens.

S. reilianum triggers distiguishable symptoms from *U. maydis* and *U. hordei* by interfering in the host's floral development. It is an unresolved question how *S. reilianum* manipulates the developmental processes of its host plant maize and causes symptoms., in the form of phyllodied inflorescence, spore formation only in the inflorescences or inducing multiple ears at a node.

1.6 Maize Floral Development

In maize the male inflorescence, the tassel, develops at the apex of the plant, whereas the female inflorescences, the ears, develop on the main shoot from axillary meristems (Veit et al., 1993). Since *S. reilianum* is able to cause symptoms in both inflorescences, it is important to know the general mechanisms of flower development to understand how *S. reilianum* interferes with the developmental program and leads to floral malformation.

1.6.1 Maize Inflorescence Architecture

During inflorescence development of tassel and ear several types of meristems develop that follow a very similar order. A first step towards development of the male inflorescence is the conversion of the shoot apical meristem into tassel inflorescence meristem (IM). In the developing tassel, IM develops to branch meristem (BM), which leades to formation of branches. At the side of each branch, spikelet pair meristems (SPM) develop that differentiate into spikelet meristems (SM), which develop to a spikelet. Eventually, each spikelet develops to two floral meristems (FM) (Veit et al., 1993). The floral meristems differentiate into upper and lower florets. The two florets are surrounded with the spikelet remnants called outer and inner glumes, which are modified leaves (Figure 4A-D). Together the axillary meristems BM, SPM, SM and FM on the inflorescence give the maize inflorescence its architecture. Similar meristem

differentiations take place in the developed ear, except that there is no formation of BM (Bennetzen and Hake, 2009).

The basic architecture of a maize floret consists of five floral whorls that form lemma, palea, two lodicules, three stamens, and in the most inner whorl a pistil formed from three carpels; two of them are fused to form the silk that surround a single ovule and one remains rudimentary (Nickerson, 1954) (Figure 4E-H). The upper floret matures in advance of the lower floret, which aborts in the ear. Another difference between tassel and ear is obvious after initiating floral organ primordia where stamens are aborted in ear florets and pistils are aborted in tassel florets giving rise to monoecious flowers (Veit et al., 1993; Bennetzen and Hake, 2009).

1.6.2 Meristem Identity and Determinacy

Any meristem could be determinate or indeterminate. Meristem determinacy refers to the capacity of the meristem for continuous activity. For example BM and IM are indeterminate meristems. Here indeterminacy reflects their continued generation of a stem axis. In contrast, the SPM, SM and FM show relative determinacy, which is reflected in the production of short branches only with defined number of organs (Bennetzen and Hake, 2009). Meristem determinacy is usually regulated via transcription factors. The *ramosa* mutants (*ra1*, *ra2* and *ra3*) show a clear contribution in specifying determinacy of the SPM. They encode a C2H2 zinc finger, a LOB domain transcription factor and a trehalose 6-phosphate phosphatase, respectively (Vollbrecht et al., 2005; Bortiri et al., 2006; Satoh-Nagasawa et al., 2006). In addition, *ra3* influences the determinacy of the SM. The determinacy of the SM is also regulated by the *BRANCHED SILKLESS1* (*BD1*), *INDETERMINATE SPIKELET1* (*IDS1*) and SISTER *INDETERMINATE SPIKELET1* (*SID1*) genes, which encode AP2 family transcription factors (Chuck et al., 1998; Chuck et al., 2002). Additionally, the *INDETERMINATE FLORAL APEX1* (*IFA1*) regulates meristem determinacy (Laudencia-Chingcuanco and Hake, 2002). Mutation of a meristem fate regulator gene could lead to abolishments or changes in meristem identity or determinacy.

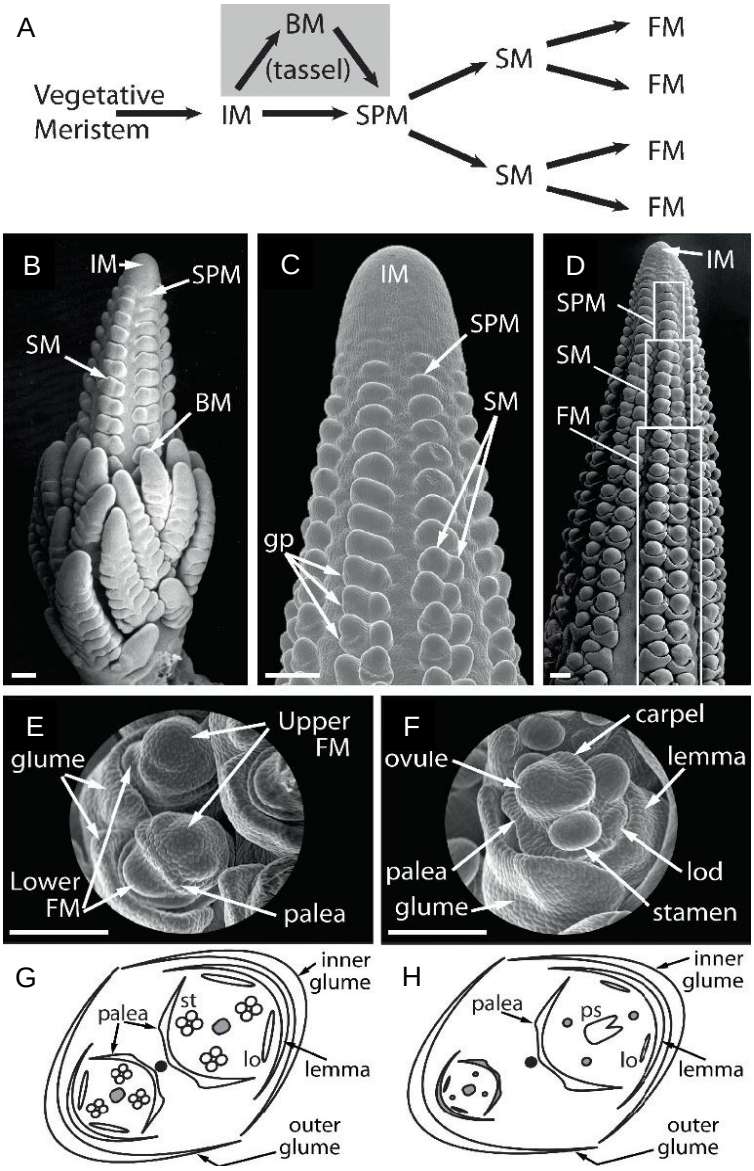

Figure 4. Inflorescence architecture of maize. (A) Scheme of the developmental progression of meristem identities during inflorescence development. (B–F) Scanning electron micrographs of developing tassel and ear through floral organ initiation. (B) Developing tassel primordium. (C) Close up of developing tassel primordium spike. (D) Developing ear primordium. (E) Floral meristems forming in spikelets. (F) Initiation of floral organ primordia. (G) Scheme of a mature staminate (tassel) spikelet. (H) Scheme of a mature pistillate (ear) spikelet. Bars = 200 μM. IM; inflorescence meristem, BM; branch meristem, SPM; spikelet pair meristem, SM; spikelet meristem, FM; floral meristem, lod; lodicule, ps; pistil. Adopted from (Bennetzen and Hake, 2009).

1.6.3 Development of Axillary Meristems

Maize undergoes two kinds of branching: vegetative, leading to leaves, and reproductive, leading to female inflorescences, the ears. The inflorescences of maize also undergo several branching events giving rise successively to BM, SPM, SM and FM (Veit et al., 1993). To branch, a group of stem cells at the meristem need to be initiated. In Arabidopsis, the initiation of these stem cells is regulated by two genes *CLAVATA* (*CLV*) and *WUSCHEL* (*WUS*). They ensure a balance of cell proliferation and meristem size. Three *CLV* genes have been identified. *CLV1* encodes a leucine rich repeat (LRR) receptor kinase, *CLV2* encodes an LRR receptor like protein, and *CLV3* is predicted to encode their ligand. *WUS* encodes a homeodomain transcription factor (Clark et al., 1997; Mayer et al., 1998; Fletcher et al., 1999; Jeong et al., 1999). The maintenance of the stem cell fate is regulated by a regulatory loop between CLV and WUS that regulates each others transcription (Schoof et al., 2000). In addition, WUS positively regulates cytokinin biosynthesis (Leibfried et al., 2005; Shani et al., 2006). This links transcriptional regulation of meristem maintenance to hormone signaling.

Hormones, cytokinins, strigolactone and auxins play a critical role in regulating branching (McSteen, 2009). Cytokinins regulate meristem size and therefore indirectly modulating branching (Shani et al., 2006). Cytokinin transport from the root towards the axillary bud promotes outgrowth (Cline et al., 1997). Conversely, transport of strigolactone in the same direction inhibits axillary meristem outgrowth (Crawford et al., 2010). Axillary meristem initiation during both vegetative and inflorescence development is also regulated by auxin. By accumulation at a certain site, auxins define the site of meristem initiation. Transport of auxin from the apex towards the root suppresses axillary meristem outgrowth leading to apical dominance (Davies et al., 1966). Apical dominance can be influenced by several endogenous and exogenous factors (Figure 5). Although hormones have been implicated in regulation of axillary meristem development (Figure 5), their exact mode of action is unknown (Barazesh and McSteen, 2008).

Increasing knowledge about the mode of action of auxins, cytokinins and strigolactones led to the proposal of two models, the “auxin transport canalization model” and the “second messenger model”, which explain apical dominance mechanistically (Domagalska and Leyser, 2011). In the auxin transport canalization model, regardless of the auxin concentration, polar auxin transport

(PAT) plays the central role in apical dominance. During basipetal movement, auxin flux is canalized gradually into a tight thread of cells , the auxin canal, resulting in a high PAT (Sachs, 1981). To be activated, the bud must also generate PAT, and export auxin to the auxin canal in the stem (Domagalska and Leyser, 2011). Meanwhile, the acropetal flow of strigolactones reduces PAT and consequently impacts on bud activity (Prusinkiewicz et al., 2009). In the second messenger model, auxin regulates a second messenger, cytokinins and strigolactones, that migrate to the axillary bud and control its activity (Domagalska and Leyser, 2011). Several studies have be conducted and support either of the two models [reviewed in (Domagalska and Leyser, 2011)].

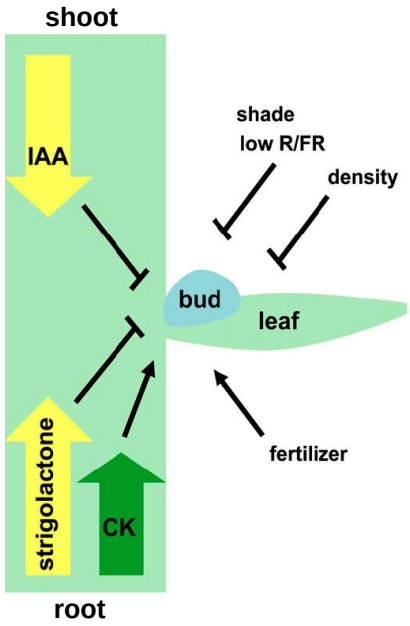

Figure 5. Model for endogenous and exogenous factors controlling bud outgrowth. The blue ball represents an axillary bud in the axil of a leaf. The endogenous factors; auxin (IAA), cytokinin (CK) and strigolactone, and the exogenous factors; shading [low red/far red (R/FR) ratio], planting density and fertilizer application determine whether or not the axillary bud grows out. Adopted from (McSteen, 2009).

Using reverse genetics in several model plants, several genes have been shown to be involved in axillary meristem initiation and outgrowth during vegetative and reproductive growth. These genes encode transcription factors, signaling components or hormone related proteins (Table 1). in maize, determination of the axillary meristems is additionally influenced by mutation in

number of transcription factor genes such as *TEOSINTE BRANCHED1*, *DELAYED FLOWERING1* and *Zea FLORICAULA/LEAFFY1* and *2* (Coe et al., 1988; Sheridan, 1988; Hubbard et al., 2002). Recently, it was shown that application of inhibitors of PAT prior to the floral transition mimics the *BARREN INFLORESCENCE2* (*BIF2*) and *BARREN STALK1* (*BA1*) inflorescence phenotypes, suggesting that they act in a similar, auxin-related pathway (Wu and McSteen, 2007). It was also found that *BA1* expression is dependent on polar auxin transport (Gallavotti et al., 2008), whereas the *BIF2* transcripts were still present in auxin inhibitor-treated plants (Wu and McSteen, 2007). This suggests a model in which *BIF2* is upstream of polar auxin transport and polar auxin transport is required for *ba1* expression (Bennetzen and Hake, 2009). This example explains how transcription factors and phytohormones interplay to regulate development of axillary meristem.

Table 1. Genes regulating axillary meristem initiation in monocots and eudicots (McSteen, 2009).

Protein	**Rice**	**Maize**	**Arabidopsis**	**Pea**	**Tomato**
Auxin efflux carrier	*OsPIN1*	*ZmPIN1*	*PIN1*	*PsPIN1*	
Ser/Thr kinase	*OsPID/OsBIF2*	*BIF2*	*PID*	*PsPID*	
Flavin mono-oxygenase	*OsYUC1*	*SPI1*	*YUC1,2,4,6*		*ToFZY*
bHLH transcription factor	*LAX*	*BA1*			
GRAS transcription factor	*MOC1/SPA*		*LAS*		*LS*
NAC transcription factor	*OsTIL1/OsNAC2*	*ZmCUC3, ZmNAC*	*CUC1,2,3*		
HD ZIP transcription factor	*OsHB3*		*REV/IFL*		
MYB transcription factor				*RAX1,2,3*	*BLIND*

1.6.4 Organ Identity and Floral Reversion

The floral meristem initiates floral organs in a defined phyllotaxy and terminates by the production of an ovule (Thompson et al., 2009). The development of each floral organ requires a combination of transcription factors that defines its identity. How these transcription factors specify the floral organ can be explained by the so-called ABCDE model of flower development. The model was initially hypothesized for the eudicots Arabidopsis and Antirrhinum. In that model, five gene classes of transcription factors A, B, C, D and E have partially overlapping target genes so that each gene class affects one to several whorls. The A and C gene classes

affect two different whorls each and have antagonistic activities, so that the loss of C results in A activity in all four whorls and vice versa. The A class genes specify sepals fate and, together with B genes, petals. The B genes specify stamens together with C genes, and the C genes alone specify carpel. The D class genes promote ovule identity. The class E genes affect all whorls and are considered to function as a scaffold for orchestrating the different ABCD transcription factors. (Coen and Meyerowitz, 1991; Weigel and Meyerowitz, 1994; Ng and Yanofsky, 2001; Ditta et al., 2004). It has been proposed that lemma/palea and lodicules of monocots correspond to sepals and petals of dicots, respectively (Ambrose et al., 2000). From works on maize and other grasses, the ABCDE model could be extended to involve monocotyledons (Yanofsky et al., 1990; Ambrose et al., 2000; Dreni et al., 2007; Thompson et al., 2009).

Disrupting the expression of any of the ABCDE class genes leads to loss of organ identity of the concerned organs (Weigel and Meyerowitz, 1994; Ditta et al., 2004; Bortiri and Hake, 2007). The class A mutants *AP2* and *APETALA1* (*AP1*) of *Arabidopsis thaliana* show conversion of sepals into carpels and petals into stamens (Jofuku et al., 1994; Weigel and Meyerowitz, 1994). The functions of the maize *AP2*-like genes *IDS1* and *SID1* seem to be partially conserved in maize, i.e., negatively regulate the C function gene *Zea AGAMOUS1* (*ZAG1*). In addition, *AP2* genes in maize have acquired novel meristem functions, initiating floral meristem and controlling spikelet meristem determinacy (Chuck et al., 2008). Mutation of the B class *SILKY* (*SI1*) in maize, transformed the lodicules into bract-like organs that resembled paleas or lemmas and converted stamens into carpels (Whipple et al., 2004). The *ZAG1* of maize shows expression restricted to carpel and its mutation leads to loss of floral meristem determinacy forming several instead of one pistil, supporting its function as a C calss gene (Schmidt et al., 1993; Mena et al., 1996). *Zea AGAMOUS2* (*ZAG2*) is a homologue of *ZAG1* that shows constrained expression to developing carpels, in particular in the ovule and extensions that form the silk. (Schmidt et al., 1993; Theissen et al., 1995; Colombo et al., 1998). *ZAG2* was placed in the D class genes according to homology to a rice D class gene, OsMADS13 (Dreni et al., 2007). In Arabidopsis class E, *SEPALLATA* (*SEP*), genes consist of four members with redundant function. Mutating all four genes led to transformation of all floral organs into leaf-like organs (Ditta et al., 2004). In rice, a *SEPALLATA*-like gene *LEAFY HULL STERILE1* (*LHS1*) was identified (Malcomber and Kellogg, 2004; Ohmori et al., 2009) and in maize, *Zea AGAMOUS3* (*ZAG3*) was shown to have an E class function. Thus, the ABCDE model can be used to draw a framework for the

developmental regulation of floral organs in grasses, nevertheless identification and characterization of new genes will be needed to uncover the differences in floral morphologies of grasses (Thompson and Hake, 2009).

S. reilianum infection leads to the formation of phyllodied inflorescences has long been known () but to date there is no detailed description of the developmental changes caused by the fungus. It is also unknown whether symptoms caused by *S. reilianum* are the results of a direct interaction of the pathogen's secreted effectors with host proteins, or a secondary consequence of hormonal and/or metabolic changes induced upon fungal infection.

1.7 Objectives of the Study

The aim of the current study was to understand the general basis of symptom development caused by *S. reilianum* infection of maize. The plant-fungus interaction was investigated both from the side of the host plant as well as from the side of the pathogen.

1. The specific objectives to achieve through maize were to:
    - Microscopically describe the floral morphologies of the infected inflorescences.
    - Investigate the molecular events underlying the floral changes caused by *S. reilianum* via analyses of the transcriptome, the hormones and the reactive oxygen species.
2. The specific objectives to be achieve through *S. reilianum* were to:
    - Technically establish a symptom evaluation system for *S. reilianum*-infected maize plants, locus specific integration for gene complementation in *S. reilianum*, and yeast two hybrid library construction for screening plant and pathogen interaction partners.
    - Study the contribution of *S. reilianum*'s unique genes, RNAi and cluster 19A genes to symptom specificity and virulence.
    - Study the localization and to identify the protein interaction partners of the potential symptom specificity effectors of *S. reilianum*.

2. RESULTS

2.1 *S. reilianum* Infection of Maize

To understand the symptoms caused by *S. reilianum* on maize, we inoculated a mixture of compatible sporidia of *S. reilianum* strains (Figure 6A) into the leaf whorl of 7-day old maize seedlings. At 16-18 hours post inoculation, calcofluor white stained leaf surfaces revealed the presence of appressoria that had developed at the tip of fungal hyphae (Figure 6B). Appressoria marked the entry point of fungal hyphae into the leaf epidermal cells. Hyphae traversed epidermal cells and colonized bundle sheath cells (Figure 6C, D). From there, *S. reilianum* progressed towards the leaf sheath and could be detected in the nodes at 15 days post inoculation. In the node, the fungus mainly proliferated around the vascular bundles (Figure 6E). Although hyphae of *S. reilianum* could be observed in all these tissues, sporulation occurred only in the male (tassel) or female (ears) inflorescences (Figure 6F). In addition to spore formation, we observed morphological changes in the inflorescences that are described in detail below.

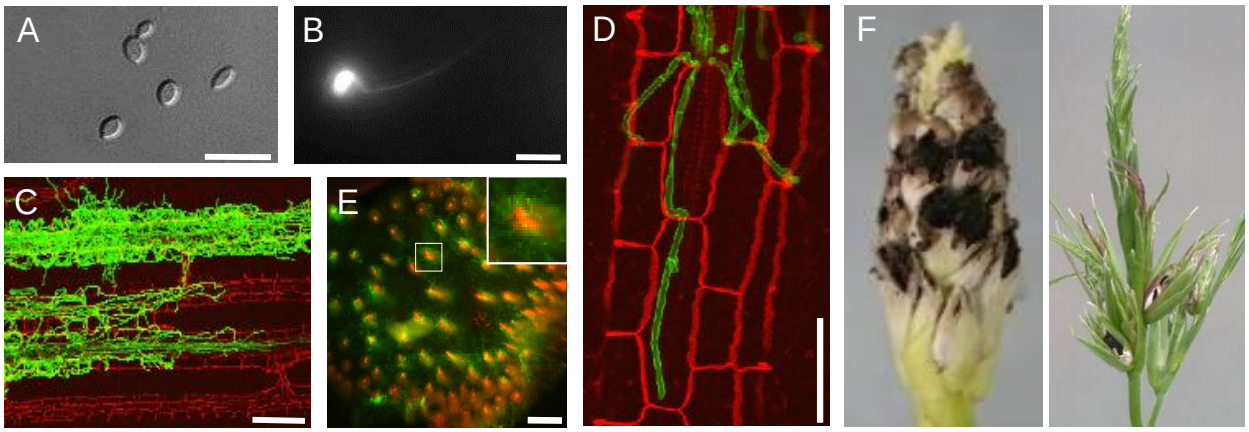

Figure 6. Morphological stages of *S. reilianum* outside, on and in *Zea mays* 'Gaspe Flint'. (A) Axenically grown haploid sporidia of *S. reilianum*. Bar = 15 µm. (B) Appressoria of *S. reilianum* penetrate the leaf surface visualized by bright field microscopy after staining with calcofluor. Bar = 10 µm. (C) In the plant leaf, fungal hyphae proliferate along leaf vascular bundles. Z-stack of a WGA-Alexaflour (green, fungal hyphae) and Propidium Iodide (red, plant cells) stained samples visualized by confocal microscopy. Bar = 100 µm. (D) A close up of fungal hyphae colonizing bundle sheath cells. Bar = 50 µm. (E) In the nodes of the plant, fungal hyphae (green) surround the plant vascular bundles (red). A cross section stained with WGA-Alexaflour and Propidium Iodide was visualized by confocal microscopy. Bar = 500 µm. (F) Spores of *S. reilianum* forming on maize ear (left) and tassel (right).

2.2 Floral Development Changes Caused by *S. reilianum*

2.2.1 *S. reilianum* Alters Ear Branching Architecture

We noticed that *S. reilianum*-infected plants showed more ear branches per plant than mock-infected ones (Figure 7A). Ear branches developed from axillary meristems borne at the axils of husk leaves (Figure 7B), indicating that *S. reilianum* infection resulted in a loss of apical dominance in ear-bearing branches. To quantify the formation of female inflorescences, we removed the husk leaves around the primary ear and counted all visible inflorescences. At eight weeks post infection, *S. reilianum*-infected plants showed on average 7.6 ears per plant, whereas mock-infected plants had only 4.3 ears per plant (Figure 7C).

To find out whether the increase in the number of ears is restricted to a branch appearing at a specific node, we determined the ear number per branch at each node. For this purpose, the 2nd node was defined as the upmost node with brace roots, and counting was towards the top. Secondary ear branches appearing from axils of husk leaves of the primary ear could be observed on any ear branches. In infected plants, subapical ears appeared at a significantly higher frequency at the 2nd to 4th nodes (Figure 7D). However, the relative increase in average ear number per branch was highest at the lowest node considered and ranged from 2.8-fold at the 2nd node to 1.1-fold at the 6th node (Figure 7D). This indicates that the increase in the total number of ears is derived from a loss of apical dominance at ear branches appearing at lower nodes.

2.2.2 *S. reilianum* Changes Morphology of Maize Flowers

An inoculation of maize seedlings with *S. reilianum* did not lead to any plant developmental defects until flowering time. When inflorescences appeared, a range of morphological changes in both male and female inflorescences could be observed in infected plants. In addition to the formation of white sori harboring dark brown fungal spores (Figure 6F), we observed the formation of phyllody in tassels and ears of infected plants (Figure 8A and B). Phyllody occurred to different extents affecting a range of spikelet numbers, from one individual spikelet to all spikelets of an inflorescence. In female inflorescences, we could distinguish two morphologic forms of phyllody, which we named “leafy” and “eary”, because they either seemed to be replaced by leaf-like structures or by ear-like structures, respectively (Figure 8A).

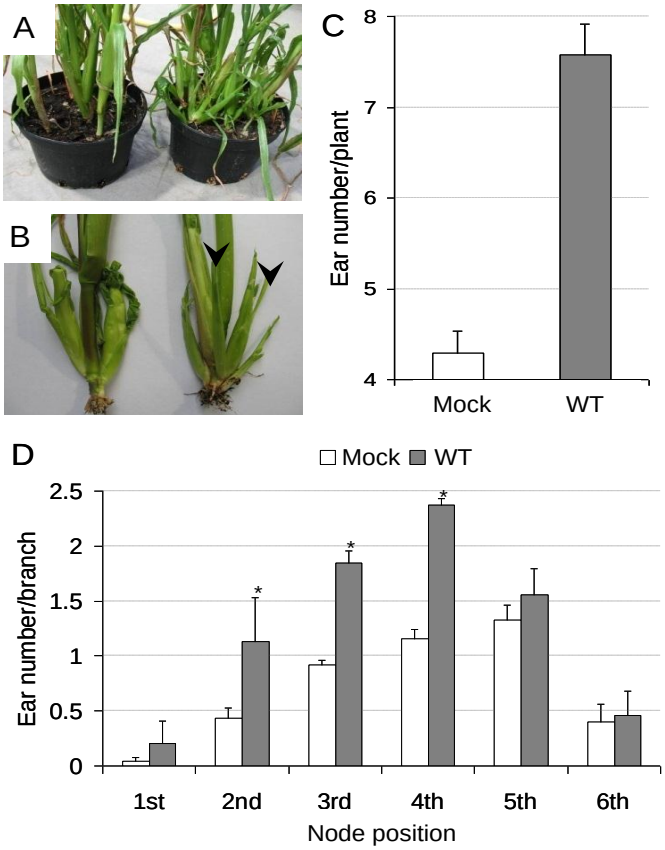

Figure 7. Effect of *S. reilianum* infection on ear number of *Zea mays* 'Gaspe Flint'. (A) *S. reilianum*-infected plants (right) show a higher ear number then mock-infected plants (left). Each pot contains 4 plants. (B) In mock-infected plants (left), ears form at apical points of a side branch. In infected plants (right), additional secondary ears (arrowheads) develop on subapical side branches of an ear-bearing side branch. (C) Quantification of the ear number per plant. Error bars represent SEM of three independent experiments with 23±2 plants per infection and replicate. The difference is significant (p-value = 0.01). (D) *S. reilianum*-infected plants significantly (*, p-value = 0.05) develop more ears per branch at the 2nd, 3rd, and 4th node. The 2nd node was defined as the upmost node with brace roots, and counting was towards the top. Error bars represent SEM of three independent experiments with more than 25 plants per infection and replicate.

Interestingly, while leafy spikelets could cover different portions of the inflorescence, eary spikelets mostly covered the whole inflorescence (Figure 8C). Ears carrying both leafy and eary spikelets were only rarely observed. In male inflorescences, we observed only one morphologic form, which we called "phyllodied tassel". In phyllodied tassels the morphologic change could affect one or more spikelets, and spikelets seemed to be replaced by ear-like structures (Figure

8B). *S. reilianum* infection of Gaspe Flint led to phyllody at a higher frequency (91%; 114 of 126 plants) in female inflorescences emerging at basal nodes, than in male inflorescences (5%; 6 of 126 plants) that form at the apex.

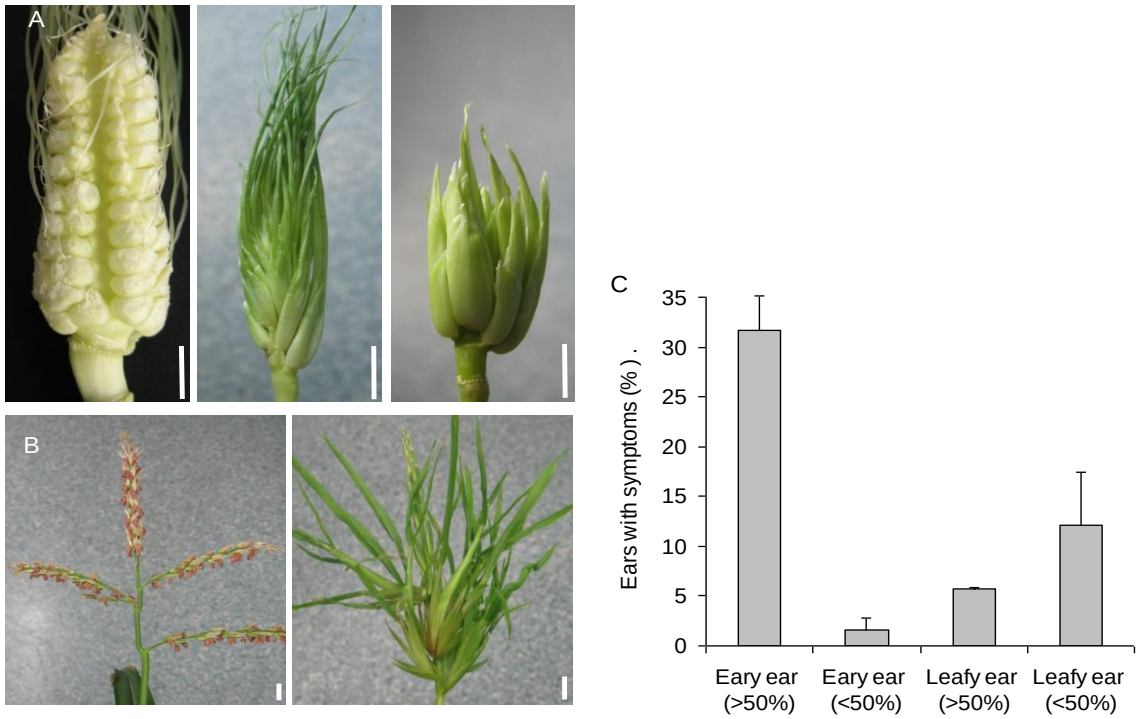

Figure 8. Phyllody caused by *S. reilianum* infection in female and male inflorescences of *Zea mays* 'Gaspe Flint'. (A) Morphology of female inflorescences of *S. reilianum*-infected (leafy ear, middle, and eary ear, right), and healthy plants (left). Bars = 1 cm. (B) Morphology of male inflorescences of *S. reilianum*-infected (phyllodied tassel, right), and healthy plants (left). Bars = 1 cm. (C) Symptom distribution of eary and leafy ears. Eary or leafy morphology could cover more (>50%) or less (<50%) than half of the inflorescence. Error bars represent standard deviation of three independent experiments with more than 25 plants each.

2.2.3 *S. reilianum* Transforms Reproductive into Vegetative Organs

To understand the floral modifications caused by *S. reilianum* infection of maize, we analyzed different spikelet developmental stages. Spikelets of female maize inflorescences (Figure 9A) are enclosed by two glumes that surround two florets, a lower one that aborts and an upper one that develops floral organs. The flower primordium produces floral organs in whorls, firstly forming the palea/lemma, then lodicules, and finally carpels that enclose the ovule, while stamen

development is arrested at an early stage (Figure 9B). Fused carpels generate the silk that is required for pollen tube guidance to assure fertilization. In male flowers, stamens develop, while female reproductive organs (carpels and ovule) are aborted.

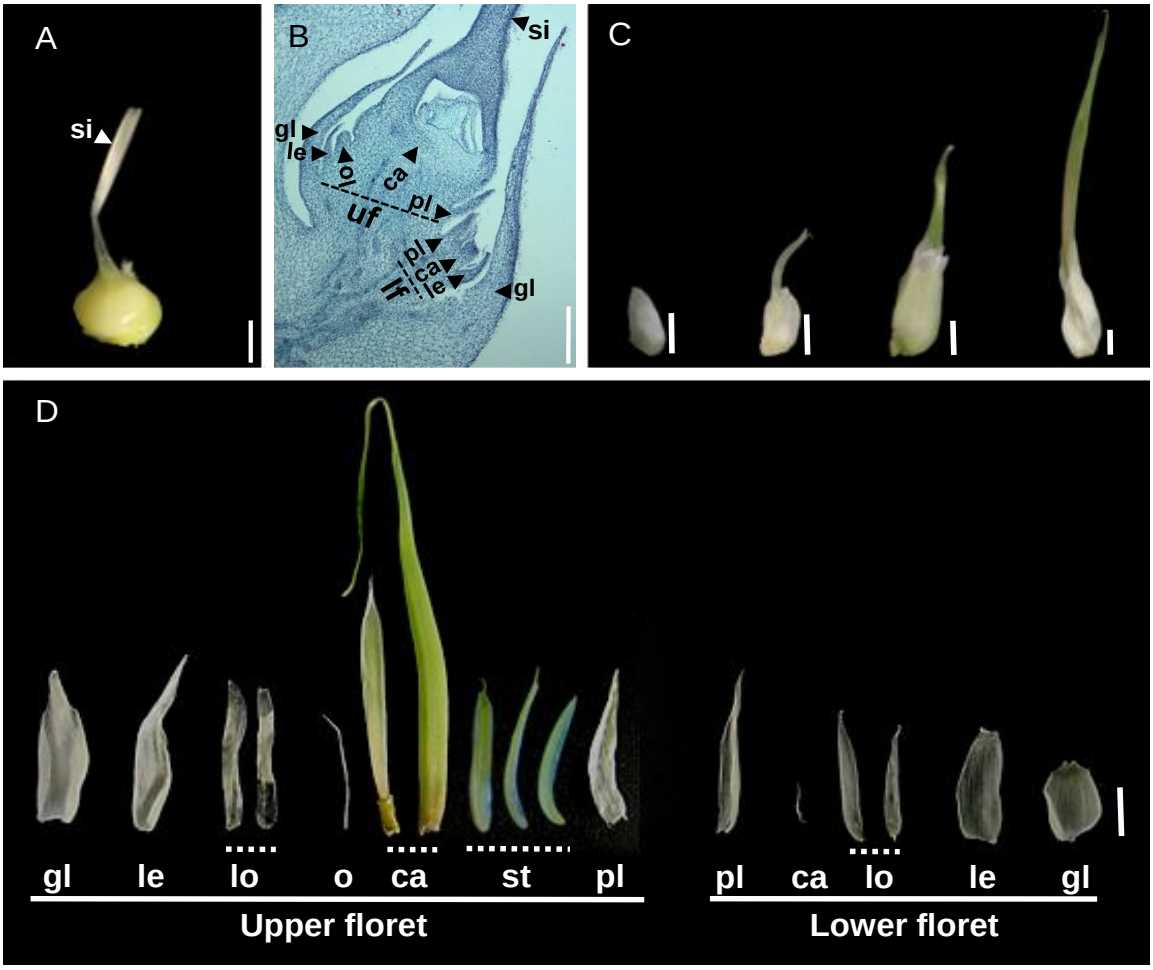

Figure 9. Spikelet development of healthy and *S. reilianum*-colonized leafy ears of *Zea mays* 'Gaspe Flint'. (A) A healthy ear spikelet. Bar = 2 mm. (B) Longitudinal section of a young healthy ear spikelet showing upper floret (uf) with developing floral organs and the aborted lower floret (lf). Bar = 1 mm. (C) Developmental stages of the leafy spikelet. The leafy spikelet first elongates, then a silk-like protrusion emerges. The protrusion elongates and thickens, and gives rise to an onion leaf-like structure. Bar = 5 mm. (D) Manually dissected floral structures of a leafy spikelet. Vegetative structures were formed at positions of all floral organs, except at stamen positions in the lower floret, indicating loss of organ identity. Tubular structures were formed at the position of the fused carpels, which infrequently enclosed a leafy and a needle-like structure. Bar = 5 mm. Floral organs forming in the healthy florets (A, B) are abbreviated by si, silk, gl, glume, le, lemma, lo, lodicules, o, ovule, ca, carpel, st, stamen, and pl, palea. In phyllodied spikelets (D), these abbreviations indicate the position at which vegetative structures appeared.

In comparison to healthy spikelets, leafy spikelets started to elongate before a silk-like protrusion emerged from the tip (Figure 9C). This protrusion grew longitudinally and radially and gave rise to a green tubular structure (Figure 9C, right). None of the floral whorls developed reproductive organs, which are readily formed in the healthy spikelet (Figure 9B, D). Instead, leaf-like organs formed in all floral whorls. In the upper floret, glume, lemma, lodicules, and palea appeared as thin, elongated, and translucent organ. In the innermost whorl, an elongated green tubular structure replaced the carpel. Within this tube-like organ, a smaller leaf-like structure was present infrequently that was folded in half to cover a transparent needle-like protrusion emerging from the center of the floret (Figure 9D). The needle like-protrusion and the folded leaf-like structure might correspond to the ovule and the rudimentary carpel, respectively, or be the result of the formation of indeterminate organs at the central whorl.

Interestingly, leaf-like organs with a yellowish to green color could be found only in upper florets of infected inflorescences at the place where stamens normally abort (Figure 9D). In the lower floret, thin elongated translucent membranous organs corresponding to glume, lemma, lodicule, and palea were formed. In the center of the lower floret, a small closed tubular structure appeared in place of the carpel (Figure 9D). In summary, vegetative structures replaced all reproductive organs indicating that *S. reilianum* infection of maize led to floral reversion. In addition, meristem termination is disturbed, leading to the formation of leaf-like organs instead of aborted stamens.

2.2.4 *S. reilianum* Modifies Floral Meristem Fate

In eary ears, spikelet development also started with spikelet elongation but, unlike in leafy ears, there was no development of a silk-like protrusion. Spikelets eventually developed two ear-like structures that contained new developing inflorescences (Figure 10A). Like in leafy spikelets, the floral whorls of eary spikelets formed vegetative structures at almost every floral whorl. While glume, lemma, lodicule and palea appeared as thin elongated translucent membranous organs, stamens appeared as thicker, leaf-like organs of yellowish to green color that resemble husk-like leaves (Figure 10B). In the center of the floret, we found a husk-like leaf that covered a newly formed inflorescence replacing the carpels (Figure 10B, inset).

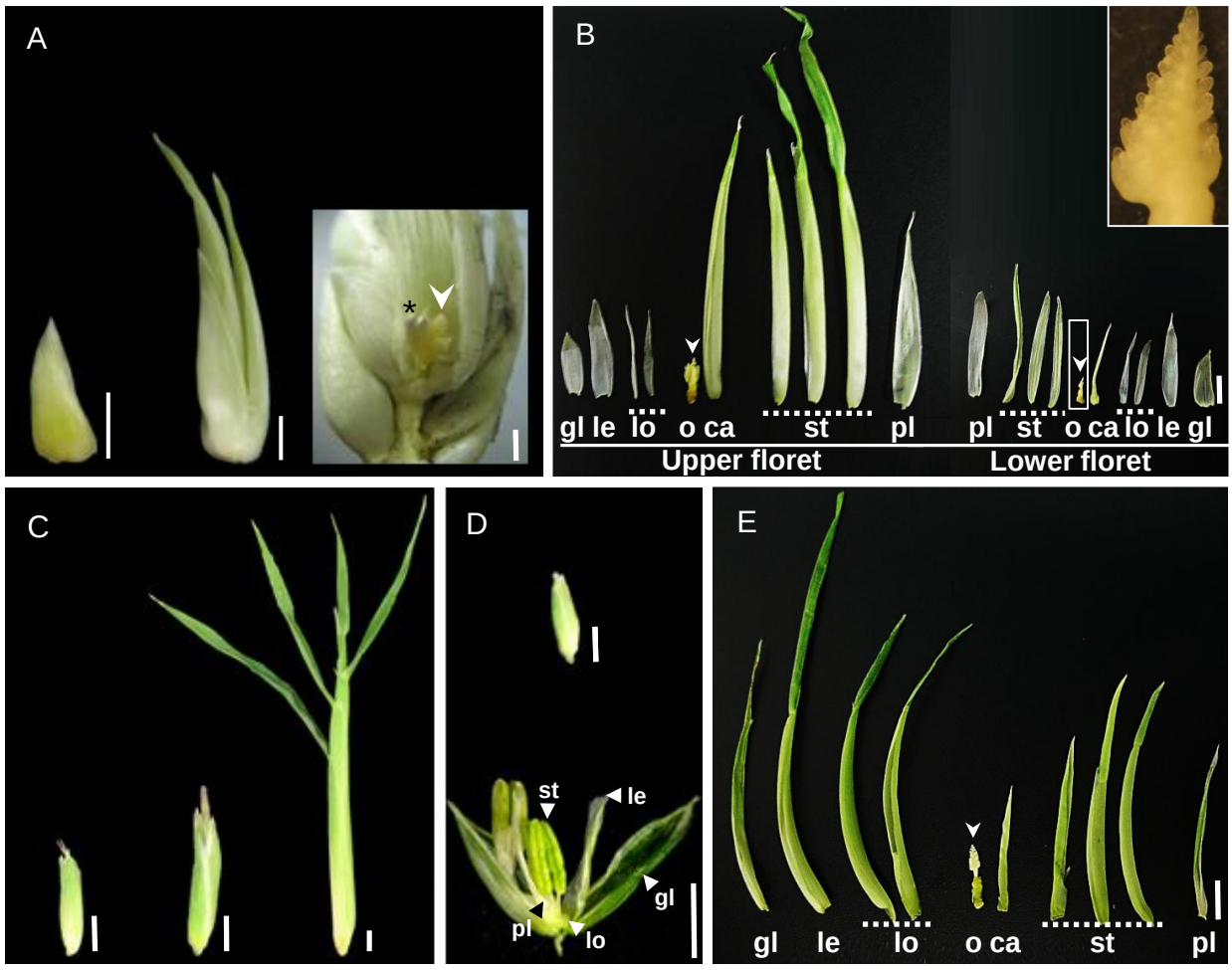

Figure 10. Loss of meristem and organ identity in spikelets of eary ears and phyllodied tassels caused by *S. reilianum* infection of *Zea mays* 'Gaspe Flint'. (A) Developmental stages of eary spikelets. Eary spikelet development starts with spikelet elongation. Elongation continues but no silk emerges, and finally two ear like structures appear that correspond to the upper and lower floret. On the right, the surrounding husk-like leaves have been partially removed to show a new developing inflorescence (arrowhead) that also bears fungal sori (star). Bars = 5 mm. (B) Manually dissected floral whorls of the eary spikelet. All the floral organs in the upper and lower floret including the two carpels that normally form the silk, were replaced by husk leaf-like structures. The most inner whorl that normally gives rise to the ovule was transformed into a new inflorescence (arrows and inset). Bar = 5 mm. (C) Spikelet developmental stages of phyllodied tassels. Bars = 5 mm. (D) Closed (top) and open (bottom) healthy spikelets of a tassel. Bars = 5 mm. (E) Manually dissected floral whorls of the upper floret of a spikelet of a phyllodied tassel spikelet. All floral organs were elongated and transformed into husk leaf-like structures, except the most inner whorl, which developed a new inflorescence (arrow). Bar = 5 mm. gl, glume; le, lemma; lo, lodicules; o, ovule; ca, carpel; st, stamens; pl, palea. Floral organs forming in the

healthy florets (D) are abbreviated by gl, glume, le, lemma, lo, lodicules, o, ovule, ca, carpel, st, stamen, and pl, palea. In phyllodied spikelets (B, E), these abbreviations indicate the position at which vegetative structures or new inflorescences appeared.

Similar morphological changes to those observed in the eary ear, could also be observed in the phyllodied tassel. Spikelets of phyllodied tassels had glumes that were elongated compared to healthy spikelets (Figure 10C, D) and developed into husk-like leaves (Figure 10C). Manual dissection of the floral whorls of the tassel spikelet revealed that most of the whorls developed husk-like leaves (Figure 10E). However, while in spikelets of healthy tassels carpel and ovule development is aborted at an early time point, the innermost whorl in spikelets of the phyllodied tassel was altered to a husk-like leaf that covered a newly developed inflorescence (Figure 10E, 11E). This suggests that in spikelets of both eary ears and phyllodied tassels most of the floral whorls developed into vegetative organs, with the exception of the most inner whorl, which developed a new inflorescence instead of ceasing meristematic activity for carpel abortion. Thus, the remnant of the floral meristem in the inner whorl has changed identity into an inflorescence meristem.

Sections of eary spikelets showed development of two inflorescences at the lower floret and the upper floret, respectively (Figure 11A). In contrast to spikelets of healthy inflorescences that developed floral organs (Figure 9B), spikelets of the newly developed inflorescence in eary spikelets developed new inflorescence meristems (Figure 11B). The newly formed inflorescences were heavily colonized by hyphae of *S. reilianum* (Figure 11C), whereas the floral organ-derived vegetative tissues were not (Data not shown). Phyllodied tassels also showed development of new inflorescences, which were more highly branched than those of eary inflorescences (Figure 11D, E). The branches of the tassel-like inflorescence had spikelet pairs similar to those of the healthy tassel but were enclosed by leafy structures (Figure 11F, G). In contrast to spikelets of healthy tassels that developed floral organs (Figure 11H), spikelets of the newly developed inflorescence in phyllodied tassel spikelets developed new inflorescence meristems (Figure 11I). Thus, the meristem remnants at the inner whorl have not only changed identity from floral to inflorescence meristem, but the newly formed inflorescence meristems have in addition lost their determinacy: instead of terminating in floral meristems, they continue to form new inflorescence meristems.

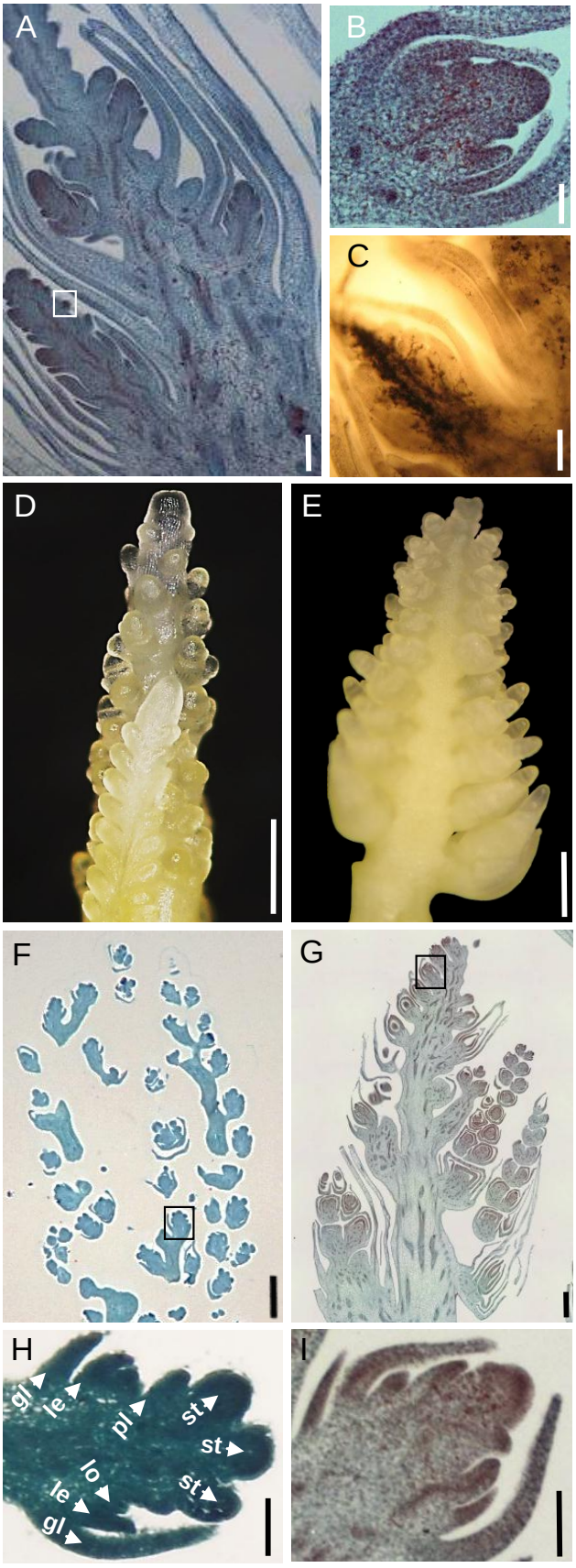

Figure 11. Loss of meristem determinacy in spikelets of eary ears and phyllodied tassels of *S. reilianum*-infected *Zea mays* 'Gaspe Flint'. (A) Longitudinal section of an eary spikelet showing development of new inflorescences in the upper and lower florets. Bar = 1 mm. (B) Magnification of the part boxed in (A) showing development of an inflorescence meristem instead of a spikelet meristem. Bar = 200 µm. (C) Longitudinal section of an eary spikelet showing massive hyphal growth of *S. reilianum* (black) in the newly formed inflorescence. Fungal hyphae were stained with Chlorazole Black E. Bar = 500 µm. (D) Tassel inflorescence of 10 day-old healthy plants showing development of a branched inflorescence. Bar = 500 µm. (E) Tassel-like inflorescence formed in the center of an infected phyllodied tassel floret. Bar = 500 µm. (F) Longitudinal section of a healthy tassel inflorescence showing development of spikelet pairs (arrows). Bar = 500 µm. (G) Longitudinal section of a newly formed tassel-like inflorescence from a phyllodied tassel floret of an infected plant showing development of spikelet pairs (arrows). Branches of the newly formed tassel-like inflorescence are enclosed within leafy structures (*). Bar = 500 µm. (H) Magnification of the part boxed in (F) showing development of floral organs. Bar = 200 µm. gl, glume; le, lemma; lo, lodicules; st, stamens; pl, palea. (I) Magnification of the part boxed in (G) showing development of an inflorescence meristem instead of a floret meristem. Bar = 200 µm. Sections were stained with O-Safranin-Fast Green staining.

2.2.5 *S. reilianum* Modulates The Floral Transcriptome

To understand the basic molecular mechanisms of *S. reilianum*-induced changes in the floral architecture of maize, we performed comparative RNA microarray analysis of healthy and *S. reilianum*-infected ears. Small ears (< 2 cm) from 20 plants each were collected at 4 weeks post inoculation, when infected ears displayed elongation of at least one spikelet (Figure 12 A). Expression patterns using Affymetrix GeneChip Maize Genome Arrays were compiled after statistical analysis of three biological replicates. Significance analysis revealed 169 differentially regulated genes, 76 down-regulated and 93 up-regulated genes (Table 2). To validate the data obtained by microarray analysis, gene expression of five randomly chosen differentially regulated genes was analyzed by quantitative Real-Time PCR (qRT-PCR). qRT-PCR analysis verified expression level changes observed by microarray analysis in all five cases (Figure 12B).

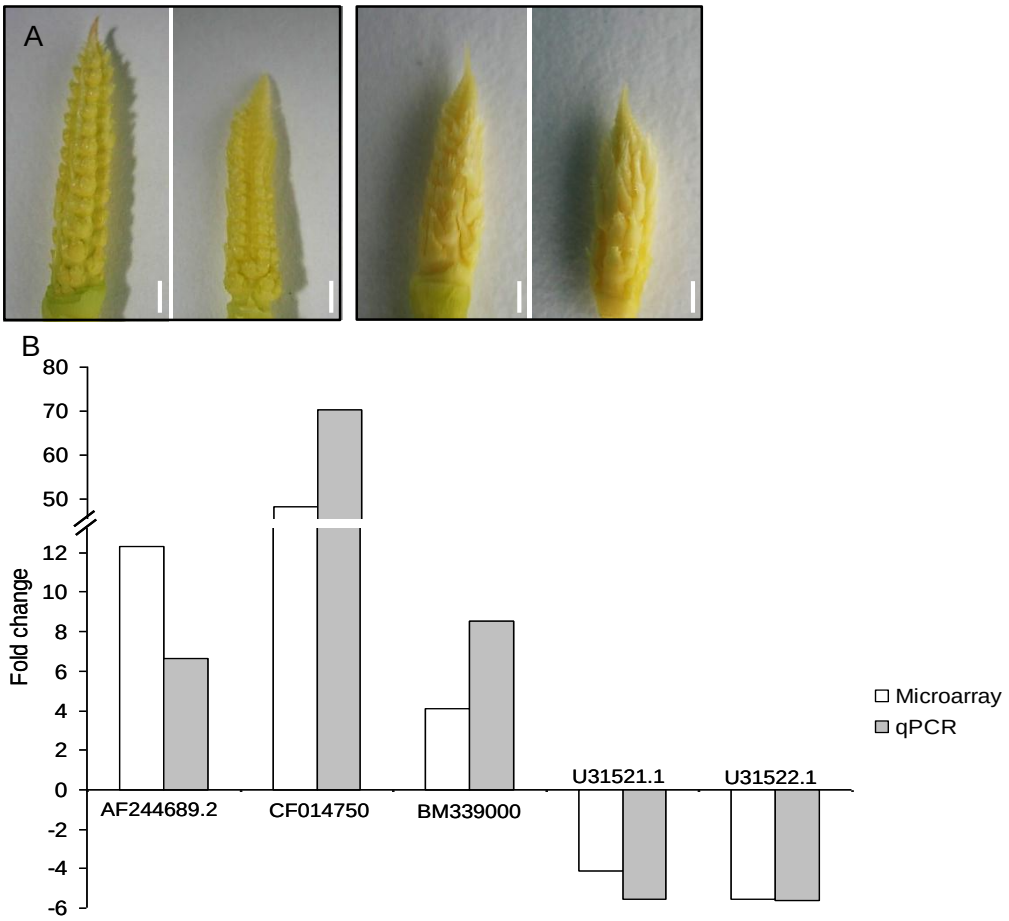

Figure 12. Morphology of samples collected for microarray analysis, and verification gene misregulation. (A) Representative developmental morphologies of mock (left) and *S. reilianum*-infected ears (right),

which were used for the microarray experiments. Bars = 200 µm. (B) Comparison of gene expression profiles determined by microarray or qRT-PCR. Similar expression values of regulated candidate genes in infected relative to healthy ears was observed using microarray and qRT-PCR analysis of the genes with the accession numbers AF244689.2, CF014750, BM339000, U31521.1 and U31522.1.

Table 2. Functional classification and approximate tissue gene expression pattern of maize genes with altered expression in *S. reilianum*-infected ears.

Accession	Fold change[a]	Annotation	Approximate gene expression pattern[b]
Biotic stress			
AF244689.2	12.3	glutathione S-transferase GST 24	ovary
BM380003	10.4	glutathione S-transferase GST 31	root; ovary
U12679.1	6.0	glutathione S-transferase IV (GSTIV)	silk; root; ovary; ear
BM381077	4.9	glutathione S-transferase GSTU6	shoot
CF626259	4.7	glutathione S-transferase GST 25	endosperm
AF244684.1	-3.8	glutathione S-transferase GST 19	ovary; ear; endosperm
BM332131	5.3	cytochrome P450 monooxygenase	aerial organs; root; embryo
BM382553	3.9	similar to cytochrome P450	ovary; shoot
BU050860	4.5	similar to putative peroxidase	ovary; ear
AY107230.1	3.2	similar to peroxidase	silk; ovary; glume
BG874182	-6.0	putative peroxidase	root
BG842197	-5.4	similar to putative peroxidase	root
CF629008	-5.1	peroxidase 1	root
AW424608	-4.3	peroxidase 1	endosperm
BM381423	-3.3	similar to putative peroxidase	endosperm; tassel
CF014750	48.3	putative sesquiterpene cyclase	silk; glume
BM379420	22.1	pathogenesis-related protein 10	endosperm; meristem
BM351351	15.3	pathogenesis related protein-1	leaf
BM379802	11.5	putative serine type endopeptidase inhibitor	ovary; root
BM079805	5.2	Ustilago maydis induced11	silk
BM379606	4.5	polygalacturonase inhibitor	sheath; ovary
BM348442	4.1	similar to glycosyl hydrolase family 17 protein	ovary; endosperm
CF649483	4.0	O-methyltransferase ZRP4	silk; ear; meristem
BM331999	3.5	xylanase inhibitor protein 1	aleurone; ovary; root
AW330894	-4.7	lichenase-2	glume; leaf; ovary
AI834666	-3.9	protease inhibitor/seed storage/LTP family protein	tassel; ear; pollen; endosperm
BM074215	-3.9	protease inhibitor/seed storage/LTP family protein	shoot; meristem
AW355997	-3.2	elicitor-responsive protein 3	ovary; root
Transcription factors			
U31522.1	-5.5	*Zea mays* MADS 1 (*ZMM1*)	pedicel; pericarp; ear; embryo
U31521.1	-4.1	*Zea* AGAMOUS2 (*ZAG2*)	pedicel; pericarp; ovary; ear
AW055920	-3.7	MADS box protein 29 (*ZMM29*)	ear; silk; pedicel; pericarp
L46397.1[a]	-2.6[a]	*Zea* AGAMOUS3 (*ZAG3*)	pedicel; ear; pericarp

Accession	Fold change[a]	Annotation	Approximate gene expression pattern[b]
L18924.1[a]	-2.3[a]	*Zea* AGAMOUS1 (*ZAG1*)	pericarp; ear
CF348980	3.9	AP2 domain containing protein	pedicel; ovary
CF637428	4.8	similar to AP2 domain-containing protein (AP28)	unknown
AI629804	5.4	MYB-related protein Hv33	aerial organs; meristem
BM075809	4.0	MYB domain protein 43	mixed tissues
AF099413.1	3.7	MYB-domain protein	unknown
AF099391.1	3.3	MYB domain transcription factor family	mixed tissues
CF045441	-3.8	NAC domain transcription factor family	endosperm
AW352507	-3.6	similar to vascular-related NAC-domain protein 7	leaf
AI670293	-3.3	NAC domain-containing protein	mixed tissues
CO533291	3.7	C2H2 zinc finger family	mixed tissues
BM380514	5.1	basic helix-loop-helix (bHLH) family protein	sheath; meristem
BG842397	4.5	nuclear transcription factor Y	meristem; embryo; shoot
Development			
CD999944	7.5	1-cys peroxiredoxin antioxidant	aleurone; embryo; endosperm
CA401976	5.2	1-cys peroxiredoxin antioxidant	endosperm
AY108635.1	9.3	seed maturation protein	embryo; endosperm
BM080758	4.9	similar to nodulin MtN3 family protein	root; aerial organs; meristem
BM338644	3.4	embryonic abundant protein	pollen; shoot
BQ539573	6.3	meiosis 5	aerial organs; meristem
AF332177.1	3.6	beta-expansin 4 (*EXPB4*)	aerial organ; meristem
AF332180.1	-3.9	beta-expansin 7 (*EXPB7*)	mixed tissues; root; silk
BM075217	-9.9	vegetative cell wall protein gp1	root
CK370036	-4.0	vegetative cell wall protein gp1	root; silk
CK369379	-4.0	L-ascorbate oxidase precursor	mixed tissues; root; silk
CK986211	-4.1	late embryogenesis abundant protein	root
AY108650.1	-3.9	lower-specific gamma-thionin	mixed tissues
CD446261	-3.3	phosphatidylethanolamine-binding proteins (*ZCN1*)	endosperm
Hormones			
AY254104.1	7.7	tryptophan synthase alpha subunit	meristem; pericarp; tassel
CF650494	5.2	similar to tryptophan synthase alpha subunit	root
CO533600	3.8	IAA-amino acid conjugate hydrolase ILR1-like 4	pollen
CK347988	-3.3	L-tryptophan:2-oxoglutarate aminotransferase	endosperm
BM339000	4.1	SAUR36 - auxin-responsive SAUR family member	meristem; aerial organs
BM379588	3.2	SAUR55 - auxin-responsive SAUR family member	mixed tissues
AY562491.1	11.5	kaurene synthase2	leaf
CF028197	3.2	gibberellin 20 oxidase 2	silk; leaf
AY105651.1	-3.4	gibberellin 20-oxidase (*GAO20*)	meristem; pericarp; pollen
CN845512	-3.8	cytokinin-O-glucosyltransferase 2	ovary; root; meristem
Signaling			
CF650678	-4.7	transducin family protein	ovary; root; meristem; endosperm
BG319707	-4.3	protein phosphatase 2C	pericarp; ear; ovary; endosperm
AY105086.1	-3.8	phosphatase	ovary; tassel; shoot

Accession	Fold change[a]	Annotation	Approximate gene expression pattern[b]
D87045.1	-3.4	protein kinase	ear
CF028241	6.2	brassinosteriod insensitive 1-associated receptor kinase 1	leaf; root
BQ528747	4.1	protein serine/threonine phosphatase	pollen
Transport			
BQ048817	-4.2	amino acid permease	ovary; endosperm; meristem
AI745852	-3.3	mechanosensitive ion channel domain-containing protein	pericarp; embryo; meristem
AI737924	-3.9	metal ion binding protein	ear; shoot
AF326489.1	-3.7	transport major intrinsic proteins PIP	root
Nuclear processes			
AY108503.1	-4.3	nuclease PA3	root; ovary; meristem
CF637079	-3.4	nuclear protein	ovary; endosperm; meristem
BG842386	-7.7	translation initiation factor	tassel; shoot; meristem
Abiotic stress			
BM381388	7.1	heat shock protein 3	ovary
L28712.1	4.1	heat shock protein 26 (*HSP26*)	endosperm
AW055615	-5.6	dehydrin 13	pollen
AY108025.1	-3.7	drought induced protein 1	root; endosperm
Energy			
AY059648.1	3.2	alternative oxidase *AOX3* precursor	ovary
CF004181	3.4	similar to citrate synthase	meristem; silk; embryo; sheath
Metabolism			
AF457950.1	-3.5	aspartate carbamoyltransferase 1	meristem; ovary; shoot
CO532055	3.4	carboxylesterase/ hydrolase	embryo; shoot; endosperm
AY103747.1	4.5	phosphoenolpyruvate carboxylase1	aerial organs; root; meristem
AW288498	4.4	chalcone synthase	silk; leaf; pericarp
AY105824.1	5.8	oleosin1	embryo; pollen; endosperm
CA400088	4.1	glycerophosphoryl diester phosphodiesterase	endosperm
U75531.1	7.7	phytase	aerial organs; meristem
CF627032	-5.0	lipid transfer protein	root; silk
CK826764	3.8	nonspecific lipid-transfer protein	meristem
CO520124	-3.5	beta-glucosidase	mixed tissues
BM381937	4.5	glyoxalase family protein	embryo; endosperm
AW573352	-3.3	similar to glucose-methanol-choline oxidoreductase	pollen
Miscellaneous			
AI667827	3.8	Brittle-1 protein (*BT1*)	endosperm
AY106977.1	-3.8	adhesive/proline-rich protein	cell culture
BM331860	-4.5	glycine-rich protein *GRP5*	mixed tissues
AY106317.1	4.4	stem 28 kDa glycoprotein precursor	tassel; meristem
CD995560	4.8	low-molecular-weight cysteine-rich protein *LCR68*	aleurone; embryo; pollen
AF365951.1	3.2	early light-induced protein	unknown
AF536189.1	4.1	bicistronic S male sterility locus	unknown
CO531219	3.9	lysosomal protective protein	mixed tissues

Accession	Fold change[a]	Annotation	Approximate gene expression pattern[b]
Unknown			
BM337251	13.1	hypothetical protein	pollen
CN844584	10.6	hypothetical protein	ovary
AY106294.1	10.4	hypothetical protein	aleurone; endosperm; embryo
BM332863	6.7	proline rich protein	aerial organ; pollen; meristem
BM347951	6.6	hypothetical protein	mixed tissues
BQ539485	6.3	hypothetical protein	root
CK827521	5.7	hypothetical protein	aerial organ; silk; leaf
AI665353	5.7	hypothetical protein	embryo; endosperm; meristem
BM341676	4.7	not assigned.unknown	ovary
BM340516	4.7	not assigned.unknown	ovary
BM337240	4.4	hypothetical protein	silk; pollen; glume; meristem ovary
BM378126	4.4	hypothetical protein	tassel; pericarp; meristem
CK985952	4.1	hypothetical protein	meristem
BM073190	4.1	not assigned.unknown	silk
BM340911	4.0	not assigned.unknown	unknown
AI833884	4.0	hypothetical protein	meristem
BM336314	3.9	not assigned.unknown	mixed tissues
CO521356	3.8	not assigned.unknown	mixed tissues
CK348021	3.8	hypothetical protein	root
BQ539474	3.7	hypothetical protein	silk; endosperm; shoot
BM072831	3.7	hypothetical protein	ovary; meristem
AI881950	3.6	not assigned.unknown	ear; tassel, endosperm; meristem
CK827054	3.6	not assigned.no ontology	mixed tissues
AY108161.1	3.5	not assigned.unknown	unknown
CF972430	3.4	hypothetical protein	Ovary; aerial organ; meristem
AY106290.1	3.3	not assigned.unknown	shoot; ovary; meristem
CK347337	3.3	hypothetical protein	endosperm
CO523535	3.3	not assigned.unknown	mixed tissues
CF633017	3.3	hypothetical protein	ovary
BM339684	3.3	not assigned.unknown	mixed tissues
BM347294	3.2	not assigned.unknown	mixed tissues
BM418233	3.2	not assigned.unknown	cell culture
BM380704	-6.2	hypothetical protein	aerial organs
CF633788	-5.8	hypothetical protein	root
CF021767	-5.3	hypothetical protein	glume; leaf; root
BM335873	-5.0	not assigned.unknown	mixed tissues; silk
AI691417	-4.9	not assigned.unknown	ear
BM340296	-4.9	hypothetical protein	mixed tissues
CA404993	-4.6	hypothetical protein	endosperm
BM078654	-4.6	hypothetical protein	aerial organs; pericarp
AI881720	-4.5	not assigned.unknown	ear
BM379705	-4.4	hypothetical protein	mixed tissues

Accession	Fold change[a]	Annotation	Approximate gene expression pattern[b]
BQ577766	-4.3	hypothetical protein	pollen
AI668207	-4.1	hypothetical protein	endosperm
CK985862	-4.0	not assigned.unknown	mixed tissues
BM339608	-4.0	not assigned.unknown	pericarp; endosperm; ear
BM382736	-4.0	hypothetical protein	root; shoot
CK827078	-3.9	hypothetical protein	silk
BM334837	-3.8	hypothetical protein	silk; glume; ovary; leaf
BM351072	-3.8	not assigned.unknown	mixed tissues
AI677123	-3.6	not assigned.unknown	embryo; endosperm
CF631293	-3.6	not assigned.unknown	root
BF727733	-3.6	not assigned.unknown	shoot; meristem
CB350776	-3.3	not assigned.unknown	mixed tissues
AI664910	-3.3	not assigned.unknown	endosperm
AI670425	-3.3	not assigned.unknown	embryo; endosperm
AI881975	-3.3	not assigned.unknown	mixed tissues
BM381305	-3.3	hypothetical protein	endosperm; meristem
BM382210	-3.2	hypothetical protein	mixed tissues
CO518294	-3.2	not assigned.unknown	mixed tissues
CA399376	-3.2	hypothetical protein	pericarp; ovary; endosperm

[a]Genes have an adjusted p-value of <0.05, except L46397.1 and L18924.1, which have adjusted p-values of 0.18 and 0.38, respectively.
[b]Estimated gene expression patterns obtained from the UniGene data base at NCBI, which were inferred from EST counts and the cDNA library sources (as reported by sequence submitters at NCBI). Libraries known to be normalized, subtracted, or otherwise biased had been removed. Tissues or organs are ordered according to their potential to express the gene.

Differentially regulated genes were manually annotated by comparison to sequence data bases available at the National Center for Biotechnology Information (NCBI) using BLAST analysis (Altschul et al., 1990), and classified according to predicted biological functions. Of the 108 genes that could be classified, most showed involvement in biotic stress (27%) and transcriptional regulation (16%). Fewer genes were predicted to have a function in development (12%), metabolism (11%), hormone biosynthesis and response (9%), or signaling (6%). A small fraction of the genes was predicted to be involved in transport (3%), nuclear processes (3%), abiotic stress (3%) or energy (2%), or grouped to several biological functions (8%). In every group, both up and down-regulated genes were represented in approximately equal parts. However, in the transcription factor group, members of the same family were regulated in the same manner. While MADS and NAC transcription factors were all down-regulated, the

members of the *AP2*, MYB, C2H2 zinc finger, and bHLH transcription factor families were up-regulated (Table 2).

To learn whether the members of transcription factor families were expressed in a tissue-specific manner, we compiled data on tissue-specific expression from the UniGene EST data base at NCBI for the differentially regulated genes. In this data base, EST counts from different cDNA libraries were used to calculate approximate gene expression patterns (number of gene ESTs per total number of ESTs in the pool) (Wheeler et al., 2006). Interestingly, all down-regulated MADS box transcription factors were estimated to be specifically expressed in reproductive organs of uninfected plants according to the calculated EST profile (Table 2) Floral organ-specific expression was also shown experimentally by in-situ hybridization for the *Zea AGAMOUS* (*ZAG*)-homologs *ZAG1* and *ZAG2*, the *AGL6*-like gene *ZAG3 (BEARDED EAR)*, and the *GLOBOSA* homolog *ZMM29* (Schmidt et al., 1993; Münster et al., 2001; Thompson et al., 2009). In Arabidopsis and maize, *AGAMOUS* (*AG*) and *APETALA2* (*AP2*) mutually repress each other (Weigel and Meyerowitz, 1994; Chuck et al., 2008). Interestingly, the two *AP2*-domain containing transcription factors with unknown function identified in this study are up-regulated (Table 2). However, whether they are regulated by *AG* is unclear.

The group of regulated genes belonging to hormone biosynthesis and response included genes potentially involved in auxin and gibberellin biosynthesis as well as auxin and cytokinin-mobilization. Two gibberellin biosynthesis genes were up-regulated, kaurene synthase 2 and gibberellin 20 oxidase 2, estimated to be expressed in the leaf according to the calculated EST profile of the UniGene data base (Table 2). In contrast, one gibberellin 20 oxidase gene that was meristem and floral organ-specifically expressed, was down-regulated in *S. reilianum*-infected relative to mock-infected ears. The up-regulation of leaf-specific and down-regulation of meristem and floral organ-specific gibberellin biosynthesis genes could either reflect the reversion of floral organs into leaf-tissue or could be the cause for the floral reversion process. Therefore, it is difficult to assess whether gibberellin concentration actively influences the observed floral reversion process. In our experiments, concentrations of gibberellins ($GA_{1, 3, 4, 5, 8, 9, 20, 34}$) in collected tissues were below detection limit (see Materials and Methods).

Three genes involved in auxin biosynthesis as well as two auxin-responsive genes were up-regulated in infected ears (Table 2). To know whether gene regulation resulted in increased auxin

levels, we measured auxin concentration of mock-infected and *S. reilianum*-infected ears. Mock-infected ears had an auxin concentration of 20 ± 0.5 pmol/g fresh weight, while that of *S. reilianum*-infected ears showed an increase of 30% (26 ± 0.7 pmol/g fresh weight; each mean of three independent biological replicates), while auxin amino acid conjugates were again below the detection limit. This *S. reilianum*-induced increase in the total auxin concentration in ears with elongating spikelets could indicate a potential role of auxin in the floral reversion process.

Most of the differentially regulated maize transcripts detected by microarray analysis had a predicted function in the response to biotic stress. Notable was the presence of 15 genes involved in detoxification of oxidative stress. Of these, nine reproductive organ or shoot expressed genes (five glutathione S-transferase, two cytochrome P450, and two peroxidase genes) were up-regulated, whereas five root or endosperm specifically expressed peroxidase genes were down-regulated (Table 2). This suggests a need for detoxification of reactive oxygen species (ROS) in *S. reilianum*-colonized inflorescence tissue, and implies that the level of ROS is higher in *S. reilianum*-colonized than in healthy inflorescences.

2.2.6 *S. reilianum*-Colonized Inflorescences Show an Elevated Level of ROS

To verify whether *S. reilianum*-colonized inflorescences contained a higher level of ROS, we prepared manual sections of young ears of infected or healthy plants that were immersed for two hours in a solution containing 3,3'-Diaminobenzidine (DAB). When supernatants were collected and absorbance of oxidized DAB at 465 nm was measured, a 15-fold increase in absorbance was detected in DAB solutions that had contained sections of infected inflorescences compared to supernatants of the healthy inflorescence sections (Figure 13A). When the DAB-treated sections were microscopically analyzed, brown oxidized DAB-precipitates could readily be detected on inflorescence sections of *S. reilianum*-infected plants but not on those of mock-infected plants (Figure 13B). DAB oxidation seemed to be specifically associated with fungal colonization and surrounded fungal hyphae that colonized leafy or eary spikelets (Figure 13C). This indicates that the presence of *S. reilianum* causes the observed increase in the ROS levels in inflorescences of infected plants, which could explain the up-regulation of reproductive-organ specifically expressed ROS detoxification genes (Table 2).

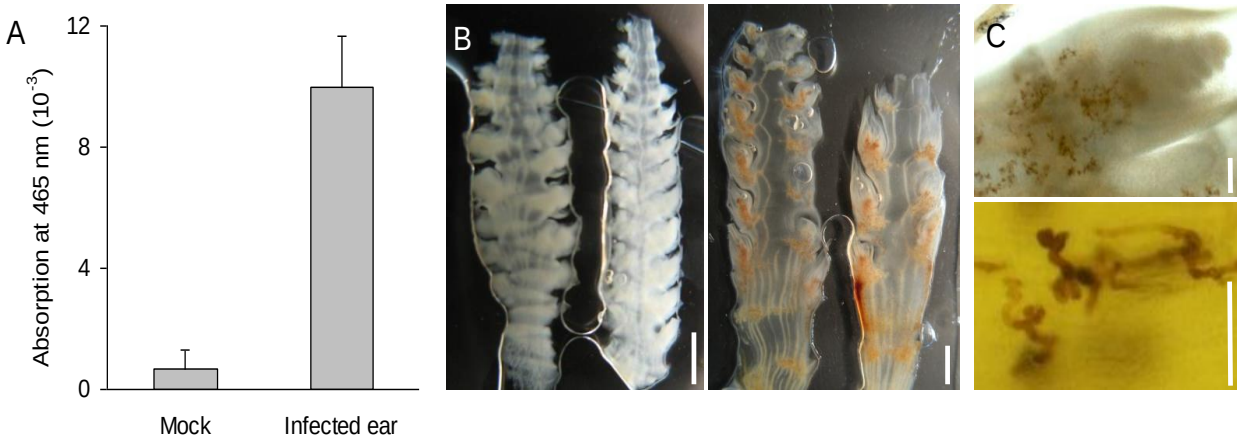

Figure 13. Detection of reactive oxygen species (ROS) in healthy and *S. reilianum*-infected female inflorescences of *Zea mays* 'Gaspe Flint'. ROS were stained and visualized by exposure to 3,3'-Diaminobenzidine (DAB). (A) DAB oxidization as a measure of ROS production in the supernatant of DAB-stained sections of female inflorescences. Error bars correspond to the standard deviation of six independent measurements. (B) Sections of healthy ears (left) and *S. reilianum*-colonized ears (right) after staining with DAB. Bar = 2 mm. (C) ROS accumulation (brown color) in sections of an eary spikelt (up) and around fungal hyphae (down). Bars = 100 µm.

2.3 Establishment of Tools for the Study of Maize-*S. reilianum* Interaction

2.3.1 Evaluation of Disease Symptoms Caused by *S. reilianum*

To quantify the strength of the interaction between maize and *S. reilianum*, a disease evaluation system is a prerequisite. So far, there is no published system for symptom severity evaluation of *S. reilianum*. Therefore, we established a disease rating method that includes both the formation of phyllodied inflorescences and inflorescences with spores by categorizing the disease symptoms into 13 categories, ordered from the weakest to the strongest symptoms (Figure 14): 1. healthy ear, 2. immature ear (does not show symptoms, but the kernels are not mature enough to be categorized as healthy), 3. ear with elongated kernels, 4. ear with >25% phyllodied kernels, 5. ear with 25-49 % phyllodied kernels, 6. ear with 50-74 % phyllodied kernels, 7. ear with 75-100 % phyllodied kernels, 8. ear with >25 % kernels filled with spores, 9. ear with 25-49 % kernels filled with spores, 10. ear with 50-74 % kernels filled with spores, 11. ear with 75-100 % kernels filled with spores, 12. tassel with phyllody and 13. tassel filled with spores. For each infected plant, each ear and tassel was ranked into one of the 14 categories.

Three measures for evaluating the virulence strength of *S. reilianum* strains were calculated, namely, disease incidence, disease severity and ear number per plant. To calculate disease incidence, each plant was placed in one of the 13 disease categories according to the highest symptom displayed on its inflorescences, and then the percents of plants in each category relative to the total plant number was calculated. To calculate the disease severity, the percent of all inflorescences falling into the same disease category from the total number of inflorescences of all plants was used as an indicator. The ear number per plant was calculated by dividing the total number of ears from all plants of one infection by the total number of plants. The three measures together can give a robust evaluation of the virulence of the *S. reilianum* strains.

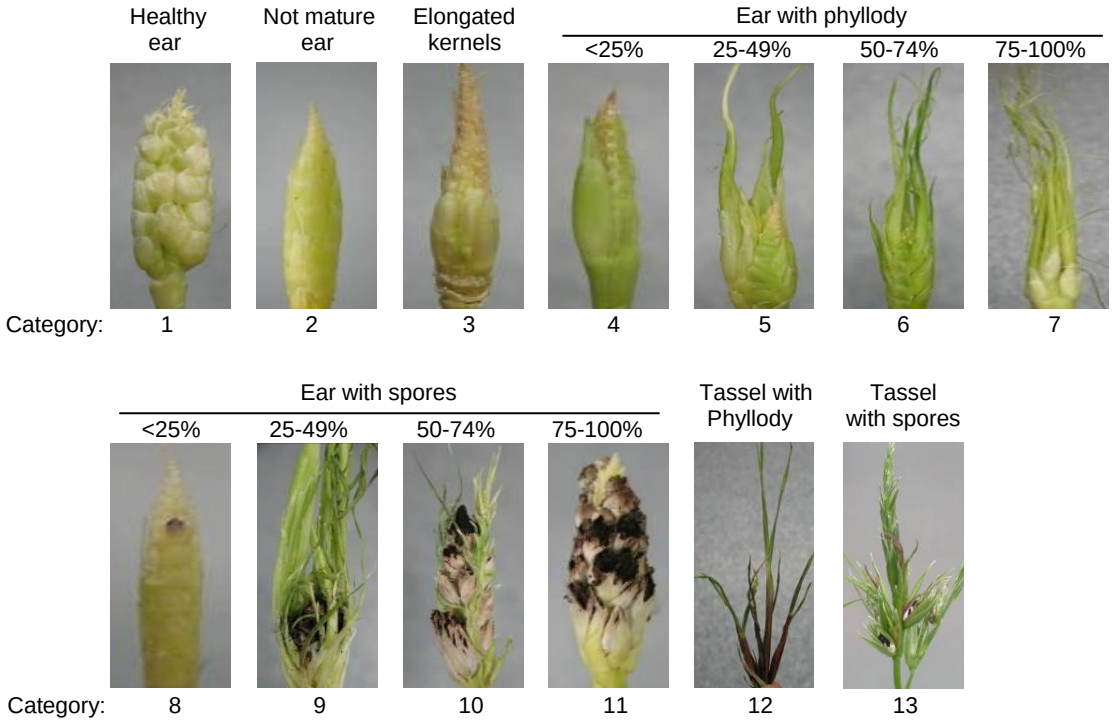

Figure 14. Symptom categories of *S. reilianum*-infected maize inflorescences. Disease symptoms were categorized into 13 categories according to the severity of the symptoms on each inflorescence, from no symptom (1) to the most severe symptom (13).

2.3.2 Establishment of a Locus-Specific Homologous Integration Strategy

For expression of a gene of interest, ideally the gene should be integrated into a specific locus on the genome. Homologous integration of a DNA fragment into a specific locus is established for *U. maydis* (Loubradou et al., 2001), a close relative of *S. reilianum*. To test whether homologous

integration at the *ip* (iron sulfur protein) locus, commonly used in *U. maydis*, could be used in *S. reilianum*, I cloned a silencing construct for *sid1*, a key player in siderophore biosynthesis, into a plasmid for integration into the *ip* locus of *S. reilianum* (p*sid1*-RNAi-cbx). The plasmid was linearized by *Nco*I and then transformed into protoplast of the *S. reilianum* strain JS161. The transformants were selected on carboxin (5 µg/ml) containing media, since the plasmid used for transformation carried a carboxin resistance cassette. Screening 200 carboxin resistant clones (*sid1*-RNAi-*cbx*^{ip}) by PCR, which were generated from 4 independent transformations, showed no integration at the *ip* locus (Figure 15). This shows that the *ip* locus does not seem to be a suitable place for use in a routine homologous integration experiments.

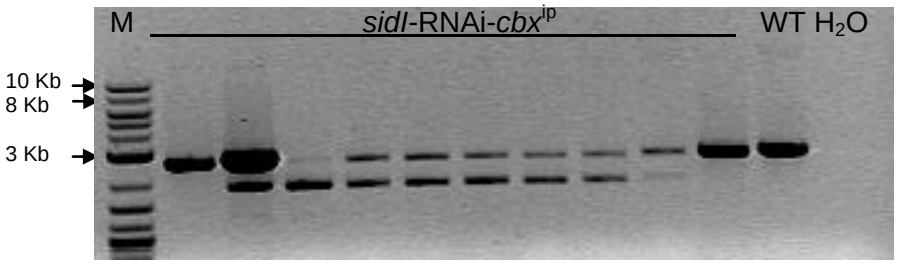

Figure 15. Verification of *sid1* silencing construct integration at the *ip* locus of *S. reilianum*. PCR was performed using the oMW6 and oMW7 primers flanking the *ip* locus. For wt locus and integrated construct at the *ip* locus 2.6 kb and 9.7 kb fragments, respectively, are expected. All candidates showed the wt fragment for the *ip* locus and additional unspecific fragment indicating no integration. M, 2-log DNA ladder (NEB).

To test, whether this is a locus-specific problem, we planed homologous integration of the *sid1* silencing construct into the intergenic region of the *mig1* locus (Figure 16A). The *mig1* locus was chosen because *mig1* in *U. maydis* is known to be highly expressed *in planta* and its deletion in *U. maydis* was very efficient and did not impair virulence. The *mig1* locus in *S. reilianum* contains 10 *mig1*-related genes (Jan Schirawski, personal communication). To construct the integration plasmid, a plasmid containing ~2 kb intergenic region sr14222 and sr14223 was generated and used to clone the *sid1* silencing construct (p*sid1*-RNAi-*mig1*). For integrating the plasmid into the intergenic region of *mig1*, either the circularized plasmid or the plasmid linearized with *Sac*I in the intergenic region (Figure 16B) were transformed into protoplast of the *S. reilianum* strain JS161. The transformants (*sid1*-RNAi-*mig1*^{mig1}) were selected onto carboxin

(5 µg/ml) containing media, since the plasmid used for transformation carried a carboxin resistance cassette. I screened 200 carboxin resistant colonies from resulting transformation with linearized or circularized plasmids using PCR. The results showed that neither the circularized nor the linearized p*sid1*-RNAi-*mig1* plasmids integrated into the *mig1* locus (Figure 16C).

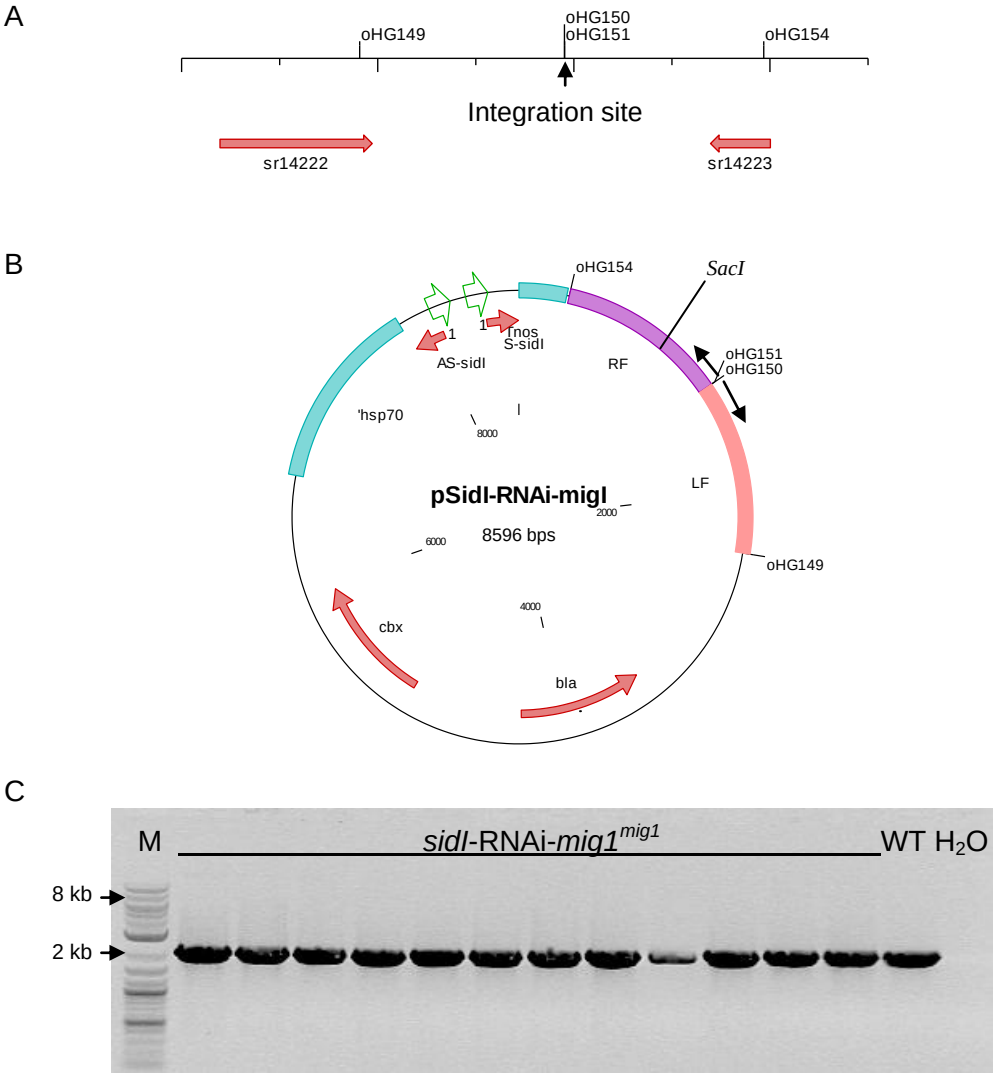

Figure 16. Physical map of *mig1* locus and *mig1* integration plasmid, and verification of integration at *mig1*. (A) Map of *mig1* locus. (B) Integration plasmid at *mig1* locus. (C) Verification of *sid1* silencing construct integration at *mig1* locus. PCR was performed using the oHG153 and oHG154 flanking the *mig1* locus. For wt locus and integrated construct at the *mig1* locus 2 kb and 8.5 kb fragments, respectively, are expected. All candidates showed the wt fragment for the *mig* locus indicating no integration. LF, *mig1* left flank; RF, *mig1* right flank; *Sac*I, the plasmid linearization site; HG150 and HG151, primers used for amplification of the whole plasmid; M, 2-log DNA ladder (NEB).

Additionally, the plasmid was amplified with primers (oHG150 and oHG151) that amplify the whole plasmid so that the intact left and right flanks are produced at the amplicon ends (Figure 16B). None of the carboxin resistant clones (*sid1*-RNAi-*mig1*^{mig1}) tested by PCR showed integration into *mig1* locus (100 clones tested), although all the transformants showed presence of the silencing construct (Figure 17A, B). These results indicate that homologous integration in *S. reilianum* under the studied conditions is not a method of choice.

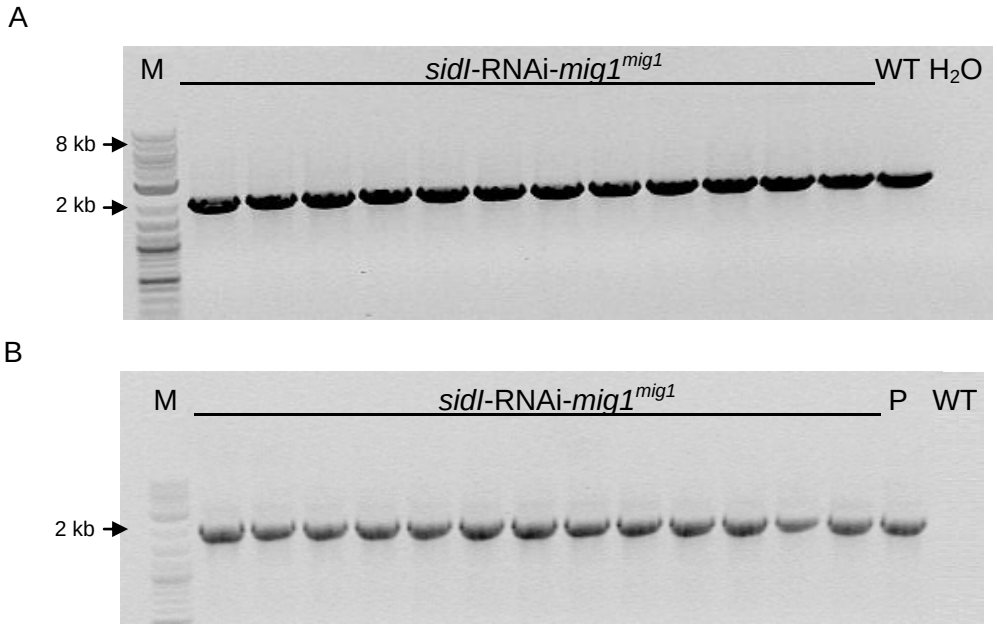

Figure 17. PCR verification of *sid1* silencing plasmid presence in the genome and integration at *mig1*. (A) Verification of *sid1* silencing construct integration at *mig1* locus. PCR was performed using the oHG153 and oHG154 flanking the *mig1* locus. For wt locus and integrated construct at the *mig1* locus 2 kb and 8.5 kb fragments, respectively, are expected. All candidates showed the wt fragment for the *mig1* locus indicating no integration. (B) Testing the presence of the *sid1* silencing construct in the tested transformants in B. PCR was performed using oHG05 and oHG151 primers located at the *mig1* flank and at the plasmid backbone, respectively, producing 1.8 kb fragement. P; positive control WT is a negative control; M, 2-log DNA ladder (NEB).

2.3.3 Establishment of a Locus-Specific-Double Homologous Recombination Strategy

To test whether double homologous recombination (DHR) could be a method of choice for integrating foreign DNA, I planned integration of hygromycin resistance cassette at the *mig1* locus by DHR. Accordingly, a hygromycin resistance cassette was cloned between 1 kb each of

the *mig1* intergenic left and right flanks (*Hyg-mig1*; Figure 18A) and the construct was transformed into *S. reilianum* protoplasts of the wt strains 5-1 and 5-2. The hygromycin resistant clones were tested for integration of the *Hyg-mig1* construct at *mig1* locus by PCR. All tested clones (20 clones from each 5-1 and 5-2) showed integration of the *Hyg-mig1* construct at the *mig1* locus to generate the strains *Hyg*^{mig1} (Figure 18B). The integration of Hyg-*mig1* construct at the *mig1* locus was also confirmed by Southern blot. To ensure that the integration at the intergenic region of *mig1* locus does not affect the pathogenicity, I tested two different compatible mating strains independently for their virulence on maize. No remarkable difference was observed in disease incidence, disease severity and ear number per plant of plants infected with wt and *Hyg*^{mig1} strains (Figure 19). These results indicate that integration at *mig1* by DHR is efficient and does not influence the virulence of *S. reilianum*.

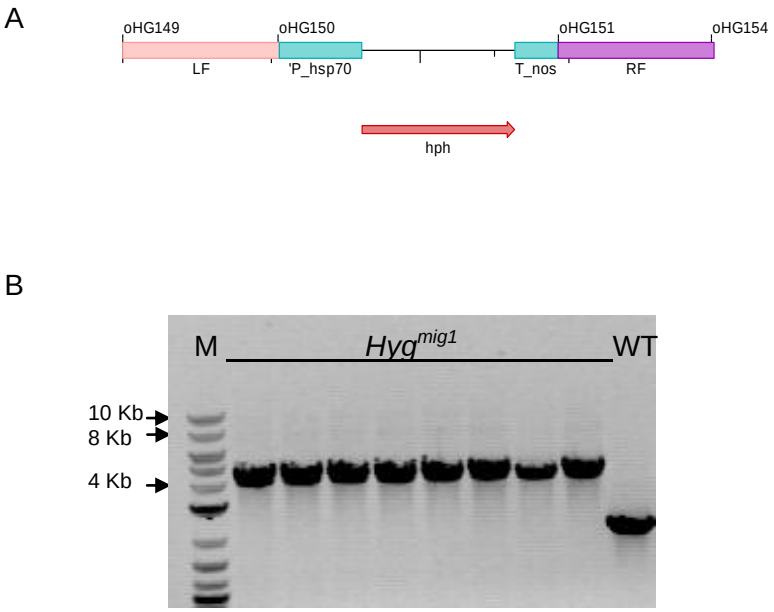

Figure 18. Integration of hygromycin resistance cassette at *mig1* locus by double homologous recombination. (A) Schematic view of the *Hyg-mig1* integration construct. LF, *mig1* left flank; RF, *mig1* right flank; hph, Hygromycin resistance gene. (B) PCR verification of the integration of the *Hyg-mig1* construct at the *mig1* locus. PCR was performed using primers oHG153 and oHG154 flanking the *mig1* locus. A 4.5 kb and 2 kb fragments are expected for successful integration of the *Hyg-mig1* construct and wt *mig1* locus, respectively. All transformants showed integration of the *Hyg-mig1* construct at *mig1* locus. M, 2-log marker (NEB).

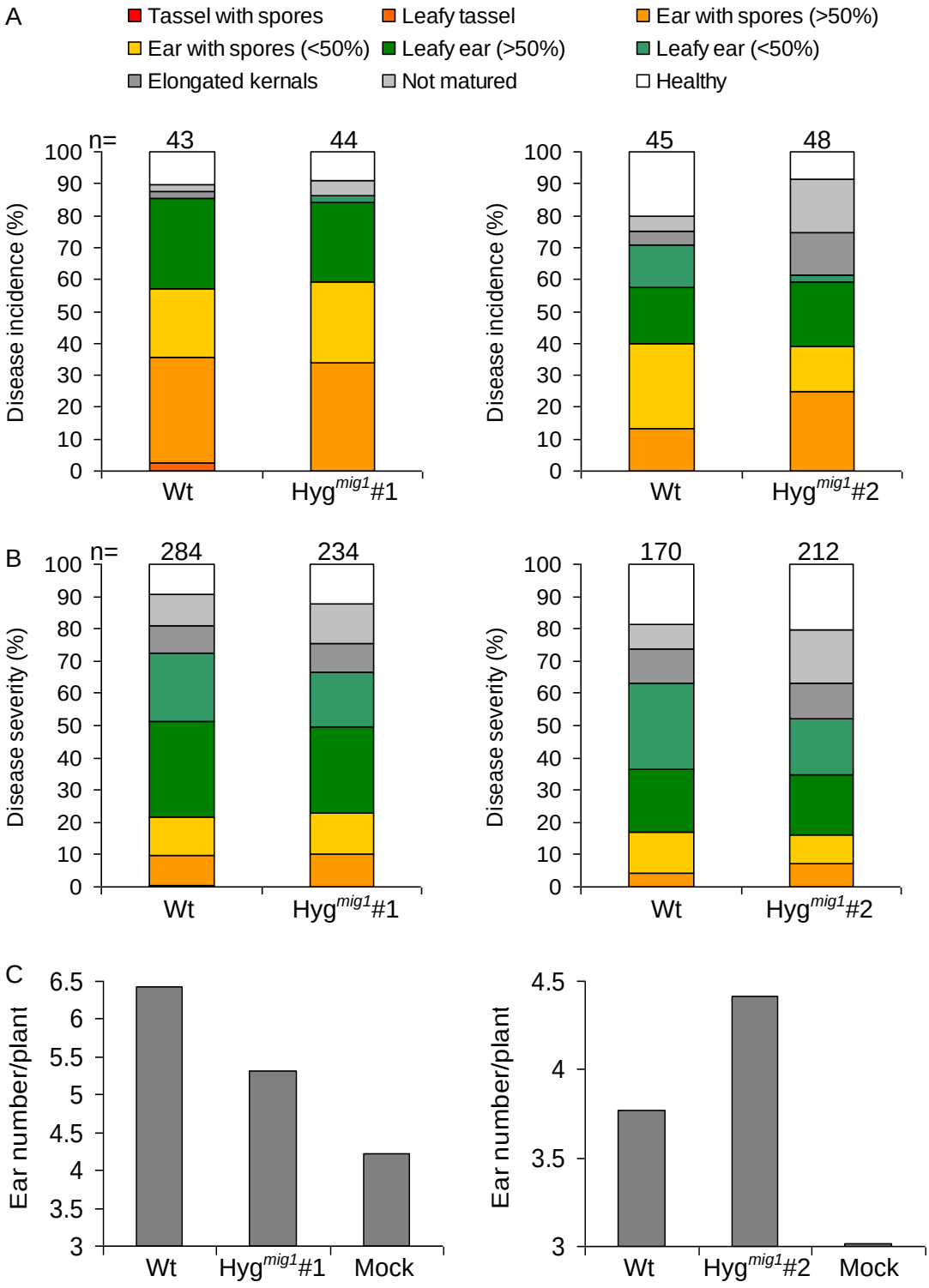

Figure 19. Virulence of *Hyg*^{mig1} and wt *S. reilianum* strains on *Z. mays* 'Gaspe Flint'. (A) Disease incidence, expressed as percent of plants displaying highest symptom (B) Disease severity, expressed as percent of inflorescences in each category from the total number of inflorescences. (C) Ear number per plant. Two independent strains with compatible mating types of the *Hyg*^{mig1} mutants (1, HG137 X

HG140; 2, HG138 X HG141) were used for infection. Wt infections were performed with the strains 5-1 and 5-2. The values are means of two independent experiments.

2.4 Genome Comparison to Identify Virulence Determinants

Genes encoding putative secreted proteins have been reported to be potential pathogenicity determinants, i.e., effectors, for *U. maydis* (Kämper et al., 2006). Genome comparison of *S. reilianum* and *U. maydis* revealed that the potential effectors of both pathogens have low sequence conservation. To identify *S. reilianum*-genes responsible for virulence and symptom development on maize, we compared the genome of *S. reilianum* with those of *U. maydis* and *U. hordei*. We aimed to identify *S. reilianum*-specific genes, or genes with low sequence identity to either *U. maydis* or *U. hordei*. First, genome comparison revealed that *S. reilianum* possesses 111 genes that do not have homologs (<20 % AA identity, E-value= $10e^{-10}$) in either *U. maydis* or *U. hordei* and are thus considered "unique" for *S. reilianum*. To select genes for functional analysis, the following criteria were applied: candidate genes should be predicted to encode secreted proteins with a reliability class = 1 or 2 and should preferably occur in clusters with other unique genes. Among the 111 unique genes 30 genes were predicted to encode secreted proteins. Then we tested whether any of the secreted proteins occurred in the neighborhood of other unique genes, even if they are not secreted, to maximize the number of candidates that can be deleted in patches. Eventually, we selected 22 unique genes for deletion (Table 3). The 22 genes included five gene clusters (unique genes that located next to each other on the genome) and six single genes, which were functionally analyzed (Chapter 2.5).

Table 3. List of *S. reilianum*-unique genes selected for functional analysis.

Entry number	TMHMM[1]	TargetP[2]	Reliability class[3]	Gene/cluster name
sr10703	1	Secretory pathway	1	*sruni1*
sr11815	1	Secretory pathway	1	*sruni2*
sr12538	0	Secretory pathway	1	*sruni3*
sr13154	4	Secretory pathway	1	*sruni4*
sr14797	1	Secretory pathway	1	*sruni5*
sr15769	1	Secretory pathway	1	*sruni6*
sr13374	0	Secretory pathway	1	5_1uni
sr13375	0	Secretory pathway	5	5_1uni
sr13413	0	Unknown	3	5_18
sr13414	0	Unknown	3	5_18

Entry number	TMHMM[1]	TargetP[2]	Reliability class[3]	Gene/cluster name
sr13415	0	Secretory pathway	1	5_18
sr13416	0	Unknown	1	5_18
sr13417	0	Unknown	2	5_18
sr13421	0	Unknown	1	5_18
sr13675	0	Unknown	3	6_1uni
sr13676	0	Secretory pathway	1	6_1uni
sr13677	0	Unknown	2	6_1uni
sr13900	0	Secretory pathway	1	7_11
sr13901	0	Secretory pathway	1	7_11
sr14791	0	Mitochondrion	5	11_1uni
sr14792	0	Unknown	1	11_1uni
sr14793	0	Unknown	2	11_1uni

[1]TMHMM server for prediction of the number of transmembrane domains.

[2]TargetP server for prediction of signal peptide.

[3]Reliabilty class for secretion rated between 1-5, where 1 is the highest probability.

Second, because *S. reilianum* and *U. hordei* systemically colonize maize and barley, respectively, and *U. maydis* locally colonizes maize, we aimed to identify *S. reilianum* genes that could contribute to the systemic colonization of maize. For this purpose, genes with high sequence conservation between *S. reilianum* and *U. hordei* and with low sequence conservation to *U. maydis* were targeted. The parameter AA identity (>20%) for the encoded genes was considered as present for comparing the genomes of the three fungi. Genome comparison resulted in 128 genes that occur in *S. reilianum* and *U. hordei*, but do not occur in *U. maydis*. Among them the genes encoding essential components for RNA interference (RNAi) were found (Figure 20). We decided to verify whether RNAi is functional in *S. reilianum* and whether it has a role in the *S. reilianum*-maize interaction (Chapter 2.6).

Third, because *S. reilianum* and *U. maydis* infect the same host, maize, and cause different symptoms, we aimed to identify *S. reilianum* genes that are responsible for symptom specificity. We hypothesized that the symptom-specific genes could have diversified between *S. reilianum* and *U. maydis* and have low sequence conservation (<57.2% AA identity). Among the genes with low sequence conservation between *S. reilianum* and *U. maydis* many occurred in cluster 19A (Figure 21). Cluster 19A of *S. reilianum* contained 29 genes, from which 24 genes have low sequence conservation with cluster 19A of *U. maydis*. Among cluster 19A genes of *S. reilianum*

24 genes encoding secreted proteins, and 7 and 13 genes absent in *U. maydis* and *U. hordei*, respectively (Figure 21). Accordingly, cluster 19A of *S. reilianum* was selected for functional analysis (Chapter 2.7).

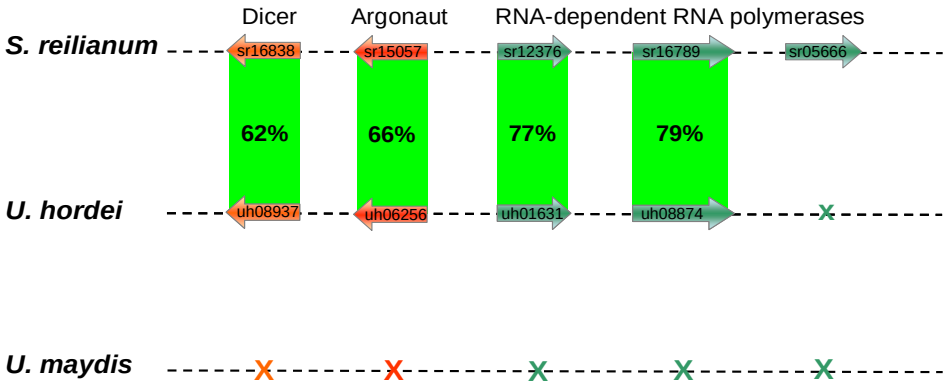

Figure 20. Schematic view of the sequence identity comparison of RNAi gene components between *S. reilianum*, *U. hordei* and *U. maydis*. The aa identity is presented in percent. The RNAi gene components are not clustered on the genomes.

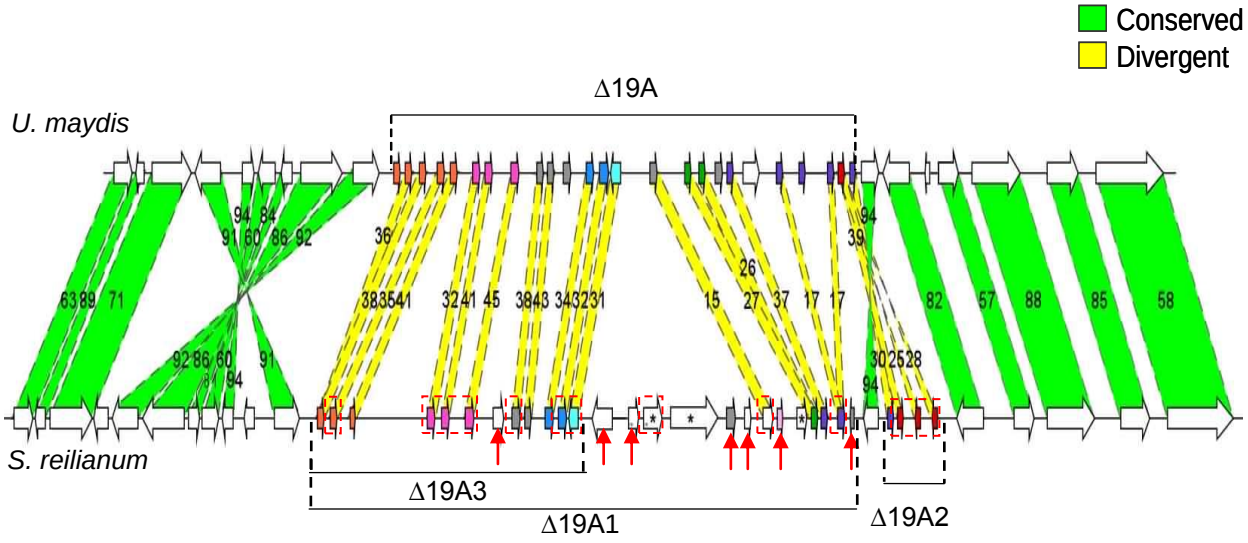

Figure 21. Diagram showing the aa sequence identity comparison of cluster 19A in *S. reilianum* and *U. maydis*. Green color corresponds to AA sequence conservation (>57.2% AA identity), and yellow color corresponds to aa sequence divergence (<57.2% AA identity). Genes boxed with red are absent in *U. hordei*. Genes indicated with red arrow are absent in *U. maydis*. Gene cluster deletions (Δ19A1, Δ19A2 and Δ19A3) are indicated by lines. Modified from picture provided by Jan Schirawski.

2.5 Contribution of *S. reilianum*-Unique Genes to Virulence

We hypothesized that the specific symptoms of *S. reilianum* could be conferred by its unique genome contents and tested this hypothesis. For that purpose, I deleted 22 *S. reilianum*-unique genes, represented by five gene clusters and six single genes (Table 3), in the JS161 strain. The gene or gene cluster deletion was confirmed by PCR and Southern blot. For each gene or gene cluster deletion, three individual mutants were selected (Table 4) to test the virulence on the 'Gaspe Flint' maize cultivar. The experiments were repeated three times for the single unique gene deletion mutants and twice for the unique gene cluster deletion mutants. Notably, deletion mutants of *sruni1* and *sruni2* reproducibly showed 5-7% and 11-13% increase in disease incidence, and 0-3% and 9-14% increase in the disease severity, respectively (Table 4; Figure 22A, B). Deletion mutants of *sruni5* and cluster 5-1uni reproducibly showed 4-14% and up to 12% reduction in disease incidence, and 8-20% and 5-12% reduction in disease severity, respectively (Table 4; Figure 22E, G). Otherwise in average, deletion mutants of *sruni3*, *sruni4*, *sruni6*, 5-18uni, 6-1uni, 7-11uni and 11-1uni did not show reproducible changes in disease incidence or in disease severity (Table 4; Figure 22C, D, F, H-K). In general, none of the unique gene deletion mutants showed significant changes in the ear number per plant in comparison with the strain JS161 (Table 4; Figure 22). These results indicate that the *S. reilianum* unique genes could modulate virulence but did not contribute to the *S. reilianum*-specific symptoms.

Table 4. Virulence of *S. reilianum*-unique-gene deletion strains. The genes were deleted in the strain JS161.

Gene/cluster deletion mutant	Mutant code	Virulence phenotype
Δ*sruni1*#11	HG40	Hypervirulent
Δ*sruni1*#12	HG41	Hypervirulent
Δ*sruni1*#13	HG42	Hypervirulent
Δ*sruni2*#1	HG43	Hypervirulent
Δ*sruni2*#8	HG44	Hypervirulent
Δ*sruni2*#16	HG45	Hypervirulent
Δ*sruni3*#10	HG46	JS161
Δ*sruni3*#12	HG47	JS161
Δ*sruni3*#14	HG48	JS161
Δ*sruni4*#5	HG49	JS161
Δ*sruni4*#10	HG50	JS161

Gene/cluster deletion mutant	Mutant code	Virulence phenotype
Δ*sruni4*#15	HG51	Reduced
Δ*sruni5*#14	HG57	Reduced
Δ*sruni5*#16	HG58	Reduced
Δ*sruni5*#17	HG59	Reduced
Δ*sruni6*#13	HG61	Reduced
Δ*sruni6*#17	HG62	Hypervirulent
Δ*sruni6*#18	HG63	JS161
Δ5-1uni#3	HG21	Reduced
Δ5-1uni#8	HG22	Reduced
Δ5-1uni#13	HG23	Reduced
Δ5-18uni#7	HG65	JS161
Δ5-18uni#10	HG66	JS161
Δ5-18uni#6	HG64	JS161
Δ6-1uni#3	HG28	JS161
Δ6-1uni#4	HG29	Reduced
Δ6-1uni#6	HG30	JS161
Δ7-11uni#7	HG24	JS161
Δ7-11uni#8	HG25	Reduced
Δ7-11uni#10	HG26	JS161
Δ11-1uni#13	HG69	JS161
Δ11-1uni#14	HG70	Hypervirulent
Δ11-1uni#15	HG71	JS161

2.6 The Role of RNAi in *S. reilianum*-Maize Interaction

Genes encoding the RNAi components were conserved in *S. reilianum* and *U. hordei* (Figure 20). Both fungi infect their host plant at the seedling stage, spread systemically through the plant and cause symptoms only in the inflorescence. The absence of the RNAi-components encoding genes from *U. maydis* that causes symptoms locally on leaf, stem or inflorescence, led us to hypothesize that RNAi could play a biological role explaining the difference in the mode of colonization between *S. reilianum*/*U. hordei* and *U. maydis*. Prior to test this hypothesis, we investigated whether RNAi is functional in *S. reilianum* by silencing *gfp* expression. To answer whether RNAi play a role in pathogenicity and in adaptation to stresses, a *dicer* deletion mutant, lacking presumably essential component of the RNAi machinery, was generated in *S. reilianum*, and its phenotype was tested *in planta* and under diverse stress conditions.

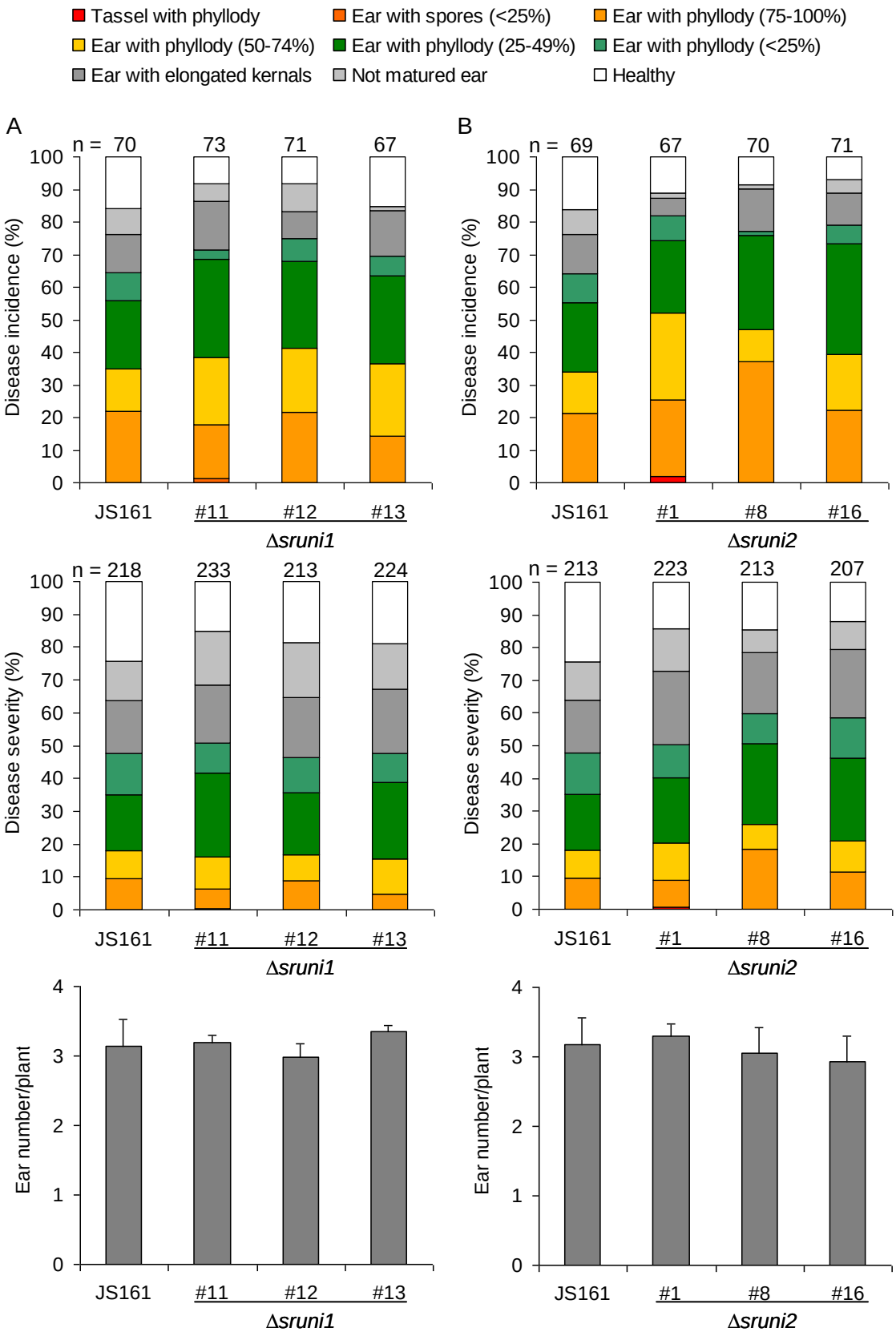
Tassel with phyllody
Ear with spores (<25%)
Ear with phyllody (75-100%)
Ear with phyllody (50-74%)
Ear with phyllody (25-49%)
Ear with phyllody (<25%)
Ear with elongated kernals
Not matured ear
Healthy
A
B
n = 70 73 71 67
n = 69 67 70 71
Disease incidence (%)
JS161 #11 #12 #13
JS161 #1 #8 #16
Δsruni1
Δsruni2
n = 218 233 213 224
n = 213 223 213 207
Disease severity (%)
Ear number/plant

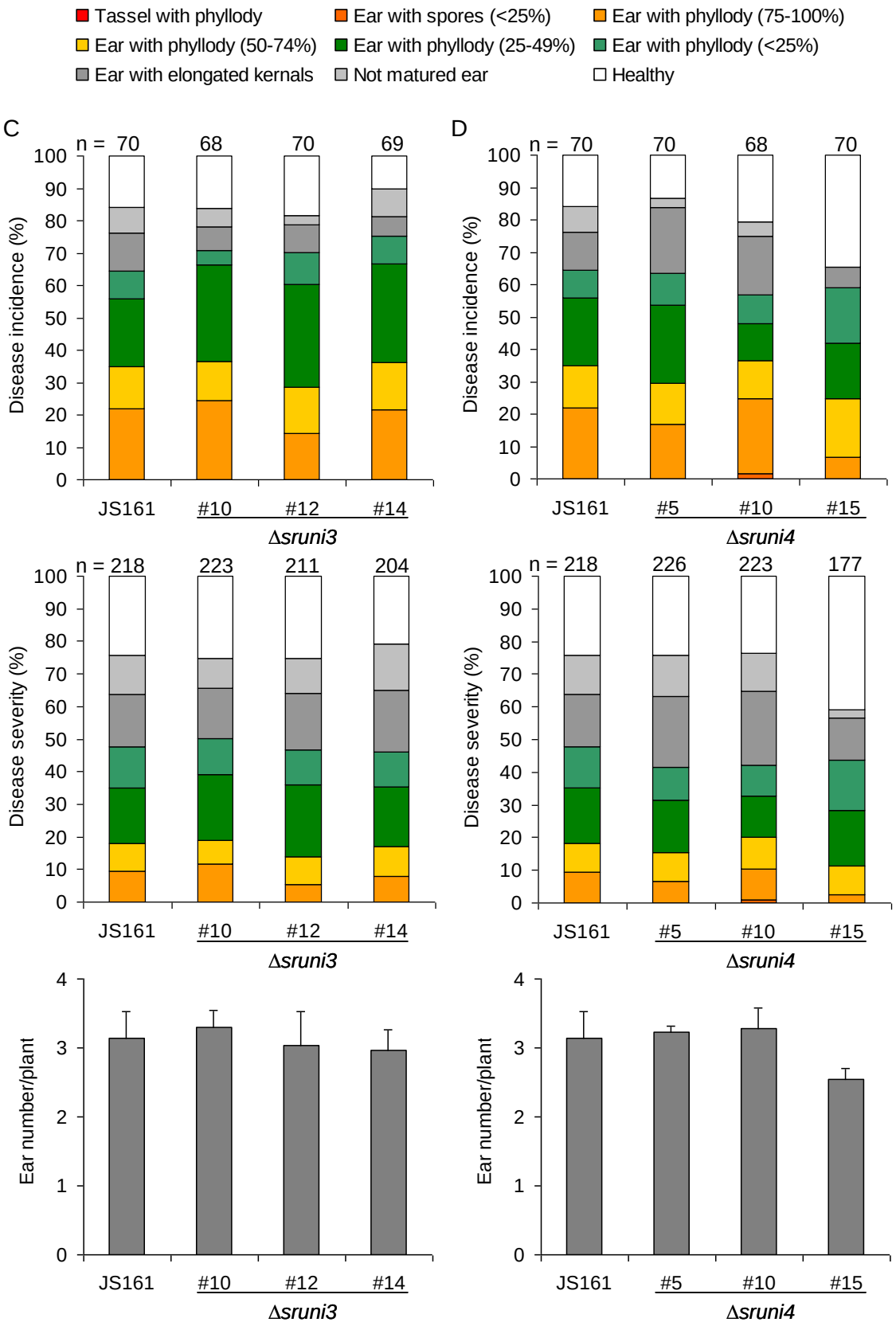
Tassel with phyllody
Ear with spores (<25%)
Ear with phyllody (75-100%)
Ear with phyllody (50-74%)
Ear with phyllody (25-49%)
Ear with phyllody (<25%)
Ear with elongated kernals
Not matured ear
Healthy
C
D
n = 70 68 70 69
n = 70 70 68 70
Disease incidence (%)
JS161 #10 #12 #14
JS161 #5 #10 #15
Δsruni3
Δsruni4
n = 218 223 211 204
n = 218 226 223 177
Disease severity (%)
Ear number/plant

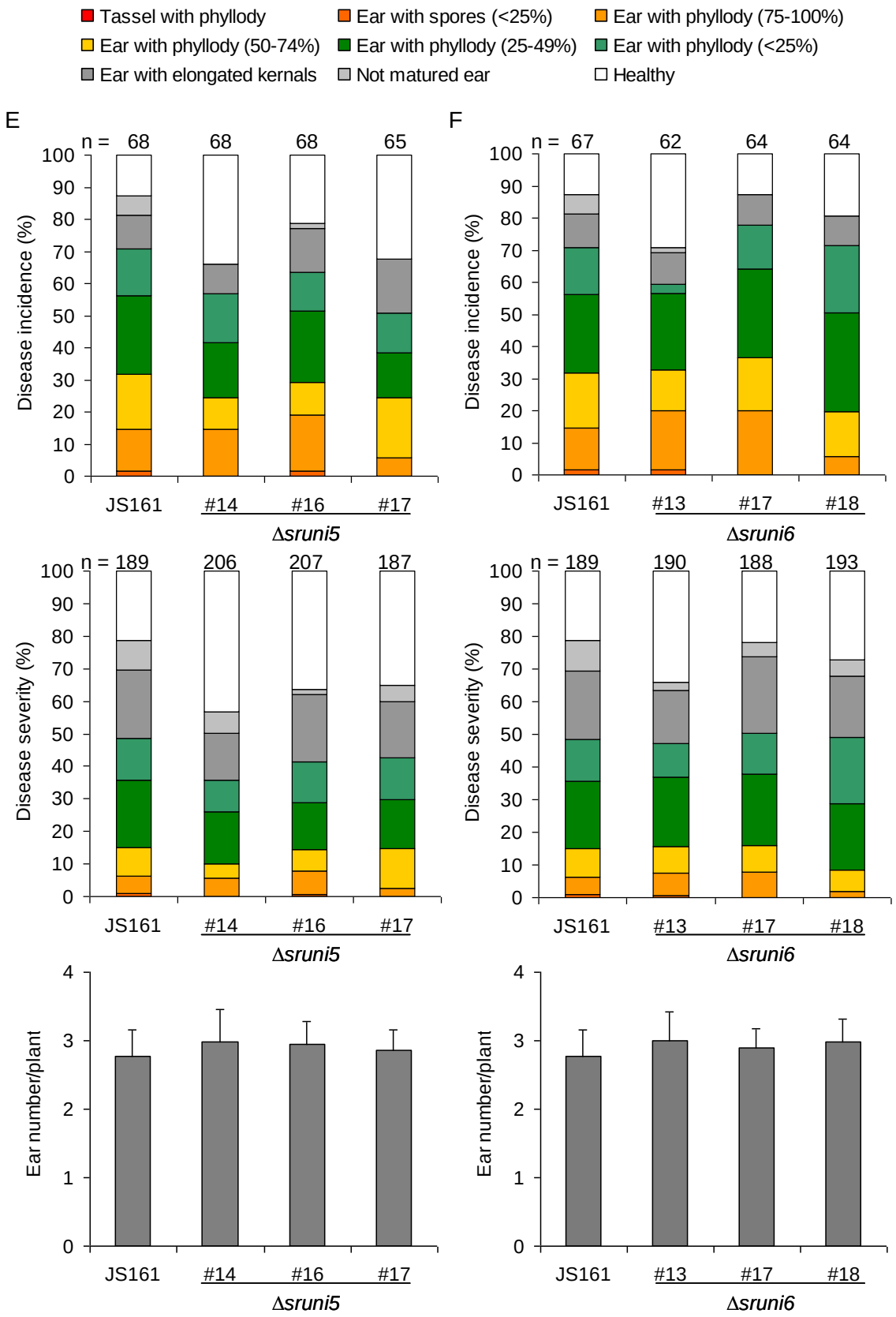
Tassel with phyllody
Ear with spores (<25%)
Ear with phyllody (75-100%)
Ear with phyllody (50-74%)
Ear with phyllody (25-49%)
Ear with phyllody (<25%)
Ear with elongated kernals
Not matured ear
Healthy
E
F
n = 68 68 68 65
n = 67 62 64 64
Disease incidence (%)
JS161 #14 #16 #17
JS161 #13 #17 #18
Δsruni5
Δsruni6
n = 189 206 207 187
n = 189 190 188 193
Disease severity (%)
Ear number/plant

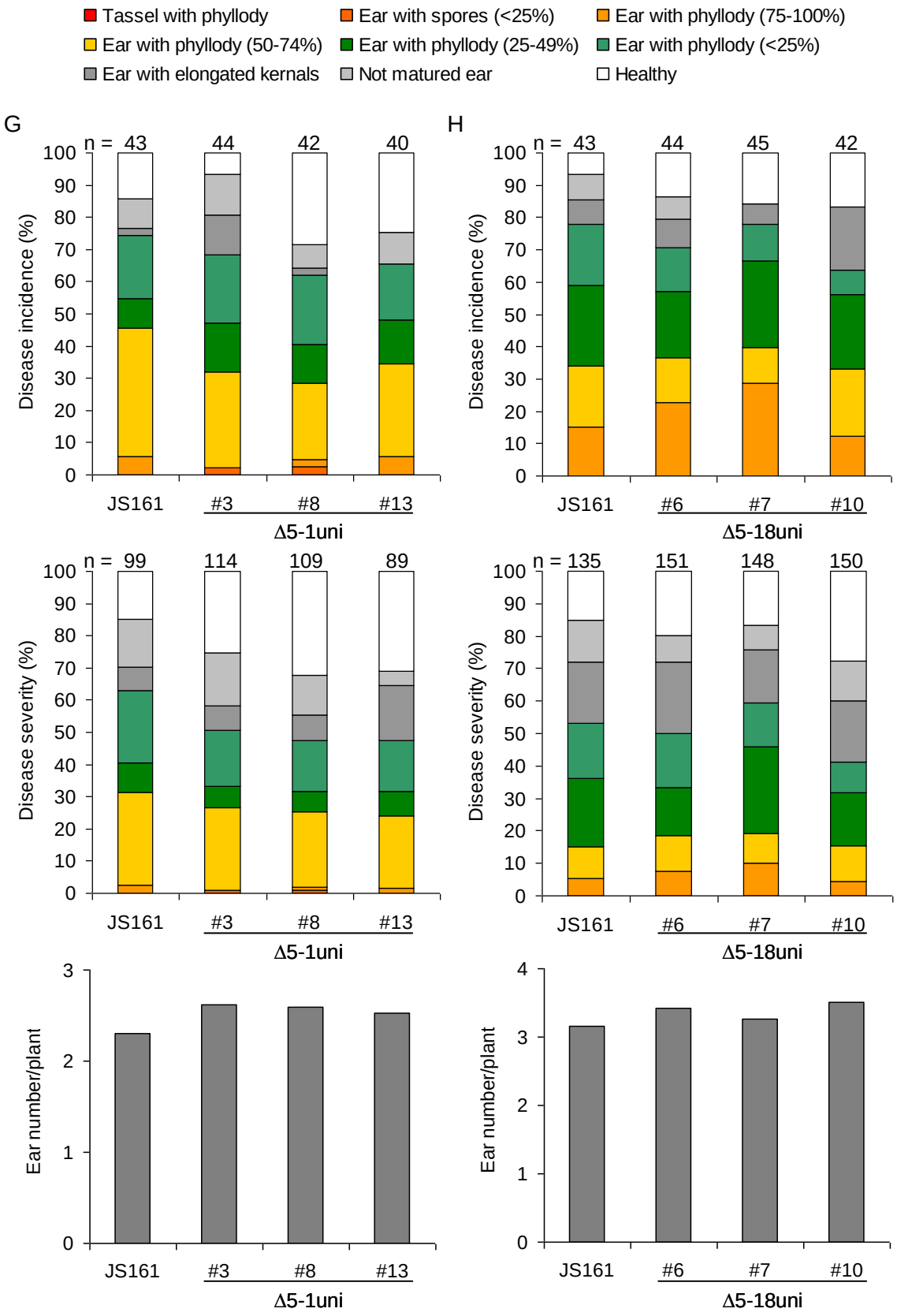
Tassel with phyllody
Ear with spores (<25%)
Ear with phyllody (75-100%)
Ear with phyllody (50-74%)
Ear with phyllody (25-49%)
Ear with phyllody (<25%)
Ear with elongated kernals
Not matured ear
Healthy
G
H
n = 43 44 42 40
n = 43 44 45 42
Disease incidence (%)
JS161 #3 #8 #13
Δ5-1uni
JS161 #6 #7 #10
Δ5-18uni
n = 99 114 109 89
n = 135 151 148 150
Disease severity (%)
Ear number/plant

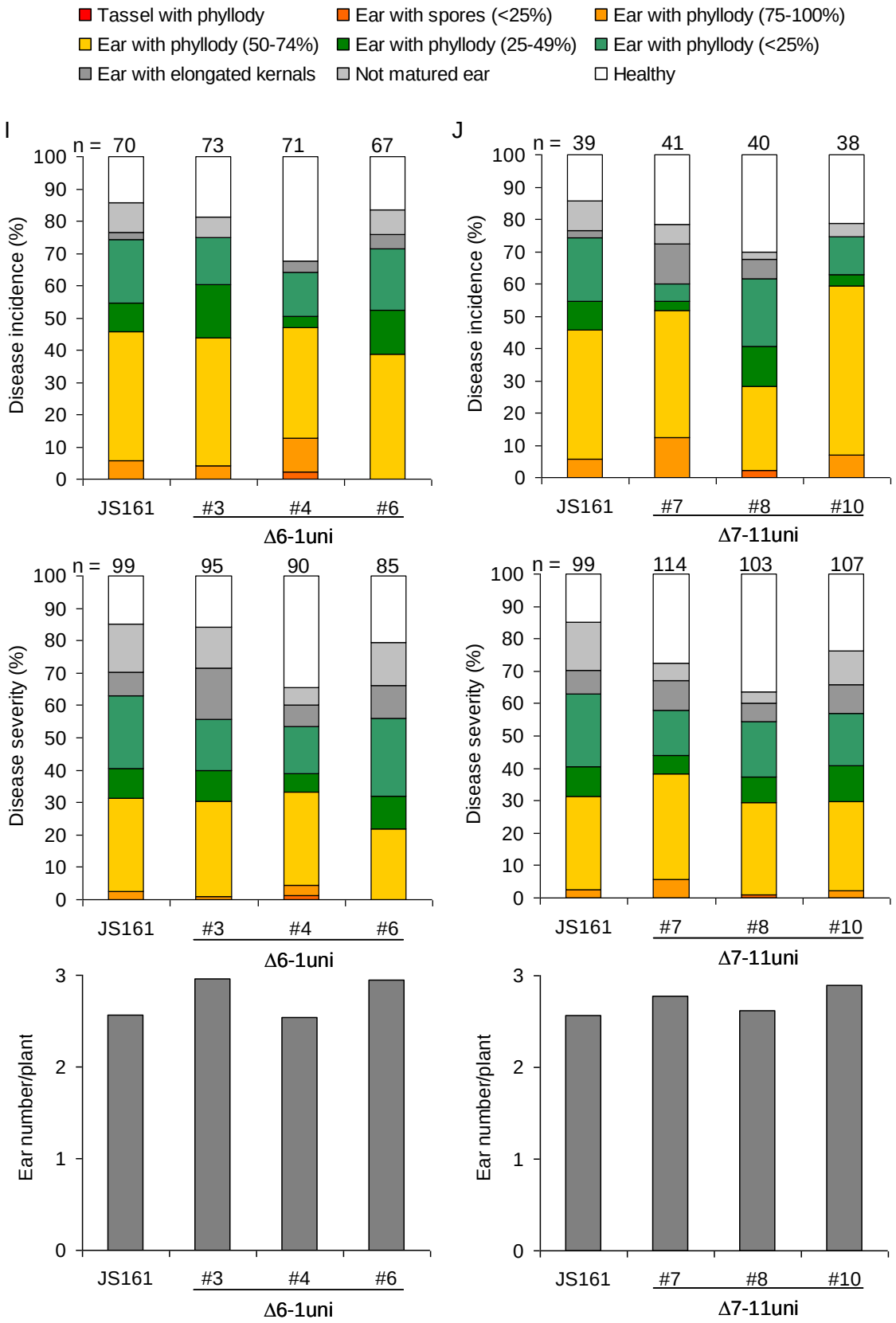
Tassel with phyllody
Ear with spores (<25%)
Ear with phyllody (75-100%)
Ear with phyllody (50-74%)
Ear with phyllody (25-49%)
Ear with phyllody (<25%)
Ear with elongated kernals
Not matured ear
Healthy
I
J
n = 70 73 71 67
n = 39 41 40 38
Disease incidence (%)
n = 99 95 90 85
n = 99 114 103 107
Disease severity (%)
Ear number/plant
JS161
#3
#4
#6
#7
#8
#10
Δ6-1uni
Δ7-11uni

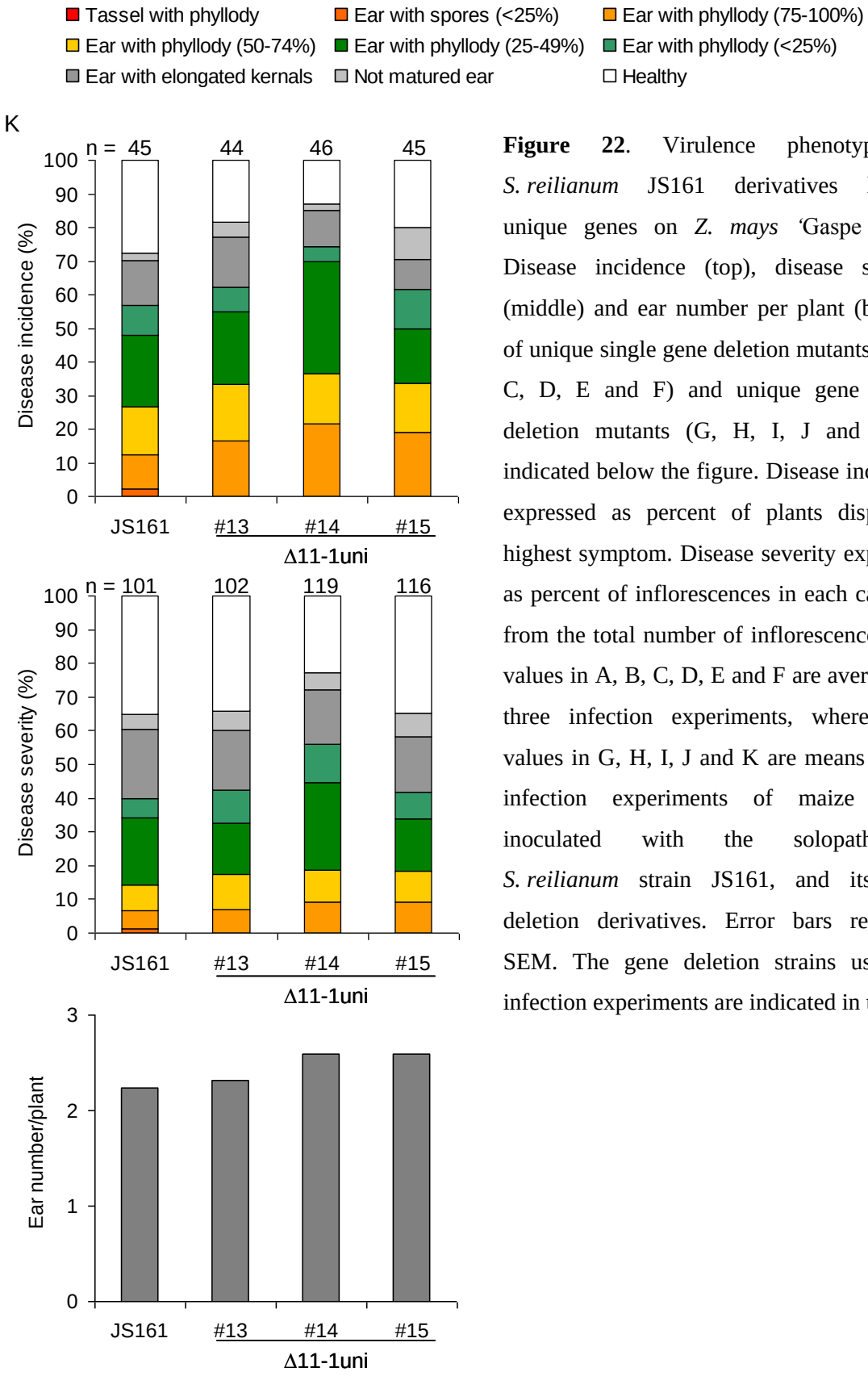

Figure 22. Virulence phenotype of *S. reilianum* JS161 derivatives lacking unique genes on *Z. mays* 'Gaspe Flint'. Disease incidence (top), disease severity (middle) and ear number per plant (bottom) of unique single gene deletion mutants (A, B, C, D, E and F) and unique gene cluster deletion mutants (G, H, I, J and K) as indicated below the figure. Disease incidence expressed as percent of plants displaying highest symptom. Disease severity expressed as percent of inflorescences in each category from the total number of inflorescences. The values in A, B, C, D, E and F are averages of three infection experiments, whereas the values in G, H, I, J and K are means of two infection experiments of maize plants inoculated with the solopathogenic *S. reilianum* strain JS161, and its gene deletion derivatives. Error bars represent SEM. The gene deletion strains used for infection experiments are indicated in table 4.

2.6.1 Proof of RNAi Functionality in *S. reilianum*

To investigate whether the RNAi machinery is functional in *S. reilianum*, two approaches for silencing *gfp* expression in a *S. reilianum* strain expressing cytoplasmic *gfp* were used. In the first approach, an artifical miRNA (amiRNA) was constructed by replacing 21 nt of the mature miRNA319a from *Arabidopsis thaliana* by 21 nt (GCCGTCCGCCCTGTGCAAAGT) that target the *gfp* mRNA sequence (nt position 615 – 631). In the second approach, an inverted repeat (IR) of 351 bp from *gfp* sequence (nt position 139 – 490) was constructed in sense and antisense directions and spaced by an intron of the *bW1* gene of *S. reilianum* to generate the IR construct. The modified amiRNA and IR constructs were cloned into the plasmid p123 to generate the p*gfp*-amiRNA and p*gfp*-RNAi, respectively. The p*gfp*-amiRNA and p*gfp*-RNAi plasmids were linearized with *NruI* and then was used to transform protoplast of *S. reilianum* 5-2 strain. The carboxin-resistant colonies were verified to have the silencing constructs by PCR and Southern blot (Data not shown). The amiRNA expressing strains reproducibly showed 6-9% reduction of GFP fluorescence in comparison to wt expressing *gfp* (Figure 23A). The IR expressing strains showed 42-47% reduction in GFP fluorescence and 49-61% reduction on *gfp* transcript level in comparison to wt expressing *gfp* (Figure 23A, B). The reduction in *gfp* expression in the IR approach shows that RNAi is functional in *S. reilianum*.

2.6.2 Characterization of *dicer* Deletion Mutant

To analyze the contribution of the RNAi machinery to virulence of *S. reilianum*, the *dicer* gene (sr16838) was deleted, and the deletion strains were verified by PCR and Southern blot. The *dicer* deletion strains were used to inoculate ‘Gaspe Flint’ maize plants and the virulence of the strains was evaluated. The *dicer* deletion mutants did not show reproducible changes in disease incidence, disease severity or ear number per plant (Figure 24A). Consistently, RT-PCR showed that *dicer* gene was expressed in cell growing liquid culture of the JS161 strain, whereas *in planta*; in infected leaves at 3 dpi and in infected ears at 4 wpi, no expression could be detected (Figure 24B).

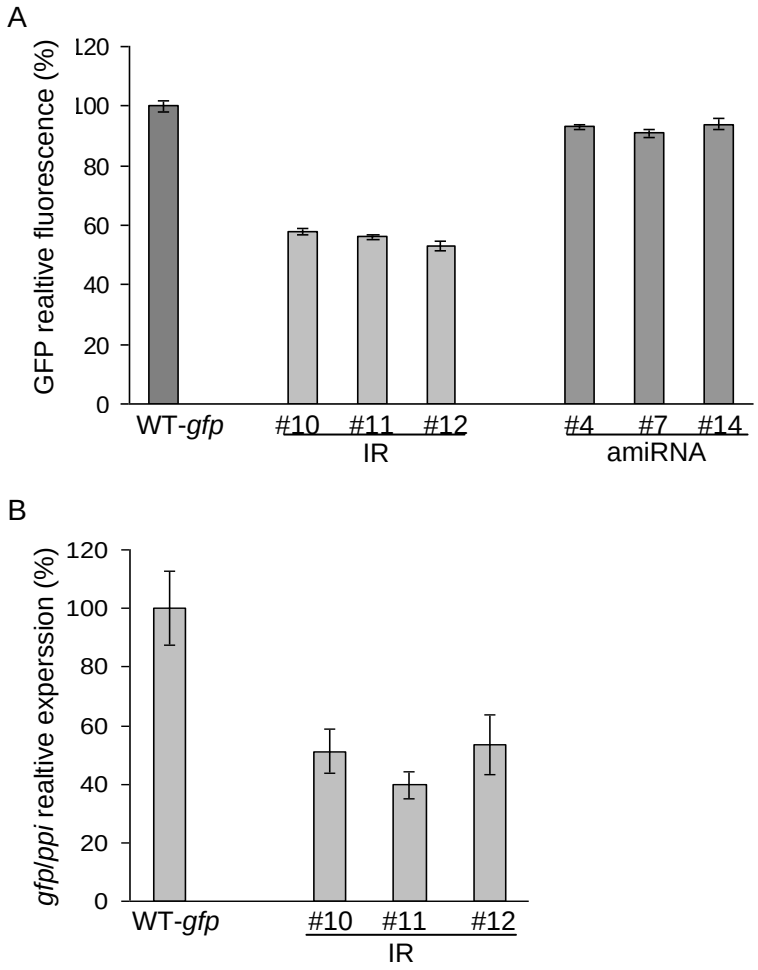

Figure 23. Verification of RNAi functionality in *S. reilianum* by GFP silencing. (A) Fluorescence measurements of GFP in *S. reilianum* strains expressing *gfp* inverted repeats (IR) or *gfp* artificial miRNA (amiRNA) relative to 5-1 strain expressing *gfp* (WT-*gfp*). (B) qPCR quantification of *gfp* transcript level (normalized to *ppi*) in IR expressing strains relative to wt. Error bars = SEM of three independent experiments.

To test whether *dicer* has a role in response to stresses, serial dilutions (0, 10^{-1}, 10^{-2}, 10^{-3}) of the *dicer* deletion strains were grown in comparison to wt under different UV (20 J and 80 J), temperature (30°C and 35°C), cell wall stress (150 µM calcofluor), oxidative stress (1.5 mM H_2O_2 and 100 µM Menadione), nutritional stress (AM and NM media) and osmotic stress (1 M NaCl and 1 M sorbitol) conditions. The *dicer* deletion mutant strains did not show differences in comparison to wt in response to any of the tested stresses (Figure 25).

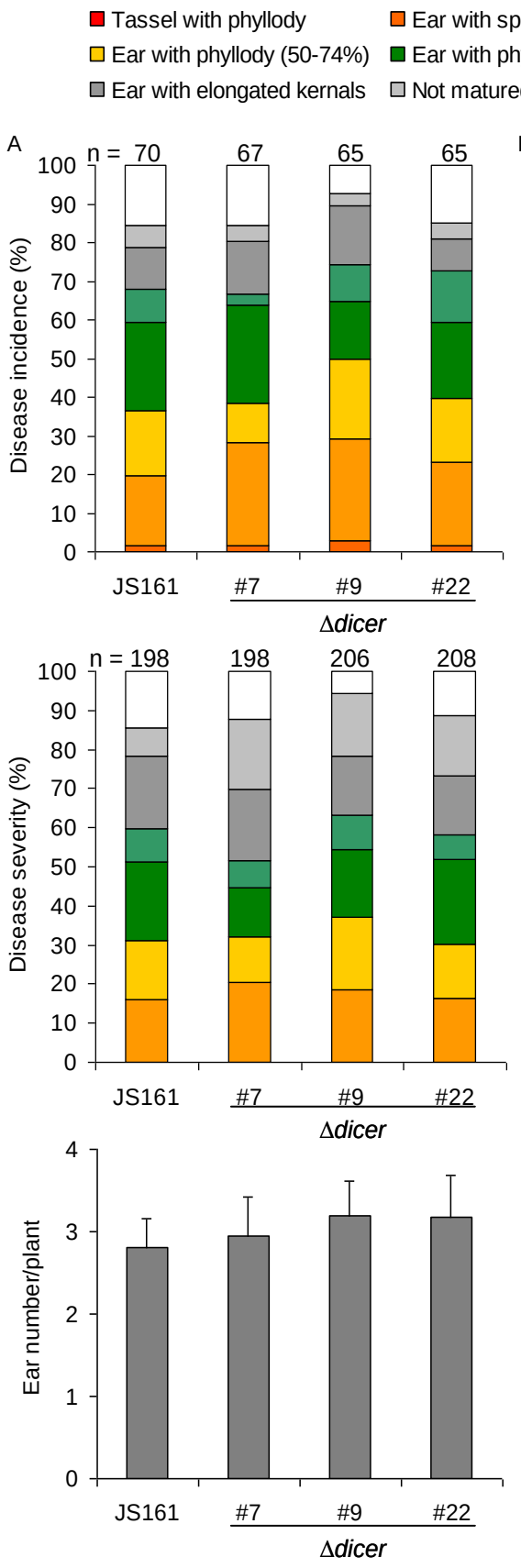

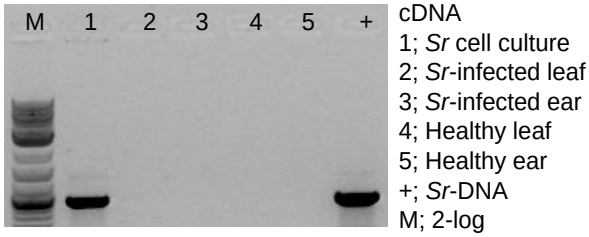

Figure 24. Virulence of *S. reilianum dicer* deletion mutants on *Z. mays* "Gaspe Flint". (A) Disease incidence (top), disease severity (middle) and ear number per plant (bottom) of *dicer* gene deletion mutants in comparison to JS161, a solopathogenic strain. Disease incidence expressed as percent of plants displaying highest symptom. Disease severity expressed as percent of inflorescences in each category from the total number of inflorescences. Three independent *dicer* deletion mutants (1, HG52; 2, HG53; 3, HG54) were used for infections. The values are means of three independent experiments. Error bars represent SEM. (B) RT-PCR showing *dicer* expression in liquid culture of JS161 and in plant material infeceted with wt of *S. reilianum* strains. *Sr*, *S. reilianum*; 2, 3rd leaf 3 days post inoculation; 3, leafy ear (stage of elongated kernel) 4 weeks post inoculation. The expression of *dicer* is detected only in liquid culture.

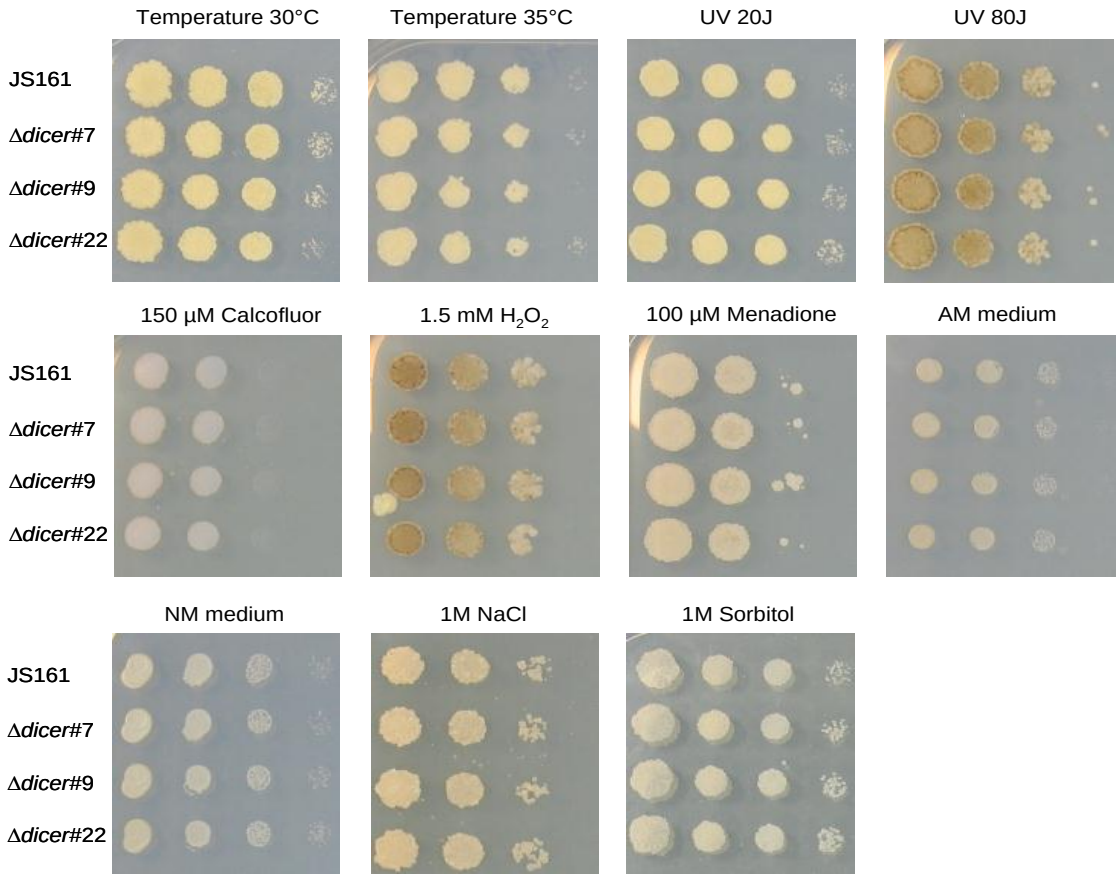

Figure 25. Response of *dicer* deletion mutants to various stresses. Serial dilutions (0, 10^{-1}, 10^{-2}, 10^{-3}) of the *dicer* deletion mutants and JS161 strains on CM medium with glucose containing the stress agent, or on AM and NM media. Stresses tested: temperature (30°C and 35°C), UV (20J and 80J), cell wall stress (150 µM calcofluor), oxidative stress (1.5 mM H_2O_2 and 100 µM Menadione) nutritional stress (AM and NM media) and osmotic stress (1 M NaCl and 1 M sorbitol).

2.7 The Role of Cluster 19A in the *S. reilianum*-Maize Interaction

2.7.1 Contribution of Cluster 19A to Pathogenicity

Cluster 19A of *S. reilianum* contains genes with a low sequence identity to those of cluster 19A of *U. maydis*. To study the role of cluster 19A of *S. reilianum* in interaction with maize, the cluster was deleted into two parts, Δ19A1 (generated by Jan schirawski) and Δ19A2, in the wild type strains 5-1 and 5-2. Deleting the cluster in two parts left the β-tubulin gene intact (Figure 21). The 19A1 deletion mutants were used to generate Δ19A1Δ19A2 double deletion mutants. The deletion of the different parts of cluster 19A was verified by PCR and Southern blot (Data not shown). Uncommonly, attempts to delete cluster 19A2 yielded 0.002% right pattern in

Southern blot. Virulence of the deletion strains was tested on 'Gaspe Flint' maize plants. Deletion of cluster 19A1A2, 19A1 and 19A2 led to 22-35%, up to 13% and 20-27% reduction in disease incidence, and 31-32%, 6% and 18-25% reduction in disease severity, respectively, in comparison to wt (Figure 26). Overall the reduced virulence of Δ19A1A2 mutants could be attributed to both parts of the cluster, 19A1 and 19A2. Notably, Δ19A1 mutants showed 27-40% and 13-25% reduced spore formation incidence and severity, respectively, in comparison to wt (Figure 26). Cluster 19A2 deletion mutants showed an overall reduction in all disease categories. Interestingly, Δ19A2 mutant did not show significant increase in ear number per plant (p-value = 0.001) in comparison to wt (Figure 26). To verify the contribution of cluster 19A2 to virulence, cluster 19A2 was deleted in the solopathogenic strain JS161, which is less virulent than the wt stains 5-1 and 5-2. Deletion of cluster 19A2 in JS161 showed 14-21% and 19-28% reduced disease incidence and severity, respectively, and did not significantly increase ear number per plant (p-value = 0.001) in comparison to the JS161 strain (Figure 27) indicating that suppression of apical dominance is conferred by a gene situated in 19A2.

To determine the target gene(s) responsible for reduced spore formation in cluster 19A1, a subdeletion of cluster 19A1 was generated resulting in cluster 19A3 deletion mutant (generated by Jan Schirawski) (Figure 21). Cluster 19A3 contains 12 genes, and their deletion was verified by PCR and Southern blot (Data not shown). The phenotype of Δ19A3 mutants on maize was tested. The Δ19A3 mutants showed 13-31% and 3-7% reduced spore formation incidence and severity, respectively (Figure 28A) indicating that the reduced spore formation of Δ19A1 mutants is at least partially conferred by 19A3.

The main effectors of *U. maydis* cluster 19A, *tin1* and *tin2* genes (*tumor inducing gene 1* and *2*) were shown to occur in the syntenic part of 19A3 of *S. reilianum* (Thomas Brefort, unpublished). To test whether sr10057 and sr10060, *tin1* and *tin2* orthologues in *S. reilianum*, are responsible for the reduced spore formation rate of the 19A3 deletion strains, the two genes were individually re-introduced at the *mig1* locus of Δ19A1A2 mutants. The mutants were verified by PCR and Southern blot. All the resulting strains showed integration of multiple copies of the integration construct. Unexpectedly, re-introduction of sr10057 or sr10060 led to further reduced spore formation rates than that of Δ19A1A2 mutants (Figure 28B). These results indicate that reduced spore formation phenotype of the 19A3 deletion strains is not caused the lack of sr10057 and sr10060.

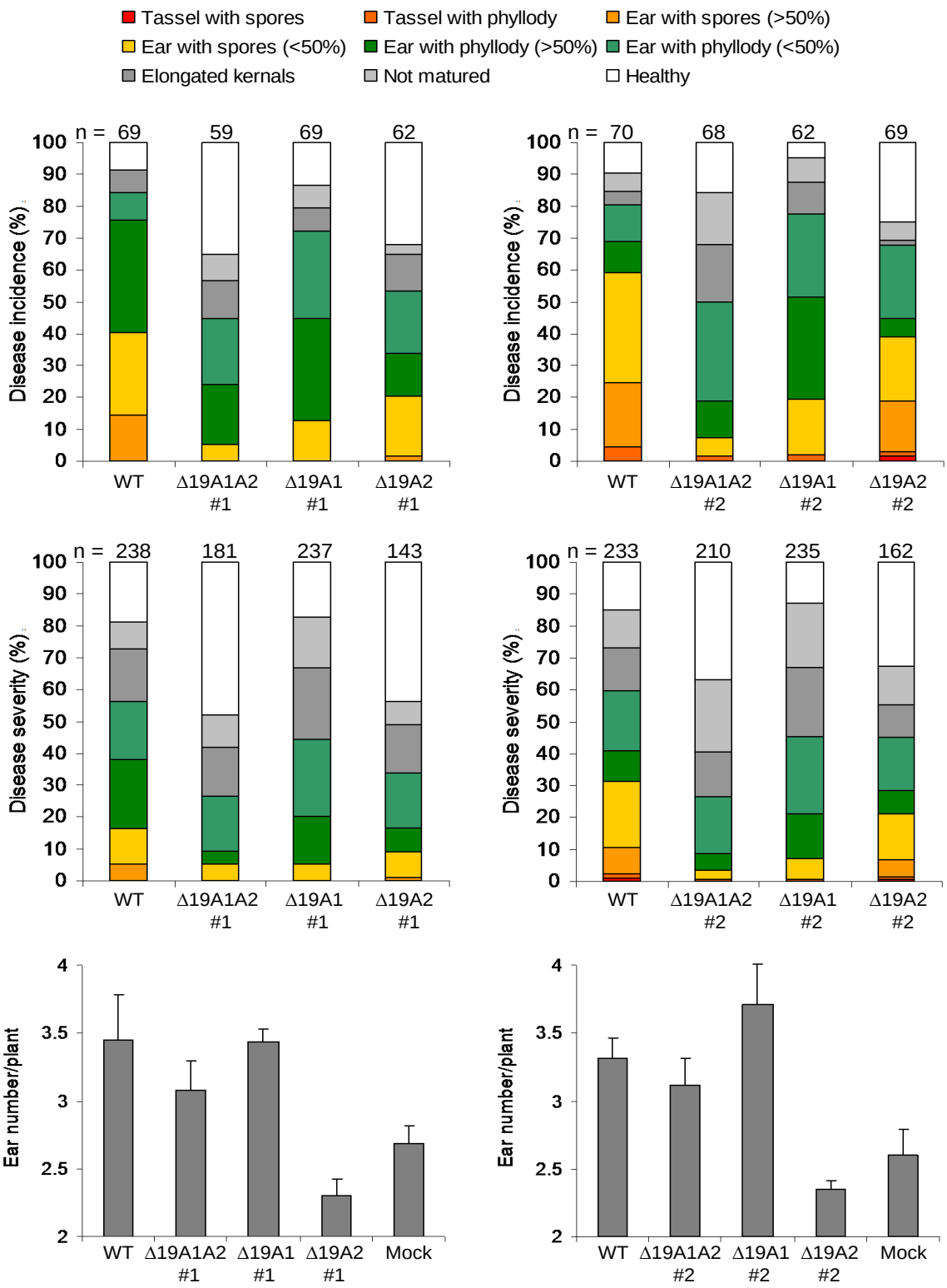

Figure 26. Virulence of *S. reilianum* cluster 19A deletion mutants on *Z. mays* 'Gaspe Flint'. Disease incidence (top), disease severity (middle) and ear number per plant (bottom) of 19A1A2, 19A1 and 19A2 gene cluster deletion mutants. Disease incidence expressed as percent of plants displaying highest

symptom. Disease severity expressed as percent of inflorescences in each category from the total number of inflorescences. Two independent compatible mating types of the Δ19A1A2 mutants (1, HG9 X HG19; 2, HG9 X HG20), Δ19A1 mutants (1, JS747 X JS751; 2, JS748 X JS752) and Δ19A2 mutants (1, HG125 X HG127; 2, HG126 X HG128) were used for infections. The values are means of three independent experiments. Error bars represent SEM.

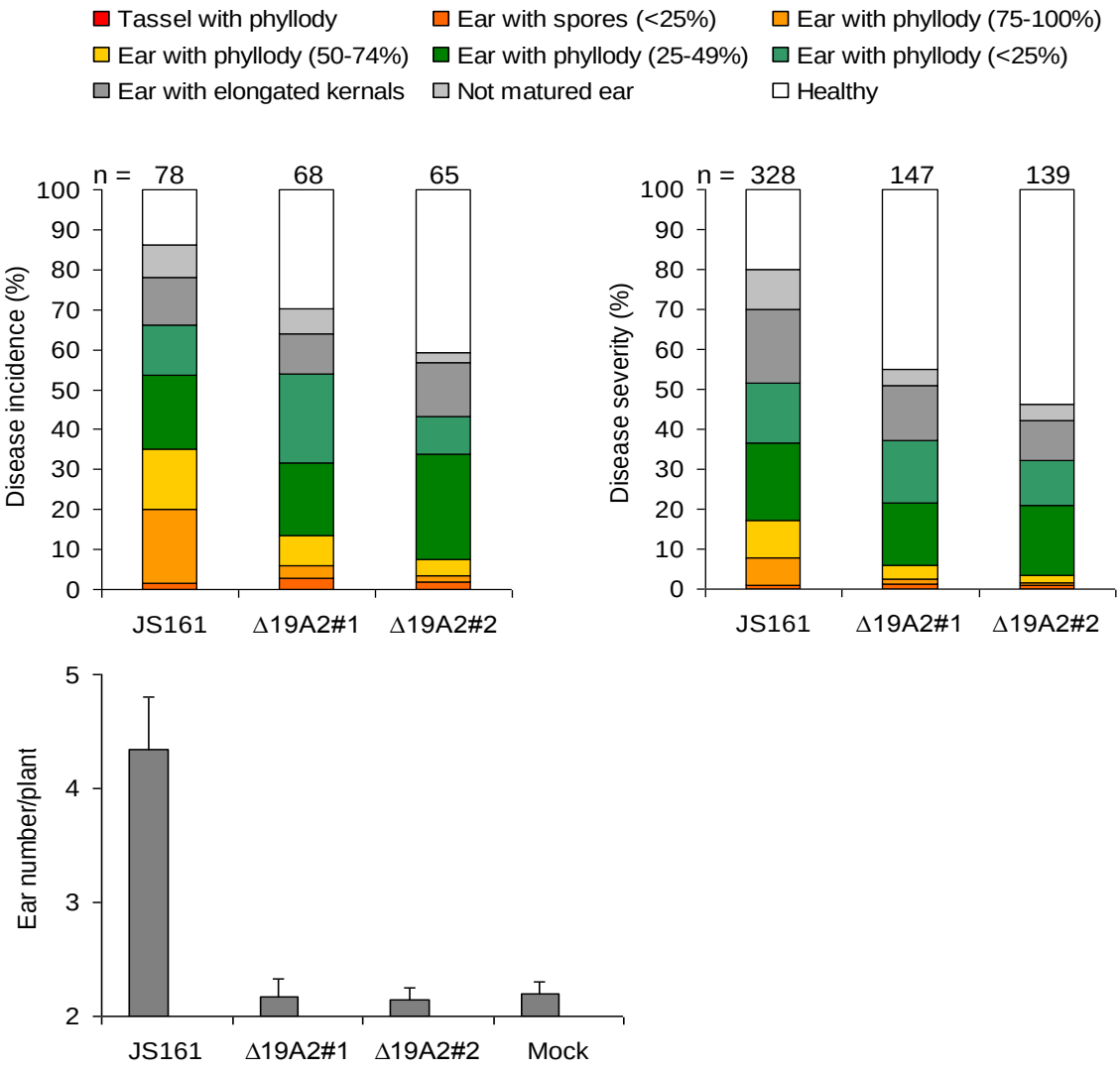

Figure 27. Virulence of the solopathogenic *S. reilianum* cluster 19A2 deletion mutants on *Z. mays* 'Gaspe Flint'. Disease incidence (top left), disease severity (top right) and ear number per plant (bottom) of Δ19A2 mutants in comparison to JS161, a solopathogenic strain. Disease incidence expressed as percent of plants displaying highest symptom. Disease severity expressed as percent of inflorescences in each category from the total number of inflorescences. Two independent Δ19A2 mutants (1, HG67; 2, HG68) were used for infections. The values are means of three independent experiments. Error bars represent SEM.

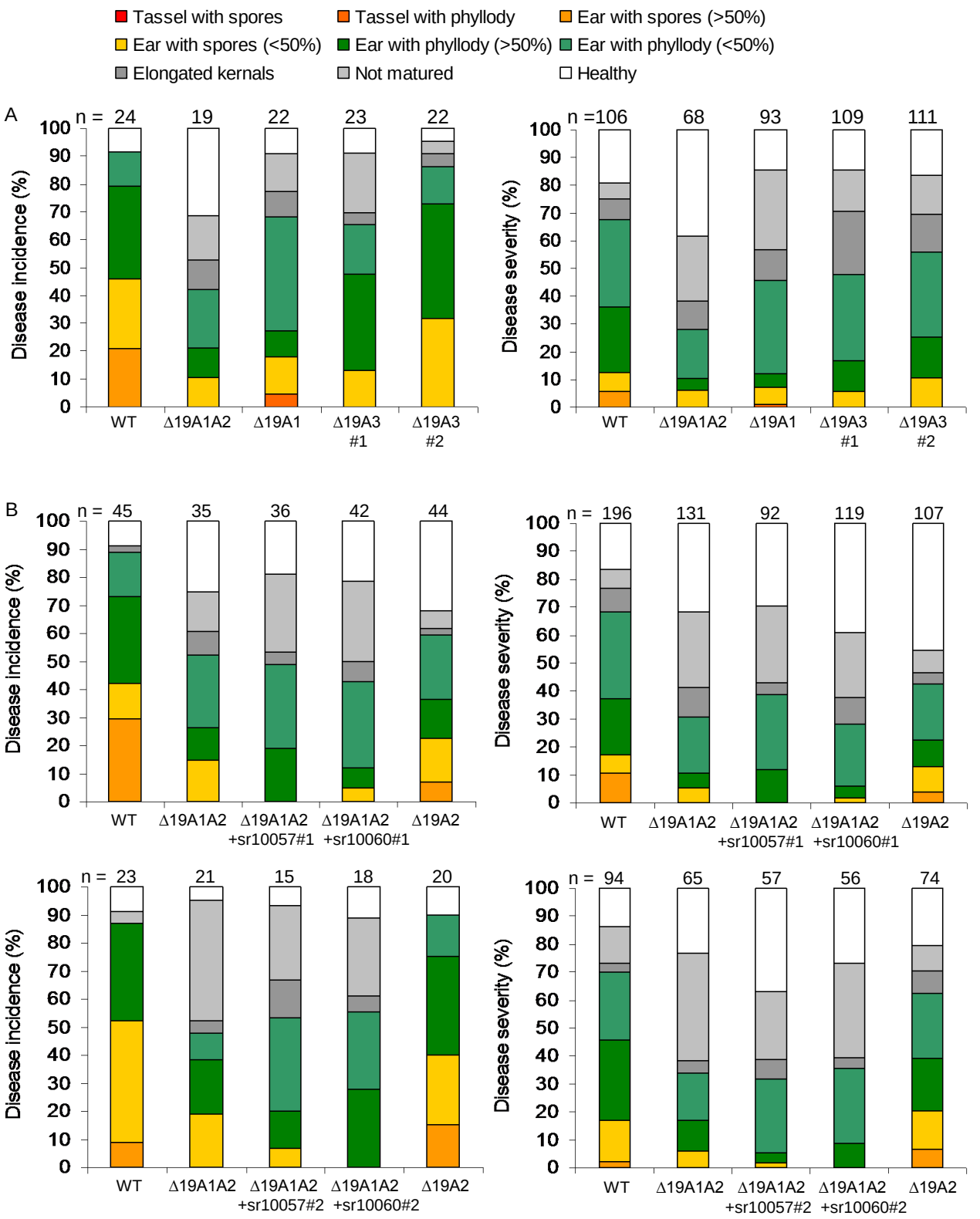

Figure 28. Pathogenicity of *S. reilianum* cluster 19A3 deletion and sr10057 and sr10060 complementation strains on *Z. mays* 'Gaspe Flint'. (A) Disease incidence (left) and disease severity (right) of Δ19A3 mutants. (B) Disease incidence (left) and disease severity (right) of sr10057 and sr10060

complementation strains in the Δ19A1A2 background strains. Disease incidence expressed as percent of plants displaying highest symptom. Disease severity expressed as percent of inflorescences in each category from the total number of inflorescences. Two independent compatible mating types of the Δ19A1A2 mutants (HG9 X HG20), Δ19A1 mutants (JS747 X JS751), Δ19A2 mutants (HG125 X HG127), Δ19A3 mutants (1, JS895 X JS900; 2, JS896 X JS901), Δ19A1A2+sr10057 (1,HG143 X HG147; 2,HG144 X HG148) and Δ19A1A2+sr10060 (1,HG150 X HG153; 2,HG151 X HG154) were used for infections. All Δ19A1A2+sr10057 and Δ19A1A2+sr10060 strains used contained multiple copies of the introduced gene. The values represent one and means of two infection experiments in A and B, respectively.

2.7.2 Influence of Cluster 19A Deletion on Proliferation Ability of *S. reilianum* in the Leaf

Inoculation of leaves with *S. reilianum* sometimes causes chlorosis at 7 dpi around the injection hole that might turn to necrosis after approximately 13 dpi (Figure 29A). Interestingly, Δ19A1A2 and Δ19A1 mutants showed chlorosis around the injection hole at 4-6 dpi that later converted to necrotic regions and led to death of the leaf tip (Figure 29A). Leaf tip death seemed to be a result of leaf tip wilting rather than extension of the necrosis from the injection hole to the tip. To quantify the contribution of cluster 19A regions to the leaf tip death phenotype, the symptoms on the 3rd leaf inoculated with Δ19A1A2, Δ19A1 and Δ19A2 mutants were quantified at 15 dpi. The Δ19A1A2 and Δ19A1 mutants showed 4.6 and 2-5 fold increase of leaf tip death incidence, respectively (Figure 29B). Δ19A2 mutants did not show differences in the rate of leaf tip death in comparison to wt (Figure 29B) indicating that the phenotype is conferred by the lack of the 19A1 genes.

To narrow down the target gene(s) of cluster 19A1 that cause leaf tip death when deleted, the phenotype of Δ19A3 mutants, and Δ19A1A2 mutants expressing sr10057 or sr10060 on the inoculated leaves was investigated at 15 dpi. The incidence of leaf tip death revealed that the phenotype is caused by deletion of cluster 19A3 genes (Figure 29C). However, reintroduction of sr10057 and sr10060 in Δ19A1A2 mutants did not change the incidence of leaf tip death in comparison to Δ19A1A2 mutants (Figure 29C). These results indicate that leaf tip death is conferred by lack of gene(s) residing in cluster 19A3, with the exclusion of the genes sr10057 and sr10060.

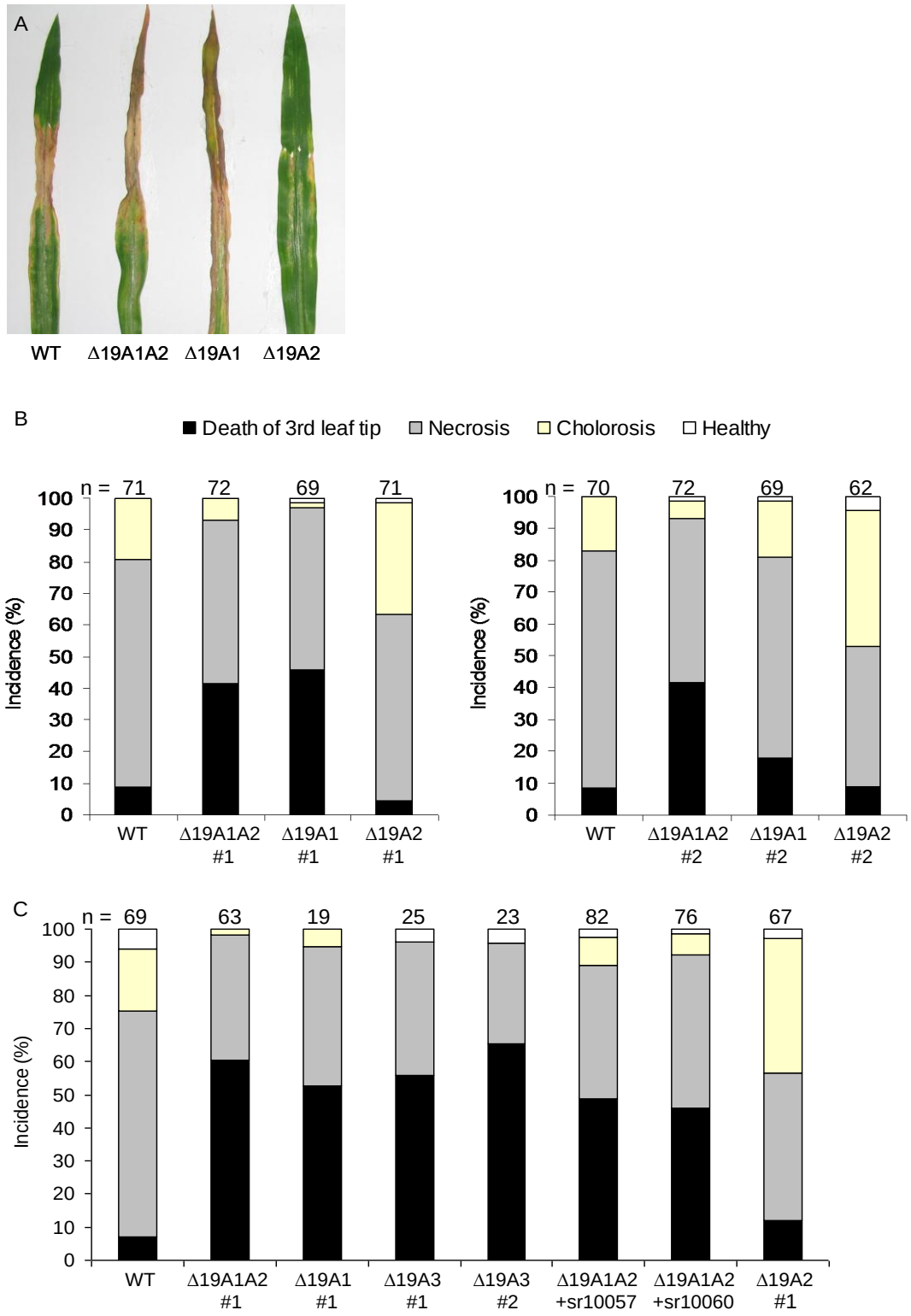

Figure 29. Leaf tip death phenotype of *S. reilianum* cluster 19A deletion strains on *Z. mays* 'Gaspe Flint' at 15 dpi. (A) Representative symptoms displayed on 3rd leaves infected with wild type (wt; 5-2 X 5-1), Δ19A1A2, Δ19A1 and Δ19A2 strains. (B) Leaf symptom incidence of Δ19A1A2, Δ19A1 and Δ19A2

mutants in comparison to WT. (C) Leaf symptom incidence of Δ19A3 mutants, and complementation mutant strains Δ19A1A2+sr10057 and Δ19A1A2+sr10060 in comparison to WT. The symptoms were evaluated on the 3rd leaf. Two independent compatible mating types of the Δ19A1A2 mutants (1, HG9 X HG19; 2, HG9 X HG20), Δ19A1 mutants (1, JS747 X JS751; 2, JS748 X JS752), Δ19A2 mutants (1, HG125 X HG127; 2, HG126 X HG128), Δ19A3 mutants (1, JS895 X JS900; 2, JS896 X JS901), Δ19A1A2+sr10057 (HG143 X HG147) and Δ19A1A2+sr10060 (HG150 X HG153) were used for infections. All Δ19A1A2+sr10057 and Δ19A1A2+sr10060 strain used contained multiple copies of the introduced gene. The values in B and C are means of three infection experiments except for Δ19A1 and Δ19A3 strains, which were evaluated only once, in C.

To monitor whether the leaf tip death is associated with a change in the proliferation behavior of *S. reilianum* mutants in the leaf, 2-cm leaf samples around the injection hole from 4 plants infected either with wt or Δ19A1A2 strains at 3 dpi were microscopically investigated. Interestingly, Δ19A1A2 mutants grew at a higher density at different locations of the leaf samples in comparison to the wild type (Figure 30A). To measure whether cluster 19A deletion strains have a higher proliferation density relative to wt in the leaf, the abundance of fungal (*ppi* gene) relative to plant DNA (*actin* gene) was quantified using qRT-PCR in leaves colonized by wt, Δ19A1A2, Δ19A1 and Δ19A2 strains. The ratio of the relative fungal DNA abundance of mutant to wt was calculated as an indicator of proliferation density. DNA was extracted from 10 pooled 3-cm 3rd leaf pieces harvested below injection hole of plants inoculated at 3 dpi with wt or mutant, and used for measuring the mutant to wt DNA ratio. Additionally, to test the proliferation density of the mutants in the node, 10 pooled 3rd nodes of infected plants were used to quantify mutant to wt DNA ratio.

In average, leaves and nodes colonized by Δ19A1A2 mutants showed a 2 fold increase of DNA abundance relative to wt (Figure 30B). However, the individual DNA quantification values between different samples colonized by Δ19A1A2 strains greatly differed leading finally to no statistical difference (p-value = 0.05). Additionally, Δ19A1 and Δ19A2 mutants did not show a dramatic change in average fungal DNA quantity in comparison to wt (Figure 30B). These results indicate that the leaf tip death is not necessarily associated with a change in the density of fungal proliferation in the leaf. Currently, the exact gene whose lack caused leaf tip death and the mechanism leading to such a phenotype is being investigated by a colleague.

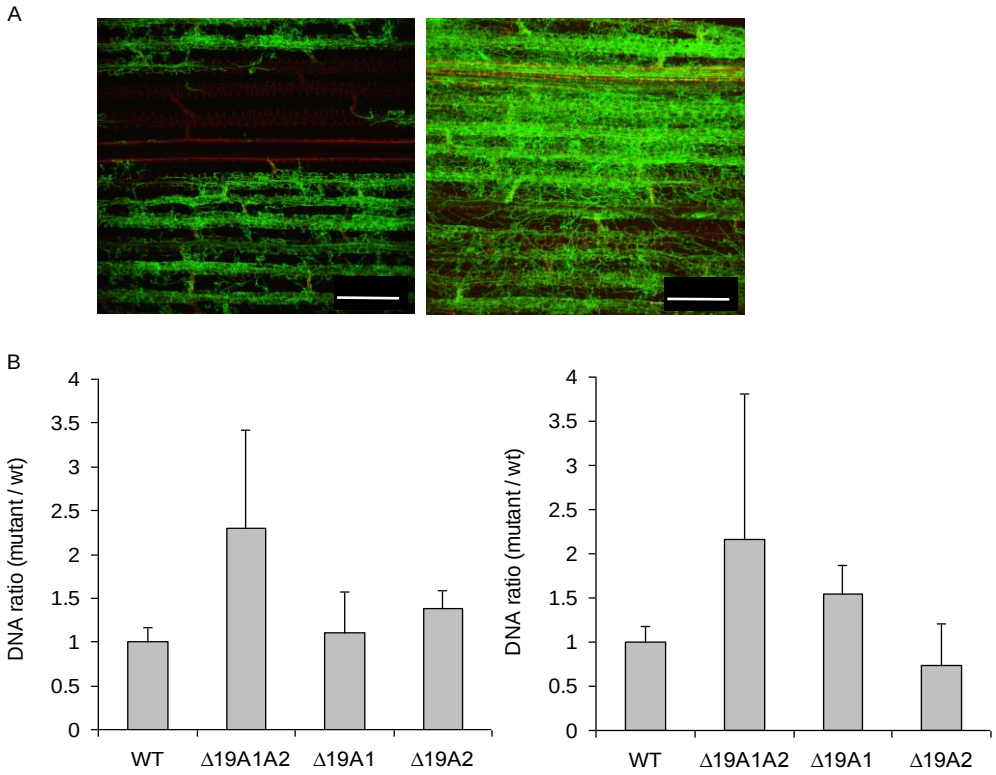

Figure 30. Proliferation density of *S. reilianum* cluster 19A deletion mutants in leaf and node of *Z. mays* 'Gaspe Flint'. (A) Representative z-stacks confocal images of WGA-Alexa Fluor and propidium iodide stained leaves (red) infected with *S. reilianum* (green) wt (left) and Δ19A1A2 mutants (right) at 3 dpi. Bars = 300 µm. (B) Quantification of relative DNA abundance of mutant and wt strains in leaves (left) and nodes (right). Fungal DNA (*ppi*) quantity was normalized by plant DNA (*actin*) quantity. DNA was extracted from 3-cm pieces of the 3rd leaves below the injection hole at 3 dpi and 3rd nodes at 15 dpi. The compatible mating types of the Δ19A1A2 mutants (HG9 X HG20), Δ19A1 mutants (JS747 X JS751) and Δ19A2 mutants (HG125 X HG127) were used for infection. Error bars represent SEM of five and three biological replicates of leaves and nodes, respectively. Each biological replicate is a pool of 10 plant samples inoculated with wt or mutant strains.

2.7.3 Identification of the Main Effectors of Cluster 19A2

Deletion of cluster 19A2 led to reduced virulence and greatly diminished suppression of apical dominance imposed by *S. reilianum*. Cluster 19A2 contains four genes (sr10073, sr10075, sr10077 and sr10079) that encode proteins predicted to be secreted. To identify the exact contribution of each gene to the deletion phenotype of cluster 19A2, the four genes were individually deleted in the wt strains (5-1 and 5-2). The deletion strains were verified by PCR and Southern blot, and the phenotype of 2 to 3 compatible stains of each gene deletion mutant

were tested individually on maize. The phenotype of the tested deletion strains showed consistency, therefore one representative pairs of compatible mating type from each gene deletion strain was used for repeating the infection experiments.

Deletion of sr10073, sr10075, sr10077, sr10079 and 19A2 led to 13%, 20%, 15%, 26% and 26% reduction in disease incidence, and 4%, 10%, 21%, 24% and 24% reduction in disease severity, respectively, in comparison to wt (Figure 31). Although deletion of sr10077 and sr10079 showed reduced disease incidence and severity (Figure 31, top, middle), the first showed increased severity of spore formation (Figure 31 middle), respectively, in comparison to wt. The reduced virulence levels shown by the individual gene deletion strains of 19A2 genes is almost equal to reduced virulence level obtained by the four-gene deletion strain, Δ19A2, indicating that the effect of the 19A2 genes is not accumulative. The sr10079 showed the highest contribution to virulence conferred by the 19A2 genes, and was named *virulence associated gene 1* (*vag1*).

An additional phenotype of 19A2 deletion strains is a reduction of the ear number per plant in comparison to wt-infected plants. Deletion of sr10077 or sr10075 exhibited significantly (p-value = 0.05) the same (2.3 ± 0.1 and 2.6 ± 0.2, respectively) number of ears per plant as mock infected plants (2.6 ± 0.1), but significantly (p-value = 0.05) lower that wt-infected plants (3.4 ± 0.2) (Figure 31). These results indicate that suppression of apical dominance imposed by wt strains of *S. reilianum* is associated with sr10077 and sr10075. Therefore we named the genes sr10077 and sr10075 *suppressor of apical dominance 1* and *2* (*sad1* and *sad2*), respectively. Because of their prominent roles in virulence and symptom formation within cluster 19A2, I functionally characterized below *sad1* (Chapter 2.8) and *vag1* (Chapter 2.9).

2.7.4 Divergence of Cluster 19A2 Effectors in Smuts

Recently, the genomes of the *S. reilianum* sorghum isolate and of *Sporisorium scitamineum* were sequenced (R. Kahmann and J. Schirawski, unpublished). To examine the divergence of cluster 19A2 effectors, a comparison of the cluster 19A2 sequence between the available smut genomes, *S. reilianum* maize and sorghum isolates, *S. scitamineum*, *U. maydis* and *U. hordei* was performed. First, the nucleotide sequences of the 19A2 genes of *S. reilianum* (maize isolate) were used to blast against the genomes of the *S. reilianum* (sorghum isolate), *U. hordei* and *S. scitamineum* to identify the 19A2 gene orthologues. Second, the nucleotide sequences of the

orthologues were translated into AA sequences, aligned, and then the AA identities to 19A2 effectors of *S. reilianum* were calculated. This comparison revealed that *S. reilianum* maize and sorghum isolates contain four genes, whereas *S. scitamineum* and *U. maydis* contain three and two genes, respectively (Figure 32).

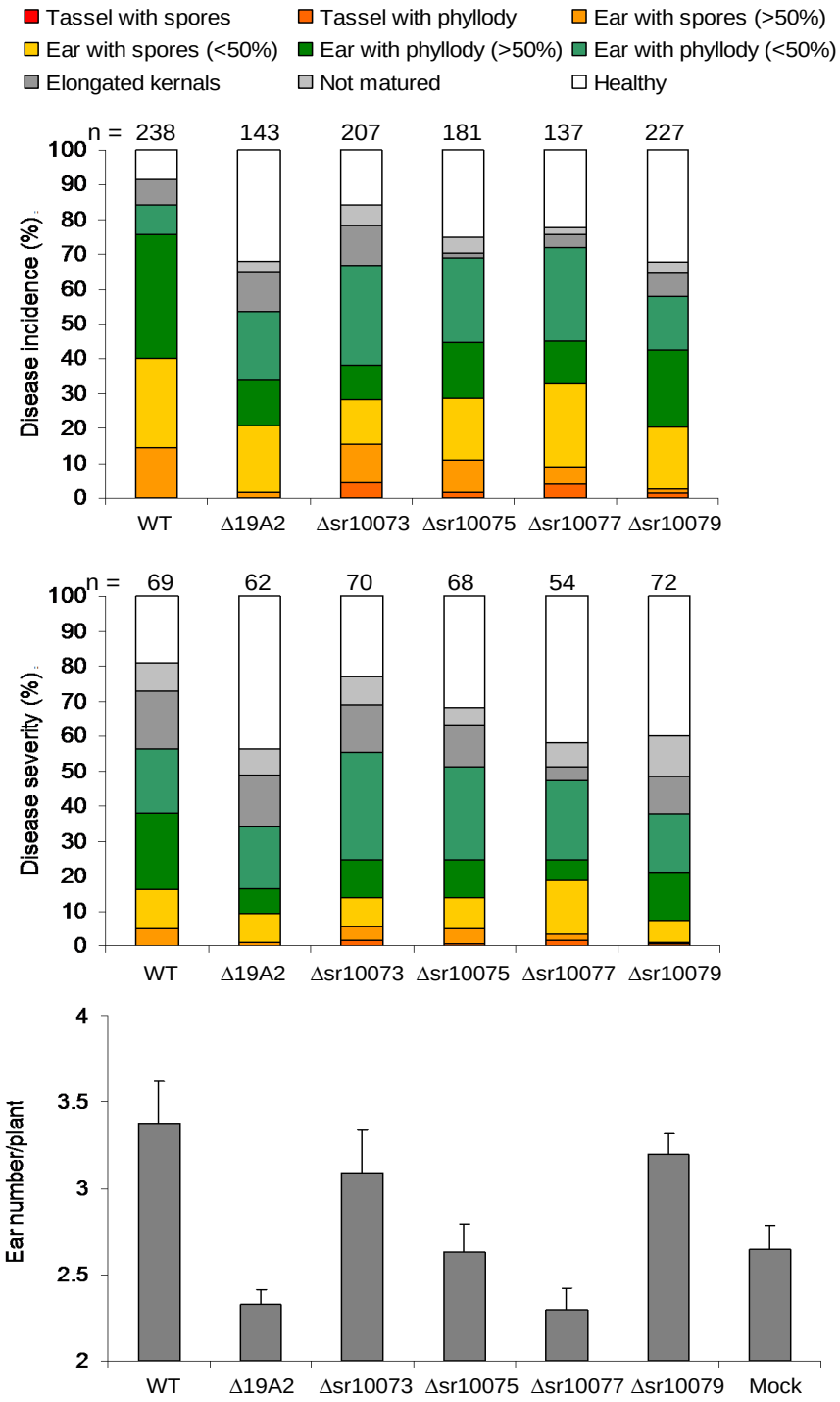

Figure 31. Virulence of the *S. reilianum* 19A2 individual gene deletion strains on *Z. mays* 'Gaspe Flint'.

Disease incidence (top), disease severity (middle) and ear number per plant (bottom) of Δ19A2 strains, and the individual gene deletions of 19A2, Δsr10073, Δsr10075, Δsr10077 and Δsr10079 strains in comparison to wt. Disease incidence expressed as percent of plants displaying highest symptom. Disease severity expressed as percent of inflorescences in each category from the total number of inflorescences. Strains with compatible mating type of the Δ19A2 mutants (HG125 X HG127), Δsr10073 mutants (HG109 X HG113), Δsr10075 mutants (HG80 X HG84), Δsr10077 mutants (HG95 X HG99) and Δsr10079 mutants (HG89 X HG92) were used for infection. The values are means of three infection experiments. Error bars represent SEM.

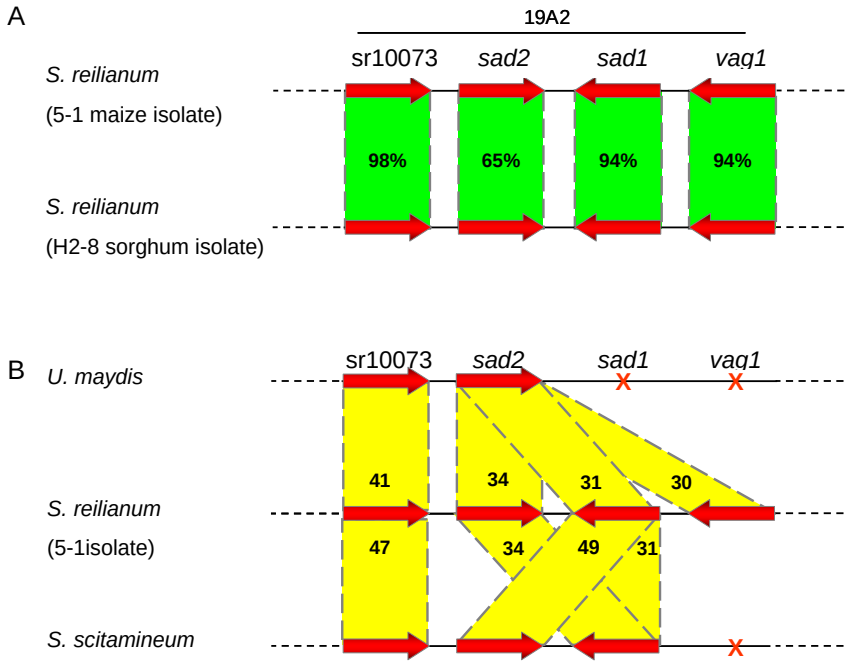

Figure 32. Schematic view of the comparison of cluster 19A2 from *S. reilianum* (maize isolate) with *S. reilianum* (sorghum isolate), *U. maydis* and *S. scitamineum*. (A) AA identity of cluster 19A2 effectors between *S. reilianum* (maize isolate) and *S. reilianum* (sorghum isolate) shows high conservation of cluster 19A2 genes. (B) AA identity of cluster 19A2 effectors between *S. reilianum* (maize isolate), *S. scitamineum* and *U. maydis*. The *sad2*, *sad1* and *vag1* seem to be paralogs in *S. reilianum*.

No orthology for any of the 19A2 genes was found in *U. hordei*. Three of the cluster 19A2 effectors showed very high (>94%) conservation between *S. reilianum* (maize isolate) and *S. reilianum* (sorghum isolate) but one (sr10075, SAD2) showed an AA identity of only 65% (Figure 32A). The AA sequence of sr10073 showed the highest level of conservation among the different smuts, whereas the AA sequence for SAD2, SAD1 and VAG1 was only weakly

conserved (Figure 32B). SAD2, SAD1 and VAG1 corresponded all to one orthologue in *U. maydis* (Figure 32B). No orthologue for VAG1 could be found in *S. scitamineum* (Figure 32B). SAD2, SAD1 and VAG1 in *S. reilianum* maize isolate showed 24-25% AA identity to each other. SAD1 showed identity to two genes in cluster 19A2 of *S. scitamineum* (Figure 32B). Intriguingly, SAD2, SAD1 and VAG1 of *S. reilianum* cluster 19A2 had 24-25% AA identity. These findings suggest that *sad2*, *sad1* and *vag1* are paralogues resulting from duplication events in *S. reilianum* maize and sorghum isolates and *S. scitamineum*.

2.8 Characterization of *sad1*

2.8.1 Complementation of *sad1*-Deletion

To ensure that loss of suppression of apical dominance is caused by deletion of *sad1* (sr10077) and not by different mutation in the genome, *sad1* was reintroduced at *mig1* locus of the two mating types of Δ*sad1* strains to generate the Δ*sad1*+*sad1* strains. The presence of *sad1* at the *mig1* locus was verified by PCR and Southern blot (Data not shown). Southern blot experiments showed that all the Δ*sad1*+*sad1* strains contained multiple copies of *sad1*. The Δ*sad1*+*sad1* strains were used to inoculate maize. Symptom evaluation of plants inoculated with the Δ*sad1*+*sad1* strains showed that re-introduction of *sad1* in multiple copies at the *mig1* locus complemented the *sad1* deletion phenotype by increasing the ear number per plant and restoring the rates of spore formation to that of wt (Figure 33).

2.8.2 Expression Pattern of *sad1*

To verify a role of *sad1* during plant colonization, the expression of *sad1* was investigated. Using RT-PCR, the *sad1* transcript could not be detect in *S. reilianum* sporidia growing in liquid culture but could be detected in hyphae growing in 3rd leaves at 3 dpi and in ears at 4 wpi (Figure 34A) indicating that *sad1* has mainly a function *in planta*. To test whether *sad1* is regulated within the different plant tissues, qRT-PCR was used to quantify the *sad1* transcripts in leaves, nodes and ears of infected plants. Using qRT-PCR, a very slight signal for the *sad1* transcript could be detected in sporidia growing in liquid culture. Therefore *sad1* expression in infected leaves, nodes and ears was calculated relative to the expression in sporidia growing in liquid culture. The relative expression of *sad1* dramatically increased more than 100 fold in infected

leaves, nodes and ears relative to axenically grown fungus (Figure 34B). The pronounced up-regulation of *sad1* in all tested plant tissues suggests that *sad1* has a pivotal role throughout growth of *S. reilianum in planta*.

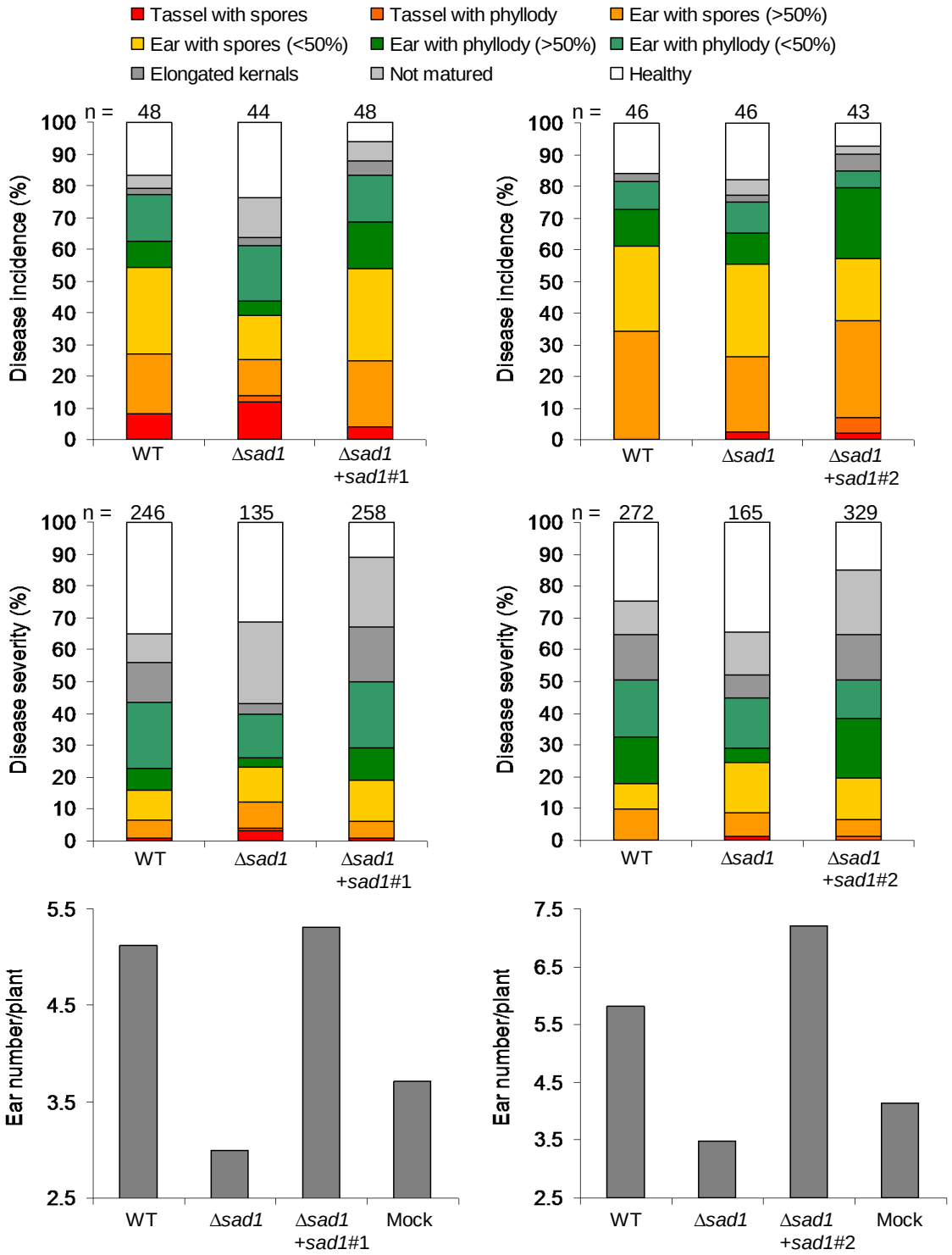

Figure 33. Virulence of *S. reilianum sad1* complementation strains on *Z. mays* 'Gaspe Flint'. Disease

incidence and disease severity of *sad1* deletion mutants and Δ*sad1+sad1* strains in comparison to wt. Disease incidence expressed as percent of plants displaying highest symptom. Disease severity expressed as percent of inflorescences in each category from the total number of inflorescences. Two independent compatible strain pairs of the Δ*sad1+sad1* mutants (1, HG163 X HG167; 2, HG164 X HG168) and one compatible strain pair of the Δ*sad1* mutants (HG95 X HG99) were used for infections. The Δ*sad1+sad1* strains carry multiple copies of *sad1* integrated at the *mig1* locus. The values are means of two infection experiments.

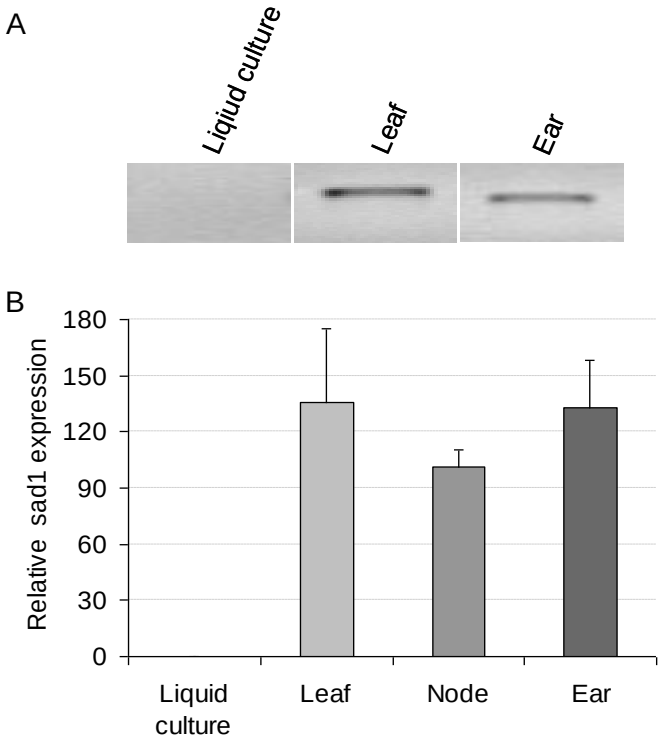

Figure 34. Expression of *sad1* in liquid culture and *in planta*. (A) The expression of *sad1* detected in *S. reilianum* sporidia growing in liquid culture (OD_{600} = 0.5), infected leaf (3 dpi) and ear (4 wpi) by RT-PCR. (B) Quantification of *sad1* transcripts by qRT-PCR in infected leaf (3 dpi), node (15 dpi) and ear (4 wpi) relative to the sporidia growing in liquid culture (OD_{600} = 0.5). The expression of *sad1* in all samples was normalized to the housekeeping *ppi* transcripts. Error bars represent SEM of three biological replicates. Each biological replicate is a pool of at least 10 samples.

2.8.3 Proliferation Behavior of the *sad1* Deletion Mutants

To test whether the proliferation of *sad1* deletion mutant is affected *in planta*, the fungal proliferation density was quantified as described in chapter 2.8.2. In infected leaf, a trend for

higher DNA abundance of *sad1* deletion mutant to wt was detected but the effect was not statistically significant (p-value = 0.05) (Figure 35). In infected nodes, there was no difference in DNA abundance of *sad1* deletion and wt strains (p-value = 0.05) (Figure 35). Theses results indicate that the phenotype of *sad1* deletion strains cannot be explained by a change in the proliferation density.

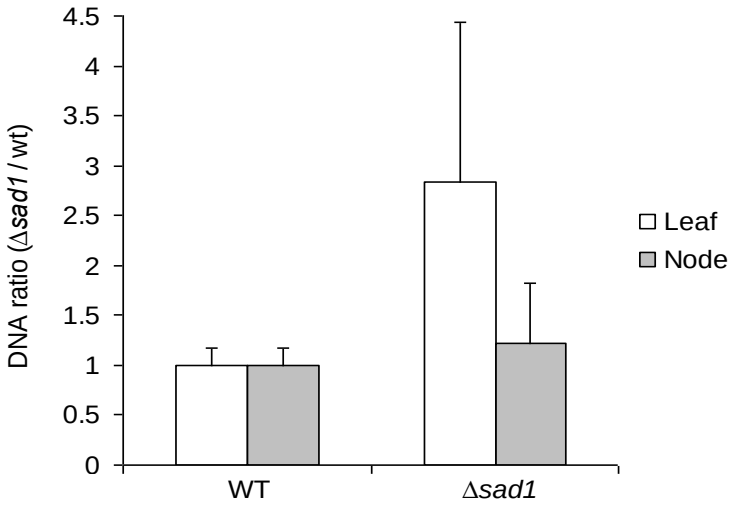

Figure 35. Proliferation density of *sad1* deletion mutant in the leaf and node of infected *Z. mays* 'Gaspe Flint'. Ratio of DNA abundance of *sad1* deletion mutant relative to wt was calculated as measure of proliferation density. Fungal DNA (*ppi*) quantity was normalized by plant DNA (*actin*) quantity. DNA was extracted from 3-cm pieces of 3rd leaves below injection hole at 3 dpi, and from 3rd nodes at 15 dpi. Error bars represent SEM of three biological replicates. Each biological replicate is a pool of 10 samples.

2.8.4 Localization of SAD1 in *S. reilianum*

For SAD1 protein localization, a *sad1-gfp* fusion construct was integrated at the *mig1* locus in the two compatible of Δ*sad1* deletion strains to generate the Δ*sad1+sad1*:*gfp* strains. The transformants were verified by PCR and Southern blot. Southern blot experiments showed that all of the generated Δ*sad1+sad1*:*gfp* strains have integration of multiple copies of the *sad1*:*gfp* fusion construct. The Δ*sad1+sad1*:*gfp* was used to infect maize. Plants infected with the Δ*sad1+sad1*:*gfp* strains did not show complementation of the *sad1* deletion mutant phenotype as ear number per plant did not increase (Figure 36A). This result indicates that the SAD1-GFP fusion protein is not functional.

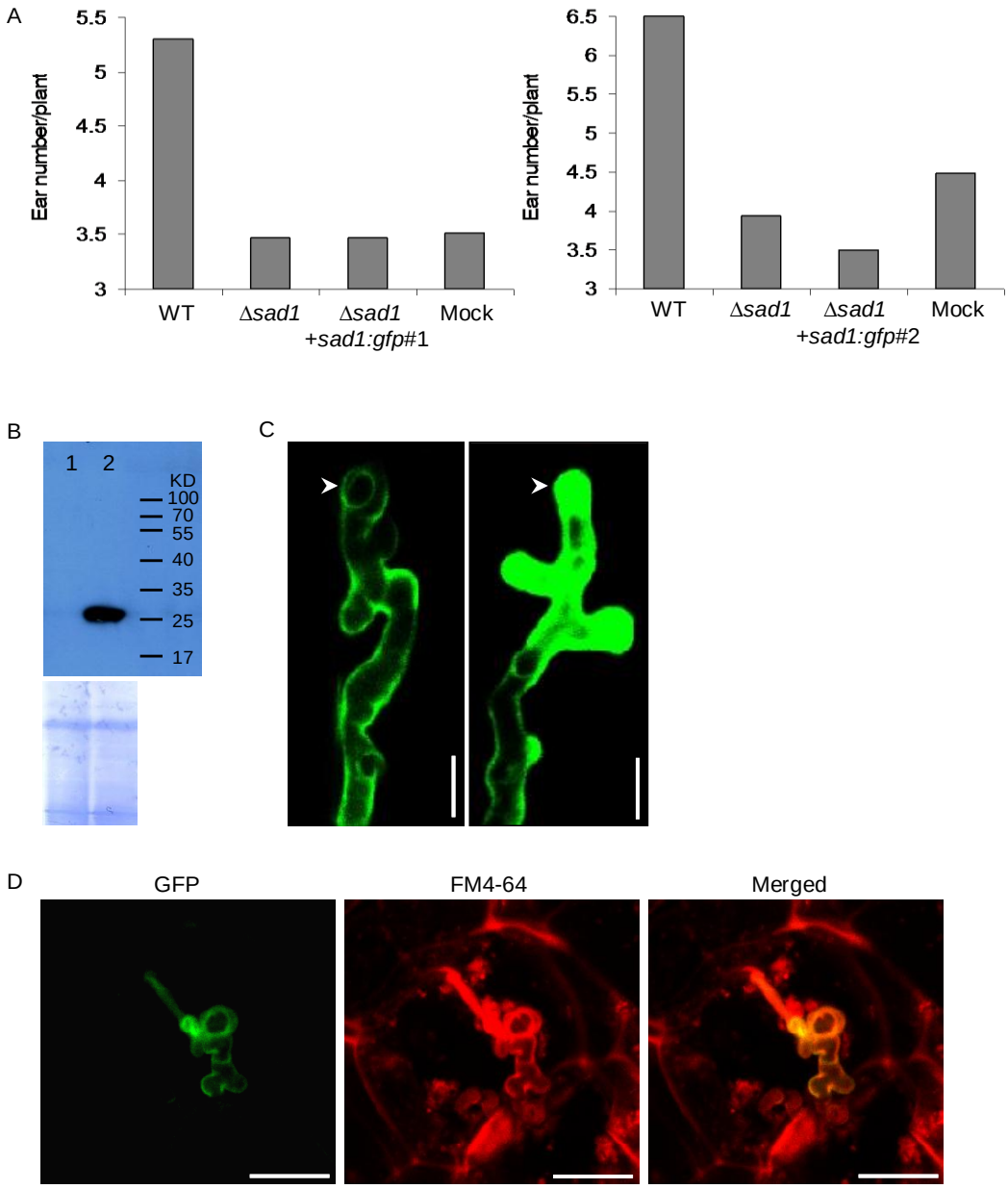

Figure 36. Localization of SAD1 *in planta*. (A) Ear number per plant of *Z. mays* 'Gaspe Flint' inoculated with *sad1* deletion mutants and Δ*sad1*+*sad1*:*gfp* strains in comparison to WT. Two independent strains of pairs of compatible mating type of the Δ*sad1*+*sad1*:*gfp* mutants (1, HG183 X HG186; 2, HG185 X HG187) and one compatible strain pair of the Δ*sad1* mutants (HG95 X HG99) were used for infections. The Δ*sad1*+*sad1*:*gfp* strains carry multiple integrated copies of the *sad1*:*gfp* construct. The values are means of two independent experiments (n in each experiment = 25 ± 2). (B) Western blot showing absence of GFP in leaves inoculated with SAD1-GFP expressing strain (1) and a detected GFP in leaves inoculated with wt expressing cytoplasmic GFP (2). The GFP was detected with a monoclonal antibody against GFP (top). For loading control, the blotting membrane was strained with Coomassie Blue

(bottom). (C) In the ear section, SAD1-GFP fusion protein showed accumulation of the fluorescence signals around fungal hypha (left) and at the hyphal tips (right). Bars = 5 µm. (D) In the ear section, co-localization of fluorescence signals of SAD1-GFP (green) with the cell membrane staining dye FM4-64 (red). Bars = 10 µm. C and D are Z-stacks of confocal images.

However, to test whether SAD1 is secreted, plant samples inoculated with the Δ*sad1+sad1*:*gfp* strains were investigated with confocal microscopy. Fluorescence signals of SAD1-GFP could not be detected in cells cultivated in liquid culture, or growing the on leaf surface, in the leaves or in leaf sheaths at 1 hour post inoculation (hpi) - 10 dpi. To verify the absence of SAD1 in the leaf, a Western blot was performed. Protein samples from leaves inoculated with Δ*sad1+sad1*:*gfp* or WT expressing cytoplasmic GFP (wt-*gfp*) as positive control, at 3 dpi were used. A GFP monoclonal antibody was used to immunodetect the fusion protein. In Western blot SAD1-GFP could not be detected in the protein extracts of leaves inoculated with Δ*sad1+sad1*:*gfp* whereas GFP could be clearly detected the samples inoculated with wt-*gfp* (Figure 36B). Surprisingly, in ear sections, a strong intercellular GFP signal could be microscopically detected around fungal hyphae and at hyphal tip (Figure 36C). The fluorescence signal of SAD1-GFP was also co-localized with the cell membrane staining dye FM4-64 (Figure 36D). The pattern of protein localization indicates that SAD1 is a secreted protein.

2.8.5 Transcriptional Regulation of the *sad1* Promoter

The *sad1* transcript was expressed in leaves and ears (Figure 34) but evidence for protein production was only visible in ears (Chapter 2.9.4). To verify whether the SAD1-mRNA is present in leaves, we replaced the *sad1* gene in wt strains with *gfp* gene and a carboxin resistance cassette by homologous recombination to generate s*ad1*p:*gfp* strains. The replacement of *sad1* by *gfp* was verified using PCR and Southern blot. In the s*ad1*p:*gfp* strains, expression of *gfp* is driven by *sad1* promoter. The s*ad1*p:*gfp* strains were used to inoculate maize. The GFP expression was investigated by fluorescence microscopy in sporidia growing in liquid culture and in the leaves at 3 dpi. In liquid culture, no GFP signal could be observed in sporidia. In leaves, the *sad1*p:*gfp* strains clearly showed GFP signal (Figure 37). These results indicate that the *sad1* promoter is transcriptionally activated *in planta* and that *sad1* transcript should be available for transcription in the leaf.

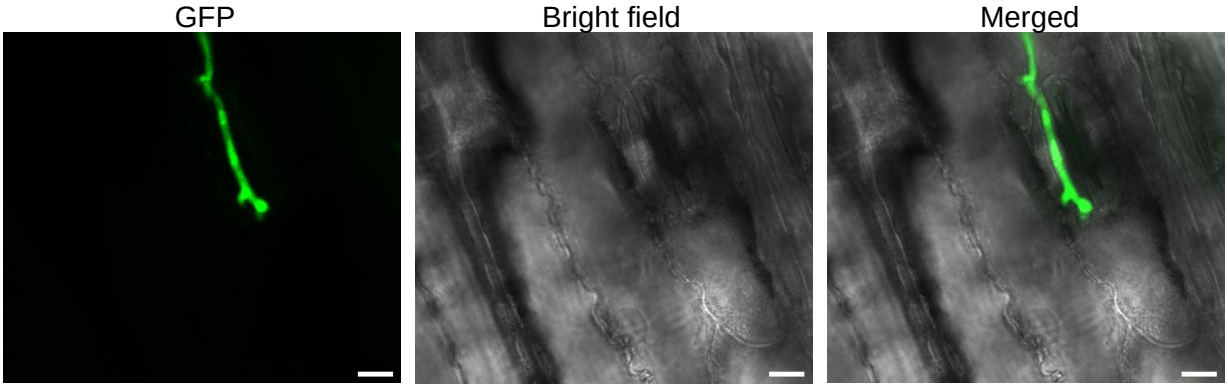

Figure 37. Promoter activity of the *S. reilianum sad1* gene in maize leaves. A fluorescence microscope image of a leaf of *Z. mays* 'Gaspe Flint' infected with a compatible combaination of the *sad1*p:*gfp* strains (YF2 5-1#1 X YF2 5-2#1) expressing *gfp* under the control of *sad1* promoter. GFP fluorescence could readily be detected in the hyphae growing in the leaf showing promoter activity of *sad1* in the infected leaf. Bars = 10 µm. This experiment was conducted by Yufei Wang.

2.8.6 Subcellular Localization of SAD1 in Plant Cells

The secreted nature of SAD1 protein opens questions: whether SAD1 is translocated into the plant cell? What is the subcellular localization of SAD1 within the plant cell? To address these questions, we plan an electron microscopic investigation of a immunogold-labeled SAD1 in infected plant tissues. Generation of strains containing tagged versions of *sad1* is currently underway. To study the subcellular localization of SAD1, SAD1 was expressed in sorghum protoplast. For that purpose, a plasmid (p*35S*p*:gfp:sad1*Δ*sp*) expressing N-terminal GFP fusion to SAD1 lacking its signal peptide, and a control plasmid (pGH215) expressing GFP only, were used to independently transform sorghum protoplasts. The transform protoplasts were investigated by fluorescence microscopy to monitor the GFP-SAD1ΔSP subcellular localization. In protoplasts transformed with p*35S*p*:gfp:sad1*Δ*sp* the GFP signals were mainly detected in the nucleus in addition to the cytoplasm, whereas in protoplasts transformed with pGH215 the GFP signals were mainly detected in the cytoplasm (Figure 38). Subcellular localization of SAD1 in the nucleus could implicate a role of SAD1 in manipulating nuclear activity by interacting with nuclear proteins or direct binding with DNA. To ensure that the subcellular localization of the GFP-SAD1ΔSP fulfils the SAD1 function, the *gfp*:*sad1* construct with sequence encoding *sad1* signal peptide is being tested for complementation of the *sad1* deletion phenotype.

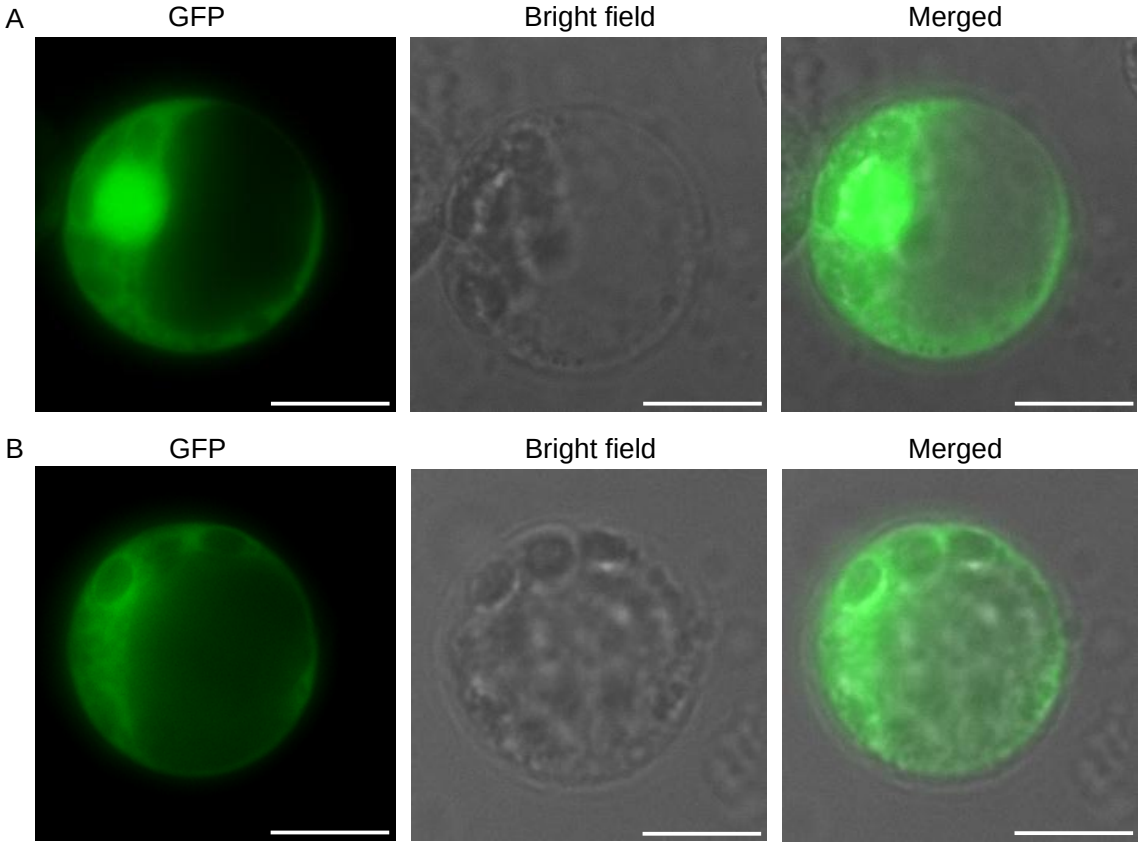

Figure 38. Subcellular localization of SAD1 in sorghum protoplast. (A) Protoplast transformed with p*35S*p:*gfp:sad1*Δ*sp* showing nuclear and cytoplasmic localization of GFP-SAD1ΔSP. (B) Protoplast transformed with a GFP expressing plasmid pGH215 showing cytoplasmic localization of GFP. Bars = 10 µm.

2.8.7 SAD1 Autoactivates *AUR1-C* and *MEL1* Transcription in Yeast

To get insight into how suppression of apical dominance is linked to function of SAD1, I aimed to identify the interaction partners of SAD1. The Matchmaker™ Gold Yeast Two-Hybrid System was used, in which a bait protein is expressed as a Gal4 DNA-binding domain (BD) fusion protein, while libraries of prey proteins are expressed as Gal4 activation domain (AD) fusion protein. I constructed the plasmid pGBKT7-BD-SAD1ΔSP, which encodes the BD followed by the c-MYC tag fused to the SAD1 protein lacking the predicted signal peptide. The pGBKT7-BD-SAD1ΔSP was transformed in the yeast strain Y2HGold to generate the Y2HGold-BD-SAD1ΔSP strain. Using Western blot, the 41 kD fusion protein BD-SAD1ΔSP could be detected in the protein extract of the Y2HGold-BD-SAD1ΔSP by a monoclonal antibody against the c-MYC tag (Figure 39A).

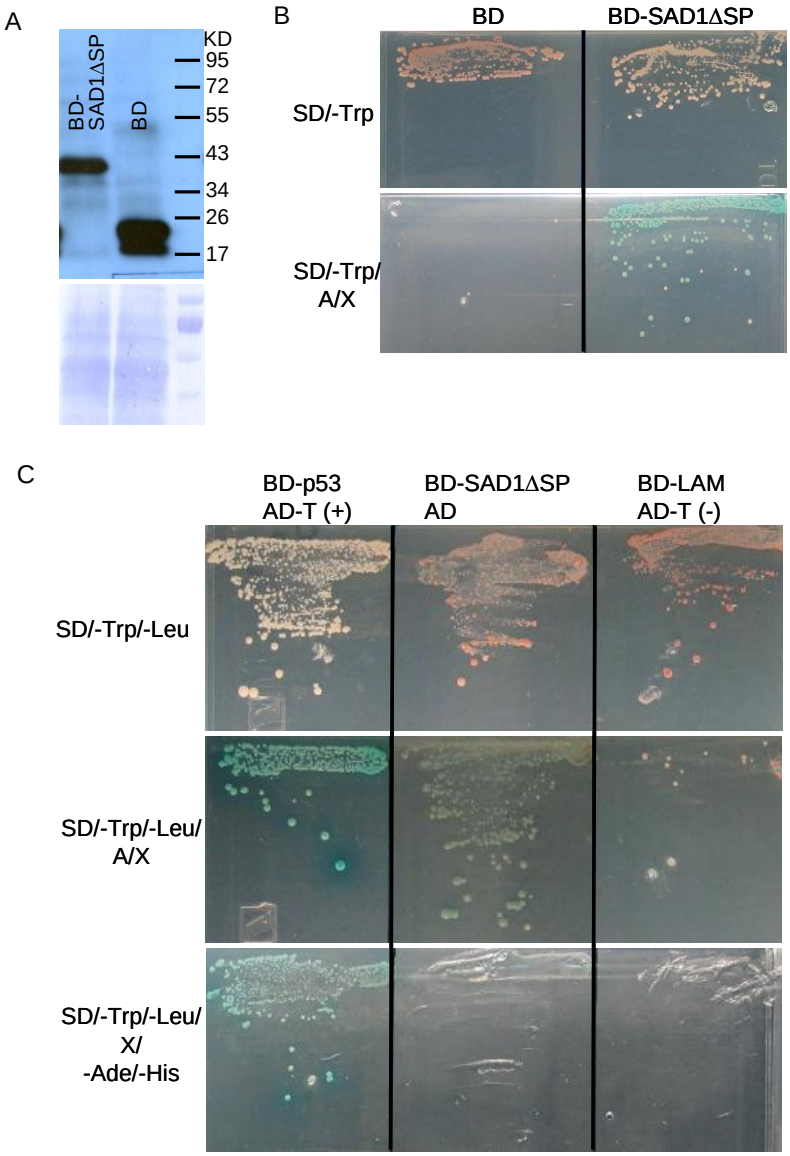

Figure 39. Transcriptional activation of reporter genes in yeast by SAD1. (A) Immunodetection of BD-SAD1ΔSP and BD in protein extracts of Y2HGold strains containing the plasmids pGBKT7-BD-SAD1ΔSP and pGBKT7-BD, respectively, with antibody specific for the c-MYC (top). For loading control, the blotting membrane was strained with Coomassie Blue (bottom). The expected size for BD-SAD1ΔSP and BD are 41 kD and 20 kD, respectively. (B) Blue colonies of the BD-SAD1ΔSP expressing yeast strain grow on SD/A/X indicating auotactivation of their reporter genes *AUR1-C* and *MEL1* by SAD1. (C) Yeast diploids containing the pGBKT7 and pGADT7 plasmids that encode the BD and AD of GAL4 only or in fusion with the SAD1ΔSP, P53, T or LAM proteins. Growth on SD/-Trp/-Leu indicates that the diploids contain both bait and prey plasmids. Growth on SD/-Trp/-Leu/A/X or SD/-Trp/-Leu/X/-Ade/-His indicates that the proteins fused to BD and AD interact. The diploid expressing SAD1ΔSP + AD could grow on SD/A/X indicating autoactivation of *AUR1-C* and *MEL1* by SAD1 as in (B). The diploid

expressing SAD1ΔSP + AD could not grow on SD/-Ade/-His indicating that SAD1 did not autoactivate the auxtrophy reporter genes *ADE2* and *HIS3*. A; Aureobasidin A, X; α-X-GAL, Trp; tryptophan, Leu; leucin, Ade; Adenin, His; histidin, (+) positive control; (-) negative control.

Preceding the screen for interaction partners, transcriptional activation of the interaction reporter genes by SAD1 was investigated. Here, four interaction reporter gene were used; *AUR1-C* (Aureobasidin A resistance gene), *MEL1* (encodes galactosidase and metabolizes α-X-GAL to produce blue color), *ADE2* (confers adenine auxotrophy) and *HIS3* (confers histidin auxotrophy). The Y2HGold-BD-SAD1ΔSP strain and a control strain Y2HGold-BD, which contains pGBKT7 plasmid lacking SAD1, were grown on SD medium supplemented with Aureobasidin A and α-X-GAL. Interestingly, in contrast to the control Y2HGold-BD strain, the Y2HGold-BD-SAD1ΔSP strain was able to grow on the medium and showed blue colony color (Figure 39B, C). These results indicate that SAD1 could autoactivates the transcription of *AUR1-C* and *MEL1*.

To test whether SAD1 also autoactivates the transcription of the *ADE2* and *HIS3* auxotrophy reporter genes. The Y2HGold-BD-SAD1ΔSP strain was mated with a yeast strain Y187-AD, which caries the empty plasmid pGADT7 encoding the AD of GAL4, and then the resulting diploids were tested for growth on SD medium supplemented with Aureobasidin A (125 ng/ml) and α-X-GAL , and/or lacking adenin and histidin (-Ade/-His). The diploid cells expressing both BD-SAD1 and AD were able to grow on SD/X/A but not on SD/-Ade/-His (Figure 39C) indicating that SAD1 can auotactivate the AUR1-C and MEL1 reporter genes but not the two auxotrophy genes (*ADE2* and *HIS3*). These results showed that the *ADE2* and *HIS3* markers can be used for selection of interaction partners of SAD1.

2.8.8 Interaction Partners of SAD1

To perform a yeast two hybrid experiment for identification of interaction partners of SAD1, a normalized cDNA library (pGADT7-PREY) was generated, which encodes maize and *S. reilianum* proteins C-terminally fused to AD that are expressed in infected leaves, nodes and ears. I transformed the pGADT7-PREY library in the yeast strain Y187 to generate the yeast prey library Y187-AD-PREY. The yeast library resulted in $2x10^6$ clones, which were mixed, aliquoted and stored at -80°C. To screen for the interaction partners of SAD1, $1x10^8$ cells of the Y2HGold-BD-SAD1ΔSP and $1x10^7$ cells of the Y187-AD-PREY were mated resulting in $5x10^5$

independent diploids growing on SD/-Trp/-Leu medium. Of these 547 diploids grew on SD/-Ade/-His medium showing putative interaction with SAD1.

To verify putative interaction and to get rid of multiple prey plasmids in those diploids, two rounds of selecting colonies growing on SD/-Trp/-Leu/-Ade/-His medium were performed ending up with 434 diploids. The plasmids encoding the SAD1 interaction partners (SAD1-IP) were isolated from all diploids and transformed in *E. coli*. The plasmids were re-isolated from *E. coli* and sequenced. The interaction partners' sequences were aligned resulting in 179 independent sequences. To prove genuine interaction of the resulting candidates, I retransformed 179 plasmids representing all detected interaction partners in the Y178 strain and mated the generated strains with the Y2HGold-BD-SAD1ΔSP and Y2HGold-BD strains. The resulting diploids were tested for interaction of the prey and bait by growth on SD/-Trp/-Leu/-Ade/-His medium (Figure 40). This analysis resulted in 139 genuine interactions, which their colonies grow on SD/-Trp/-Leu/-Ade/-His medium in the presence of BD-SAD1ΔSP only. In addition, 34 false positive interactions were shown to grow on SD/-Trp/-Leu/-Ade/-His medium in the presence of BD-SAD1ΔSP and BD indicating autoactivation effect. Five diploids failed to grow on SD/-Trp/-Leu/-Ade/-His showing no interactions with SAD1.

The sequences for the 139 genuine interaction partners were annotated by comparison to nucleotide database (BLASTN, NCBI) (Altschul et al., 1990) and functionally classified according to their biological function. Interestingly, large portion of the annotated interaction partners with known function belonged to transcription, ubiquitination and signaling functional groups (Table 5). Additionally, five SAD1 interaction partners, MIS1, TGA1, Fimbriata-like protein, ZAG1 and ZmLD had a function in floral development (Table 5). Importantly, the *S. reilianum* effecter MIG1 interacted with SAD1 (Table 5) suggesting that SAD1 could function in an effector complex. These results draw a frame work for SAD1 function where at least interaction of SAD1 with proteins involved in transcription, ubiquitination and signaling could explain the role of the protein *in planta*.

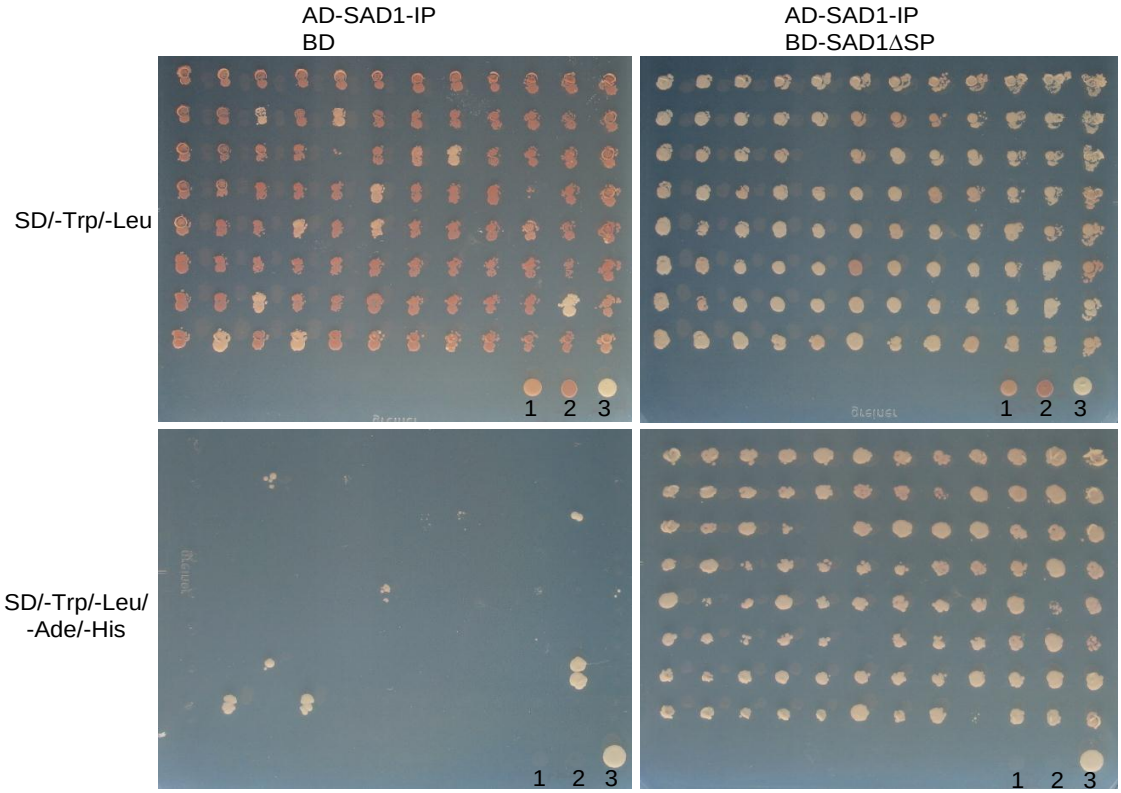

Figure 40. Identification of SAD1 interaction partners. Yeast diploids expressing SAD1 interaction partners (AD-SAD1-IP) and either BD (left) or BD-SAD1ΔSP (right) were inoculated on SD/-Trp/-Leu (top) and SD/-Trp/-Leu/-Ade/-His (bottom) media. Growth on SD/-Trp/-Leu medium shows that the prey and bait plasmids are present, whereas growth on SD-Ade/-His medium shows that prey and bait interact. 1 and 2 are negative controls (1; BD-SAD1 + AD, 2; BD-LAM + AD-T), and 3 is positive control (BD-P53 + AD-T).

Table 5. List of SAD1 Interaction Partners Identified by Yeast Two Hybrid.

Name IP [N, C]	**Recovery (X)**	**Accession**	**Annotation**
Development			
SAD1-IP1	4	AF467541	putative aldehyde dehydrogenase MIS1 (MIS1)
SAD1-IP2[N]	3	AY883559	teosinte glume architecture 1 (TGA1)
SAD1-IP3	2	NM_001177122	Fimbriata-like protein
Transcription			
SAD1-IP4[N]	5	NM_001111851.	*Zea mays* AGAMOUS 1 (ZAG1)
SAD1-IP5[N]	4	NM_001112378	helicase RH2 protein-like
SAD1-IP6[N]	4	NM_001158297	polypyrimidine tract-binding protein
SAD1-IP7[N]	3	NM_001155221	arginine/serine-rich splicing factor 10
SAD1-IP8[N]	3	EU955917	RNA-binding protein-like
SAD1-IP9[N]	3	EU962463	zinc finger protein-like 1 mRNA

Name IP [N, C]	Recovery (X)	Accession	Annotation
SAD1-IP10[N]	2	NM_001154418	zinc finger, C3HC4 type family protein
SAD1-IP11[N]	2	NM_001175194	transcription factor PIF3
SAD1-IP12[N]	2	EU964022	DNA-directed RNA polymerase II subunit J
SAD1-IP13[N]	1	NM_001196711	putative nucleic acid binding protein
SAD1-IP14[N]	1	BT083965	putative polynucleotide adenylyltransferase
SAD1-IP15[N]	1	AF166527	flowering-time protein isoforms alpha and beta (ZmLD)
SAD1-IP16 [N]	1	EZ728980	putative transcription elongation factor 1 homolog
Nuclear processes			
SAD1-IP17[N]	5	NM_001175076	nucleolar complex protein 2 homolog
SAD1-IP18[N]	1	NM_001155749	GTP-binding nuclear protein Ran-A1
SAD1-IP19[N]	1	EU963722	replication factor A
SAD1-IP20[N]	1	NM_001174927	DNA polymerase delta small subunit
SAD1-IP21[N]	1	NM_001111755	single myb histone3 (SMH3)
Ubiquitination			
SAD1-IP22	7	EU965267	similar to SAM domain of Anks family protein
SAD1-IP23	4	NM_001147846	probable E3 ubiquitin-protein ligase
SAD1-IP24	2	NM_001155504	probable E3 ubiquitin-protein ligase
SAD1-IP25[C]	2	U29161	MubG7 ubiquitin fusion protein gene
SAD1-IP26	2	BT066423	ubiquitin-associated protein
SAD1-IP27[C]	2	NM_001152740	E3 ubiquitin-protein ligase RGLG2
SAD1-IP28[C]	2	EU940814.1	E3 ubiquitin-protein ligase KEG
SAD1-IP29	2	BT067186	S-phase kinase-associated protein 1-interacting partner 14
SAD1-IP30	1	EU971426	S-phase kinase-associated protein 1-interacting partner 5
SAD1-IP31	1	NM_001139323	probable ubiquitin carrier protein E2
SAD1-IP32	1	EU947130	ubiquitin carboxyl-terminal hydrolase 26
Signaling			
SAD1-IP33	6	NM_001153317	probable phosphatase 2C
SAD1-IP34	2	NM_001111427	pyruvate dehydrogenase (lipoamide) kinase1 (pdlk1)
SAD1-IP35	2	EU954821	casein kinase II subunit beta-4
SAD1-IP36	2	NM_001158779	kinase APK1B
SAD1-IP37	1	NM_001158059	calcium-dependent protein kinase (CDPK) substrate
SAD1-IP38	1	NM_001165853	serine/threonine-protein kinase CTR1
SAD1-IP39	1	NM_001156570	serine/threonine-protein phosphatase 5
SAD1-IP40	1	EU960993	WD-repeat protein-like
SAD1-IP41	1	NM_001175835.	serine/threonine-protein kinase CTR1
Defense			
SAD1-IP42	4	DQ237917	TVLP1 induced during incompatible disease interaction
SAD1-IP43	2	NM_001158127	protease 2
SAD1-IP44	2	NM_001149532	pore-forming toxin-like protein Hfr-2
SAD1-IP45	11	NM_001137280	chorismate mutase
SAD1-IP46	1	AK229483	beta-1,3-glucanase
SAD1-IP47	1	EU969433	avr9 elicitor response protein
Effector			
SAD1-IP48	3	sr02613	*MIG1*

Name IP [N, C]	Recovery (X)	Accession	Annotation
Transport			
SAD1-IP49	5	NM_001136832	Probable potassium transporter
SAD1-IP50	2	AF272758	kinesin heavy chain (KIN13)
SAD1-IP51	2	NM_001176496	ADP-ribosylation factor GTPase-activating protein AGD2
SAD1-IP52	2	EU962421	triose phosphate/phosphate translocator
SAD1-IP53	1	NM_001175501	cell division control protein 48 homolog
SAD1-IP54	1	NM_001174517	putative copper-transporting ATPase
SAD1-IP55	1	EU976570	vacuolar ATP synthase catalytic subunit A
Protein biosynthesis			
SAD1-IP56	2	NM_001158959	40S ribosomal protein S29 mRNA
SAD1-IP57	13	BT024101	60 kDa chaperonin
SAD1-IP58	1	EU959231	mitochondrial elongation factor G
SAD1-IP59[C]	1	NM_001158850	T-complex protein 1 subunit gamma
Metabolism			
SAD1-IP60[C]	5	L23548	alcohol dehydrogenase (ADH1-S)
SAD1-IP61	3	NM_001156978	transaldolase 2
SAD1-IP62	3	NM_001155106	cysteine desulfurase
SAD1-IP63	2	EU952885	3-dehydroquinate synthase
SAD1-IP64	2	NM_001149213	Aminotransferase y4uB
SAD1-IP65	2	EU954542	ATP synthase C chain
SAD1-IP66	1	NM_001158819	stachyose synthase precursor
SAD1-IP67[C]	1	NM_001158838	UDP-sugar pyrophospharylase
SAD1-IP68[C]	1	NM_001158006	beta-galactosidase precursor
SAD1-IP69[C]	1	NM_001112255	glutamine synthetase1 (GLN1)
Cytoskeleton trafficking			
SAD1-IP70[C]	4	NM_001154731	actin7 (ACT7)
SAD1-IP71[C]	1	NM_001112152	profilin 5 (PRO5)
SAD1-IP72[C]	1	AF412282	actin-1
Miscellaneous			
SAD1-IP73	9	EU325985	RuBisCo subunit binding-protein beta subunit
SAD1-IP74[C]	2	NM_001153975	copine-1
SAD1-IP75[C]	1	AY772416	peroxisomal targeting signal 1 receptor short form (PEX5)
SAD1-IP76	1	EU967561	ATP binding protein
SAD1-IP77[C]	1	AF090447	22 kDa alpha zein
SAD1-IP78	1	EU964459	ENT domain containing protein
Unknown			
SAD1-IP79	9	EU956885	unknown
SAD1-IP80	5	NM_001147681	unknown
SAD1-IP81	5	XM_002458201	unknown
SAD1-IP82	4	unknown	unknown
SAD1-IP83	4	NM_001176366	unknown
SAD1-IP84	4	NM_001175437	unknown
SAD1-IP85	4	NM_001147847	unknown
SAD1-IP86	4	AY105415	unknown

Name IP [N, C]	Recovery (X)	Accession	Annotation
SAD1-IP87	4	EU952389	unknown
SAD1-IP88	4	FJ909097	unknown
SAD1-IP89	3	NM_001138777	unknown
SAD1-IP90	3	unknown	unknown
SAD1-IP91	3	XM_002459720	unknown
SAD1-IP92	3	NM_001147794	unknown
SAD1-IP93	2	EZ049005	unknown
SAD1-IP94	2	EU973079	unknown
SAD1-IP95	2	NM_001150894	unknown
SAD1-IP96	2	NM_001149677	unknown
SAD1-IP97	2	NM_001196640	unknown
SAD1-IP98	2	EU970950	unknown
SAD1-IP99	2	NM_001143503	unknown
SAD1-IP100	2	EU970455	unknown
SAD1-IP101	2	NM_001152817	unknown
SAD1-IP102	2	BT037014	unknown
SAD1-IP103	2	NM_001138124	unknown
SAD1-IP104	2	XM_002436662	unknown
SAD1-IP105	2	XM_002461939	unknown
SAD1-IP106	2	XM_002447971.	unknown
SAD1-IP107	2	EU947192	unknown
SAD1-IP108	1	NM_001196794	unknown
SAD1-IP109	1	NM_001165499	unknown
SAD1-IP110	1	unknown	unknown
SAD1-IP111	1	EZ091105	unknown
SAD1-IP112	1	XM_002436271	unknown
SAD1-IP113	1	unknown	unknown
SAD1-IP114	1	XM_002442110	unknown
SAD1-IP115	1	NM_001152450	unknown
SAD1-IP116	1	NM_001174716	unknown
SAD1-IP117	1	NM_001137844	unknown
SAD1-IP118	1	XM_002466376	unknown
SAD1-IP119	1	EU952389	unknown
SAD1-IP120	1	NM_001175212	unknown
SAD1-IP121	1	NM_001137520	unknown
SAD1-IP122	1	XM_002462618	unknown
SAD1-IP123	1	XM_002438743	unknown
SAD1-IP124	1	NM_001175213	unknown
SAD1-IP125	1	unknown	unknown
SAD1-IP126	1	NM_001150484	unknown
SAD1-IP127	1	XM_002467492.	unknown
SAD1-IP128	1	XM_002445936	unknown
SAD1-IP129	1	NM_001175235	unknown
SAD1-IP130	1	EU976041	unknown

Name IP [N, C]	Recovery (X)	Accession	Annotation
SAD1-IP131	1	NM_001149012	unknown
SAD1-IP132	1	NM_001151504	unknown
SAD1-IP133	1	AC206303	unknown
SAD1-IP134	1	BT087990	unknown
SAD1-IP135	1	NM_001150065	unknown
SAD1-IP136	1	NM_001138154	unknown
SAD1-IP137	1	XM_002467701	unknown
SAD1-IP138	1	FJ910859	unknown
SAD1-IP139	1	unknown	unknown

[N, C] Known or predicted to localize to cell nucleus (N) or cytoplasm (C).

2.8.9 Bioinformatic Analysis of SAD1

To predict interaction domains of SAD1, the protein sequence was analyzed via the protein computational prediction servers; SignalP, PROSITE and BDM-PUB (Emanuelsson et al., 2007; Li et al., 2009; Sigrist et al., 2010). SignalP 3.0 revealed presence of a secretion signal peptide (probability = 1), which is likely cleaved between AA position 24 and 25 of SAD1 (probability = 0.833) (Figure 41). PROSITE predicted three phosphorylation sites within the SAD1 sequence; two predicted to be protein kinase C phosphorolytion sites at AA positions 86-88 and 108-110, and one predicted to be casein kinase II phosphorylation site at AA position 163-166 (Figure 41). Additionally two N-myristoylation sites were predicted at AA positions 21-26 and 27-32 (Figure 41). BDM-PUB predicted an ubiquitination site at lysine (K) position 118 with score 1.69 (threshold = 0.3) (Figure 42).

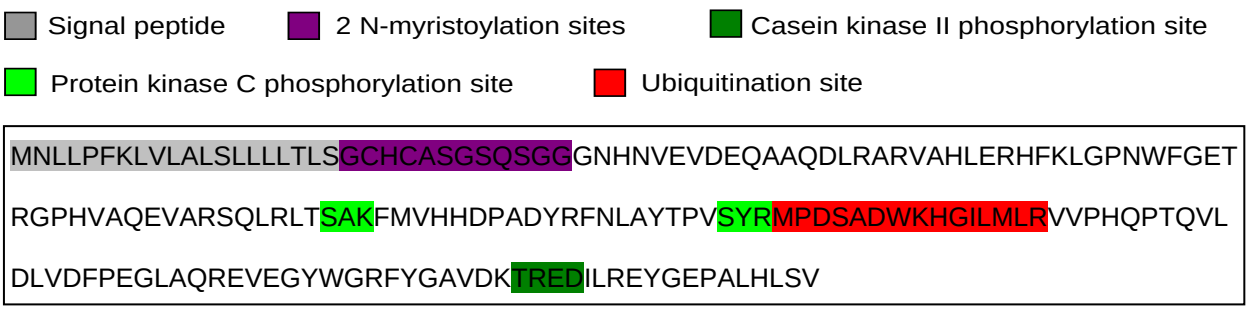

Figure 42. SAD1 domain prediction analysis. Protein sequence of SAD1 highlighted with different colors corresponding to predicted domains. Signal peptide domain was predicted by SignalP 3.0 server. N-myristoylation and phosphorylation sites were predicted by PROSITE server. Ubiquitination recognition domain (red) and ubiquitination site (K) was predicted by BDM-PUB server.

2.9 Characterization of *vag1*

2.9.1 Complementation of *vag1*-Deletion

To confirm the reduced virulence phenotype of the *vag1* (sr10079) deletion, *vag1* was re-introduced at the *mig1* locus of the two compatible Δ*vag1* strains to generate the Δ*vag1+vag1* strains. Integration of *vag1* at the *mig1* locus was verified by PCR and Southern blot. Southern blot analysis showed that all the Δ*vag1+vag1* strains contained multiple copies of *vag1*. Maize infection with the Δ*vag1+vag1* strains showed that re-introduction of *vag1* in multiple copies at the *mig1* locus could complement the *vag1* deletion phenotype by restoring the rates of spore formation to that of wt (Figure 43).

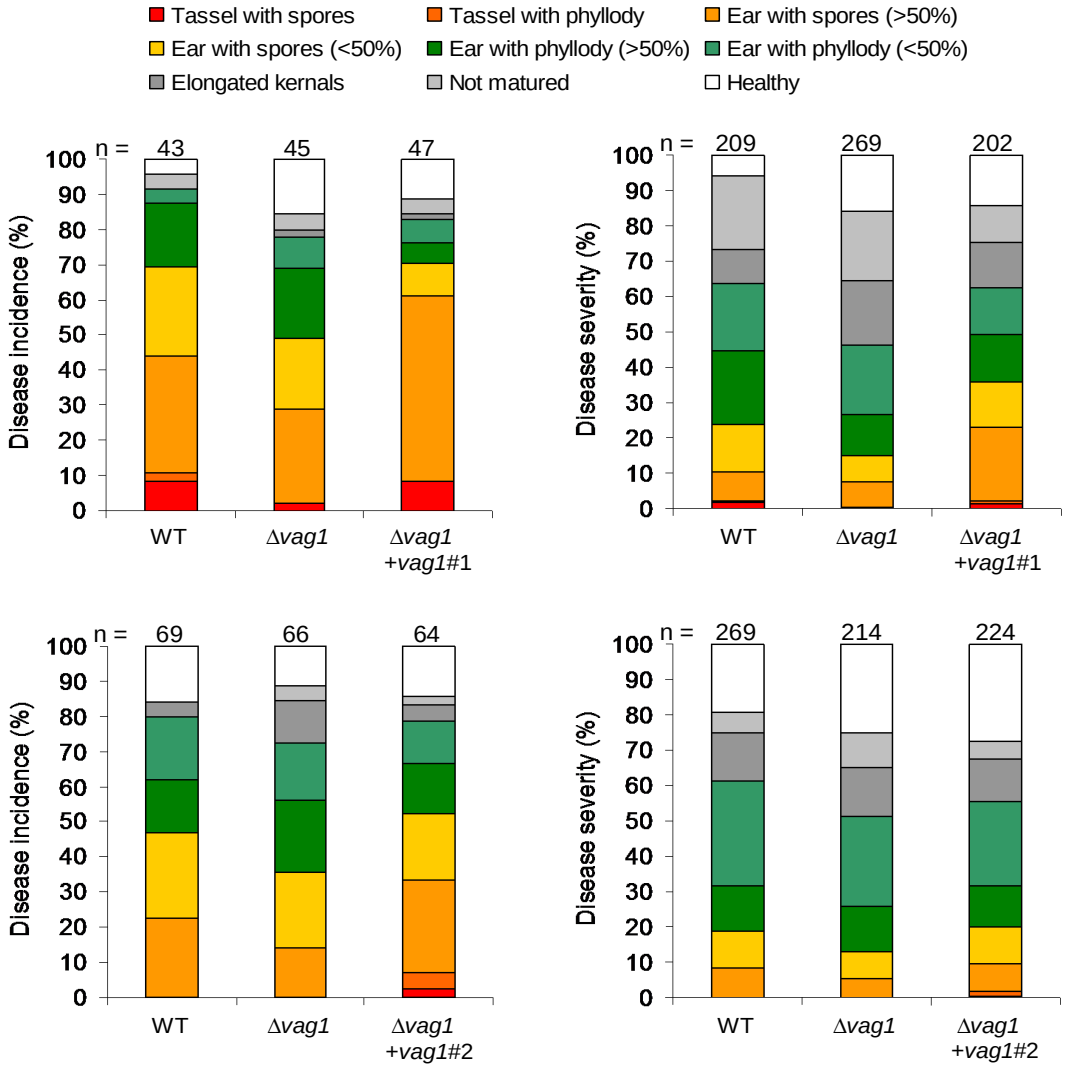

Figure 43. Virulence of *S. reilianum vag1* complementation strains on *Z. mays* 'Gaspe Flint'. Disease

incidence (left) and disease severity (right) of *vag1* deletion mutants and Δ*vag1+vag1* strains in comparison to WT. Disease incidence expressed as percent of plants displaying highest symptom. Disease severity expressed as percent of inflorescences in each category from the total number of inflorescences. Two independent compatible strain pairs of the Δ*vag1+vag1* mutants (1, HG157 X HG161; 2, HG158 X HG162) and one compatible strain pairs of the Δ*vag1* mutants (HG89 X HG92) were used for infections. The Δ*vag1+vag1* strains carry multiple integrated copies of the *vag1*. The values are means of two and three infection experiments in top and bottom experiments, respectively.

2.9.2 Expression Pattern of *vag1*

The expression pattern of *vag1* was examined. Using RT-PCR the *vag1* transcript could be detected in *S. reilianum* sporidia growing in liquid culture, hyphae growing in 3rd leaves at 3 dpi and in ears at 4 wpi (Figure 44A). To get insight into the regulation of *vag1* transcripts, qRT-PCR was used to quantify the *vag1* transcripts *in planta* relative to that of sporidia in liquid culture. The expression of *vag1* dramatically increased to more than 70 fold in infected leaves, nodes and ears relative to expression in liquid culture (Figure 44B). The up-regulation of *vag1 in planta* supports a function during plant colonization.

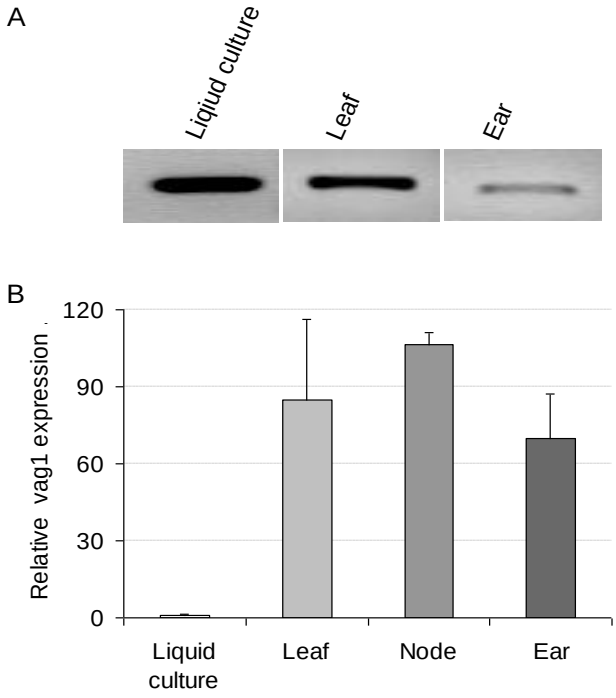

Figure 44. Expression of *vag1* in liquid culture and *in planta*. (A) The expression of *vag1* detected in *S. reilianum* sporidia growing in liquid culture (OD_{600} = 0.5), in infected leaves (3 dpi) and ears (4 wpi)

by RT-PCR. (B) Quantification of *vag1* transcripts by qRT-PCR in infected leaves (3 dpi), nodes (15 dpi) and ears (4 wpi) relative to the sporidia in liquid culture (OD_{600} = 0.5). The expression of *vag1* in all samples was normalized to the housekeeping *ppi* transcripts. Error bars represent SEM of three biological replicates. Each biological replicate is a pool of at least 10 samples.

2.9.3 Proliferation Behavior of the *vag1* Deletion Mutant

To understand how *vag1* could contribute to reduced spore formation in the inflorescences, the proliferation density of the *vag1* deletion strains was examined as indicated in chapter 2.8.2. In infected leaves, *vag1* deletion mutants showed a significantly higher ratio of DNA abundance of mutant to wt (p-value = 0.05) (Figure 45) indicating that *vag1* deletion mutant hyperproliferated in the leaf. Interestingly, in nodes, the *vag1* deletion mutant showed a significant reduction (two third) in fungal DNA in comparison to wt (p-value = 0.05) (Figure 45) indicating that proliferation was reduced in the *vag1* deletion mutant, suggesting that the mutant was hindered before reaching the inflorescence.

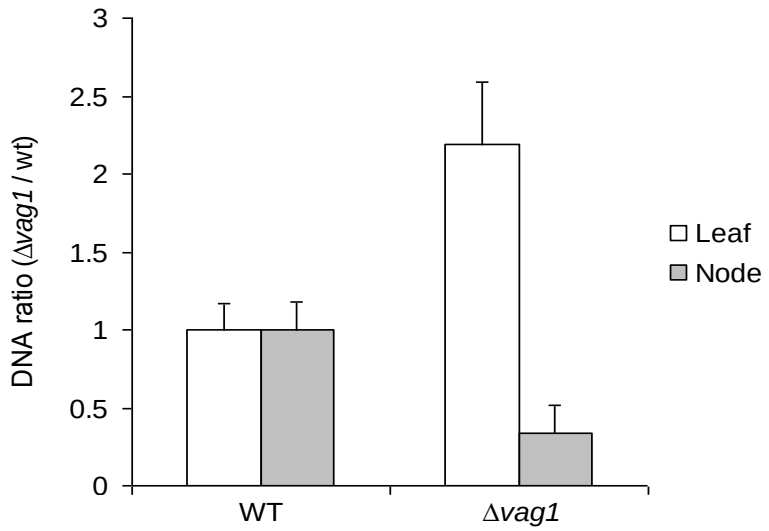

Figure 45. Proliferation density of *vag1* deletion mutant in the leaves and nodes of infected *Z. mays* 'Gaspe Flint'. Ratio of DNA abundance of *vag1* deletion mutant to relative to wt was calculated as measure of mutant proliferation density. Fungal DNA (*ppi*) quantity was normalized by plant DNA (*actin*) quantity. DNA was extracted from 3-cm pieces 3rd leaves below the injection hole at 3 dpi and 3rd nodes at 15 dpi. Each biological replicate is a pool 10 plant tissue infected with wt or mutant strains. Error bars represent SEM of three biological replicates.

2.9.4 Localization of VAG1 in *S. reilianum*

For VAG1 protein localization, *vag1* was fused to *gfp* and the fusion construct was integrated at the *mig1* locus in the two compatible Δ*vag1* strains to generate the Δ*vag1+vag1*:*gfp* strains. The transformants were verified by PCR and Southern blot. In Southern blot analysis showed that the Δ*vag1+vag1-gfp* strains contained multiple copies of the *vag1*:*gfp* fusion construct. Introduction of *vag1:gfp* at *mig1* in multiple copies resulted in complementation of the *vag1* deletion phenotype by restoring the rates of spore formation to that of wt (Figure 46A) indicating that the VAG1-GFP fusion protein is functional.

To monitor VAG1 localization, GFP fluorescence of Δ*vag1+vag1*:*gfp* strains was investigated by confocal microscopy. GFP signals were detected in sporidia, conjugation hyphae and dikaryotic filaments of Δ*vag1+vag1*:*gfp* strains on leaves 1-2 dpi (Figure 46B). I could not detect GFP signals in leaves or leaf sheaths at 2-7 dpi. Surprisingly, in ear sections, GFP signal could be detected around fungal hyphae and at hyphal tips (Figure 46C). The pattern of VAG1 localization indicates that the protein is secreted.

2.9.5 Bioinformatic Analysis of VAG1

To get insight into the probable functions of VAG1, the VAG1 sequence was analyzed via the protein domain computational prediction servers; SignalP and PROSITE (Emanuelsson et al., 2007; Li et al., 2009; Sigrist et al., 2010). SignalP 3.0 revealed presence of a secretion signal peptide (probability = 0.99), which is likely cleaved between AA positions 25 and 26 of VAG1 (probability = 0.763) (Figure 47). PROSITE predicted seven phosphorylation sites within the VAG1 sequence; three are predicted to be protein kinase C phosphorolytion sites at AA positions 61-63,119-121 and 149-151, and four are predicted to be casein kinase II phosphorylation sites at AA positions 39-42, 46-49, 73-76 and 154-157. Additionally, two N-myristoylation sites at AA positions 68-73 and 135-140, and a nuclear localization signal at AA position 120-134 were predicted (Figure 47). BDM-PUB predicted an ubiquitination site at lysine (K) position 52 with score 1.46 (threshold = 0.3) (Figure 47).

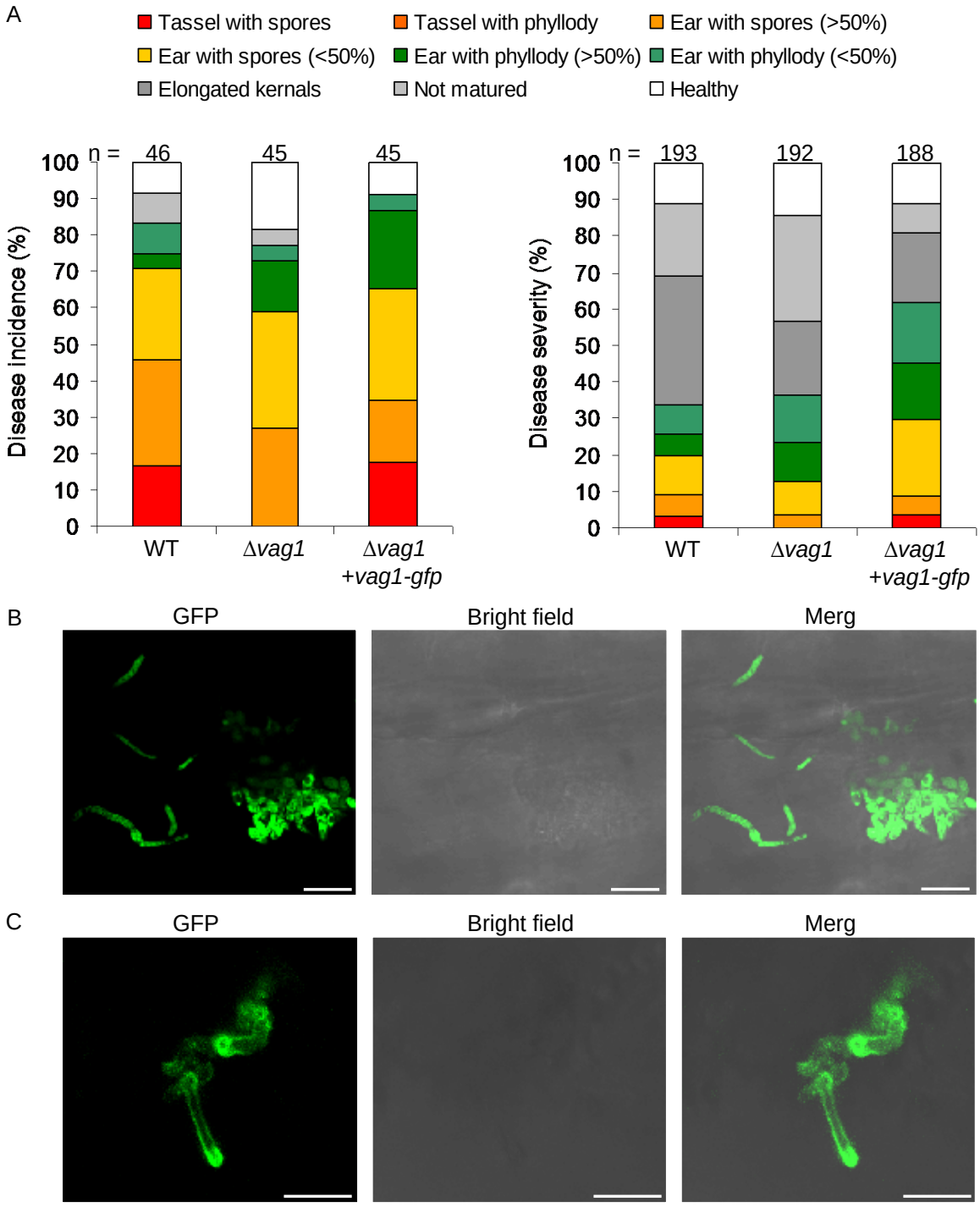

Figure 46. Localization of VAG1 *on* and *in planta*. (A) Disease incidence (left) and disease severity (right) of *vag1* deletion and Δ*vag1+vag1*:*gfp* strains in comparison to WT on *Z. mays* 'Gaspe Flint'. Disease incidence expressed as percent of plants displaying highest symptom. Disease severity expressed as percent of inflorescences in each category from the total number of inflorescences. One compatible strain combination of the Δ*vag1+vag1*:*gfp* mutants (HG189 X HG196) and of the Δ*vag1* mutants (HG89

X HG92) were used for infection. The Δ*vag1+vag1*:*gfp* strains carry multiple integrated copies of the *vag1*:*gfp* construct. The values are means of two independent experiments. (B) GFP signal of the VGA1-GFP fusion protein showing accumulation of the signals in sporidia, conjugation tubes and dikaryotic filaments on the leaf surface. Bars = 20 µm. (C) Intercellular GFP signal around hyphae and at the hyphal tips in a section of an ear. B and C are z-stacks of confocal images.

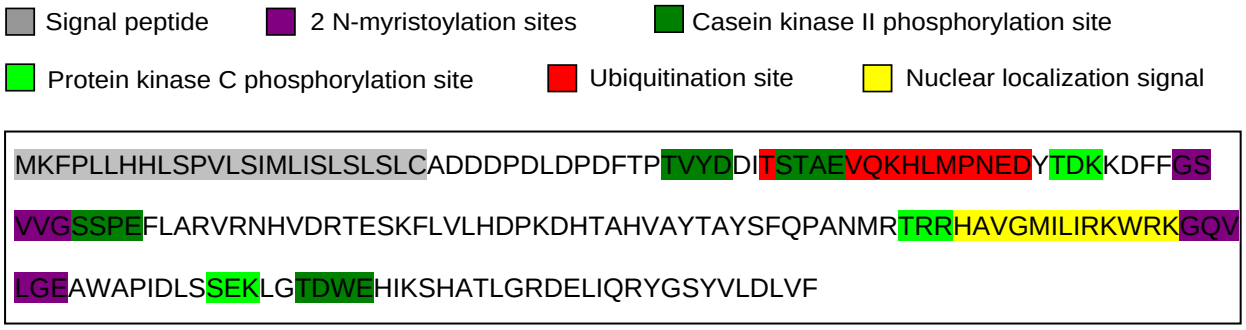

Figure 47. VAG1 domain prediction analysis. Protein sequence of VAG1 highlighted with different colors corresponding to the predicted domains. Signal peptide domain was predicted by SignalP 3.0 server. N-myristoylation, phosphorylation sites and the nuclear localization signal were predicted by the PROSITE server. Ubiquitination site (K) was predicted by BDM-PUB server. The phosphorylation site STAE overlaps with the ubiquitination recognition domain TSTAEVQKHLMPNED.

3. DISCUSSION

The core objective of the current work was to understand the symptoms caused by *S. reilianum* infection of maize. Understanding the host and pathogen factors that are involved in disease development could provide an insight into the mechanisms by which the pathogen is able to overtake the plant immune system and cause symptoms. In this work, I investigated the head smut symptoms from both the maize and the *S. reilianum* sides. From the maize side, the developmental changes in maize inflorescence and branching architectures that are caused by *S. reilianum* were dissected. From the *S. reilianum* side, pathogen effectors that were associated with virulence and symptom development were identified and characterized.

3.1 Molecular Dissection of *S. reilianum* Symptoms in Maize

S. reilianum caused a number of developmental changes in the inflorescences of infected maize plants. Infected ears showed loss of meristem identity and determinacy, and loss of organ identity. Loss of organ identity occurred at all floral organs (glume, lemma, lodicule, carpel, palea and stamen) in leafy ears (Figure 9). In eary ears and phyllodied tassels, floral organs showed reversion into vegetative structures, with the exception of the most inner whorl that developed an inflorescence (Figure 10). Additionally, *S. reilianum* induced suppression of apical dominance in the branches of female inflorescences (Figure 7).

3.1.1 How Could Infection of Maize by *S. reilianum* Lead to Different Morphologies of the Colonized Inflorescences?

The developmental decision of leafy or eary ear formation might be made by the crucial timing of inflorescence invasion by *S. reilianum*. If the fungus invades the female inflorescence at an early time point of inflorescence development before the appearance of silk tissue, it can redirect the developmental program of the floral meristem to that of an inflorescence meristem and thus cause the development of ears instead of flowers. If the fungus reaches the female inflorescence after silk development and initiation of floral organs, it redirects the floral developmental program to a vegetative program giving rise to leafy ears.

In healthy plants, each of the spikelet meristems differentiates into two florets that both initiate all floral organs including carpel and stamen. Then floret development continues differently in

male and female inflorescences: Whereas in male florets the carpel primordia are aborted, in female inflorescences the complete lower floret and the stamen primordia of the upper floret are aborted (Veit et al., 1991). In the female inflorescence, the inner whorls develop three carpels, two that elongate and fuse to form the tubular silk, and one that remains rudimentary (Nickerson, 1954; Dellaporta et al., 1991). Inside the carpels, the ovule develops (Dellaporta et al., 1991).

In eary ears, a husk-like leaf forms an open structure developed at the position of carpel primordia (Figure 10B), suggesting that loss of organ identity occurred before fusion of carpel primordia was complete. In contrast, in leafy ears, the impact of *S. reilianum* on carpel development must have occurred after carpel fusion was completed, since a closed tubular onion leaf-like structure developed. In some cases, two more vegetative structures within the tubular structure could be observed that might either be the result of indeterminate growth of carpel primordia preceding loss of organ identity, or correspond to the rudimentary carpel and the ovule (Figure 9). In such cases, the primordia of the rudimentary carpel and the ovule could have been initiated but organ development was not yet terminated before *S. reilianum* exerted its effect. If in eary ears, *S. reilianum* colonized the inflorescence at an early stage of inflorescence development, all spikelets would be equally affected. Accordingly, we observed that most of the spikelets on eary ears were completely converted to eary spikelets (Figure 8C). Thus, the different morphologies of the *S. reilianum*-colonized inflorescences are most likely a result of differences in the developmental states of the florets at the time of fungal colonization.

The spatial and temporal colonization pattern of *S. reilianum* might also be responsible for the observed loss of apical dominance at ear branches appearing at basal nodes (Figure 7D). Ears develop first at the more apical nodes, and ears that appear at lower nodes are formed later. Since young seedling plants were used for infection, *S. reilianum* enters the plant via leaves developing from basal nodes. This enables the fungus to reach lower nodes first. Thus, it has time to colonize the sub-meristematic tissue before development of the inflorescence meristem. Any *S. reilianum*-induced hormonal or metabolic changes would therefore immediately affect inflorescence development. In contrast, *S. reilianum* might reach the primordia at higher nodes only after inflorescence development has completed. In this case, any *S. reilianum*-induced hormonal or metabolic changes would have little impact on inflorescence morphology. Such a scenario would also explain why female inflorescences on infected plants show phyllody much more frequently (91%, see above) than male inflorescences (5%). Since the male inflorescence

emerges from the plant apex, the fungus might only rarely be able to reach it before the completion of tassel development.

The conversion to vegetative growth could have the potential advantage for the fungus to be provided with nutrients generated by photosynthetic activity of the green leaf-like tissue. If eary ears develop, the fungus can profit in two ways: First, the husk leaves of the newly developing inflorescence will provide nutrients by photosynthesis, while the additional inflorescences will enlarge the tissue suitable for fungal proliferation and spore formation.

3.1.2 *S. reilianum* Infection Leads to Loss of Floral Organ Identity

A reversion of floral organs into vegetative structures implies a change in the identity of affected organs. Floral organ identity is regulated by a number of homeotic transcription factors including those of the MADS and the AP2 families (Coen and Meyerowitz, 1991). According to the ABCDE model that was developed for dicots, transcription factors belong to five functional classes that determine floral organ identity in different combinations (Coen and Meyerowitz, 1991; Weigel and Meyerowitz, 1994; Ng and Yanofsky, 2001; Ditta et al., 2004). While genes that carry out B, C, D, and E functions were identified in rice and maize, information about an A function outside the higher eudicots is ambiguous (Yanofsky et al., 1990; Ambrose et al., 2000; Dreni et al., 2007; Thompson et al., 2009). While AP2 carries out A function in Arabidopsis, diverse functions have been described for AP2-like genes in monocots and dicots (Tang et al., 2007; Chuck et al., 2008; Maeo et al., 2009). This suggests that monocots might follow different regulatory networks to govern floral development, and that AP2-like genes regulate additional developmental processes in monocots.

It has been proposed that lemma/palea and lodicules of monocots correspond to sepals and petals of dicots, respectively (Ambrose et al., 2000). In dicots, the organ identity of sepals is governed by A class genes, while that of petals is defined by A and B class genes (Weigel and Meyerowitz, 1994). Active B and C class genes define organ identity of stamens, C class genes of carpels and D class genes of ovules (Weigel and Meyerowitz, 1994; Colombo et al., 1995). E class genes work as scaffolds and are required for organ identity of all floral whorls (Ditta et al., 2004). In *S. reilianum* infected leafy ears, floral organs corresponding to lemma, lodicule, stamen and carpel have lost their organ identity and have reverted to vegetative leaf-like organs. This

could indicate that *S. reilianum* affects the function of A, B, C, and D genes, or of E genes to cause loss of floral organ identity.

Transcriptional analysis of young *S. reilianum* infected ears showed that the E class resembling gene *ZAG3* (*BDE*) (Thompson et al., 2009) was down-regulated (Table 1). In addition, the C class gene *ZAG1* (Mena et al., 1996) was down-regulated. Two AP2 family genes were up-regulated (Table 1) indicating an A class-typical antagonistic regulation to the C class genes (Chuck et al., 2008) but whether the two AP2 family genes fulfill other A class functions is unknown. One gene likely belonging to the B class of floral transcription factors, *ZMM29* (Münster et al., 2001) was down-regulated (Table 1). *ZAG2*, a gene that is homologous to the rice D class gene *OsMADS13* (Dreni et al., 2007) and whose expression is constrained to the ovule and extensions that form the silk (Schmidt et al., 1993; Colombo et al., 1998), was also down-regulated, as was its homolog *ZMM1* (Theissen et al., 1995). According to the UniGene data base, the B, C, D, E class transcription factors, as well as one AP2-family protein were found to be specifically expressed in floral organs (Table 1). *S. reilianum* infection apparently greatly impacts the transcriptional profile of A, B, C, D, and E class genes, supporting the observation that in infected inflorescences vegetative organs develop in place of floral organs. While *S. reilianum* infection might affect the regulation of floral organ identity genes directly it is more likely that the infection has an impact on regulatory mechanisms acting upstream of flower development such as meristem identity, local hormone concentration, or general metabolite levels that all may affect gene expression.

In this respect, it is remarkable that ROS accumulation was observed around fungal hyphae in colonized inflorescences (Figure 13). While it is unclear, whether ROS generation stems from the fungus or the plant, it is obvious that ROS are detected by the plant, since we observed a dramatic increase in the expression level of plant genes involved in detoxification of oxidative stress (Table 1). In plants, ROS are known to have a role in signaling and development (Gapper and Dolan, 2006; Møller and Sweetlove, 2010). Therefore, it is possible that the morphological changes induced by *S. reilianum* colonization of the inflorescence are an indirect result of the increased ROS levels in the plant cells. Possibly, this indirect effect is exerted via redox-regulation of glutaredoxins, that have recently been shown to play a crucial role in floral organ development (Xing and Zachgo, 2008; Li et al., 2009; Li et al., 2009). On the other hand, the increased ROS levels in infected floral tissues might be a result of down-regulation of a specific

MADS box transcription factor. It has recently been shown in rice that a mutation in the C class gene *MADS3* leads to ROS accumulation, which may be responsible for the observed decreased pollen viability (Hu et al., 2011).

3.1.3 *S. reilianum* Infection Changes Meristem Identity and Induces Meristem Indeterminacy

In eary ears, the floral whorls corresponding to lemma/palea, lodicule, stamen and carpel showed loss of organ identity leading to formation of vegetative organs, similar to what happens in leafy ears. However, in eary ears, the whorl that corresponded to the ovule developed an inflorescence (Figure 10). This indicates that the remnants of stem cells in the floral meristems did not terminate in forming ovules. Instead, the floral meristems changed identity to inflorescence meristems. These new inflorescence meristems showed loss of meristem determinacy: Transition of spikelet to floral meristems did not occur but spikelets developed inflorescence meristems (Figure 11). In addition, these newly formed inflorescences were heavily colonized by fungal hyphae, and fungal growth was prominent in the core of the inflorescence and did not extend to the surrounding vegetative organs (Figure 13). Apparently, inflorescences are preferred substrates for fungal growth. Thus, abolishing meristem determinacy may be advantageous for proliferation of the fungus, because more inflorescence tissue for colonization would be available.

How could fungal presence induce these described changes? Meristem determinacy was shown to be regulated by three *AP2* family genes, *INDETERMINATE SPIKELET1* (*IDS1*), *SISTER of INDETERMINATE SPIKELET1* (*SID1*) and *BRANCHED SILKLESS1* (*BD1*) (Chuck et al., 2002; Chuck et al., 2008). Of these, only *IDS1* was represented on the arrays and did not show changes in transcript level. However, two uncharacterized *AP2* family genes were up-regulated in *S. reilianum*-infected ears and one of them was found to have a flower-specific expression pattern (Table 1). This could hint at a role of these AP2 family members in regulating meristem determinacy.

Floral meristem identity has been shown to be additionally regulated by two redundantly acting genes, *ZAG1* and *ZAG3* (Thompson et al., 2009). The *zag1 zag3* double mutants show a severe ear phenotype, in which the floral meristems fail to develop floral organs but instead produce

branch-like structures that initiate ectopic meristems (Thompson et al., 2009). The indeterminate meristem phenotype in the *zag1 zag3* double mutants is very similar to the occurrence of inflorescence meristems that continuously differentiate into additional meristems observed in *S. reilianum*-infected eary ears (Figure 11). Since both *ZAG1* and *ZAG3* were down-regulated in young *S. reilianum*-infected ears (Table 1) their down-regulation could at least partially explain the changes in meristem fate caused by *S. reilianum* even though it is unknown how the infection influences the transcription levels of *ZAG1* and *ZAG3*.

3.1.4 *S. reilianum* Triggers Suppression of Apical Dominance

S. reilianum infected plants show an increase in the number of ears per branch (Figure 7). This observation can be explained by a loss of apical dominance leading to activation and outgrowth of the axillary meristems on the ear shank. Shanks of ears lacking silks show outgrowth of the subapical ear meristems in many maize inbred lines (Virginia Walbot, personal communication). Because loss of carpel identity precludes silk formation, the observed change of carpel identity induced by *S. reilianum* could explain the increased ear number per branch. How outgrowth of axillary meristems in maize is regulated has not been deeply studied. However, two C2H2 zinc-finger transcription factors, *RAMOSA1* (*RA1*) and *INDETERMINATE1* (*ID1*), have been identified that have a role in axillary meristem fate. Whereas *RA1* determines the fate of second-order meristems (Vollbrecht et al., 2005), *ID1* controls the transition from vegetative to reproductive growth in maize, and *id1* mutants fail to form ears (Colasanti et al., 1998). Neither RA1 nor ID1 was found to be regulated in in the microarray experiments. While one C2H2 zinc-finger family member was up-regulated in young *S. reilianum*-infected ears (Table 1), it is unknown whether the gene has a function in the regulation of meristem outgrowth.

In addition to an increased number of ears per branch, *S. reilianum*-infected plants exhibited an increased ROS level in colonized ears (Figure 7). A similar finding has been described for the *Epichloe festucae*-perennial ryegrass interaction. Perennial ryegrass infected with *E. festucae* strains lacking the stress-activated mitogen-activated protein kinase gene *sakA* showed an elevated ROS level and excessive tillering (Eaton et al., 2010), thereby linking ROS accumulation with loss of apical dominance.

Initiation of vegetative and reproductive development in maize has recently been shown to be mediated by the tryptophan aminotransferase VANISHING TASSEL2, an enzyme involved in auxin biosynthesis (Phillips et al., 2011). One gene encoding an L-tryptophan 2-oxoglutarate aminotransferase was down-regulated upon maize infection with *S. reilianum* (Table 1) possibly linking auxin to the observed developmental defects in infected inflorescences. Axillary meristem initiation in maize has been shown to be regulated by *BARREN INFLORESCENCE2* (*BIF2*), which encodes a serine/threonine protein kinase (McSteen and Hake, 2001; McSteen et al., 2007). BIF2 has been shown to interact with BARREN STALK1 (BA1), a bHLH protein required for the initiation of axillary meristems in maize (Gallavotti et al., 2004; Skirpan et al., 2008). BIF2 and BA1 have been implicated in polar auxin transport (Wu and McSteen, 2007; Gallavotti et al., 2008). It was suggested that *BIF2* functions upstream of polar auxin transport and that polar auxin transport is required for *BA1* expression (Bennetzen and Hake, 2009). This indicates a tight connection of auxin regulators involved in axillary meristem initiation. Generation of local auxin maxima is known to be necessary for axillary meristem formation (Gallavotti et al., 2008). Interestingly, the auxin content of young *S. reilianum*-infected ears at 4 wpi showed an increase of 30% relative to control ears. This increase was detectable although complete inflorescences were collected at a stage where the inflorescences only partially showed symptoms. Thus, we cannot exclude a local auxin accumulation to much higher concentrations than the measured one. PAT plays the central role in apical dominance, regardless the auxin concentration. (Sachs, 1981). For activation of the axillary bud, the bud must generate PAT, and export auxin to the stem (Domagalska and Leyser, 2011). Hence, local auxin maxima could be responsible for axillary meristem activation and consequently lead to the observed increase in the number of ears per branch in *S. reilianum*-infected plants.

Interestingly, an elevation of the level of auxin was observed in infected ears at 4 wpi but the increased ear number per plant was observed at 7-8 wpi. In the future, auxin concentrations should be determined in infected and healthy ears at 5, 6 and 7 wpi to cover the interval of suppression of apical dominance. Remarkably, zeatin, a cytokinin, was elevated 3 fold in *S. reilianum*-infected ears (77 ± 10 pmol/g fresh weight) in comparison to healthy ears (26 ± 8 pmol/g fresh weight) at 7 wpi. Zeatin could not be detected at 4 wpi (see Materials and Methods). Since cytokinin is negatively regulated by auxin (Nordström et al., 2004; Tanaka et al., 2006), elevated cytokinin levels from 4 wpi to 7 wpi could be the results of reduced auxin

levels at 7 wpi. Nevertheless cytokinin can promote axillary bud outgrowth even in the presence of apical auxin (Sachs and Thimann, 1967). Thus the *S. reilianum*-induced cytokinin could directly activate axillary bud even in the presence of high auxin levels. Auxin levels should also be measured at 7 wpi in the future to verify whether auxin concentration is associated with suppression of apical dominance.

3.1.5 Proposal for *S. reilianum*-Mediated Changes in Inflorescence and Branching Architectures

S. reilianum infection of *Zea mays* 'Gasp Flint' induced loss of apical dominance and led to two major modifications of the inflorescences. Loss of organ identity was evident in leafy ears, eary ears and phyllodied tassels. Loss of meristem identity and determinacy was exclusive to eary ears and phyllodied tassels. The timing of *S. reilianum* colonization relative to the developmental state of the colonized inflorescence could be decisive for the outcome of the floral modification resulting in leafy or eary ears. *S. reilianum* colonized inflorescences showed higher levels of ROS, auxin and cytokinin, and misregulation of floral regulatory transcription factors. In accordance with the expectations of the ABCDE model, we observed up-regulation of A and down-regulation of B, C, D and E class genes. Together, these changes might explain, how *S. reilianum* modulates floral architecture of maize inflorescences (Figure 48). While floral gene regulation might be a secondary consequence of increased ROS or auxin levels, it could also be that *S. reilianum* directly regulates key players controlling floral gene expression, e.g. via secretion of small effector proteins that are translocated into the plant cells. Future experiments will clarify whether and how ROS, auxin, cytokinin or fungal secreted effectors contribute to symptom development of *S. reilianum*.

3.2 Characterization of Symptom and Virulence Determinants in *S. reilianum*

In this work, several novel effector genes with impact on virulence of *S. reilianum* were identified and functionally characterized. To four of the candidate genes (sr10057, sr10060, *sruni1*, *sruni2*) avirulence functions could be attributed. The genes of clusters 19A, cluster 5-1uni, and *sruni5* exhibited virulence function. In addition to a function in virulence, genes of cluster 19A3 were associated with leaf tip death in infected plants. The *sad1* and *sad2* were involved in suppression of apical dominance.

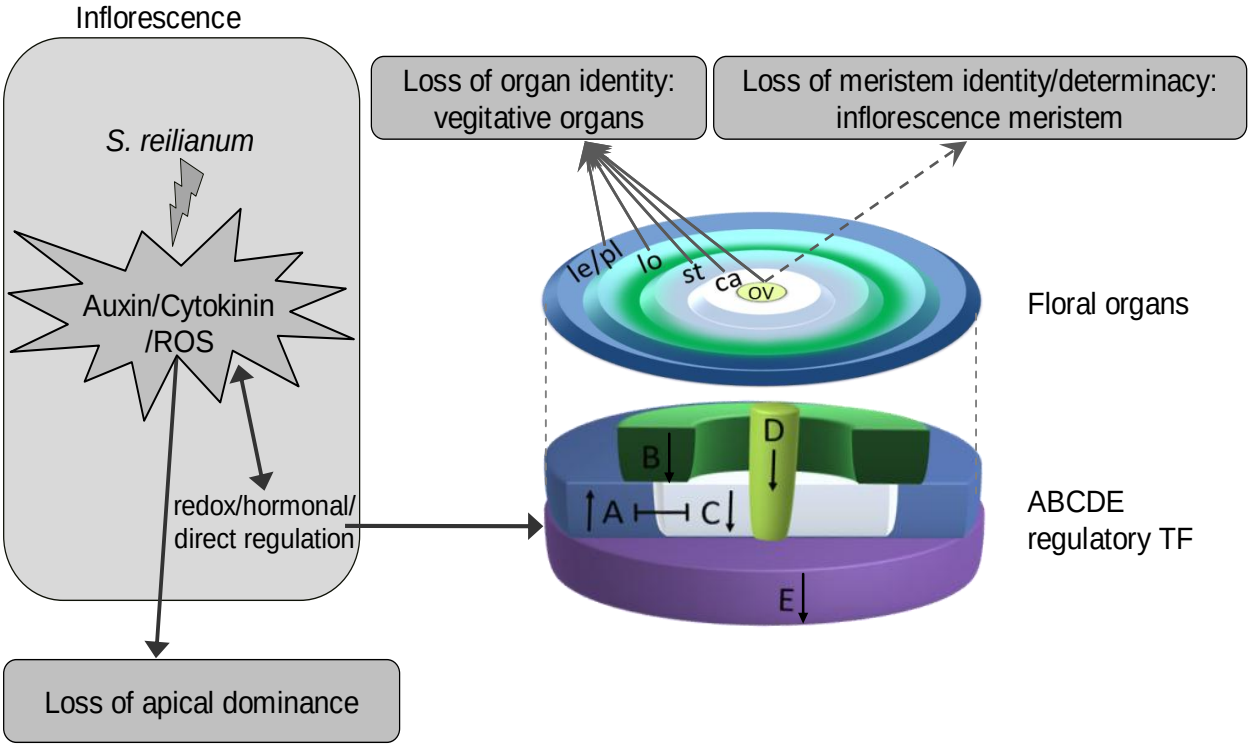

Figure 48. Hypothetical model of changes in inflorescence and branching architectures of maize induced by *S. reilianum*. Fungal colonization leads to ROS, auxin and cytokinin accumulations in the inflorescence. Possibly, increased ROS, auxin or cytokinin concentrations at the infected ear axillary meristems lead to promoting outgrowth of the subapical inflorescence meristems leading to suppression of apical dominance and consequently a change in branching architecture. Additionally, loss of organ identity triggered by *S. reilianum* could be the result of an altered expression of the A-, B-, C-, D- and E-class genes. Altering expression of the ABCDE regulators could be the result of a direct regulation by fungal secreted proteins, or of an indirect regulation by auxin, cytokinin and/or ROS. Alternatively, increased accumulation of auxin, cytokinin and ROS could be the result of modulation of the ABCDE regulators. *S. reilianum* could trigger loss of meristem identity and determinacy (dashed arrow), if it reached the floral meristem before stem cells terminate into an ovule. Black arrows indicate up- or down-regulation of ABCDE transcription factors. Lemma (le), palea (pl), lodicule (le), stamen (st), carpel (ca), ovule (ov).

3.2.1 Genome Comparison as Tool for Effector Identification

I sought to identify *S. reilianum* genes contributing to suppression of apical dominance, spore formation and leaf tip death in infected plants. *S. reilianum* is a close relative of *U. maydis* and *U. hordei* (Begerow et al., 2006). Nevertheless the three fungi differ in the mode of plant

colonization and symptom formation (Lübberstedt et al., 1999; Singh and Mathur, 2004; Brefort et al., 2009). Therefore, the genome sequences of *S. reilianum*, *U. maydis* and *U. hordei* were compared. The genome comparison resulted in three categories of gene candidates. The first gene category was constrained to the unique genes of *S. reilianum* that did not exist in *U. maydis* or *U. hordei*. Possibly the *S. reilianum* unique genes could be responsible for properties of *S. reilianum* that are not displayed by the close relatives, e.g., phyllody formation. The second gene category represented genes that occurred in *S. reilianum* and *U. hordei* but were absent in *U. maydis*. *S. reilianum* and *U. hordei* colonize the plant systemically (Lübberstedt et al., 1999; Singh and Mathur, 2004), while *U. maydis* has a local mode of plant colonization (Snetselaar and Mims, 1992). Therefore genes of the second category could be involved in determining the mode of colonization. The third gene category involved genes that were predicted to encode proteins with low sequence conservation between *S. reilianum* and *U. maydis*, maize pathogens that cause different symptoms. Genes of this category could encode symptom determinants. Because selecting gene candidates this way is high risk, and each category contained a large number of genes, it was reasonable to choose some candidates from each category for functional analysis (Chapter 2.4).

From the first category, I deleted 22 *S. reilianum* unique genes that occurred on the genome as six individual genes and 5 gene clusters (Chapter 2.5). Because an effector should interact with proteins from the host cell, secretion from the pathogen is an essential property. In *U. maydis* it was shown that genes predicted to encode secreted proteins were potential virulence factors that facilitate maize infection (Kämper et al., 2006). Therefore the unique gene candidates were selected based on their potential to encode secreted proteins. However, deletions of *sruni1* or *sruni2* led to increased susceptibility of *S. reilianum* on maize ‘Gaspe Flint’, whereas deletion of *sruni5* or gene cluster 5-1uni led to reduced susceptibility (Figure 22A, B, G). Otherwise, no remarkable difference in virulence could be observed by deletion of the other unique candidate genes. Thus virulence determinants could be identified from the first category, and none of the unique genes studied in this work was involved in symptom specificity.

From the second gene category, the genes encoding the RNAi components were found only in *S. reilianum* and *U. hordei* (Figure 20). RNAi was proven to be functional in *S. reilianum* (Figure 23). Nevertheless deletion of the only *dicer*, a key player in RNAi, in *S. reilianum* did not lead to a change in virulence or in behavior under different stresses (Figure 24, 25). It has

been shown that *dicer2* of *Magnaporthe oryzae* was functional in RNAi, whereas *dicer1* had an unknown function (Kadotani et al., 2004). Also Dicer like 2 functioned as antiviral defense mechanism in *Cryphonectria parasitica*, whereas Dicer like 1 did not show phenotypic difference to wt (Segers et al., 2007). *U. maydis* can be infected by *U. maydis virus H1* (Voth et al., 2006). So far it is unknown whether *S. reilianum* can be infected with any mycoviruses. Since *U. maydis* does not harbor RNAi components, *dicer* could have a defensive function against viral attack in *S. reilianum*. Accordingly, the susceptibility of the *dicer* deletion to *U. maydis virus H1* should be tested. In the future, *gfp* silencing efficiency should be tested in the *dicer* deletion mutant of *S. reilianum* to verify whether *dicer* is at all involved in RNAi.

From the third gene category, gene cluster 19A was predicted as the largest region with low sequence conservation between *S. reilianum* and *U. maydis*, which differ in symptom formation (Schirawski et al., 2010). The gene cluster is predicted to encode 29 proteins; among them 24 putatively secreted proteins (Figure 21). 19A deletion led to reduced level of spore formation (Figure 26) and appearance of leaf tip death (Figure 29A). Reduced spore formation could be assigned to different parts of 19A (Figure 26), whereas leaf tip death could be restricted to 19A3 (Figure 21, 29B). In addition, deletion of 19A2 showed abolishment of the suppression of apical dominance symptom (Figure 21, 31). Thus these findings articulated the power of genome comparison in identification of potential pathogen effectors that functions as symptom determinants.

3.2.2 19A, 5-1uni and *sruni5* Genes Enhance Virulence of *S. reilianum*

The Δ19A1A2, Δ19A1, Δ19A2 and Δ19A3 mutants exhibited reduced disease incidences and severities (Figure 21, 26, 28A) indicating that the three deleted regions of 19A are contributing to virulence. The reduced virulence of Δ19A1A2 was shown to be an additive effect resulting from deletion of both 19A1 and 19A2 (Figure 26). Δ19A1 mutant was particularly reduced in spore formation. By RNA sequencing analysis, we could find out that the genes of 19A1 were differentially regulated. Some genes were expressed in sporidia, *S. reilianum*-inoculated leaves and ears, and others showed constrained expression to leaf or ear (H Ghareeb, J. Schirawski, unpublished). Genes that are expressed in the ear could have direct or indirect impact on spore formation. Genes that are not expressed in the ear could have an indirect influence on spore formation and could promote pathogen fitness in colonized leaf or node tissues. Further work is

underway to dissect the individual contributors of cluster 19A1 to virulence (J. Schirawski, personal communication).

The four genes of 19A2 were predicted to encode secreted proteins and were shown to be highly expressed *in planta* (H Ghareeb, J. Schirawski, unpublished). Therefore their contribution to virulence was further studied. Individual deletions of the four genes of 19A2, Δsr10073, Δ*sad2*, Δ*sad1* and Δ*vag1*, were generated. The Δsr10073, Δ*sad2*, Δ*sad1* and Δ*vag1* mutants showed reduced disease incidences and severities, which were mearly equal to that of Δ19A2 (Figure 31). This indicates that the proteins encoded by cluster 19A2 might not function individually but might interact to form an effector complex. The 19A2 genes have 2 orthologues in cluster 19A of *U. maydis*, *tin4*, *tumor inducing gene 4*, (orthologue of sr10073) and *tin5*, *tumor inducing gene 5*, (orthologue of *sad2*, *sad1* and *vag1*) (Figure 21). After having identifyed a role of 19A2 genes in virulence, the orthologues of 19A2 genes were deleted in *U. maydis*. Consistently, deletion of *tin4* and *tin5* led to reduced tumor formation (T. Brefort and R. Kahmann, personal communication). Thus the virulence function of 19A2 genes could be conserved among smuts. To verify a conserved virulence function of 19A2 genes of *S. reilianum*, and of *tin4* and *tin5* of *U. maydis*, a complementation study should be performed by expressing the 19A2 genes of *S. reilianum* in the *U. maydis* Δ*tin4* and Δ*tin5* mutants and expressing the *tin4* and *tin5* genes in the Δ19A2 strains of *S. reilianum*.

Deletion of *sruni5* and unique gene cluster 5-1uni led to reduced disease incidence and disease severity (Figure 22). 5-1uni contains two genes sr13374 and sr13375. The genes *sruni5*, sr13374 and sr13375 were predicted to encode secreted proteins (Table 3). Secretion of their encoded protein is still to be experimentally proven. However, using RNA sequencing, *sruni5*, sr13374 and sr13375 were shown to be expressed in sporidia and up-regulated in *S. reilianum*-inoculated leaves. Additionally, *sruni5* and sr13374 were dramatically up-regulated in *S. reilianum*-colonized ears (H. Ghareeb and J. Schirawski, unpublished). Up-regulation of *sruni5*, sr13374 and sr13375 *in planta* and the putative secretion of their encoded proteins supported their function as effectors.

Since *sruni5*, 19A and 5-1uni were shown to encode virulence determinants they could function to promote pathogen fitness and enhance disease development on maize. The mechanism by which these virulence proteins impart susceptibility is still to be investigated. However, their

mode of action in mediating virulence could be similar to some known effectors. The bacterial virulence effectors are the most intensively studied. They are known so far to suppress the host defense by targeting three plant processes, namely protein turnover, RNA homeostasis, and phosphorylation pathways (Rooney et al., 2005; Römer et al., 2007; Block et al., 2008; Xiang et al., 2008).

3.2.3 sr10057, sr10060, *sruni1* and *sruni2* Fulfill Avirulence Functions

The genes *tin2* and *tin3* are two of the major effectors of cluster 19A of *U. maydis*. They encode secreted virulence proteins that facilitate tumor formation on maize (T. Brefort and J. Kahmann, personal communication). sr10057 and sr10060 that occur in the cluster 19A3 of *S. reilianum* are orthologues of *tin2* and *tin3*, respectively (J. Schirawski, personal communication). Since the *S. reilianum* Δ19A1A2 and Δ19A3 mutants induced leaf tip death and showed reduced disease incidence and severity (Figure 26, 29A), the contributions of sr10057 and sr10060 to these phenotypes was investigated. The two genes were individually re-introduced in the Δ19A1A2 mutant to test whether they can complement the mutant phenotypes. Regarding leaf tip death, no difference could be observed between Δ19A1A2 and Δ19A1A2+sr10057 and Δ19A1A2+sr10060 (Figure 29B) indicating that neither gene is involved in leaf tip death. Interestingly, Δ19A1A2+sr10057 and Δ19A1A2+sr10060 mutants showed less spore formation than the Δ19A1A2 strains (Figure 28) indicating that both genes could have avirulence functions. If they do have avirulence function, gene deletion should lead to hypervirulent strains. Deletion analyses of the two genes are currently underway.

sr10057 and sr10060 show only low sequence conservation to *tin2* (38%) and *tin3* (32%), respectively. In addition, expression of sr10057 under control of *tin2* promoter in the *ip* locus of the *U. maydis* Δ*tin2* mutant or expression of sr10060 under control of *tin3* promoter in the *ip* locus of the *U. maydis* Δ*tin3* mutant did not complement the virulence or loss of anthocyanin phenotypes of *U. maydis* deletion strains (T. Brefort, personal communication). Together, these results indicate that sr10057 and sr10060 have a different function in *S. reilianum* than their orthologues, *tin2* and *tin3*, in *U. maydis*. Δ19A mutants of *U. maydis* were unable to form tumors on leaves of maize seedlings (Kämper et al., 2006), but readily did so on adult leaves and tassels (Skibbe et al., 2010). Phenotype discrepancies of the Δ19A strains of *U. maydis* on the different plant tissues were suggested to be due to differential gene expression (Skibbe et al., 2010). *tin2*

and *tin3* were shown to be highly up-regulated in leaves of seedling but not in the adult leaves or tassels (Skibbe et al., 2010). In contrast, the transcripts of sr10057 and sr10060 were shown to be up-regulated in *S. reilianum*-infected leaves and ears at 3 dpi and 4 wpi (H. Ghareeb and J. Schirawski, unpublished). Hence, the different functions of sr10057 and sr10060 in *S. reilianum*, and their orthologues *tin2* and *tin3* in *U. maydis* can be explained by diversifications of their AA sequence and by differences in expression patterns.

The Δ*sruni1* and Δ*sruni2* mutants showed increased disease incidence and severity in comparison to wt. Although complementation of the phenotypes by re-introduction of the deleted still needs to be performed to establish the casual link between phenotype and gene loss, the hypervirulence phenotypes of the Δ*sruni1* and Δ*sruni2* mutants indicate that the two deleted genes fulfill avirulence functions. All four proteins with potential avirulence function deleted in this study (SR10057, SR1060, SRUNI1 and SRUNI2) were predicted to harbor signal sequence for secretion. Additionally, transcripts of sr10057, sr10060, *sruni1* and *sruni2* could be detected in infected plant materials using RNA sequencing (H. Ghareeb and J. Schirawski, unpublished). Whereas the highest expression of sr10057 was in the leaves, the highest expression of sr10060 was in the ears. Transcripts of *sruni1* were detected in infected ears but not in infected leaves or sporidia. The *sruni2* transcripts were detected in sporidia and infected leaves and it was dramatically up-regulated in infected ears. (H. Ghareeb and J. Schirawski, unpublished). Hence, putative role could be postulated for *sruni1*, *sruni2* and sr10060 in the ears, and for sr10057 in leaves. Protein secretion and the roles *in planta* of the four genes will have to be experimentally proven.

The avirulence function of sr10057, sr10060, *sruni1* and *sruni2* could be a result of a change in the fitness of *S. reilianum* whenever they are expressed. The negative impact on pathogen fitness can be a result of attenuation in mutant growth and/or aggressiveness (De Wit, 1997). According to Guard model, recognition of an avirulence protein (AVR) by its cognate resistance protein (R) would trigger defense mechanisms and restrict pathogen progression on the host (van der Biezen and Jones, 1998). Thus increased susceptibility of plants inoculated with the Δ*sruni1* or Δ*sruni2* strains could be explained by partial prevention of *S. reilianum* recognition by the host defense system. Similarly, reduced susceptibility of plants inoculated with Δ19A1A2 mutants expressing sr10057 or sr10060 could be explained by enhanced recognition of *S. reilianum* by the plant immune system. Assuming perception of SR10057, SR1060, SRUNI1 and the SRUNI2 in maize

cultivar Gaspe Flint, it will be indispensible to screen for their interaction partners. Identification of the plant cognate proteins could explain how these avirulence effectors trigger host immunity.

Harboring AVR can be considered a disadvantage for the pathogen but likely this is not the case. Coevolution of AVR-R interactions has been described by Guard model (van der Biezen and Jones, 1998; Dangl and Jones, 2001). The model was developed for the flax-flax rust system, where virulence (*avr*) and resistance cognate (*R*) genes have signatures of diversifying selection. Twelve variants of the *AvrL567* gene were found in 6 flax rust strains. Transient expression of 7 variants in flax leaves expressing *L5*, *L6,* or *L7 R* genes induced HR (hypersensitive cell death response) but not in that lacking expression of the *R* genes. Expression of the other 5 variants did not lead to HR could be observed. This demonstrated a diversified function of *AvrL567* variants resulting in 7 avirulence and 5 postulated virulence variants (Ellis et al., 2007). The *R* gene *L6* of flax seemed to have evolved from fusion of *L7* and *L11*. Rust strains carrying *AvrL567*, *AvrL11*, and *I* were virulent flax plants carrying *L7* and *L11* but avirulent on plants carrying *L6*. Transient expression of *L6* and *L6L11RV*, an allele of *L6* in which 11 AA were derived from *L11*, in combination with the seven *AvrL567* avirulence variants showed that *L6* recognized all variants, whereas *L6L11RV* recognized only one variant. These findings indicated that *avr* evolved to escape recognition by *R*, and *R* evolved tp improve *avr* perception (Ellis et al., 2007). Such *R*-*avr* interactions have been applicable also in other pathosystems (van der Biezen and Jones, 1998). AVR encoding genes have been also identified in *U. maydis* (Kämper et al., 2006; Schirawski et al., 2010) but their cognate *R* genes are still to be identified. So far no *R*-*avr* interactions have been described for the maize-*S. reilianum* pathosystem.

If SR10057, SR1060, SRUNI1 and SRUNI2 negatively impact on *S. reilianum* fitness, why would not *S. reilianum* dispense them to promote virulence on maize 'Gaspe Flint'? This question can be answered in the light of Guard model. Gaspe Flint possibly evolved cognate proteins that perceived SR10057, SR1060, SRUNI1 and SRUNI2. Nevertheless in other maize cultivars that do not possess their cognate proteins, the four effectors could support virulence and enhance colonization performance of the fungus. In other words, SR10057, SR1060, SRUNI1 and SRUNI2 might have had virulence functions, which can no longer be displayed on Gaspe Flint because of perception by cognate R proteins. To support this explanation, the sr10057, sr10060, *sruni1* and *sruni2* deletion mutants will need to be tested whether they show reduced virulence on other maize cultivars.

3.2.4 Does *S. reilianum* Require All Effectors for Disease Establishment?

Deletion of 17 *S. reilianum* unique genes, including 7 genes predicted to encode secreted proteins, did not lead to observable changes in virulence (Figure 22C, D, F, H-K). Nevertheless, transcripts of all of these genes were clearly detected in infected maize tissues (H. Ghareeb and J. Schirawski, unpublished). The unique genes of *S. reilianum* do not exist in the close relatives *U. maydis* and *U. hordei*. Probably the unique genes have recently evolved after speciation, and coevolved during interaction with the newly developed cultivars of maize. Supposingly, the unique proteins could enhance virulence on the cultivars that they coevolved with. Then it is reasonable not to observe a change in virulence, if Gaspe Flint does not harbor interaction partners of proteins encoded by the deleted 17 unique genes. Alternatively, the absence of phenotypes of the 17 gene deletions can be explained by the Decoy model (van der Hoorn and Kamoun, 2008) assuming that those genes encode AVR proteins. The Decoy model is a variant of the Guard model for R-AVR interaction. In the Decoy model, an AVR protein is indirectly perceived via a decoy, an effector target with no function in host defense or susceptibility that is required for R protein function. Accordingly, decoy modifications, phosphorylation, degradation..etc, by the effector will not be recognized by plants lacking the R protein, and consequentially no phenotype might be observed for this effector (van der Hoorn and Kamoun, 2008). Thus Gaspe Flint could lack the R cognate proteins of the encoded proteins of some deleted unique genes.

S. reilianum survives 2-3 months within the host from seedling till flowing stages. During that long time, *S. reilianum* encounters several barriers. First, *S. reilianum* proliferates in the leaf, node and inflorescence tissues (Figure 6). Second, *S. reilianum* has contacts with different cell types, namely, epidermal, mesophyll, bundle sheath and parenchyma cells (Figure 6) and (Martinez et al., 2000). Third, during biotrophic growth, the pathogen is subject to variable environmental conditions that influence the interaction with the host (Chapter 1.2). Likely *S. reilianum* developed various strategies to overcome tissue, cell and environmental barriers during biotrophic growth to keep compatibility with the host. Thus the phenotypes of the 17 gene deletions may be more pronounced under different conditions from those used here. Alternatively, the 17 unique genes could have such a marginal role in virulence that their contribution cannot be measured, or they could have no role in virulence.

None of gene deletions of putative effectors in *S. reilianum* led to a strong effect on virulence. That is not a surprising outcome, because resistance to *S. reilianum* was revealed to be an additive trait (Bernardo et al., 1992; Wisser et al., 2006; Chen et al., 2008). According to the Guard model (van der Biezen and Jones, 1998; Dangl and Jones, 2001), virulence of *S. reilianum* should also be conferred by large pool of effectors to counteract the additive resistance in the host. Consequently, identifying genes conditioning quantitative resistance or virulence will be challenging because of their modest phenotypic effects as has been also suggested by Wisser et al., 2006. Although several efforts have been exerted to identify resistance loci against *S. reilianum* using QTL, so far there is no resistance gene identified against the pathogen (Bernardo et al., 1992; Lübberstedt et al., 1999; Chen et al., 2008; Li et al., 2008). Thus any contribution, even if a little, of the identified virulence and *avr* genes could be meaningful in shaping pathogenicity of *S. reilianum*. Also, identification of *avr* genes will simplify identification of their cognate *R* genes, which will finally support pyramiding resistance against *S. reilianum*.

3.2.5 Gene Cluster 19A3 Inhibits Leaf Senescence

Intriguingly, deletion of cluster 19A of *S. reilianum* led to enhanced leaf tip death (Figure 29A, B). This phenotype was more specifically conferred by deletion of 19A1 or 19A3 (Figure 29C). Further analysis showed that the leaf tip death phenotype is conferred by deletion of only three genes (sr10050, sr10051 and sr10052) of cluster 19A (Y. Zhao, personal communication). The three genes belong to a gene family and are orthologues of the five *tumor induced gene 1* genes (*tin1.1-1.5*) of *U. maydis* (J. Schirawski, personal communication). Whereas the transcripts of sr10052 could not be detect *in planta*, the transcript levels of sr10050 and sr10051 were up-regulated in infected ears relative to sporida. Only transcripts of sr10050 could be detected in infected leaves (H. Ghareeb and J. Schirawski, unpublished). Their pattern of expression could indicate that lack of sr10050 is essential for triggering leaf tip death. Nevertheless, the phenotype of sr10050 deletion still needs to be experimentally proven.

The Δ19A1 mutant did not show differences in the proliferation pattern (as visualized by microscopy, not shown) or proliferation density (measured by qRT-PCR) in the leaves at 3 dpi in comparison to wt (Figure 30B). Therefore the proliferation behavior of the 19A1 mutant at 3 dpi can be excluded as reason for enhanced leaf tip death. However, the leaves inoculated with the

Δ19A1 and Δ19A3 mutants exhibited earlier chlorosis than wt, at 4 to 6 in comparison to more than 7 dpi. Chlorosis extended later preceeding leaf tip death (Figure 29A). Chlorosis is the result of chlorophyll disintegration, which is a sign of leaf senescence (Munné-Bosch and Alegre, 2004). Leaf senescence is different from programmed cell death (PCD) in that in PCD the cell death rate is fast and localized or limited to tissue or cell types (Lim et al., 2007). The leaf tip death, here, was preceded by chlorosis and wilting of the leaf tip. Thus a role of PCD in the dynamics of leaf tip death caused by Δ19A1 and Δ19A3 mutants can be excluded. It seems that the leaf tip death caused by Δ19A1 and Δ19A3 mutants is a result of accelerated leaf senescence.

Leaf senescence can be induced by several stresses such as pathogen attack, wounding, drought or nutrient deficiency, in particular nitrogen deficiency (Lim et al., 2007). Senescence can be triggered by a change in the internal hormone levels. Low cytokinin, high ethylene, high auxin, high abscisic acid, high jasmonic acid and high salicylic acid concentrations result in enhanced senescence [reviewed by (Lim et al., 2007)]. These hormones can be modulated in response to pathogen attack [reviewed by (Pieterse et al., 2009)]. Also ROS is elevated during leaf senescence (Pastori and Trippi, 1993). In addition, high sugar accumulation also has been hypothesized to play a role in senescence (Van Doorn, 2008).

Possibly sr10050, sr10051 and sr10052 could function as suppressors of leaf senescence as has been shown for the XopD effector, a type III effector from *Xanthomonas campestris* pathovar *vesicatoria* (Xcv). XopD was shown to suppress leaf senescence in infected tomato through reducing chlorophyll loss, reducing salicylic acid levels, and changing mRNA abundance of senescence- and defense-associated genes. XopD encodes a Cys protease that localizes to subnuclear foci and binds to the host DNA (Kim et al., 2008). To test whether sr10050, sr10051 and sr10052 have a role in inhibiting leaf senescence, the concentration of hormones, ROS, sugar, and nitrogen should be measured in the leaves inoculated with the leaf tip death inducing mutants.

3.2.6 Gene Cluster 19A2 Encodes Suppressors of Apical Dominance

Maize infection with strains lacking cluster 19A2 did not lead to increased ear number per plant (Figure 26, 27). Thus, suppression of apical dominance induced by wt (Chapter 3.1.4) could be

attributed to 19A2 genes. By testing the individual deletion strains of the four genes of 19A2, it was shown that suppression of apical dominance is conferred by *sad1* and *sad2* (Chapter 2.7.3). Notably, the Δ*sad1* mutants showed more prominent contribution to suppression of apical dominance than the Δ*sad2* mutants (Chapter 2.7.3). The phenotype of Δ*sad1* mutants could be complemented by re-introduction of *sad1* in the Δ*sad1* mutants (Figure 33). Verification of *sad2* deletion phenotype still needs to be confirmed by gene complementation analysis. SAD1 and SAD2 show low (25%) AA sequence identity (Chapter 2.7.4). Analysis of transcript level showed that *sad1* was 4 times higher expressed than *sad2* in infected leaves, nodes and ears (Data not shown). Although SAD1 and SAD2 showed diversification in transcript regulation and AA sequence, strains lacking either proteins failed to suppress apical dominance. Because *sad1* and *sad2* are placed next to each other, deletion of *sad2* could have impeded transcription of *sad1*, thereby showing the same phenotype of Δ*sad1* mutants. To verify this option, *sad1* transcripts could be quantified in plant tissues infected with Δ*sad2* mutants. Alternatively, SAD1 and SAD2 could influence the biosynthesis or signaling of different pathways, e.g., auxin and cytokinin, which could individually regulate apical dominance.

3.2.7 Molecular Functions of SAD1 Effector

SAD1 suppressed apical dominance in the female inflorescences of maize. To change a biological function in the host, SAD1 should be translocated into the apoplast or the host cell. Indeed, SAD1 was predicted to have secretion signal (Figure 42). In the ear, SAD1 was localized around fungal hyphae and hyphal tips, and colocalized with the cell membrane (Figure 36), indicating that SAD1 is secreted. The *sad1* expression was highly up-regulated *in planta* (Figure 34). Accordingly, SAD1 could have interacted with the host cells, thereby leading to changes in the branching architecture.

SAD1 was localized at the nucleus and cytoplasm of sorghum protoplasts (Figure 38). The same pattern of localization was observed in Arabidopsis and tobacco (C. Löfke and T. Teichmann, unpublished). Consistently, SAD1 interacted at least with 19 and 14 plant proteins known or predicted to function in the nucleus and cytoplasm, respectively (Table 5). Additionally, transcriptional activation of *AUR1-C* and *MEL1* reporter genes in yeast by SAD1 lacking its signal peptide indicated that SAD1 has a nuclear function (Figure 39). This supports a nuclear localization of SAD1 in the host cell, although no nuclear localization signal could be predicted

in SAD1 using PROSITE. SAD1 and VAG1 were suggested to be paralogos (Chapter 2.7.4). VAG1 was predicted by PROSITE to possess a nuclear localization signal (Figure 47). Thus it is not clear whether the nuclear localization of SAD1 is mediated by interaction with a protein that localizes to the nucleus or by recognition of a diversified nuclear localization signal different from that of VAG1.

The role of SAD1 in the nucleus could be either direct and or indirect. A direct role could be by binding to specific promoters of plant genes and modulating their transcription. To examine the direct nuclear function of SAD1, DNA-SAD1 interaction analysis should be undertaken to identify *cis* elements binding SAD1. These results can then be validated by determining the change in expression of SAD1 target genes. An indirect role of SAD1 could be mediated through interaction with host nuclear proteins by inhibiting or activating their function. The latter scenario is more likely based on identification of the SAD1 plant interaction partners with nuclear function (Table 5). To test the significance of indirect nuclear function of SAD1, the SAD1 interaction domain(s) with the plant nuclear proteins should be mapped and mutated. The mutated SAD1 versions should be reintroduced in Δ*sad1* mutant and then complementation of the deletion phenotype should be examined. Complementation analysis with *sad1* fused to a nuclear export signal, which can act against the nuclear localization, can reveal the importance of direct or indirect nuclear localization of SAD1. However, translocation into and nuclear localization of SAD1 in plant cells should be proven in infected maize tissue. To this end, we are currently working on generating a tagged version of SAD1 suitable for immunogold labeling of SAD1 in plant tissues infected with *S. reilianum*.

SAD1 was predicted to harbor phosphorylation sites (Figure 42). The phosphorylation sites were also predicted in the SAD1 paralogoues, SAD2 (Data not shown) and VAG1 (Figure 47). In consistence, SAD1 interacted with 5 plant kinases and 2 plant phosphatases (Table 5) suggesting that SAD1 interferes with host signaling. Additionally, SAD1 interacted with a MIG1 family member, a putative effector that is up-regulated *in planta* (H. Ghareeb and J. Schirawski, unpublished). Therefore, it is possible that SAD1 mediates its function via an effector complex. Verification of this complex will provide a new insight into the dynamics of effector function. In the future, phenotypes of *S. reilianum* strains lacking MIG1 or expressing truncated versions MIG1 that lost interaction with SAD1 should reveal the significance of this effector complex *in planta*.

SAD1 also interacted with several plant interaction partners that are involved in development, defense, transport, cytoskeleton trafficking, protein biosynthesis and metabolism (Table 5). These results could indicate several roles of SAD1 *in planta*. It cannot be excluded that some interactions do not take place in the native situation. Little is known about the SAD1 interaction partners. So far, none of the SAD1 interaction partners had a described function that can provide a direct link to suppression of apical dominance. Because of the large number of interaction partners identified for SAD1 (Table 5), a screen for the significant interaction partners should be done. To this end, the domains of SAD1 interacting with identified partners could be mapped. This can be carried out by testing the loss of interaction of SAD1 interaction partners with truncated versions of SAD1. In parallel, the phenotype of *S. reilianum* expressing the truncated versions of SAD1 should be monitored. Interaction partners interacting with SAD1 domains whose deletion disrupted protein function should be important for SAD1 function and should be further studied.

3.2.8 Shaping the Role of SAD1 in Suppression of Apical Dominance

How can SAD1 mediate suppression of apical dominance? Δ*sad1* mutants did not show a change in proliferation density in leaves and nodes compared to wt (Figure 35). Therefore attenuation in the mutant fitness can be excluded as a reason for loss of suppression of apical dominance by Δ*sad1* mutants. Apical dominance has long been known to be controlled by basipetal movement of auxin from the apex to suppress axillary meristem outgrowth (Davies et al., 1966). To test whether SAD1 modulates auxin, transgenic Arabidopsis plants expressing SAD1 were generated. Intriguingly, the transgenic plants showed slower growth, late flowering and seemed to have more inflorescence branches in comparison to the progenitor Arabidopsis plants. Additionally, there is preliminary evidence that SAD1 negatively regulates auxin in the roots of these transgenic plants (C. Löfke and T. Teichmann, unpublished). The influence of SAD1 on auxin levels in the Arabdiposis inflorescence still needs to be investigated. The auxin pattern in the inflorescence of Arabidopsis should be more informative and comparable to the observed effect of SAD1 on apical dominance in the female inflorescence of maize. However, to verify the effect of SAD1 on auxin, the concentration of auxin or expression of auxin marker genes, *PIN1* or *DR5*, in ears and shanks should be compared between samples infected with Δ*sad1* or wt strains. Since suppression of apical dominance is observed at 7 wpi, the auxin analysis should be

performed at 5, 6 and 7 wpi. SAD1 could impact on auxin biosynthesis, signaling or even more important on polar auxin transport (PAT) leading to depletion of apical dominance.

An example of a pathogen effector influencing auxin is known for plant-phytoplasma interaction (Hoshi et al., 2009). Tengu-su inducer (TENGU), a secreted virulence protein of a plant-pathogenic phytoplasma, was shown to be responsible of inducing witches' broom and dwarfism (Hoshi et al., 2009). Witches' broom results from lack of apical dominance leading to dense emergence of branches resembling broom. Expressing *tengu* in Tobacco and Arabidopsis plants resulted in plants exhibiting symptoms of witches' broom and dwarfism. The *tengu*-transgenic plants showed down-regulation of auxin-responsive genes suggesting that TENGU inhibited auxin-related pathways, thereby influencing plant development (Hoshi et al., 2009).

In maize, inflorescences development is dependent on *BIF2*, a serine/threonine-protein kinase known to be involved in PAT (McSteen and Hake, 2001; McSteen et al., 2007; Wu and McSteen, 2007; Gallavotti et al., 2008). Among the SAD1 interaction partners are three different serine/threonine-protein kinases. If one of these kinases is involved in auxin transport or biosynthesis, they could link SAD1 to suppression of apical dominance by auxin depletion.

Alternatively, SAD1 could dampen the apical dominance by impeding biosynthesis, signaling or transport of cytokinin or strigolactone. I suggested that cytokinins induced by *S. reilianum* could contribute to suppression of apical dominance (Chapter 3.1.4). Since cytokinin is negatively regulated by auxin (Nordström et al., 2004; Tanaka et al., 2006), elevated cytokinin levels could be the result of reduced auxin levels caused by presence of SAD1. However, cytokinins can promote axillary bud outgrowth even in the presence of apical auxin (Sachs and Thimann, 1967). Additionally, the acropetal movement of strigolactone from the root inhibits axillary meristem outgrowth (Crawford et al., 2010). Thus SAD1 could either induce cytokinin or inhibit strigolactone to activate axillary buds outgrowth. ROS was associated with loss of apical dominance in perennial ryegrass after infection with the Δ*sakA* mutant of *E. festucae* (Eaton et al., 2010). Therefore it will be reasonable to compare the cytokinins, strigolactones and ROS levels in the roots, shanks and ears of plants infected with Δ*sad1* mutant and wt strains to, and mock-infected plants at 4, 5, 6 and 7 wpi. To provide an understanding for the role of SAD1 in suppressing apical dominance, SAD1 could be expressed in Arabidopsis lines expressing

fluorescently tagged marker genes involved in signaling and transport of auxin, cytokinins and strigolactones to further narrow down the function of SAD1 on a molecular level.

3.2.9 Organ-Specific Degradation of SAD1 and VAG1

SAD1 and VAG1 were shown to be expressed and secreted in the ears (Figure 36, 46), although I could not detect the two proteins in the leaves (Figure 36 and Chapter 2.9.4). The transcripts of SAD1 and VAG1 were shown by qRT-PCR (Figure 34, 44) and RNA sequencing (H. Ghareeb, J. Schirawski, unpoblished) to be highly expressed in leaves, nodes and ears: Expression in the leaves was further proven for *sad1* by *gfp* fusion to the *sad1* promoter (Figure 37). Thus the transcripts of *sad1* and *vag1* were made but the encoded proteins could not be detected in the leaves. SAD1 and VAG1 likely undergo a common regulatory process on the post-transcriptional or post-translational level. Astonishingly, constitutive expression of GFP-SAD1 in Arabidopsis was shown to be constrained to the inflorescence and the root. Expression in leaves was only limited to guard cells (C. Löfke and T. Teichmann, unpublished). Expression of SAD1 in Arabidopsis provided supporting evidence to the absence of SAD1 observed in maize leaves. Hence, SAD1 is likely produced in leaves and then degraded via unknown process that is conserved in leaves of monocots and dicots.

SAD1 and VAG1 were predicted to possess ubiquitination sites (Figure 42, 47) suggesting that their absence in maize and Arabidposis leaves is a result of protein ubiquitination and degradation. In consistence, I identified 11 different plant interaction partners of SAD1 that are involved in ubiquitination, including 4 different E3 ubiquitin ligases. This supports the involvement of ubiquitination in processing of SAD1 and VAG1 in the leaves. Organ-specific degradation of SAD1 and VAG1 could uncover a new insight into the organ-specific functions of pathogen effectors. The ubiquitination of the two proteins can be examined by application of ubiquitination inhibitors to leaves of Arabidopsis expressing GFP-SAD1 or GFP-VAG1, and maize leaves infected with *S. reilianum* expressing SP-GFP-SAD1 or SP-GFP-VAG1. Alternatively, the ubiquitination sites of SAD1 and VAG1 can be mutated. Detection of the proteins by GFP fluorescence in leaves can be as evidence of an ubiquitination-mediated organ-specific degradation of SAD1 and VAG1. An efficient ubiquitination and degradation of the two proteins could reflect a possibly undesired negative function of SAD1 and VAG1 in leaves. Alternatively, degradation could keep the defense system busy leading to evasion recognition of

other pathogen's effectors. It will be interesting to investigate the effect *in planta* of *S. reilianum* expressing SAD1 and VAG1 with mutated ubiquitination sites.

E3 ubiquitin ligase CMPG1 was identified by Y2H to interact with AVR3a, an effector of *Phytophthora infestans*. CMPG1 is required for cell death trigged by another effector called infestin 1. AVR3a suppressed infestin 1-triggered cell death. It was shown that AVR3a stabilized CMPG1, thereby mediated suppression of cell death (Bos et al., 2010). Whether SAD1 fulfils a similar function in stabilizing its interacting E3 ubiquitin ligases still needs to be investigated.

3.2.10 VAG1 is an Effector with Avirulence and Virulence Functions

Deletion of *vag1* led to reduced spore formation, which could be restored by re-introduction of *vag1* (Figure 43). VAG1 was predicted to have a secretion signal and was proven to be localized around fungal hyphae and hyphal tips in colonized ears (Figure 46, 47) indicating that VAG1 is a secreted protein. The transcript of *vag1* was detected in the sporidia and was up-regulated in the leaves, nodes and ears (Figure 44). Accordingly, VAG1 is suggested to play an important role all through the life cycle of *S. reilianum*. The influence of VAG1 on spore formation could either be direct or an indirect result of affecting virulence.

Intriguingly, the Δ*vag1* mutant exhibited hyperproliferation in the leaf followed by significantly reduced proliferation density in the node (Figure 45). The enhanced fitness of the Δ*vag1* mutant in the leaf could reflect an avirulence function of VAG1, whereas the reduced fitness of the mutant in the node could indicate a virulence function of VAG1. The avirulence function can explain the suggested ubiquitination-mediated VAG1 degradation in the leaf (Chapter 3.2.9). Thereby the hyperprolifeartion of Δ*vag1* mutant in the leaf could be due to evading recognition by the defense system of the plant. In contrast, the inhibited proliferation of Δ*vag1* mutant in the node indicated that VAG1 promotes compatibility with the host. Thus VAG1 could have different functions in an different tissues. The virulence function of *vag1* seemed to be more essential for *S. reilianum* that it has impacted on spore formation indirectly. The predicated nuclear localization signal and phosphorylation sites in VAG1 discussed in chapter 3.2.7 , could propose a role of the protein in impeding nuclear activity and signaling of the host, thereby balance compatibility with the host.

4. MATERIALS AND METHODS

4.1 Materials

4.1.1 Maize Plants

Seeds of the early flowering cultivar Gaspe Flint were obtained from Prof. Regine Kahmann, Max Planck Institute for Terrestrial Microbiology, Marburg, Germany.

4.1.2 *S. reilianum* Strains

The *S. reilianum* strains generated and used in thisstudy are listed below (Table 6).

Table 6. List of *S. reilianum* strains used in this study.

Name	Genotype*	Progenitor strain	Resistance**
5-1	*a2 b2*	wt	-
5-2	*a1 b1*	wt	-
HG09	*a2 b2* Δcluster19A1A2#20	JS747	P+H
HG15	*a2 b2 sgfp*^{ectopic} *egfp*-RNAi^{ectopic}#6	JS113	H+C
HG16	*a2 b2 sgfp*^{ectopic} *egfp*-amiRNA^{ectopic}#8	JS113	H+C
HG17	*a2 b2 sgfp*^{ectopic} *egfp*-amiRNA^{ectopic}#14	JS113	H+C
HG19	*a2 b2* Δcluster 19A1A2#40	JS751	P+H
HG20	*a2 b2* Δcluster 19A1A2#69	JS751	P+H
HG21	*a1 mfa2.1 bW1 bE2* Δcluster 5-1uni#3	JS161	P+H
HG22	*a1 mfa2.1 bW1 bE2* Δcluster 5-1uni#8	JS161	P+H
HG23	*a1 mfa2.1 bW1 bE2* Δcluster 5-1uni#13	JS161	P+H
HG24	*a1 mfa2.1 bW1 bE2* Δcluster 7-11uni#7	JS161	P+H
HG25	*a1 mfa2.1 bW1 bE2* Δcluster 7-11uni#8	JS161	P+H
HG26	*a1 mfa2.1 bW1 bE2* Δcluster 7-11uni#10	JS161	P+H
HG28	*a1 mfa2.1 bW1 bE2* Δcluster 6-1uni#3	JS161	P+H
HG29	*a1 mfa2.1 bW1 bE2* Δcluster 6-1uni#4	JS161	P+H
HG30	*a1 mfa2.1 bW1 bE2* Δcluster 6-1uni#6	JS161	P+H
HG34	*a2 b2 sgfp*^{ectopic} *egfp*-RNAi^{ectopic}#5	JS113	H+C
HG35	*a2 b2 sgfp*^{ectopic} *egfp*-RNAi^{ectopic}#10	JS113	H+C
HG38	*a2 b2 sgfp*^{ectopic} *egfp*-amiRNA^{ectopic}#4	JS113	H+C
HG40	*a1 mfa2.1 bW1 bE2* Δ*sr10703*#11	JS161	P+H
HG41	*a1 mfa2.1 bW1 bE2* Δ*sr10703*#12	JS161	P+H
HG42	*a1 mfa2.1 bW1 bE2* Δ*sr10703*#13	JS161	P+H
HG43	*a1 mfa2.1 bW1 bE2* Δ*sr11815*#1	JS161	P+H
HG44	*a1 mfa2.1 bW1 bE2* Δ*sr11815*#8	JS161	P+H
HG45	*a1 mfa2.1 bW1 bE2* Δ*sr11815*#16	JS161	P+H

Name	Genotype*	Progenitor strain	Resistance**
HG46	*a1 mfa2.1 bW1 bE2* Δ*sr12538*#10	JS161	P+H
HG47	*a1 mfa2.1 bW1 bE2* Δ*sr12538*#12	JS161	P+H
HG48	*a1 mfa2.1 bW1 bE2* Δ*sr12538*#14	JS161	P+H
HG49	*a1 mfa2.1 bW1 bE2* Δ*sr13154*#5	JS161	P+H
HG50	*a1 mfa2.1 bW1 bE2* Δ*sr13154*#10	JS161	P+H
HG51	*a1 mfa2.1 bW1 bE2* Δ*sr13154*#15	JS161	P+H
HG52	*a1 mfa2.1 bW1 bE2* Δ*Dicer*#7	JS161	P+H
HG53	*a1 mfa2.1 bW1 bE2* Δ*Dicer*#9	JS161	P+H
HG54	*a1 mfa2.1 bW1 bE2* Δ*Dicer*#22	JS161	P+H
HG55	*a1 mfa2.1 bW1 bE2* Δ*sr13154*#8	JS161	P+H
HG56	*a1 mfa2.1 bW1 bE2* Δ*sr13154*#9	JS161	P+H
HG57	*a1 mfa2.1 bW1 bE2* Δ*sr14797*#14	JS161	P+H
HG58	*a1 mfa2.1 bW1 bE2* Δ*sr14797*#16	JS161	P+H
HG59	*a1 mfa2.1 bW1 bE2* Δ*sr14797*#17	JS161	P+H
HG61	*a1 mfa2.1 bW1 bE2* Δ*sr15769*#13	JS161	P+H
HG62	*a1 mfa2.1 bW1 bE2* Δ*sr15769*#17	JS161	P+H
HG63	*a1 mfa2.1 bW1 bE2* Δ*sr15769*#18	JS161	P+H
HG64	*a1 mfa2.1 bW1 bE2* Δcluster 5-18uni#6	JS161	P+H
HG65	*a1 mfa2.1 bW1 bE2* Δcluster 5-18uni#7	JS161	P+H
HG66	*a1 mfa2.1 bW1 bE2* Δcluster 5-18uni#10	JS161	P+H
HG67	*a1 mfa2.1 bW1 bE2* Δcluster 19A2#3	JS161	P+H
HG68	*a1 mfa2.1 bW1 bE2* Δcluster 19A2#27	JS161	P+H
HG69	*a1 mfa2.1 bW1 bE2* Δcluster 11-1uni#13	JS161	P+H
HG70	*a1 mfa2.1 bW1 bE2* Δcluster 11-1uni#14	JS161	P+H
HG71	*a1 mfa2.1 bW1 bE2* Δcluster 11-1uni#15	JS161	P+H
HG80	*a2 b2* Δ*sr10075*#4	5-1	H
HG81	*a2 b2* Δ*sr10075*#5	5-1	H
HG82	*a2 b2* Δ*sr10075*#6	5-1	H
HG84	*a1 b1* Δ*sr10075*#4	5-2	H
HG85	*a1 b1* Δ*sr10075*#5	5-2	H
HG86	*a1 b1* Δ*sr10075*#6	5-2	H
HG88	*a2 b2* Δ*sr10079*#4	5-1	H
HG89	*a2 b2* Δ*sr10079*#5	5-1	H
HG90	*a2 b2* Δ*sr10079*#6	5-1	H
HG91	*a1 b1* Δ*sr10079*#4	5-2	H
HG92	*a1 b1* Δ*sr10079*#5	5-2	H
HG93	*a1 b1* Δ*sr10079*#6	5-2	H
HG95	*a2 b2* Δ*sr10077*#4	5-1	H
HG96	*a2 b2* Δ*sr10077*#5	5-1	H
HG97	*a2 b2* Δ*sr10077*#6	5-1	H
HG99	*a1 b1* Δ*sr10077*#4	5-2	H

Name	Genotype*	Progenitor strain	Resistance**
HG100	*a1 b1* Δ*sr10077*#5	5-2	H
HG101	*a1 b1* Δ*sr10077*#6	5-2	H
HG103	*a1 mfa2.1 bW1 bE2 hpt*^{mig1}#1	JS161	P+H
HG104	*a1 mfa2.1 bW1 bE2 hpt*^{mig1}#2	JS161	P+H
HG105	*a1 mfa2.1 bW1 bE2 hpt*^{mig1}#3	JS161	P+H
HG109	*a2 b2* Δ*sr10073*#1	5-1	H
HG110	*a2 b2* Δ*sr10073*#4	5-1	H
HG111	*a2 b2* Δ*sr10073*#7	5-1	H
HG113	*a1 b1* Δ*sr10073*#4	5-2	H
HG114	*a1 b1* Δ*sr10073*#5	5-2	H
HG115	*a1 b1* Δ*sr10073*#9	5-2	H
HG125	*a2 b2* Δcluster 19A2#10	5-1	H
HG126	*a2 b2* Δcluster 19A2#42	5-1	H
HG127	*a1 b1* Δcluster 19A2#39	5-2	H
HG128	*a1 b1* Δcluster 19A2#85	5-2	H
HG137	*a2 b2 hpt*^{mig1}#9	5-1	H
HG138	*a2 b2 hpt*^{mig1}#11	5-1	H
HG139	*a2 b2 hpt*^{mig1}#12	5-1	H
HG140	*a2 b2hpt*^{mig1}#9	5-2	H
HG141	*a2 b2hpt*^{mig1}#10	5-2	H
HG142	*a2 b2hpt*^{mig1}#11	5-2	H
HG143	*a2 b2* Δ19A1A2+*sr10057*^{mig1M}#3	HG09	P+H+C
HG144	*a2 b2* Δ19A1A2+*sr10057*^{mig1M}#10	HG09	P+H+C
HG147	*a1 b1* Δ19A1A2+*sr10057*^{mig1M}#2	HG20	P+H+C
HG148	*a1 b1* Δ19A1A2+*sr10057*^{mig1M}#3	HG20	P+H+C
HG150	*a2 b2* Δ19A1A2+*sr10060*^{mig1M}#2	HG09	P+H+C
HG151	*a2 b2* Δ19A1A2+*sr10060*^{mig1M}#10	HG09	P+H+C
HG153	*a1 b1* Δ19A1A2+*sr10060*^{mig1M}#2	HG20	P+H+C
HG154	*a1 b1* Δ19A1A2+*sr10060*^{mig1M}#3	HG20	P+H+C
HG157	*a2 b2* Δ*sr10079*+*sr10079*^{mig1M}#1	HG89	H+C
HG158	*a2 b2* Δ*sr10079*+*sr10079*^{mig1M}#3	HG89	H+C
HG161	*a1 b1* Δ*sr10079*+*sr10079*^{mig1M}#4	HG92	H+C
HG162	*a1 b1* Δ*sr10079*+*sr10079*^{mig1M}#6	HG92	H+C
HG163	*a2 b2* Δ*sr10077*+*sr10077*^{mig1M}#6	HG95	H+C
HG164	*a2 b2* Δ*sr10077*+*sr10077*^{mig1M}#7	HG95	H+C
HG165	*a2 b2* Δ*sr10077*+*sr10077*^{mig1M}#12	HG95	H+C
HG167	*a1 b1* Δ*sr10077*+*sr10077*^{mig1M}#4	HG99	H+C
HG168	*a1 b1* Δ*sr10077*+*sr10077*^{mig1M}#1-1	HG99	H+C
HG169	*a1 b1* Δ*sr10077*+*sr10077*^{mig1M}#1-8	HG99	H+C
HG183	*a2 b2* Δ*sr10077*+*sr10077:egfp*^{mig1M}#20	HG95	H+C
HG185	*a2 b2* Δ*sr10077*+*sr10077:egfp*^{mig1M}#22	HG95	H+C

Name	Genotype*	Progenitor strain	Resistance**
HG186	*a1 b1* Δ*sr10077+sr10077:egfp*^{mig1M}#12	HG99	H+C
HG187	*a1 b1* Δ*sr10077+sr10077:egfp*^{mig1M}#13	HG99	H+C
HG189	*a2 b2* Δ*sr10079+sr10079:egfp*^{mig1M}#7	HG89	H+C
HG196	*a1 b1* Δ*sr10079+sr10079:egfp*^{mig1M}#4	HG92	H+C
YF2 5-1 #1	*a2 b2* Δ*sr10077+sr10077*p:*egfp*^{sr10077M}#1	5-1	C
YF2 5-2 #1	*a1 b1* Δ*sr10077+sr10077*p:*egfp*^{sr10077M}#1	5-2	C
JS64	*a1 b1 sgfp*^{ectopic}	5-2	H
JS113	*a2 b2 sgfp*^{ectopic}	5-1	H
JS161	*a1 mfa2.1 bW1 bE2*	5-2	P
JS747	*a2 b2* Δcluster 19A1	5-1	P
JS751	*a1 b1* Δcluster 19A1	5-2	P
JS895	*a2 b2* Δcluster 19A3	5-1	H
JS896	*a2 b2* Δcluster 19A3	5-1	H
JS900	*a1 b1* Δcluster 19A3	5-2	H
JS901	*a1 b1* Δ cluster 19A3	5-2	H

4.1.3 *Saccharomyces cerevisiae* Strains

The *S. cerevisiae* strains generated and used in this study are listed below (Table 7).

Table 7. List of *S. cerevisiae* strains used in the current study.

Name	Description	Genotype	Progenitor strain	Selection*
yHG1	Y2HGold	*MATa, trp1-901, leu2-3, 112,ura3-52, his3-200, gal4Δ, gal80Δ, LYS2 : : GAL1UAS–Gal1TATA–His3, GAL2UAS–Gal2TATA–Ade2 URA3 : : MEL1UAS–Mel1TATA AUR1-C MEL1*	-	-
yHG2	Y187	*MATα, ura3-52, his3-200, ade2-101, trp1-901, leu2-3, 112, gal4Δ, gal80Δ, met–, URA3 : : GAL1UAS–Gal1TATA–LacZ,MEL1*	-	-Leu/Amp
yHG3	Y187-pGADT7-T	pGADT7-T	yHG2	-Leu/Amp
yHG4	Y187-pGADT7	pGADT7	yHG2	-Try/Kan
yHG5	Y2HG-pGBKT7	pGBKT7	yHG1	-Try/Kan
yHG6	Y2HG-pGBKT7-53	pGBKT7-53	yHG1	-Try/Kan
yHG7	Y2HG-pGBKT7-lam	pGBKT7-lam	yHG1	-Try/Kan
yHG8	Y2HG-pGBKT7-sad1Δsp	pGBKT7-sad1Δsp	yHG1	-Leu/-Try/-His/-Ade/A/X

Name	Description	Genotype	Progenitor strain	Selection*
yHG9	H-pGBKT7-53+pGADT7-T	pGBKT7-53, pGADT7-T	yHG6+ yHG3	-Leu/-Try/-His/-Ade/A/X
yHG10	H-pGBKT7-lam+pGADT7-T	pGBKT7-lam, pGADT7-T	yHG7+ yHG3	-Leu/-Try
yHG11	H-pGBKT7-sad1Δsp+pGADT7	pGBKT7-sad1Δsp, pGADT7	yHG8+ yHG4	-Leu/-Try

*Leu; Leucin, Try; Tryptophan, His; Histidin, Ade; Adenin, A; Aureobasidin, X; X-α-Gal, Amp; ampicillin resistance, Kan; kanamycin resistance.

4.1.4 *Escherichia coli* Strains

The *E. coli* strains TOP10 [Genotype: F- mcrA Δ(mrr-hsdRMS-mcrBC) Φ80lacZΔM15 ΔlacX74 deoR recA1 araD139Δ(ara-Leu)7697 galU galK rpsL (StrR) endA1 nupG] and DH5α [Genotype: F-Φ80dlacZΔM15 Δ(lacZYA-argF) U169 deoR recA1 endA1 hsdR17(rk-, mk+) phoA supE44 λ- thi-1 gyrA96 relA1] were obtained from Invitrogen (Karlsruhe, Germany), and Stellar [*F–, endA1, supE44, thi-1, recA1, relA1, gyrA96, phoA, Φ80d lacZΔ M15, Δ(lacZYA-argF) U169, Δ(mrr-hsdRMS-mcrBC), ΔmcrA, λ–*] was obtained from Clontech (Saint-Germain-en-Laye, France). The TOP10 and Stellar strains were used for preparation of chemically competent cells, and DH5α was used for preparation of electro competent cells.

4.1.5 Oligonucleotides

The oligonucleotides designed and used in this study are listed below (Table 8).

Table 8. List of oligonucleotides and their use.

Name	Sequence	Use (amplification of)
oHG009	GATCTTTGCTCAGGGCGGACTGCTCTCTCTTTTGTATTCC	backbone of plasmid pRS300 for generation of *gfp* artificial microRNA
oHG010	GAGCAGTCCGCCCTGAGCAAAGATCAAAGAGAATCAATGA	backbone of plasmid pRS300 for generation of *gfp* artificial microRNA
oHG011	GAGCCGTCCGCCCTGTGCAAAGTTCACAGGTCGTGATATG	backbone of plasmid pRS300 for generation of *gfp* artificial microRNA
oHG012	GAACTTTGCACAGGGCGGACGGCTCTACATATATATTCCT	backbone of plasmid pRS300 for generation of *gfp* artificial microRNA
oHG013	CTGCAAGGCGATTAAGTTGGGTAAC	*gfp* artificial microRNA

Name	Sequence	Use (amplification of)
oHG014	GCGGATAACAATTTCACACAGGAAACAG	*gfp* artificial microRNA
oHG015	GCTAAGCTTTCCGGCTCGTATGTTGTG	hsp70 promotor
oHG016	CTGGTACCAGACGTCGCGGTGAGTTCAG	hsp70 promotor
oHG017	GTGGTACCAGACGTTGTGGCTGTTGTAG	*sgfp* antisense
oHG018	GTTCGGCCCTGAGGGCCAGCTGACCCTG AAGTTCATC	*sgfp* antisense
oHG019	GTGAGGCCGTCACGGCCCTGCGAGACAA AGAAGC	interon sequence of *bW* transcription factor
oHG020	GTGAGGCCGTCTGGGCCGTGAGTACCTG TCCCTTTC	interon sequence of *bW* transcription factor
oHG021	GTGAGGCCCAGACGGCCTTCATCTGCAC CACCGGCAAG	s*gfp* sense
oHG022	CTAGGCGGCCGCCCTTGATGCCGTTCTTC TG	s*gfp* sense
oHG023	GTGTGGATGCGGTAATTCAG	deletion confirmation of cluster 19A2
oHG024	TCGGATGGCTAGCATCAAAC	deletion confirmation of cluster 19A2
oHG025	TCGCTGTTGGTGGACAAGTG	RT-PCR of *Dicer*
oHG026	TCGGTCATTGCGGGTCATTC	RT-PCR of *Dicer*
oHG027	TGGAGCTCGAGTTTGTAGTC	left flank of knockout construct for *S. reilianum* unique gene cluster 5-1
oHG028	ATCTAGGCCATCTAGGCCGTCCGCATAG ATCTGCACTG	left flank of knockout construct for *S. reilianum* unique gene cluster 5-1
oHG029	ATCTAGGCCTGAGTGGCCGTGGCGGTGA TGTCAGGATG	right flank of knockout construct for *S. reilianum* unique gene cluster 5-1
oHG030	TCAATCCGCGTGTCTCCAAC	right flank of knockout construct for *S. reilianum* unique gene cluster 5-1
oHG031	AGGGCATGGTCGAGATCAAC	whole knockout construct for *S. reilianum* unique gene cluster 5-1
oHG032	CGAGCTGGCTCAACGGATTC	whole knockout construct for *S. reilianum* unique gene cluster 5-1
oHG033	TCGGGCATGGCATTCATGTC	left flank of knockout construct for *S. reilianum* unique gene cluster 6-1
oHG034	ATCTAGGCCATCTAGGCCGTGCCGTGGT GTCTCGAATC	left flank of knockout construct for *S. reilianum* unique gene cluster 6-1

Name	Sequence	Use (amplification of)
oHG035	ATCTAGGCCTGAGTGGCCCTGTCGACGATGCAATGATG	right flank of knockout construct for *S. reilianum* unique gene cluster 6-1
oHG036	TCAGCCACGACAATGTCAAC	right flank of knockout construct for *S. reilianum* unique gene cluster 6-1
oHG037	GACCCGAGACATGCGAAGAG	whole knockout construct for *S. reilianum* unique gene cluster 6-1
oHG038	GCTGCATGGCCTTGCGATAC	whole knockout construct for *S. reilianum* unique gene cluster 6-1
oHG039	GAATCCTGTACGCCTACATC	left flank of knockout construct for *S. reilianum* unique gene cluster 7-11
oHG040	ATCTAGGCCATCTAGGCCCGGCAAGGAACCACTTAATC	left flank of knockout construct for *S. reilianum* unique gene cluster 7-11
oHG041	ATCTAGGCCTGAGTGGCCCTCAGTGCCCTTCTTATACC	right flank of knockout construct for *S. reilianum* unique gene cluster 7-11
oHG042	TAGTTAGGAGCCGGGACTTG	right flank of knockout construct for *S. reilianum* unique gene cluster 7-11
oHG043	ACCGTCCTTCCATGCTCTAC	whole knockout construct for *S. reilianum* unique gene cluster 7-11
oHG044	ACATTGCGCAGCAAACATCC	whole knockout construct for *S. reilianum* unique gene cluster 7-11
oHG047	ATCTAGGCCTGAGTGGCCATCGTTCGTTGGCGGTCTTG	right flank of knockout construct for *S. reilianum* unique gene cluster 11-1
oHG048	CTTCGCGCTGGGCTACTTTG	right flank of knockout construct for *S. reilianum* unique gene cluster 11-1
oHG050	TAATCTTCGGCTGCTTCACC	whole knockout construct for *S. reilianum* unique gene cluster 11-1
oHG051	GTGAGCAAGGGAGGAGATAG	deletion confirmation of *S. reilianum* unique gene cluster 5-18
oHG052	CCATCATTCGCAGTAGACAC	deletion confirmation of *S. reilianum* unique gene cluster 5-18
oHG053	TGCTCCGGCTTGACATAACC	deletion confirmation of *S. reilianum* unique gene cluster 5-1
oHG054	AAGCGGGAAGCAACCCATAC	deletion confirmation of *S. reilianum* unique gene cluster 5-1
oHG055	CGTCGTTTACCAGTCCTTTC	deletion confirmation of *S. reilianum* unique gene cluster 6-1
oHG056	CCTGATCCACATCTGCATAG	deletion confirmation of *S. reilianum* unique gene cluster 6-1
oHG057	GCCCTTGCATTCGAAGAAAC	deletion confirmation of *S. reilianum* unique gene cluster 7-11
oHG058	GTAGGTGAGGCTCGCTAAAC	deletion confirmation of *S. reilianum* unique gene cluster 7-11

Name	Sequence	Use (amplification of)
oHG059	GAACAGCGGGAAGAGTATGG	deletion confirmation of *S. reilianum* unique gene cluster 11-1
oHG060	GACTCTGAGCCCGAAAGTAG	deletion confirmation of *S. reilianum* unique gene cluster 11-1
oHG061	ACATGTACGGCGACGAAGAC	left flank of knockout construct for *S. reilianum* unique gene cluster 5-18
oHG063	ATCTAGGCCTGAGTGGCCTCACGATCTG ACCCATAAGG	right flank of knockout construct for *S. reilianum* unique gene cluster 5-18
oHG064	GCATGTCGATACGCTAGAAC	right flank of knockout construct for *S. reilianum* unique gene cluster 5-18
oHG065	GTGCTCGTGGTGACAGAGAC	whole knockout construct for *S. reilianum* unique gene cluster 5-18
oHG066	GAGGTTCTCCGCCACCATTG	whole knockout construct for *S. reilianum* unique gene cluster 5-18
oHG073	CCTAGCGCACAGTACAACTC	left flank of knockout construct for *S. reilianum* unique gene *sr10703*
oHG074	ATCTAGGCCATCTAGGCCCGCAACTGTG GTTCAGAAAG	left flank of knockout construct for *S. reilianum* unique gene *sr10703*
oHG075	ATCTAGGCCTGAGTGGCCCGAAGGAGGA GGAGCAGAAG	right flank of knockout construct for *S. reilianum* unique gene *sr10703*
oHG076	CTTCCCGCAAGGTAGGATCG	right flank of knockout construct for *S. reilianum* unique gene *sr10703*
oHG077	CGCCGGGATAGAGTTCTGAC	whole knockout construct for *S. reilianum* unique gene *sr10703*
oHG078	GGATCGAAGAAGCCGAGACC	whole knockout construct for *S. reilianum* unique gene *sr10703*
oHG079	GCTCGCAAAGTGCACAACTC	left flank of knockout construct for *S. reilianum* unique gene *sr11815*
oHG080	ATCTAGGCCATCTAGGCCCGGGTGGTCA TTCCAAGTAG	left flank of knockout construct for *S. reilianum* unique gene *sr11815*
oHG081	ATCTAGGCCTGAGTGGCCAACTCTGAGG ACCGCAGTAG	right flank of knockout construct for *S. reilianum* unique gene *sr11815*
oHG082	GTGGTGGTGGTGATCATTCG	right flank of knockout construct for *S. reilianum* unique gene *sr11815*
oHG083	GGCCTTGCGGTTTGACGTTC	whole knockout construct for *S. reilianum* unique gene *sr11815*
oHG084	ACCCACTGCACCTGCAAGAG	whole knockout construct for *S. reilianum* unique gene *sr11815*
oHG085	CTGGCGCCTAATTTCGATATCC	left flank of knockout construct for *S. reilianum* unique gene *sr12538*
oHG086	ATCTAGGCCATCTAGGCCAACGCCGAGA CGTCCAATAC	left flank of knockout construct for *S. reilianum* unique gene *sr12538*

Name	Sequence	Use (amplification of)
oHG087	ATCTAGGCCTGAGTGGCCTCCGCGATTGTCGAGTGTAG	right flank of knockout construct for *S. reilianum* unique gene *sr12538*
oHG088	CGAGCAAAGAGGCCTTTGTG	right flank of knockout construct for *S. reilianum* unique gene *sr12538*
oHG089	CAGCGTTCTTGACCGGGTTC	whole knockout construct for *S. reilianum* unique gene *sr12538*
oHG090	CGGTGACGCTGCTCCAATTC	whole knockout construct for *S. reilianum* unique gene *sr12538*
oHG091	GCGAGATGAGCAAGGACTAC	left flank of knockout construct for *S. reilianum* unique gene *sr13154*
oHG092	ATCTAGGCCATCTAGGCCGGAACGATGGCTTGATAGAG	left flank of knockout construct for *S. reilianum* unique gene *sr13154*
oHG093	ATCTAGGCCTGAGTGGCCGGTCTCGATCCGATACCTTTC	right flank of knockout construct for *S. reilianum* unique gene *sr13154*
oHG094	AGGTGTCGGCCATAGCTTC	right flank of knockout construct for *S. reilianum* unique gene *sr13154*
oHG095	ATCACGTCCATCGTCAAACC	whole knockout construct for *S. reilianum* unique gene *sr13154*
oHG096	GCTCAGCCTGTATTTGAACC	whole knockout construct for *S. reilianum* unique gene *sr13154*
oHG099	ATCTAGGCCTGAGTGGCCTCGGTTTCGCAGACGTTC	right flank of knockout construct for *S. reilianum* unique gene *sr14797*
oHG100	AAGACCTCGCAGTCGTCAC	right flank of knockout construct for *S. reilianum* unique gene *sr14797*
oHG102	TGTGCCTCGCGATCAGCTAC	whole knockout construct for *S. reilianum* unique gene *sr14797*
oHG103	AAGCCGGGTAGACAAATTGC	left flank of knockout construct for *S. reilianum* unique gene *sr15769*
oHG104	ATCTAGGCCATCTAGGCCTCCGCGTCATATACCGTTAG	left flank of knockout construct for *S. reilianum* unique gene *sr15769*
oHG105	ATCTAGGCCTGAGTGGCCCAATCTCCCGTTCGGTTTCC	right flank of knockout construct for *S. reilianum* unique gene *sr15769*
oHG106	GTCGAATGGGCTCGAATCAG	right flank of knockout construct for *S. reilianum* unique gene *sr15769*
oHG107	TTCTTACCACGCATGGTTCC	whole knockout construct for *S. reilianum* unique gene *sr15769*
oHG108	GCCCACTCGATCTACATTTAGC	whole knockout construct for *S. reilianum* unique gene *sr15769*
oHG111	AAGACTGGGAGACGTGTTAC	deletion confirmation of *S. reilianum* unique gene *sr10703*
oHG112	TGGAGACGCTCATCATACTG	deletion confirmation of *S. reilianum* unique gene *sr10703*

Name	Sequence	Use (amplification of)
oHG113	GAGCTCTCGGTGACTGTTG	deletion confirmation of *S. reilianum* unique gene *sr11815*
oHG114	GGCCTGCATACGCTCATTG	deletion confirmation of *S. reilianum* unique gene *sr11815*
oHG115	GAGACCGGGCTGATGTTACG	deletion confirmation of *S. reilianum* unique gene *sr12538*
oHG116	GCATGGTGGGAGGATCAGAG	deletion confirmation of *S. reilianum* unique gene *sr12538*
oHG117	GGCGTCTTGGTGCTTTCTCC	deletion confirmation of *S. reilianum* unique gene *sr13154*
oHG118	CGCGAGCCTGGTGATACTTG	deletion confirmation of *S. reilianum* unique gene *sr13154*
oHG119	CTCTCGGCATGCTTCGCTAC	deletion confirmation of *S. reilianum* unique gene *sr14797*
oHG120	TGCTGTTCGCACTCCTCTTC	deletion confirmation of *S. reilianum* unique gene *sr14797*
oHG121	CGAGCGATGCTACCAACAAG	deletion confirmation of *S. reilianum* unique gene *sr15769*
oHG122	TGATAGAAGCGCGTGTTGTG	deletion confirmation of *S. reilianum* unique gene *sr15769*
oHG127	TTGGCAGCACACGCATCTAC	left flank of knockout construct for *S. reilianum* unique gene *sr14797*
oHG128	ATCTAGGCCATCTAGGCCTGGCGAGACT TTGCATTCCG	left flank of knockout construct for *S. reilianum* unique gene *sr14797*
oHG129	GTACTACCTAGGGAGTGACTAC	whole knockout construct for *S. reilianum* unique gene *sr14797*
oHG136	ACACCTCGCTGGCTGTCACT	left flank of knockout construct for *S. reilianum* unique gene cluster 5-18
oHG137	ATCTAGGCCATCTAGGCCTGGACACGGG CAAGATGACG	left flank of knockout construct for *S. reilianum* unique gene cluster 5-18
oHG138	CGCTGGCTGTCACTCGATTG	whole knockout construct for *S. reilianum* unique gene cluster 5-18
oHG139	GCGGATCTTGAAGTTCAC	qRT-PCR for *gfp*
oHG140	CGACGGCAACTACAAGAC	qRT-PCR for *gfp*
oHG143	CCGCCAGAATCATGTCCAAC	qRT-PCR for *ppi*
oHG144	CATGAACTGCGGGATGACAC	qRT-PCR for *ppi*
oHG145	GGATGCCATAGCCCAGATCG	left flank of knockout construct for *S. reilianum* unique gene cluster 7-11

Name	Sequence	Use (amplification of)
oHG146	ATCTAGGCCATCTAGGCCAATACGGTTG CGCTCTGAGG	left flank of knockout construct for *S. reilianum* unique gene cluster 7-11
oHG147	CCTGGCCCACATTGATAAGC	whole cluster 19A2
oHG148	GTACACGGCGTATTCGTTCC	whole cluster 19A2
oHG149	TCGCAACGAGGAAACGAGAC	left flank of *mig1* locus
oHG150	ATCTAGGCCATCTAGGCCCGGCCTACCC AATCTTCAACG	left flank of *mig1* locus
oHG151	ATCTAGGCCTGAGTGGCCCTGACGGTAA CGGCCGAAAC	right flank of *mig1* locus
oHG152	CGCTTTTGCCACTGCTTCC	right flank of *mig1* locus
oHG153	CCGTGGTATCTGAAGCAATC	whole *mig1* integration construct
oHG154	CCGCCTTGTTGTTCATGG	whole *mig1* integration construct
oHG156	TGGTAAGCTTGATGGCCGAACGTGGTAA C	Hygromycin cassette
oHG157	CGAATCGATGATGGCCGAACGTGGTAAC	Hygromycin cassette
oHG158	ATCTAGGCCTGAGTGGCCAGGAAGAGGG CATTCTGG	right flank of knockout construct for *sr10073*
oHG159	CTGTGGCGATATGAGAGC	right flank of knockout construct for *sr10073*
oHG160	GGCCGAGACTGAGTTCATGTGC	left flank of knockout construct for *sr10075*
oHG161	ATCTAGGCCATCTAGGCCAGTGGGCTCG ATCAACAGTCC	left flank of knockout construct for *sr10075*
oHG162	ATCTAGGCCTGAGTGGCCGCGTTTGATG CTAGCCATCC	right flank of knockout construct for *sr10075*
oHG163	CCAACGGCAACCTCAATACC	right flank of knockout construct for *sr10075*
oHG164	CGAGCATGCAAGACCTCATGG	whole knockout construct for *sr10075*
oHG165	GCGTTTGATGCTAGCCATCC	left flank of knockout construct for *sr10077*
oHG166	ATCTAGGCCATCTAGGCCAACGGCAACC TCAATACC	left flank of knockout construct for *sr10077*
oHG167	ATCTAGGCCTGAGTGGCCGTTGGAAAGG CGATGTAGAACC	right flank of knockout construct for *sr10077*

Name	Sequence	Use (amplification of)
oHG168	TCGCTGAGCAGAACTTCAACC	right flank of knockout construct for *sr10077*
oHG169	CTCTCATATCGCCACAGTTCG	whole knockout construct for *sr10077*
oHG170	GCTCGCAAATGTTGCAAGG	whole knockout construct for *sr10077*
oHG171	CCGTTGGAAAGGCGATGTAGAACC	left flank of knockout construct for *sr10079*
oHG172	ATCTAGGCCATCTAGGCCTCGCTGAGCA GAACTTCAACC	left flank of knockout construct for *sr10079*
oHG173	GCGGCTTCAAGCAAGGTAGG	whole knockout construct for *sr10079*
oHG174	TCCAAGCGCAAGAATCTCTG	whole knockout construct for *sr10073*
oHG175	GTTACCGCCTCAGCTCTTTCC	whole knockout construct for *sr10075*
oHG176	AGCACCTCGCCGAAATCTCC	deletion confirmation of *sr10073*
oHG177	AATCGTAGCAGCGCGACTGG	deletion confirmation of *sr10073*
oHG178	GAATGCCATGCTTCCAATCG	deletion confirmation of *sr10077*
oHG179	TCTGCCCTTCAAACTTGTCC	deletion confirmation of *sr10077*
oHG180	AACGAATACGCCGTGTACGC	deletion confirmation of *sr10079*
oHG181	ATCTAAGCCCGGTGCTTTCC	deletion confirmation of *sr10079*
oHG183	CAACCTCGAGCGGCCTACCCAATCTTCA ACG	left flank of inverted *mig1* locus
oHG184	CAACCTCGAGTCTGACGGTAACGGCCGA AAC	right flank of inverted *mig1* locus
oHG186	GTGGAGGAGCCCTACATACC	qRT-PCR for *sr10073*
oHG187	CAGCGGGCTTATCAATGTGG	qRT-PCR for *sr10073*
oHG188	ATGCGCCTTCTACTCCAACG	qRT-PCR for *sr10075*
oHG189	CCGCTCTTTGCAACTCTTCG	qRT-PCR for *sr10075*
oHG190	CATGAGAATGCCATGCTTCC	qRT-PCR for *sad1*

Name	Sequence	Use (amplification of)
oHG191	TTCATGGTGCATCACGATCC	qRT-PCR for *sad1*
oHG192	ATTGGAGCCCATGCCTCACC	qRT-PCR for *vag1*
oHG193	TGGCGTACACGGCGTATTCG	qRT-PCR for *vag1*
oHG194	TGCGCCGCTCAGCATGACATAC	confirmation of construct integration at *mig1* locus
oHG195	ACGTCGCTGACTGGAGGCTTTG	confirmation of construct integration at *mig1* locus
oHG196	ATCACGGCCTCTAAGGCCGTTTGATGCTAGCCATCC	complementation construct of *sad1*
oHG197	ATCACGGCCTCTAAGGCCGGCTTCAAGCAAGGTAGG	complementation construct of *vag1*
oHG198	ATCAAGGCCATCTAGGCCTGATGAAGCGCCTCAAGTCG	complementation construct of *vag1*
oHG199	GACACGAGGTGTTCGCAACGAGGAAACGAGAC	left flank of inverted *mig1* locus
oHG200	GACACCTCGTGCCGCCTTGTTGTTCATGG	right flank of inverted *mig1* locus
oHG202	ATCACGGCCTCTAAGGCCAATACGCAAACCGCCTCTC	*egfp*-nos terminator
oHG205	GATCACGGAGTGGCAGGTGCAGTGAGCAAGGGCGAGGAG	*egfp*-nos terminator
oHG206	GATCACTCCGTGTACTGATAAATGGAGAGCAGG	localization construct of *sad1*
oHG207	GATCAGTCCCTGGAACACCAAGTCCAGGAC	localization construct of *sad1*
oHG210	ATCTAGAATTCAGTGGCTCTCAGAGCGGCGG	*sr10077* fusion with GAL4-binding domain for yeast two hybrid
oHG211	ATCTAGGATCCCTATACTGATAAATGGAGAGCAGG	*sr10077* fusion with GAL4-binding domain for yeast two hybrid
oHG212	TAGGCGTGCTGGAGGAAGTG	qRT-PCR for AF244689.2
oHG213	TTGCTGGCGGTGAAGAAGGC	qRT-PCR for AF244689.2
oHG214	CACATGAGTACTGGCTTCAC	qRT-PCR for CF014750
oHG215	TGCCACGAACGGTACTAGAG	qRT-PCR for CF014750
oHG216	AGGAGCGCCTTCTCAACATC	qRT-PCR for BM339000

Name	Sequence	Use (amplification of)
oHG217	CCACACGGCAGTGTTTGTAG	qRT-PCR for BM339000
oHG218	CTTGCGGTCGTTCAACTAGG	qRT-PCR for AY562491.1
oHG219	TTCTCACGATGGGCGTTAGG	qRT-PCR for AY562491.1
oHG220	TGTCACTCAAGGAGCTGAAG	qRT-PCR for U31521.1
oHG221	AGGGTCATGTGGTCATTCTG	qRT-PCR for U31521.1
oHG222	GTGACTCTGTGGGAAACTTG	qRT-PCR for U31522.1
oHG223	TTGGTCCTGAGGTTCATGTG	qRT-PCR for U31522.1
oHG230	TCAGAATTCGGCCATTACGG	interacting gene sequence from pGADT7
oHG231	TGCACGATGCACAGTTGAAG	interacting gene sequence from pGADT7
oJS485	AGCCGGTGGTGAAGAAGTGC	left flank of knockout construct for *sr10073* and cluster 19A2
oJS486	ATCTAGGCCATCTAGGCCAAGCTCAGGC TCGACCATCC	left flank of knockout construct for *sr10073* and cluster 19A2
oJS487	ATCTAGGCCTGAGTGGCCTGGCGTGTCTT CTCTGAAGC	right flank of knockout construct for *sr10079* and cluster 19A2
oJS488	CTGCATGACGGTTCGTTTCG	right flank of knockout construct for *sr10079* and cluster 19A2
oJS489	GAACTCCTCGCGCAGTTTGG	whole knockout construct for cluster 19A2
oJS490	GTCGAATGTGGCGCTGATCC	whole knockout construct for cluster 19A2
oJS588	ATCACGGCCTCTAAGGCCATGCAGGCGT TCAATGTTGG	sr10057 for integration at *mig1* locus
oJS589	ATCAAGGCCATCTAGGCCAGTTTCGCTC GCTGATTTGG	sr10057 for integration at *mig1* locus
oJS495	ATCATGGCCTCTAAGGCCGCGTCATGGG TAGGTGTAAAC	sr10060 for integration at *mig1* locus
oJS496	ATCTAGGCCATCTAGGCCACGCTAGCCA GGTCTGATAGTG	sr10060 for integration at *mig1* locus
oJS568	ATATAGGCCTGAGTGGCCGCGATTCGCT CCTTCTTTGC	right flank of knockout construct for *dicer*
oJS569	ATCTAGGCCATCTAGGCCCTCATGTGCGT GCCGTTCTAC	left flank of knockout construct for *dicer*

Name	Sequence	Use (amplification of)
oJS570	TCAGCGCCAAACGCAAACC	left flank of knockout construct for *dicer*
oJS554	GTCGCGTGGTTTGAAGTTGG	right flank of knockout construct for *dicer*
oBH73	ACCTCACCGACCACCTAATG	qRT-PCR of maize *actin*
oBH74	ACCTGACCATCAGGCATCTC	qRT-PCR of maize *actin*

4.1.6 Plasmid Vectors

The plasmids constructed and used in this study are listed below (Table 9).

Table 9. List of plasmids and their usage.

Plasmid name	Use and description	Reference
pRS300	It contains an Arabidopsis miRNA gene called *miR319a* to be used as template for generating amiRNA that can silence gene expression.	Detlef Weigel, Max Planck Institute, Tübingen
p*gfp*-RNAi	For silencing *gfp* using inverted repeats. A 337 pb sense and a 351 bp antisense fragment of *gfp*, and a 302 bp fragment of *bW1* intron were amplified using oHG21 + oHG22, oHG20 + oHG19 and oHG18 + oHG17, respectively, from gDNA of *S. reilianum* strain JS64, which contains ectopic copy of *gfp*. Sense, antisense and *bW1* intron were digested with *Acc65I* + *SfiI*, *SfiI*, and *NotI* and *SfiI*, respectively, and then ligated. The hsp70 promoter (1326 bp) from pCM54 was digested with *Acc65I* and *HindIII*, and was then ligated with sense-intron-antisense construct to generate the silencing construct, which was ligated into p123 digested with *HindIII* and *NotI*.	This study
p*gfp*-amiRNA	For silencing *gfp* using amiRNA. Overlap extension PCR using the primers oHG9 + oHG14 and the template pRS300 was performed to replace 21 bp miRNA of the Arabdiposis gene *miR319a* with 21 bp for *gfp* according to WMD3 web (http://wmd3.weigelworld.org/cgi-bin/webapp.cgi?page=Help). A 487 bp fragment encoding miRNA for *gfp* was digested with *Acc65I* and *NotI*. The hsp70 promoter (1326 bp) from pCM54 was digested with *Acc65I* and *HindIII*, and was then ligated with the 487 bp fragment to generate the silencing construct, which was ligated into p123 digested with *HindIII* and *NotI*.	This study
p*mig1*	For integration at *mig1* locus 1 kb of right and left flanks of *mig1* locus were amplified with oHG149 + oHG150 and oHG151 + oHG154, respectively, digested with *DraIII* and then ligated. The ligated fragment and p123 were digested with *BsaBI* and then ligated together.	This study
pTOPO-*sad1-egfp*	A 1655 bp *sad1* with promoter fragment and a 1174 bp *gfp* fragment were amplified with oHG206 + oHG172 and oHG205 +	This study

Plasmid name	Use and description	Reference
	oHG202, respectively, digested with *DraIII* and then ligated into pTOPO	
p*mig1-sad1-egfp*	For integration of *sad1* fused to *gfp* at *mig1* locus A 2396 bp *sad1-gfp* was digested from pTOPO-*sad1-egfp* with *PvuII* and *EcoRI* and ligated into p*mig1*	This study
pTOPO-*vag1-egfp*	A 2473 bp *vag1* with promoter fragment and a 1174 bp *gfp* fragment were amplified with oHG207 + oHG198 and oHG205 + oHG202, respectively, digested with *AlwNI* and then ligated into pTOPO	This study
p*mig1-vag1-egfp*	For integration of *sad1* fused to *gfp* at *mig1* locus A 3626 bp *vag1-gfp* was digested from pTOPO-*sad1-egfp* with *SfiI* and *NcoI* and ligated into p*mig1*	This study
pGBKT7-BD-SAD1ΔSP	Expressing N-terminal SAD1 without signal peptide sequence fused to GAL4 binding domain for yeast two hybrid screen A 490 bp fragment of *sad1* without signal peptide was amplified with oHG210 + oHG211, digested with BamHI and EcoRI, and then ligated into pGBKT7	This study
pGADT7-SfiI	Modified pGADT7 by inserting a *SfiI* cutting sites at the GAL4 activation domain for directional cloning of the cDNA library	Bio S&T INC., Lachine, QC, Canada
pGADT7-T	T-antigen gene fused to GAL4 activation domain as control	Clontech, Saint-Germain-en-Laye, France
pGBKT7-53	Expressing P53 fused to GAL4 binding domain as positive interaction with T-antigen	Clontech, Saint-Germain-en-Laye, France
pGBKT7-LAM	Expressing LAM protein fused to GAL4 binding domain as negative interaction with T-antigen	Clontech, Saint-Germain-en-Laye, France
pGH215	GFP expressing vector under the control of *ubi* promoter for protoplast transformation	Jochen Kumlehn, IPK, Gatersleben
p*35Sp:gfp:sad1*Δ*sp*	GFP:SAD1ΔSP fusion expressing vector under the control of 35S promoter for protoplast transformation	Christian Löfke, Göttingen University
pNEB-Sr-Cbx	For integration at the *S. reilianum* succinate dehydrogenase locus	M. Wagenknecht
p123	For construction of *gfp* gene fusions.	C. Aichinger
pBS-Cbx(+)	To obtain the carboxin resistance cassette with *SfiI* digestion or PCR amplification	(Brachmann et al., 2004)
pBS-hnn	To obtain the hygromycin resistance cassette with *SfiI* digestion or PCR amplification	(Kämper, 2004)
pNEBUH	Self replicating plasmid containing hygromycin resistance cassette for testing the *S. reilianum* protoplast transformation efficiency	G. Weinzierl,
pNEBUC	Self replicating plasmid containing carboxin resistance cassette for testing the *S. reilianum* protoplast transformation efficiency	G. Weinzierl,
TOPO®TA	For cloning PCR fragments with TA cloning	Invitrogen, Karlsruhe

4.1.7 Chemicals and Suppliers

All chemicals used in the stated experiments were of molecular biology grade supplied by

Sigma, Fluka, Clonetech, Merck, Roche, Bio-Rad, Difco or Roth. Exceptions are indicated in the text.

4.1.8 Commercial Kits

The commercial kits used in this study are listed below (Table 10).

Table 10. List of kits and their suppliers.

Kit name	Supplier
DIG-HIGH-Prime	Roche, Mannheim
GenElute™ Gel Extraction	Sigma-Aldrich, Dürheim
GenElute PCR DNA Purification	Sigma-Aldrich, Dürheim
iQ SYBR Green Supermix	Bio-Rad, München
Matchmaker Gold Yeast Two Hybrid System	Clontech, Saint-Germain-en-Laye, France
RNeasy Plant Mini Kit	Qiagen, Hilden
DNeasy Plant Mini Kit	Qiagen, Hilden
TOPO TA Cloning Kit	Invitrogen, Karlsruhe
Plasmid Mini	Qiagen, Hilden
CompactPrep Plasmid Maxi	Qiagen, Hilden
InnuPREP PCRpure	Analytikjena, Jena
InnuPREP Gel Extraction	Analytikjena, Jena
In-Fusion Advantage PCR Cloning	Clontech, Saint-Germain-en-Laye, France
RevertAid™ First Strand cDNA Synthesis	Fermentas, St. Leon-Rot
CDPstar	Roche, Mannheim
Agilent RNA 6000 Nano Reagents	Agilent, Böblingen
One-Cycle cDNA Synthesis Kit	Affymetrix, Santa Clara, California
GeneChip IVT Labeling Kit	Affymetrix, Santa Clara, California
GeneChip® Maize Genome Array	Affymetrix, Santa Clara, California
ECLReagenz	GE Healthcare, München

4.1.9 Enzymes

The enzymes used in the current study are listed below (Table 11).

Table 11. List of enzymes and their suppliers.

Enzymes	Supplier
Lysozyme	Merk, Nottingham
Novozym 234	Novo Nordisc, Copenhagen, Denmark
Restriction enzymes	New England Biolabs GmbH, Frankfurt
Antarctic Phosphatase	New England Biolabs GmbH, Frankfurt
T4 Polynucleotide Kinase	Fermentas, St. Leon-Rot
Phusion DNA-Polymerase	New England Biolabs GmbH, Frankfurt
Taq-Polymerase Fermentas (St. Leon-Rot)	Fermentas, St. Leon-Rot
KOD Xtreme™ Hot Start DNA Polymerase	Merk, Nottingham
T4-DNA-Ligase	Roche, Mannheim
RNAse A	Serva, Heidelberg
RNase-Free DNase Set	Qiagen, Hilden

4.1.10 Media

YEPSL Medium Modified from (Tsukuda et al., 1988)

10 g/l	Tryptone
10 g/l	Yeast extract
10 g/l	Sucrose

CM Medium (Holliday, 1974; Banuett and Herskowitz, 1989)

1.5 g/l	NH4NO3
1 g/l	Yeast extract
2.5 g/l	Casamino Acids
0.5g/l	Hering sperm DNA
10 ml/l	Vitamin solution (see below)
62.5 ml/l	salt solution (see below)
20 g/l	Agar (only for solid medium)
pH 7.0	
40 ml/l	50% Glucose (after autoclaving the medium)

PD Medium

24 g/l	Potato Dextrose Broth
20 g/l	Agar (only for solid medium)

Regeneration Medium (Schulz et al., 1990)

10 g/l	Tryptone
10 g/l	Yeast extract
10 g/l	Sucrose
182.2 g/l	Sorbitol
20 g/l	Agar (only for solid medium)

NSY Glycerin Medium (Holliday, 1974)

8 g/l	Nutrient Broth
10 g/l	Yeast extract
5 g/l	Sucrose
696 ml/l	Glycerin

Ammonium Minimal (NM) Medium

3 g/l	$(NH_2)SO_4$
62.5 ml/l	Salt solution
pH 7.0	
20 g/l	Agar (only for solid medium)
20 ml/l	50% Glucose (after autoclaving the medium)

Nitrat Minimal (NM) Medium

3 g/l	KNO_3
62.5 ml/l	Salt solution
pH 7.0	
20 g/l	Agar (only for solid medium)
40 ml/l	50% Glucose (after autoclaving the medium)

Water Agar Medium

10 g/l	Agar

YT Medium (Sambrook and Russell, 2001)

8 g/l	Trypton
5 g/l	Yeast extract
5 g/l	NaCl
20 g/l	Agar (only for solid medium)

SOC Medium (Sambrook and Russell, 2001)

20 g/l	Tryptone
5 g/l	Yeast extract
10 mM	NaCl
2.5 mM	KCl
10 mM	$MgCl_2$
10 mM	$MgSO_4$
pH 7.0	
20 mM	Glucose (after autoclaving the medium)

YPDA Medium

20 g/l	Difco peptone
10 g/l	Yeast extract
0.03 g/l	Adenine hemisulfate
20 g/l	Agar (only for solid medium)
pH= 6.5	
40 ml/l	50% Glucose (after autoclaving the medium)

SD Medium

6.7 g/l	Yeast nitrogen base without amino acids
100 ml/l	Appropriate sterile 10X dropout solution (see below)
20 g/l	Agar (only for solid medium)
pH= 5.8	
40 ml/l	50% Glucose (after autoclaving the medium)

4.1.11 Medium Additives

Trace Elements Solution (Holliday, 1974)

60 mg/l	H3BO3
140 mg/l	MnCl2 x 4 H2O
400 mg/l	ZnCl2
40 mg/l	NaMoO4 x 2 H2O
100 mg/l	FeCl3 x 6 H2O
40 mg/l	CuSO4 x 5 H2O

Salt Solution (Holliday, 1974)

16 g/l	KH2PO4
4 g/l	Na2SO4
8 g/l	KCl
4 g/l	MgSO4 x 7 H2O
1.32 ml/l	CaCl2 x 2 H2O
8 ml/l	Trace elements solution (see above)

Vitamin Solution (Holliday, 1974)

100 mg/l	Thiamin
50 mg/l	Riboflavin
50 mg/l	Pyridoxin
200 mg/l	Calcium pantothenate
500 mg/l	p-Aminobenzoic acid
200 mg/l	Nicotinic acid
200 mg/l	Cholin chloride
1000 mg/l	Myo-Inositol

10X Dropout Solution

200 mg/l	L-Adenine hemisulfate salt

200 mg/l	L-Arginine HCl
200 mg/l	L-Histidine HCl monohydrate
300 mg/l	L-Isoleucine
1000 mg/l	L-Leucine
300 mg/l	L-Lysine HCl
200 mg/l	L-Methionine
500 mg/l	L-Phenylalanine
2000 mg/l	L-Threonine
200 mg/l	L-Tryptophan
300 mg/l	L-Tyrosine
200 mg/l	L-Uracil
1500 mg/l	L-Valine

X-α-Gal

Dissolve 5-bromo-4-chloro-3-indolyl- α-D-galactopyranoside (Clontech, Saint-Germain-en-Laye, France) in N,N dimethylformamide (DMF) at a concentration of 20 mg/ml. The final concentration in medium is 40 μg/ml X-α-Gal.

X-β-Gal

Dissolve 5-bromo-4-chloro-3-indolyl-β-D-galactopyranoside (Sigma-Aldrich, Dürheim) in N,N dimethylformamide (DMF) at a concentration of 20 mg/ml. The final concentration in medium is 40 μg/ml.

Antibiotics

The antibiotics used in the current study are listed below (Table 12).

Table 12. List of antibiotics, their final concentration and suppliers.

Antibbiotic	Final concentration	Supplier
Ampicillin	100 μg/ml	Sigma-Aldrich, Dürheim
Kanamycin	50 μg/ml	Duchefa, Haarlem, The Netherland
Spectinomycin	100 μg/ml	Duchefa, Haarlem, The Netherland
Carboxin	5 μg/ml	Riedel-de Haën, Seelze
Hygromycin	150 μg/ml	Duchefa, Haarlem, The Netherland

Antibbiotic	Final concentration	Supplier
Aureobasidin	125-300 ng/ml	Clontech, Saint-Germain-en-Laye, France

4.1.12 Antibodies

Mouse anti c-myc epitope monoclonal antibody (Roche, Mannheim)

Goat anti-mouse IgG-Horseradish Peroxidase (Promega, Mannheim)

Anti-digoxigenin (DIG) antibody (Roche, Mannheim)

4.1.13 Miscellaneous Materials

Nylonmembran positively charged (Roche, Mannheim)

Nylonmembran Hybond N+ (GE Healthcare, München)

Medical X-Ray screen film blue sensitive (CEA, Strängäs, Sweden)

4.2 Growth Conditions

4.2.1 Cultivation of Maize

Pots 13 cm were filled with soil Type T (Frühstorfer Pikiererde, Germany) and five maize seeds were sown and watered daily. The maize (*Z. mays*) cultivar Gaspe Flint was grown in a greenhouse under the following conditions; day conditions; 28°C, 40% relative humidity and minimum 28000 Lux light with additional 90000 Lux sun radiation for 15 h, night conditions; 20°C and 60% relative humidity for 9 h. Between day and night shifts 2.5 h and 3.5 h of light ramping was included to simulate sunset and sunrise, respectively

For microarray experiments the plants were transferred from the greenhouse to a phytochamber (Vötsch, Balingen-Frommern, Germany) six days post sowing the seeds. The growth conditions in the phytochamber were like in the greenhouse with the exception of 1 h ramping between day and night shifts.

4.2.2 Cultivation of Sorghum

Sorghum bicolor (L.) Moench (Tall Polish) was obtained from Institut für Pflanzengenetik und Kulturpflanzenforschung (Gatersleben, Germany). Seeds were sown in vermiculite for 5 days in

a phytochamber under the following conditions; 28°C, 50% relative humidity and minimum 28000 Lux light with for 15 h, night conditions; 20°C and 60% relative humidity for 9 h. Seedlings were left afterwards in dark for a week.

4.2.3 Cultivation of *S. reilianum*

S. reilianum strains were grown on regeneration agar or PD solid media supplemented with the appropriate antibiotic at 28°C. The strains were also grown in YEPSL, PD or CM liquid media under constant agitation of 200 rpm. Strains were preserved on the solid medium up to three weeks or stored at -80°C in NSY glycerin medium.

4.2.4 Cultivation of Yeast

Yeast (*Saccharomyces cerevisiae*) strains were grown on YPDA medium or SD medium supplemented with the proper dropout and antibiotic at 30°C´for 3-5 days. Liquid cultures were grown under constant agitation of 250 rpm. Strains were preserved on the solid medium for four weeks or stored at -80°C in YPDA medium with 25% Glycerol.

4.2.5 Cultivation of *E. coli*

E. coli strains were grown on YT solid medium or liquid cultures supplemented with the appropriated antibiotic at 37°C overnight. Liquid cultures were grown under constant agitation of 200 rpm. Strains to be preserved were stored at -80°C in YT medium with 10% Glycerol.

4.3 Nucleic Acids Extraction, Modification and Cloning

4.3.1 Plasmid Extraction from *E. coli*

Plasmid extraction was achieved by the boiling lysis method (Sambrook and Russell, 2001) with some modifications. A 2 ml overnight culture of *E. coli* strain was centrifuged for 2 min at 13000 rpm in benchtop centrifuge (Heraeus Biofuge 15). After decanting the supernatant the cell pellet was stored at -20°C at least for 20 min and then was thoroughly resuspended in 325 µl STET buffer with 25 µl lysozyme solution (10 µg/µl). Cell suspension was heated at 99°C for 1 min. The lysis mixture was centrifuged for 15min at 13000 rpm and the cell pellet was removed with a toothpick. Plasmid DNA was precipitated by the addition of 40 µl 3 M sodium acetate (pH 5.3)

and 400 µl isopropanol the tube was inverted several times. The plasmid DNA was precipitated by centrifugation for 10 min at 13000 rpm. The supernatant was aspirated and the pellet washed with 500 µl 70% ethanol and then centrifuged for 5 min at 13000 rpm. The supernatant was aspirated and the pellet was dried at room temperature. The pellet was dissolved in 100 µl TE with 20 mg/ml RNase A at 50°C for 15 min and stored at -20°C.

1 M Tris-HCl pH 8.0

563 mM	Tris-HCl
437 mM	Tris-Base

STET buffer

50 mM	Tris-HCl, pH 8.0
50 mM	Na_2-EDTA
8 %	Sucrose
5%	Triton X-100

Lysozyme solution

10 mg/ml	Lysozyme
10 mM	Tris-HCl, pH 8.0

4.3.2 Plasmid Extraction from Yeast

Plasmid extraction was performed according to (Robzyk and Kassir, 1992) with some modifications. A single colony of yeast was grown in a 2 ml SD liquid medium for 1-2 days and then centrifuged in 2 ml tubes with 200 µl glass beads for 5 min at 13000 rpm in benchtop centrifuge (Heraeus Biofuge 15). The supernatant was aspirated and the cell pellet was stored at -20°C for at least 20 min, and then 100 µl Yeast-STET buffer were added and vortexed for 5 min followed by adding 50 µl Yeast-STET and vortexing for 3 min. Cell suspension was heated at 99°C for 3 min and then cooled on ice for 3 min. The mixture was centrifuged at 13000 rpm and 4°C for 10 min, and 100 µl supernatant were mixed with 50 µl ammonium acetate (7.5 M). The

mixture was incubated at -20°C for 1 h and then centrifuged at 4000 rpm and 4°C for 20 min. Plasmid DNA was precipitated by mixing 75 supernatant with 150 µl cold ethanol followed by centrifugation at 4000 rpm and 4°C for 20 min. The supernatant was aspirated and the pellet was dried at room temperature. The pellet was dissolved in 20 µl water and then stored at -20°C.

Yeast-STET Buffer

8%	Sucrose
50 mM	Tris-HCl pH 8.0
50 mM	EDTA pH 8.0
5%	Triton X-100

4.3.3 Genomic DNA Extraction from Maize

The plant tissues were ground with liquid nitrogen and 100 mg were mixed with 400 µl *Ustilago* lysis buffer, 500 µl phenol-chloroform mixture (1:1) and 200 µl glass beads. Mixture was vortexed for 15 min using Vibrax shaker at maximum speed. After centrifuging at 13000 rpm, 20 min, RT, the upper phase was transferred to a fresh tube and phenol-chloroform extraction was repeated. The DNA was precipitated with the addition of 0.1 V 3 M Na-acetate and 2.5 V ethanol 96% and centrifugation at 13000 rpm, 15 min. The supernatant was aspirated and the pellet was washed with 500 µl ethanol 70% then centrifuged at 13000 rpm, 10 min. The supernatant was aspirated and the pellet left to dry at room temperature. The DNA pellet was resuspended in 50 µl TE with 20 mg/ml RNase A at 55°C for 15 min and the DNA was stored at -20°C.

***Ustilago* Lysis Buffer**

50 mM	Tris-HCl, pH 7.5
50 mM	Na_2-EDTA
1 %	SDS

Phenol:Chloroform

0.5 Vol	Phenol
0.5 Vol	Chloroform
Equalibrate with	TE

4.3.4 Genomic DNA Extraction from *S. reilianum*

This is a modified version of the method by (Hoffman and Winston, 1987). A single colony of *S. reilianum* was grown in 2 ml YEPSL liquid medium at 28°C with 200 rpm shaking for 36-40 h. The cell culture was centrifuged with 200 µl glass beads at 13000 rpm for 5 min. Supernatant was aspirated and pellet was frozen at -20°C for at least 20 min. The cells were resuspended in 500 µl *Ustilago* lysis buffer and 600 µl phenol-chloroform mixture (1:1). Mixture was vortexed for 15 min using Vibrax shaker at maximum speed. After centrifuging at 13000 rpm, 25 min, RT, the upper phase was transferred to a fresh tube. The DNA was precipitated with the addition of 1 ml of ethanol 96% and centrifugation at 13000 rpm, 15 min. The supernatant was aspirated and the pellet left to dry at room temperature. The DNA pellet was resuspended in 50 µl TE with 20 mg/ml RNase A at 55°C for 15 min and stored at -20°C.

4.3.5 RNA Extraction from Maize

A 2 cm piece below the injection hole of the third leaves at 3 dpi, first nodes at 15 dpi and ears at 4 weeks post inoculation (wpi) with 1-2 cm length from healthy or *S. reilianum* infected plants were collected in liquid nitrogen. Only infected ears that showed elongation of the kernels without any leafy structures were collected. Each ear sample was collected from 20 plants and the whole experiment was independently repeated three times. The samples were ground with liquid nitrogen, and 10 volumes TRI Reagent (Sigma) were added and mixed together. The mixture was incubated 15 min at room temperature and then 0.2 volume chloroform was added followed by short vortexing. The mixture was centrifuged at 13000 rpm and 4°C for 15 min. The aqueous phase was mixed with the same volume of phenol: chloroform: isoamyl alcohol (25:24:1) and centrifuged at 13000 rpm and 4°C for 15 min. The aqueous phase was mixed with the same volume of isopropanol and centrifuged at 13000 rpm and 4°C for 15 min. RNA was precipitated by centrifugation at 13000 rpm and 4°C for 15 min. The supernatant was aspirated and the RNA was washed with 2 ml 80% ethanol by inverting the tubes several times. RNA was precipitated by centrifugation at 13000 rpm for 10 min and the supernatant was aspirated. The cell pellet was dried at room temperature and then dissolved in the same volume of the plant sample weight using RNase free water at 50°C and 550 rpm for 10 min. DNAse treatment was performed using RNase-Free DNase Set (Qiagen) and then the RNA was cleaned up with RNeasy Plant Mini Kit (Qiagen). The RNA quality analyzed on a 1% TBE agarose gel and by

Bioanalyzer 2100 (Agilent), and the RNA purity and concentration were analyzed with the NanoDrop ND-1000 or Nanodrop 2000c (Thermo Fisher Scientific). The RNA samples were stored at -80°C until use.

4.3.6 RNA Extraction from Fungal Liquid Culture

A single colony of *S. reilianum* was inoculated in YEPSL liquid medium for 8-12 h. This culture was used to inoculate 50 ml CM medium overnight until OD600nm= 0.5. The cell culture was centrifuged at 3500 rpm for 5 min. The supernatant was discarded and the cell pellet was immediately frozen in liquid nitrogen and stored at –80°C until RNA extraction. The frozen pellet was resuspended in 1.5 ml TRI Reagent (sigma) and the mixture was transferred into 2 ml tubes containing 200 µl glass beads. The mixture was vortexed at Vibrax shaker at maximum speed for 10 min and then 300 µl chloroform were added followed by short vortexing. The mixture was incubated for 3 min at room temperature and then centrifuged at 13000 rpm and 4°C for 15 min. The aqueous phase was transferred into new tube and mixed with the same volume of isopropanol by inverting the tube several times. RNA was precipitated by centrifugation at 13000 rpm and 4°C for 15 min. The supernatant was aspirated and the RNA was washed with 1 ml 80% ethanol by inverting the tubes several times. RNA was precipitated by centrifugation at 13000 rpm for 10 min and the supernatant was aspirated. The cell pellet was dried at room temperature and then dissolved in 50 µl RNase free water at 50°C and 550 rpm for 10 min. DNAse treatment was performed using RNase-Free DNase Set (Qiagen) and then the RNA was cleaned up with RNeasy Plant Mini Kit (Qiagen). The RNA quality analyzed on a 1% TBE agarose gel and by Bioanalyzer 2100 (Agilent), and the RNA purity and concentration were analyzed with the Nanodrop 2000c (Thermo Fisher Scientific). The RNA sample was stored at -80°C.

4.3.7 RNA Concentration

RNA was mixed with 0.1 V 5 M NaCl and 2 V cold ethanol 96%, incubated for 45 min at -70°C and centrifuged at 13000 rpm and 4°C for 10 min. The pellet was washed with 1 ml 75% ethanol and then centrifuged for 13000 rpm and 4°C for 10 min. The ethanol was aspirated and the pellet was dried at room temperature then dissolved in an appropriate amount of RNase-free water.

4.3.8 Polymerase Chain Reaction

Polymerase chain reaction (PCR) was carried out to amplify a DNA fragment and to confirm the presence or absence of DNA sequence. For cloning purposes Phusion and KOD Xtreme were used, and for only checking the genotype recombinant DNA Taq polymerase (Fermentas, St. Leon-Rot) was used. The PCR reactions were set up as following:

PCR component	Phusion	KOD Xtreme	Taq polymerase
DNA template	10-100 ng	10-100 ng	10-100 ng
PCR buffer	10 (5X)	25 (2X)	2.5 (10X)
dNTPs	0.4 µl (25 mM)	10 µl (2 mM)	0.2 µl (25 mM)
Forward primer	1 µl	1.5 µl	0.5 µl
Reverse primer	1 µl	1.5 µl	0.5 µl
Enzyme	0.25 U	1 U	1.25 U
DMSO	-	-	0.75 µl
1.5 M $MgCl_2$	-	-	1.5 µl
Water	rest	rest	rest
Total	50 µl	50 µl	25 µl

For DNA amplification a TPersonal thermocycler (Biometra, Göttingen) was used. The following cycling conditions were applied:

PCR cycle	Phusion	KOD Xtreme	Taq polymerase
1. Initial denaturation	98°C/30 s	94°C/2 min	94°C/2 min
2. Denaturation	98°C/15 s	94°C/30 s	94°C/20 s
3. Annealing	60-68°C/30 s	62°C/15 s	60-63°C/20 s
4. Extension	72°C/30 s/kb	68°C/1 min/kb	72°C/1 min/kb
Number of cycles (step 2-4)	32	40	35
Final extension	72°C/10 min	68°C/10 min	72°C/10 min
Storage	4°C	4°C	4°C

4.3.9 Overlap Extension PCR

To join several DNA fragments together an overlap extension PCR was performed according to (Heckman and Pease, 2007). The primers were designed to posses 15-20 b overlap to the joining fragment. Each fragment was amplified with Phusion or KOD Xtreme independently for 12-20 cycles and then the fragments were mixed together in 1:1 or 1:2:1 ratio and they amplification was continued for additional 20 cycles. The fragment mix was amplified by Phusion or KOD Xtreme to generate the joined fragments with the following PCR programs:

PCR cycle	Phusion	KOD Xtreme
1. Initial denaturation	98°C/30 s	94°C/2 min
2. Denaturation	98°C/15 s	94°C/30 s
3. Annealing	60-68°C/60 s	62°C/60 s
4. Extension	72°C/30 s/kb	68°C/1 min/kb
Number of cycles (step 2-4)	12	20
Mix PCR products	-	-
Number of cycles (step 2-4)	20	20
Final extension	72°C/10 min	68°C/10 min
Storage	4°C	4°C

4.3.10 Quantitative Real Time Polymerase Chain Reaction

To quantify the gene expression, a quantitative real time polymerase chain reaction (qRT-PCR) was performed according to (Ghareeb et al., 2011). Perceeding qRT-PCR, reverse transcription of 1 µg total RNA in 10 µl reaction volume was performed with the RevertAid H Minus First Strand cDNA Synthesis Kit (Fermentas) using the oligo dT primer, according to the manufacturer's instructions. The cDNA was used for qRT-PCR.

The qRT-PCR mixture contained 7.5 µl cDNA (diluted 18 X), 10 µl iQ SYBR Green 2x Supermix (Bio-Rad) and 300 nM from forward and reverse primers in 20 µl total volume. PCR was performed using the CFX384 real-time PCR detection system (Bio-Rad). Cycling parameters were the same for all primers; initial 95°C for 6 min, followed by 40 cycles of 95°C for 30 s, 60°C for 1 min, plate read step, then product melting curve 55–95°C. The results were analyzed with CFX Manager V1.6 (Bio-Rad).

4.3.11 DNA Digestion

Plasmids and genomic DNA were digested with restriction enzymes (NEB, Frankfurt) for 1-16 h under the appropriate temperature. The digested DNA was elctrophoretically separated on TAE agarose gel to analyze the digestion pattern. The DNA digestion reaction typically contained:

0.5-2 µg	DNA
2 µl	10X enzyme buffer (NEB buffer 1-4)
0.2 µl	100X BSA (if required)
0.5-2 U	Restriction enzyme
Fill to 20 µl	Water

The digestion reaction was incubated for 4-16 h.

4.3.12 DNA Ligation

The Ligation of DNA fragments were perfomed using T4 DNA Ligase (Roche, Mannheim). The DNA fragment were mixed in 1:2:1 (left flank: resistance cassette: right flank) ratio for gene deletion constructs and 1:3 (vector: insert) ratio for plasmid constructions. A typical ligation reaction consisted of:

50-500 ng	Digested DNA flanks, insert or/and vector
3 µl	10x T4 DNA Ligase buffer
1 U	T4 DNA Ligase
Add to 30 µl	Water

The ligation reaction was incubated at 16°C overnight or at 22 for 1-4 h.

4.3.13 Gel Electrophoresis of Nucleic Acids

Nucleic Acids were analyzed and visualized by elctrophoretical separation on a 0.8-2% TAE or TBE agarose gel. The proper weight of agarose LE was added in 1X TAE or 0.5X TBE buffers and boiled until agarose was completely melted. Ethidium bromid was added to a final concentration 1 µg/ml. The gel was cooled to ~60°C and then was poured in closed cassette with the appropriate comb. After solidification, the gel was placed in electrophoresis tank filled with the same buffer as the gel (1X TAE or 0.5X TBE bufferes). DNA or RNA samples were mixed

with loading buffer and loaded in the wells along with 5 µl DNA 2-log ladder (NEB, Frankfurt). The samples were electrophoreticallay separated with 70-150 V for 0.3-4 h.

1X TAE Buffer

40 mM	Tris-Acetat
1 mM	Na_2-EDTA

0.5X TBE Buffer

50 mM	Tris-Borat, pH 7,9
1 mM	Na_2-EDTA

6X Loading Buffer

50%	Sucrose
0.25%	Bromphenolblau
10 mM	HCl, pH 7.9
1 mM	Na2-EDTA

4.3.14 Southern Blot

Blotting of DNA separated by gel electrophoresis on nylon membrane was performed according to (Southern, 1975) with some modifications. Briefly 2.5-5 µg genomic DNA were digested with the appropriate restriction enzyme(s). The digested DNA was electrophoretically separated on 0.9% TAE agarose gel, photo documented with a linear, and then the gel was incubated in 0.25 M HCl for 15 min with gentle agitation. The gel was neutralized to denature the DNA by incubation in 0.4 M NaOH for 15 min with gentle agitation. The DNA was transferred on a positively charged nylon membrane (Roche) by capillary transfer overnight using 0.4 M NaOH as a transfer buffer and hand towels as capillary force. Positions of the lanes and DNA ladder were marked on the membrane with a pencil. Membranes were air-dried and crosslinked by UV exposure (302 nm, 120 mJ/cm^2). All the following steps were performed in a hybridization oven with rolling. The membrane was prehybridized in 20 ml Southern hybridization buffer and incubated at 65°C for 1 h and then hybridized with the labeled DNA probe (see below) at 65°C

overnight. The DNA probe was recovered and the membrane was washed twice with Southern wash buffer at 65°C each for 20 min. All the following steps were performed at room temperature. The membrane was washed with DIG wash buffer for 5 min. Blocking of the membrane was achieved by incubation in DIGII for 30 min. The membrane was incubated with 5 ml α-DIG-Antibody-solution (1:10000 in DIGII) for 30 min and then washed twice with DIG wash buffer each for 15 min. The membrane was equilibratet in DIGIII for 5 min and then incubated with 5 ml CDPStar solution (1:200 in DIGIII). The CDPStar solution was recovered and the membrane was sealed in a plastic bag. The membrane was incubated at 37°C for 15 min and then incubated with chemiluminescence sensitive film in dark for 1-20 min in a closed cassette. The film was develop and fixed using developing machine (QX-60, Konica).

Na-Phosphate Buffer, 1 M, pH 7.0

142 g/l	Na2HPO4 (1 M)-solution 1
138 g/l	NaH2PO4xH2O (1 M)-solution 2

Add solution 2 until pH 7.0

Southern Hybridization Buffer

0.5 M	Na-Phosphate buffer, pH 7.0
7%	SDS

Southern Wash Buffer

0.1 M	Na-Phosphate buffer, pH 7.0
1%	SDS

DIGI Buffer

0.1 M	Maleic Acid
0.15 M	NaCl
pH 7.5	With ~40ml/l NaOH (5 M)

DIGI Wash Buffer

97.7%	DIGI buffer

0.3%	Tween-20

Blocking Solution

90%	DIGI buffer
10%	Blocking reagent

DIGII Buffer

1 Vol	Blocking solution
9 Vol	DIGI buffer

DIGIII Buffer

0.1 M	Tris-HCl pH 9.5
0.1 M	NaCl
0.05 M	MgCl2x6H2O

Southern Antibody Solution

1 µl	Anti-Digoxigenin-AP
10 ml	DIG2 buffer

CDP-Star Buffer

50 µl	CDP-Star
10 ml	DIG3 buffer

4.3.15 DNA Probe Labeling

DNA probes used for Southern blot hybridization were labeled by denaturing ~300 ng (16 µl) PCR product of the whole DNA construct at 95°C for 5 min, cooling for 1 min in ice cold NaCl and then mixing with 4 µl High DIG Prime labeling mix (Roche). The mixture was incubated at 37°C for 16-20 h. The labeling reaction was stopped by adding 1 µl 0.5 M EDTA and incubating at 65°C for 10 min. The labeled probe was then mixed with 20-50 ml Southern hybridization buffer and boiled at 95°C for 5 min immediately before hybridization. The probe was stored at –20°C and reused several times.

0.5 M EDTA

182,1 g/l Na_2-EDTA, pH 8.0

4.3.16 Maize Transcriptome Analysis

To analyze the changes in transcriptome of infected ears at early stage of malformation the Affymetrix Gene Chip Maize Genome arrays were performed for 3 independent experiments. RNA amplification was performed according to the manual of the One-Cycle cDNA Synthesis Kit (Affymetrix, Santa Clara, California). cRNA labeling and cRNA fragmentation and labeling were performed according to the manual of the GeneChip IVT Labeling Kit (Affymetrix, Santa Clara, California). Array hybridization, washing and staining was performed according to the Midi_Euk2V3 protocols using GeneChip Fluidics Station 400 and then the arrays were scanned with Affymetrix GSC3000 scanner (Affymetrix, Santa Clara, California).

The signal data from the microarrays were processed using the GCOS v1.4 software package (Affymetrix, Santa Clara, California). The software was used to produce presence-absence calls and to normalize the signal intensities from each array with scaling the target signal to 300 and using the default parameters. The produced files were used to analyze the statistical significant difference using the Biocondactor v2.3 package. Genes with adjusted p-value < 0.05 were considered to be significantly regulated.

4.4 Cell Transformation

4.4.1 Determination of Cell culture Densities

Densities of liquid cell culture were determined photometrically with visible light at 600 nm using a Novospec II Spectrophotometer (PharmaciaBiotech) or NanoDrop 2000C (Thermo Fisher Scientific). To ensure that a linear correlation between culture density and optical density at 600 nm (OD_{600nm}) the cultures were diluted to a measured value of below 0.8 after determining the zero value with the pure medium in which the cells were cultivated.

4.4.2 *S. reilianum* Protoplast Transformation

Protoplast and transformation of *S. reilianum* were prepared according to (Schulz et al., 1990; Gillissen et al., 1992) with some modifications. A single fungal colony was used to inoculate 2

ml YEPSL liquid medium and incubated at 28°C for 8 – 12 h. This culture was used to inoculate 100 ml of YEPSL, which was incubated at 28°C with constant shaking at 200 rpm. Cells were grown overnight to an OD_{600nm}= 0.6–0.8 and subsequently centrifuged at 3500 rpm (Beckmann Biofuge) for 5 min. The supernatant was discarded and the pellet resuspended in 50 ml SCS buffer. Cells were centrifuged at 3500 rpm for 10 min and the supernatant was discarded. Protoplasts were produced by resuspending the cells in 2 ml of Novozyme solution (Novo Nordisc, Copenhagen, Denmark) and incubating at room temperature for 5-10 min until ~50% of the cells produced protoplast. The formation of protoplasts was confirmed by microscopy. Protoplasting was stopped by adding 20 ml SCS buffer and centrifuging the solution at 2300 rpm for 15 min. The supernatant was discarded and the pellet was washed twice with SCS and once with STC, respectively, by carefully resuspending the pellet in 20 ml of either buffers and centrifuging at 2300 rpm for 15 min. Finally protoplasts were resuspended in 500 µl ice-cold STC buffer and dispensed into 70 µl aliquots and either used directly for transformation or stored at -80°C.

For transformation of the protoplast a 70 µl aliquot of protoplasts was mixed with ~5 µg DNA and 1.5 µl heparin sodium sulfate (50 mg/mL) and kept on ice for 10 min. Protoplasts were carefully mixed with 500 µl of cold STC/40% PEG solution and incubated on ice for a further 15 min on ice. The entire mixture was plated onto regeneration medium supplemented with the appropriate antibiotic. Plates were incubated at 28°C for 4-6 days or until distinct colonies appeared. Single colonies were picked using sterile toothpicks and streaked onto PD or regeneration medium-plates supplemented with the appropriate antibiotic to obtain single colonies. Putative transformants were picked as single colonies and verified by PCR and Southern blot.

SCS Solution

20 mM	Na-Citrat, pH 5.8
1 M	Sorbitol

The solution was sterile filtered

STC Solution

10 mM	Tris-HCl, pH 7.5

100 mM	CaCl2
1 M	Sorbitol

The solution was sterile filtered

STC/PEG

15 ml	STC
10 g	PEG4000

4.4.3 Rubidium Chloride Transformation of *E. coli*

Chemically competent *E. coli* cells were prepared according to (Cohen et al., 1972) with some modifications. A single colony of Top10 or Stellar *E. coli* strains was grown in 10 ml YT medium supplemented with 0.5 mM $CaSO_4$ and 0.5 mM $MgSO_4$overnight. The culture was incubated with 190 rpm constant shaking at 37°C. Next morning, 100 ml YT medium were inoculated with 1 ml overnight culture until an $OD_{600nm} \approx 0.5$-0.6 was reached. The culture was centrifuged at 3000 rpm (Beckmann Biofuge) for 15 min at 4°C. After discarding the supernatant, the cells were resuspended carefully in 33 ml ice cold RF1 solution and incubated on ice for 30-60 min. Thereafter the cells were centrifuged again at 3000 rpm for 15 min at 4°C. The cell pellet was resuspended in 330 µl ice-cold RF2 solution and incubated on ice for 15 min and finally aliquoted in 30 µl and stored at -80°C. For testing the competence efficiency of the cells 0.1 ng pUC19 plasimd was used to transform the cells.

For the transformation of the cells one aliquot was thawed on ice and then diluted with 270 µl RF2 solution. From diluted cells 50 µl were mixed with 2-5 µl ligation mixture or 5 ng plasmid DNA and incubated on ice for 30 min. The cells were heat-shocked at 42°C for 45 sec, cooled on ice immediately and 250 µl SOC medium were applied to the cells and incubated at 37°C for 1 h with 190 rpm constant shaking. The transformation mixture was plated onto YT plates containing the appropriate antibiotic concentration (see above) and incubated at 37°C overnight.

RFI Solution

100 mM	RbCl
50 mM	$MnCl_2$ x 4 H_2O

30 mM	K-Ac
10 mM	$CaCl_2$ x 2 H_2O
15%	Glycerin in ddH_2O
pH 5.8	Filter sterilize

RFII Solution

10 mM	RbCl
10 mM	MOPS
75 mM	$CaCl_2$ x 2 H_2O
15%	Glycerin in ddH_2O
pH= 5.8	Filter sterilize

4.4.4 Electro Transformation of *E. coli*

A single colony of D5Hα *E. coli* strain was grown in 10 ml YT medium overnight. The culture was incubated with 190 rpm constant shaking at 37°C. Next morning, 500 ml YT medium were inoculated with 5 ml overnight culture until an $OD_{600nm} \approx 0.5$-0.8 was reached. The culture was kept on ice for 15-30 min and then centrifuged at 3000 rpm (Beckmann Biofuge) for 15 min at 4°C. After discarding the supernatant, the cells were resuspended carefully in 500 ml ice cold water and then centrifuged at 3000 rpm for 15 min at 4°C. The cell pellet was resuspended in 250 ml ice-cold water and centrifuged as previously indicated. The cell pellet was resuspended in 10 ml ice-cold 10% glycerol and centrifuged once again. Finally the cells were resuspended in 500 µl ice-cold 10% glycerol. The cells were aliquoted in 40 µl aliquots and stored at -80°C.

For the transformation of the cells one aliquot was thawed on ice, mixed with 2-5 µl ligation mixture (previously dialysed), transferred to a pre-chilled electroporation cuvette and then placed in the electroporator (Gene Pulser, Bio-Rad). The cells then were subjected to electirical pulse (25 mF, 2.5 kV, 200 W) for 4-5 msec. Thereafter the cuvette were immediately put on ice and 500 µl SOC medium were applied to the cells and incubated at 37°C for 1 h with 190 rpm constant shaking. The transformation mixture was plated onto YT plates containing the appropriate antibiotic concentration (see above) and incubated at 37°C overnight.

4.4.5 Yeast Transformation

The transformation was carried according to (Gietz and Schiestl, 2007) and Yeastmaker™ Yeast Transformation System 2 (Clontech, Saint-Germain-en-Laye, France) with some modifications. A 2-3 mm single colony of yeast was inoculated in 3 ml YPDA liquid medium and incubated at 30°C with 250 rpm constant shaking for 8-12 h. From this culture 20 µl were used to inoculate 200 ml YPDA liquid medium and incubated as previously indicated for 16-20 h until OD_{600nm}= 0.4-0.5 is reached. The culture was centrifuged at 700 g for 5 min. Cell pellet was resuspended in 120 ml water and centrifuged once again. The cell pellet was resuspended in 1 ml 1.1X TE buffer. The cells either used immediately for transformation or kept on ice for some hours.

For transformation, the cell suspension was mixed with 1 ml denatured DNA carrier (2 mg/ml; Clontech, Saint-Germain-en-Laye, France), 0.75 1.1X TE buffer and 1.05 ml 1 M LiAc. For each transformation 35 µl were mixed with 0.2-1 µg plasmid and then 60 µl 50% PEG 3350 (Clontech, Saint-Germain-en-Laye, France) were added and mixed with 300 rpm shaking for 5 min. The mixture was heat shocked in an incubator at 42°C for 70 min with mixing each 20 min. The cells were centrifuged at 1500 g for 10 min, resuspended in 50 µl water and 15-50 µl were plated on selection plates. Plates were incubated at 30°C for 3-5 days.

10X TE

12.1 g/l	Tris-Base
3.7 g/l	Na_2-EDTAx2H_2O
pH 7.5	

10X LitAc (1M)

66 g/l	LitAc
pH=7.5	

1.1X TE/LitAc

1.1 Vol	10 x TE
1.1 Vol	10 x LitAc
7.8 Vol	H_2O

LitAc/PEG

8 Vol	50% PEG3350
1 Vol	10 x TE
1 Vol	10 x LitAc

4.4.6 Transformation of Sorghum Protoplast

Sorghum protoplast preparation and transformation were performed according to (Yoo et al., 2007) with some modifications. Leaves of 12 day-old plants were collected from 20 plants, cut carefully into 0.5 cm strips with sharp scissor without wounding. Leaf strips were dipped quickly in 10 ml enzyme solution using flat-tip forceps and then incubated overnight in a phytochamber with low indirect light at 21°C. Gently swirl the enzyme solution to release the protoplasts. A 75 µm nylon mesh (laboratory sifters, Carolina Biological Supplies) was wetted with 1 ml W5 solution, placed on a falcon tube. The enzyme solution was applied to the nylon mesh and then the falcon tube was centrifuged at 100 g for 3 min. Most of supernatant was carefully removed, protoplast pellet was resuspended in 10 ml cold W5 solution by gentle swirling and then centrifugation was repeated once again; meanwhile the protoplasts were counted using a hemacytometer. Washing with W5 solution was repeated and then the protoplasts were kept on ice for 3-5 h. The supernatant was carefully removed and the protoplast pellet was resuspended in MMG solution to reach a density of 2-4x 10^6 protoplasts/ ml.

For protoplast transformation 10 µl plasmid (10-20 µg) were mixed with 100 µl protoplast and gently mixed and then 110 µl PEG-calcium transfection solution were added and then mix completely by gently tapping the tube. The transfection mixture was incubated for up to 15 min at room temperature and then 400 µl W5 solution were added and gently mixed by inverting the tube to stop the transfection process. The mixture was centrifuged at 100 g for 2 min, the supernatant was carefully removed and then the protoplasts were resuspended in 1 ml WI solution and incubated overnight in a phytochamber at 21°C. As much as possible of the WI solution was removed and then the protoplasts were analyzed by fluorescence microscopy.

Enzyme Solution

20 mM	MES, pH 5.7

Heat to 70°C for 3 min

1.5%	Cellulase R10
0.4%	Macerozyme R10
0.4 M	Mannitol
20 mM	KCl

The mix was warmed up to 55°C for 10 min to inactivate DNases and proteases and then it was cooled down to room temperature. The following was added:

10 mM	CaCl2
5 mM	β-mercaptoethanol
0.1%	BSA

The final enzyme solution was filtered through a 0.45 mm filter into a Petri dish.

W5 Solution

2 mM	MES, pH 5.7
154 mM	NaCl
125 mM	$CaCl_2$
5 mM	KCl

WI Solution

4 mM	MES, pH 5.7
0.5 M	Mannitol
20 mM	KCl

MMG Solution

2 mM	MES, pH 5.7
0.4 M	Mannitol
15 mM	$MgCl_2$

PEG-Calcium Transfection Solution

40%	PEG4000
0.2 M	Mannitol

100 mM $CaCl_2$

4.5 Virulence Analysis

4.5.1 Generation of Gene Deletion in *S. reilianum*

To test the contribution of the gene candidates to virulence gene deletion was accomplished according to (Kämper, 2004) in the *S. reilianum* wt stains 5-1 and 5-2 and/or the solopathogenic strain JS161 (Schirawski et al., 2010). A construction of the deletion was first simulated in Clone Manager V9 software. For each gene deletion a replacement construct was generated by PCR amplification of ~1 kb DNA fragments of the gene flanking regions, which were then cleaned up with GenElute PCR DNA Purification (Sigma). The gene flanks and a resistance cassette (hygromycin or carboxin) were digested with SfiI enzyme as indicated above to generate combatable ends. The fragments were electrophoretically separted on 1% TAE agarose gel, cut from the gel and then cleaned up from with GenElute™ Gel Extraction (Sigma). The fragments were ligated together as indicated above. The ligated fragments were electrophoretically separted on 1% TAE agarose gel, cut from the gel and then cleaned up from with GenElute™ Gel Extraction. The cleaned product was used for PCR amplification of the whole construct in 3 PCR reaction tubes (each 50 µl) using Phusion enzyme and nested primers. The PCR product was cleaned up directely or from 1% TAE agarose gel using the GenElute PCR DNA or GenElute™ Gel Extraction, respectively. The Deletion construct was concentrated with adding 2.5 V ethanol and 0.1 V sodium acetate, pH 5.8 and thecentrifuging at 13000 rpm for 20 min. The pellet was washed with 70% ethanol and centrifuged for at 13000 rpm for 10 min. The pellet was dried at room temperature and dissolved in 15 µl water. For protoplast transformation of S. reilianum 5 µl of concentrated deletion construct was used (see above). The antibiotic resistant single colonies were used for genomic DNA extraction and gene deletion was confirmed by PCR and Southern blot.

4.5.2 Gene Integration at the *mig1* Locus

To verify the role of the deleted gene in virulence or to localize the protein *in planta* integration of constructs for gene complementation or protein localization was achieved by double homologous recombination at the *mig1* locus in the *S. reilianum* wt stains 5-1 and 5-2. The

integration construct was first simulated in Clone Manager V9 software. For each construct-integration ~1 kb DNA fragments of the *mig1* flanking regions and the gene of interest with or without fusion to *egfp* were amplified and then cleaned up with GenElute PCR DNA Purification. The *mig1* gene flanks, the gene of interest and the carboxin resistance cassette were digested with SfiI enzyme as indicated above to generate combatable ends. The fragments were electrophoretically separated on a 1% TAE agarose gel, cut from the gel and then purified using GenElute™ Gel Extraction. The *mig1* left flank and the gene of interest, and the resistance cassette (hygromycin or carboxin) and *mig1* right flank were individually ligated, again purified from the gel and the two halves of the integration construct were ligated as indicated above.

The ligated fragments were electrophoretically separted on 1% TAE agarose gel, cut from the gel and then purified using GenElute™ Gel Extraction. The cleaned product was used for PCR amplification of the whole construct using KODextreem enzyme and nested primers. The PCR product was cleaned up from 1% TAE agarose gel using the InnuPREP Gel Extraction (Analytikjena) and eluted in 15 µl of water. For protoplast transformation of *S. reilianum* 5 µl of concentrated deletion construct was used. The carboxin resistant single colonies were used for genomic DNA extraction and gene deletion was confirmed by PCR and Southern blot.

4.5.3 Inoculum Preparation and Mating Test of *S. reilianum*

S. reilianum strains were inoculated in 2ml YEPSL medium and incubated at 28°C with 200 rpm shaking for 8-12 h. These cultures were used to inoculate 50 ml PD liquid medium overnight until OD_{600nm}=0.5 - 1.0 was reached. The culture was centrifuged at 3500rpm for 5min. Cell pellets were resuspended in H2O to a calculated OD_{600nm}=2.0. Either 5 µl of solopathogenic strains (JS161 strain derivatives) or of the mixed strains with different mating types (5-1 and 5-2 derivatives) were dropped on water agar medium, sealed with Parafilm and left for 1-7 days at room temperature then microscoped to observe formation of dikaryotic filaments as an indication of the mating success.

4.5.4 Plant Pathogenicity Test

To test virulence of *S. reilianum* mutants on maize and *in planta* growth, *S. reilianum* inocula were used to inoculate 7 days old maize seedlings. The inocula were applied into the leaf whorl

using a syringe and a needle. The plants were not watered for a 24 h upon inoculation. Usually 25 plants per strain were tested. From each mating type 2-3 strains of each mutant were tested for virulence at least in three independent experiments.

4.5.5 Fungal Genomic DNA Quantification *in planta*

To quantify fungal proliferation *in planta* DNA quantification was taken as measure. From each 10 plants 2 cm below injection hole of infected leaves or first nodes were collected and pooled. The experiment was repeated 3 times. The DNA concentration was measured and 70 ng were used for quantitative real time PCR (see below). The primers oHG143 and oHG144 (for amplification of peptidylprolyl isomerase) were used to quantify fungal genomic DNA and the primers oBH73 and oBH74 (for amplification of maize actin) were used for plant genomic DNA. The fungal genomic DNA was normalized by dividing the quantification values of fungal by the plant genomic DNA.

4.6 Protein-Protein Interaction "Yeast Two Hybrid"

4.6.1 Yeast cDNA Library Construction

RNA for normalized cDNA library construction was obtained from three maize tissues infected with *S. reilianum*; infected third leaf (2 cm below injection hole) 3 days post inoculation (dpi), infected first node 15 dpi and infected ears 4 wpi (smaller than 2 cm). Each tissue was collected from three independent experiments, which each included 20 plants. The quality and purity of RNA from each individual experiment and tissue was checked by bioanalyzer 2100 (Agilent) and NanoDrop ND-1000 (Thermo Fisher Scientific). Equal RNA amounts from the pooled RNA of each tissue were mixed to make the RNA sample for cDNA library construction. A normalized cDNA library was constructed by Bio S&T, Lachine, QC, Canada. Briefly, 100 µg of total RNA were used for mRNA extraction and cDNA synthesis followed by cDNA normalization using a modified SMARTTM cDNA synthesis method. The cDNA was amplified, purified, digested with *SfiI* for directional cloning into the pGADT7 (modified to include *SfiI* site at the multiple cloning site), ligated and transformed into *E. coli*. Cells were plated into LB solid medium plates with ampicilin and incubated at 37°C overnight. Colonies were collected from plates with LB with 10% glycerol and using glass beads. The *E. coli* cells were kept at -80 in 1

ml aliquots. A portion of the *E. coli*-containing cDNA library was grown overnight in LB liquid medium with ampicilin. The pGADT7 containing the cDNA library was isolated and used from transforming yeast to construct the yeast two hybrid library.

4.6.2 Yeast-Two Hybrid Library Generation

The Yeast two hybrid library was constructed according to Make Your Own Mate and Plate Yeast Two Hybrid Library System and Yeastmaker™ Yeast Transformation System 2 (Clontech, Saint-Germain-en-Laye, France) with some modifications. A 2-3 mm single colony of the yeast strain Y187 was inoculated in 3 ml YPDA liquid medium and incubated at 30°C with 250 rpm constant shaking for 8-12 h. From this culture 5 µl were used to inoculate 50 ml YPDA liquid medium and incubated as previously indicated for 16-20 h until OD_{600nm}= 0.15-0.3 is reached. The culture was centrifuged at 700 g for 5 min. Cell pellet was resuspended in 100 ml YPDA liquid medium and left to grow at 30°C with 250 rpm constant shaking for 3-5 h until OD_{600nm}= 0.4-0.5 is reached. The culture was centrifuged at 700 g for 5 min. The cell pellet was resuspended in 30 ml water and centrifuged once again. The cell pellet was resuspended in 1.2 ml 1.1X TE buffer. The cells were used immediately for transformation of cDNA library.

For transformation, the 600 µl cell suspension were mixed with 15 µg cDNA library, 20 µl denatured DNA carrier (10 mg/ml; Clontech, Saint-Germain-en-Laye, France) and 2.5 ml PEG/LiAc solution. The transformation mixture was incubated at 30°C for 45 min with gentle mixing every 15 min. Thereafter 160 µl DMSO were added to the mixture and then incubated in a water bath at 42°C for 20 min with mixing every 10 min. The cells were centrifuged at 700 g for 5 min, resuspended in 3 ml YPD Plus Medium (Clontech, Saint-Germain-en-Laye, France) and incubated at 30°C with 250 rpm shaking for 90 min. The transformed culture was centrifuged once again. This transformation was performed 10 times individually in two independent experiments and the cell pellets were polled and resuspended in 15 ml 0.9% NaCl. In each experiment the cell suspensions were plated on 100 SD/-Leucine soild medium plates (150 µl per plate). Plates were incubated at 30°C for 4 days, and then chilled at 4°C for 1 day (experiment 1) and 5 h (experiment 2). The colonies in each plate were collected using 5 ml freezing medium (YPDA with 25% glycerol and 50 µg/ml kanamycin) and glass rod. The medium collected from the first experiment was used to collected cells from the plates of second experiment. Cell suspension was collected in one container, well mixed and distributed in 1 ml

aliquots for direct use or 50 ml aliquots for long term storage. Aliquots were stored at -80°C until used. Cell density of the library was calculated using a hemocytometer and titering 10^{-4}, 10^{-5}, 10^{-6} and 10^{-7} dilutions of the library on SD/-Leucine (SD/-Leu) solid plates.

4.6.3 Yeast-Two Hybrid Screening

The yeast two hybrid screening was performed according to Matchmaker™ Gold Yeast Two-Hybrid System (Clontech, Saint-Germain-en-Laye, France). To prepare for the yeast-two hybrid screening with SAD1 the *sad1* gene without the signal peptide was cloned into pGBKT7 (pGBKT7–SAD1) so that it fuses with the GAL4 DNA binding domain. The plasmid was transformed into the yeast strain Y2HGold. As controls, the empty plasmid pGBKT7 and pGBKT7-53 (containing p53 coding sequence), and pGADT7 (empty prey plasmid), pGADT7-T (containing T antigen coding sequence) and pGADT7-Lam (containing the Lam coding sequence) were transformed into the Y2HGold and Y187 strains, respectively. The Y2HGold and Y187 strains can mate.

To test whether SAD1 has autoactivation effect on the screening selectable markers the yeast strain Y2HGold containing pGBKT7–SAD1 was mated with the strain Y187 containing pGADT7 and as controls the strain Y2HGold containing pGBKT7-53 was mated with the stain Y187 containing either pGADT7-T (resulting in positive interaction) pGADT7-Lam (resulting in negative interaction). The mating was performed by mixing 2-3 mm single colony from each strain in 2X YPDA liquid medium. The mixture was incubated at 30°C with 50 rpm shaking for 20-24 h. The mating events were selected on SD/-Leu/-Tryptophan (Trp) double dropout (DDO). The autoactivation of the selectable markers was analyzed by growing the zygotes on DDO with 125-300 ng Aureobasidin A and X-α-Gal (DDO/A/X) or DDO lacking adenine and histidin (QDO) solid medium.

To screen for the interaction partners of SAD1 a single colony of the Y2HGold strain containing pGBKT7-SAD1 was inoculated in 70 ml SD/-Trp liquid medium and incubated at 30°C with 250 rpm shaking until OD_{600nm}= 0.8. The culture was centrifuged at 1000 g for 5 min then the cell pellet was resuspended in 4 ml SD/-Trp liquid medium and combined with 200 µl of Y187 containing the cDNA library (see above) in a sterile 2 L flask. To allow mating 45 ml 2X YPDA liquid medium (with 50 µg/ml kanamycin) were added and the culture was incubated at 30°C

with 50 rpm shaking for 24 h. The mated culture was centrifuged at 1000 g for 10 min and then resuspended in 10 ml 0.5X YPDA (with 50 µg/ml kanamycin). Each 200 µl mating suspension were spread on high stringency medium (QDO). Additionally, dilution serials 10^{-3}, 10^{-5} and 10^{-6} were prepared and 100 µl of each dilution was spread on SD/-Leu, SD/-Trp and DDO plate to estimate the mating efficiency and calculate the total number of screened clones. The plates were incubated at 30°C for 5 days.

The growing colonies were singled out twice on QDO with 300 ng/ml Aureobasidin (QDO/A). Colonies that survived were used to isolate plasmids, which were individually used to transform *E.coli*, then plasmids were isolated from *E. coli* and sequenced. The sequences were grouped and a representative plasmid (pGADT7-PREY) for each group was retransformed in the Y187 strain to generate Y187+pGADT7-PREY. The Y187+pGADT7-PREY strains were gown in 150 µl liquid SD/-Leu medium in 96 well at 30°C and shaking at 280 rpm for two days. Meanwhile, the Y2HGold strains containing either pGBKT7-SAD1 or pGBKT7 were grown in 20 ml SD/-Trp medium at 30°C and 250 rpm until OD_{600nm}= 5-6 was reached. To verify the interaction, 75 µl of Y187+pGADT7-PREY were mixed with 75 µl Y2HGold strains containing either pGBKT7-SAD1 or pGBKT7 in 96 well microtiter plates and incubated overnight at 30°C with shaking at 50 rpm. The cell mixtures were printed on DDO and QDO plates using 96-prong replicator and incubated at 30°C for 3-4 days.

4.6.4 Protein Extraction from Yeast

A single colony of yeast strains were grown in 3 ml SD liquid medium with the appropriate dropout and incubated at 30°C with 250 rpm constant shaking for 8-12 h. This culture was used to inoculate 50 ml SD liquid medium with the appropriate dropout and incubated as indicated overnight until OD_{600nm}= 0.4-0.6 is reached. The culture was placed in a tube halfway filled with ice and then centrifuged at 700 g and 4°C for 5 min. Cell pellet was resuspended 30 ml cold water and centrifuged once again. The pellet was immediately frozen in liquid nitrogen and stored at –80°C until use.

The cracking buffer was prewarmed to 60°C and then quickly added to the cell pellet so that each 7.5 OD_{600nm} was treated with 10 µl cracking buffer. The cell pellet was resuspended and aliquot of the 100X PMSF stock solution was added to the protein extraction buffer each ~7 min.

Cell disruption occurred by adding 300 µl glass beads, heating the samples at 70°C for 10 min and then by vortexing vigorously for 1 min. The mixture was centrifuged at 13000 rpm and 4°C for 5 min. The supernatant was kept on ice and the pellet was boiled in a water bath at 100°C for 3-5 min. The mixture was vigorously vortexed and then centrifuged at 13000 rpm and 4°C for 5 min. The supernatant was combined with the first supernatant. The protein extracts were stored at –80°C until use.

Yeast Protein Extraction Buffer

8 M	Urea
5%	SDS
40 mM	Tris-HCl, pH 6.8
0.1 mM	EDTA
0.4 mg/ml	Bromophenol blue

Immediately before use add:

10 µl/ml	β-mercaptoethanol
50 µl/ml	PMSF (0.1742 g/10 ml)
70 µl/ml	Protease inhibitor Complete, Roche (1 tablet/2.8ml)

4.6.5 Denaturing SDS-Polyacrylamide Gel Electrophoresis

To separate proteins a denaturing SDS-polyacrylamide gel electrophoresis (SDS-PAGE) was performed using the Mini-PROREAN® 3 system (BioRad) and discontinuous polyacrylamide (PAA) gels. A 10% resolving gel was poured between to glass plates and overlaid with isopropanol. After the gel was polymerized for 30-45 min, isopropanol overlay was removed and the gel surface was rinsed with water. Water excess was removed with a filter paper. A 4% stacking gel was poured on the top of the resolving gel, a comb was inserted and the gel was allowed to polymerize for 30-45 min. The gels were placed in a hand towel paper, wetted with gel running buffer and then kept in a plastic bag until use.

Protein samples were denatured by boiling for 5 min. Each PAA gel was placed into the electrophoresis tank and submerged in 1x running buffer and then the combs were removed. A

pre-stained molecular weight ladder (PageRuler 15-130 KDa, Fermentas) and denatured protein samples were loaded onto the gel and run at 130 V until the ladder resolved enough.

10% Resolving Gel

6.1 ml	H_2O
2.5 ml	1.5 M Tris-HCl, pH 8.8
50 µl	20 % SDS
3.3 ml	30 % Acrylamide/Bis solution, 29:1 (BioRad)
5 µl	TEMED
75 µl	10 % Ammonium persulfate

4% Stacking Gel

4.1 ml	H_2O
2.5 ml	0.5 M Tris-HCl, pH 6.8
50 µl	20 % SDS
1.3 ml	30 % Acrylamide/Bis solution, 29:1 (BioRad)
10 µl	TEMED
100 µl	10 % Ammonium persulfate

10X Running Buffer

30.28 g/l	Tris
144.13 g/l	Glycine
10 g/l	SDS

4.6.6 Western Blot

For protein immunoblot proteins were run on PAA gel. A PVDF membrane was activated in methanol for 10 min, meanwhile the cassette glass was removed. The gel and membrane were incubated in 1X transfer buffer for 10 min on a rotary shaker. The blotting apparatus (Mini Trans-Blot® Cell, BioRad) was assembled according to the manufacturer instructions. Transfer was carried out at 100 V for 70 min. The transfer cassette was dismantled and membrane was

washed for 5 min in TBS-T before membranes were blocked for 1 h at room temperature in TBS-T containing 5 % blotting grade milk powder (Roth). The blocking solution was removed and the membrane was washed briefly with TBS-T. The membrane was incubated with anti-c-Myc mouse monoclonal antibody (1:5000 in TBS-T with 2 % milk powder) and slowly shaken on a rotary shaker at 4° C overnight. The primary antibody solution was recovered and membrane was washed 3 times each for 15 min with TBS-T at room temperature on a rotary shaker.

Primary antibody was detected using a horseradish peroxidase-conjugated goat anti-mouse diluted 1:5000 in TBS-T with 2% milk powder. Membranes were incubated in the secondary antibody solution for 1 h at room temperature by slowly rotating. The antibody solution was recovered and membrane was washed as described above. For signal detection the kit was used by mixing and applying the mixture on the membrane in a plastic page. After 5 min the excess of detection mixture was removed using a hand towel. The plastic bag was sealed and luminescence was detected by exposing the membrane to chemiluminescence sensitive film in dark for 1-20 min in a closed cassette. The film was develop and fixed. The membrane was stained with coomassie blue solution for 1-2 min and then destained until a good contrast was obtained.

10X Transfer Buffer

58.2 g/l Tris
29.3 g/l Glycine
12.5 g/l 10% SDS
pH 9.2
Immediately before use add to 1X buffer:
20% Methanol

10X TBS-T Buffer

100 mM Tris
1.5 M NaCl
pH 7.5
Immediately before use add to 1X buffer:
0.05 % Tween 20

Coomassie Blue Staining Solution

0.1%	Coomassie Brilliant Blue R-250 (Sigma)
50%	Methanol
10%	Glacial acetic acid

Coomassie Blue Destaining Solution

40%	Methanol
10%	Glacial acetic acid

4.7 Microscopy, Staining and Image Processing

4.7.1 Confocal, Fluorescence and Light Microscopy

Microscopy samples were freshly collected and prepared by laying ~1 cm infected leaf or thin section of infected ear on a glass slid and immediately fixed on a slid with the help of a drop of water and cover slip. For cell culture samples, cells from logarithmically growing cultures were placed on a thin 1% agarose layer. The samples were immediately observed using a Zeiss Axioplan II and Axio Observer.Z1 microscopes (Zeiss, Jena, Germany). For microscoping calcofluor the DAPI filter (excitation at 365 nm and emission at >397 nm) was used. For GFP and WGA the FITC filter (excitation at 450-490 nm and emission at 515-565 nm) was used. For microscoping propidium-iodide-stained samples the Rhodamin filter (excitation at 546 nm and emission at >590 nm) was used. All fluorescence observations were captured using a CoolSNAP-HQ CCD camera (Photometrics, Tucson, AZ, USA) or AxioCam MRm (Zeiss, Jena, Germany). The colored images were captured using AxioCam ICc 1 (Zeiss, Jena, Germany). Image processing, including adjustment of brightness, contrast and gamma-values and image merging were performed using the imaging software MetaMorph v6.2 (Universal Imaging, Downing Town, PA, USA) or AxioVision v4.3 (Zeiss, Jena, Germany).

Confocal images were captured using TCS-SP5 microscope (Leica, Bensheim, Germany). The type of laser and Excitation and emission wavelengths used are listed in (Table 13). Images were processed using LAS AF v1.8 (Leica, Bensheim, Germany).

Table 13. Laser types used in confocal microscopy and their use.

Laser	Excitation	Emission	Purpose
405 Diode	405 nm	415-460 nm	Autofluorescence
Argon-Laser	488 nm	495-530 nm	GFP
Argon Laser	488 nm	500-540 nm	Alexa Fluor 488
561 nm DPSS Laser	561 nm	580-660 nm	Propidium-iodid
561 nm DPSS Laser	561 nm	640-750 nm	FM4-64

4.7.2 Calcofluor White Staining

Calcofluor staining was used to stain fungal appresorium or fungal structures *on planta*. The inoculated leaf 1-2 dpi was dipped in Calcofluor White (100 ng/ml Fluorescent Brightener 28) for 30 s and then washed once with water. The stained sample was placed on a slide and used for microscopic analysis using the DAPI filter.

4.7.3 Inflorescence Sectioning

Inflorescence fixing and sectioning was performed according to (Huijser et al., 1992) with some modifications. Inflorescences were collected, husk leaves were removed and then emerged in formaldehyde-acetic acid-ethanol fixing solution for 24-48 h at 4°C. During incubation the tissue was vacuum infiltrated. The tissues were transferred to 70% ethanol solution and kept at -20°C until use. After fixation the tissues were dehydrated in a series of increasing ethanol concentrations with 0.1% eosin. The ethanol was replaced by a series of increasing histoclear : ethanol concentrations and subsequently the tissues were embedded in Paraplast Plus (Roth) at 60°C overnight. The paraplast was replaced with fresh molten paraplast twice a day for 5 days. Finally, the tissues were vacuum-infiltrated in a petri dish and then quickly cooled down on ice-water.

The paraplast blocks were cut into 15 µm sections on the proper orientation and then the ribbons were floated on a silicon coated slides with some water (Thermo Fisher Scientific). Slides were placed on a heat stretching plate at 42°C. After stretching of the sections, water was removed and the slides were incubated on the heat stretching plate at 42°C for 24-48 h.

Formaldehyde-Acetic Acid-Ethanol Solution

2.5%	Formaldehyde
5%	Acetic Acid
60%	Ethanol

4.7.4 Safranin-Fast Green Staining

To visualize the modifications in inflorescence structures safranin-fast green staining was performed. The fixed tissue slides were incubated in histoclear twice each for 10 min followed by double washes with 100% ethanol for 2 min. The tissues were hydrate in a series of decreasing ethanol concentrations (95%-30%) each for 5 min. The tissues were stained in 0.1% safranin o-solution for 10 min and then washed with 30% ethanol. The staining was fixed with 1% $NaHCO_3$ followed by wash in 50% and 30% ethanol each for 5 min. The tissues were stained with 0.2% fast green (FCF) solution and then washed twice with 100% ethanol. Finally the slides were placed in histoclear for 5 min, dried, mounted in entellan and covered carefully with a cover slip.

4.7.5 Chlorazole Black E Staining

For visualization of fungal structures and pattern of proliferation *in planta* an appropriate fraction of the leaf (usually the third leaf, up to 3 cm below the injection hole) was soaked in ethanol overnight. The ethanol was discarded and the leaf segments were rinsed once with water. A 10% KOH solution was added and incubated at room temperature overnight or at 90°C for about 3-4 h. After carefully discarding of the KOH solution and rinsing with water, the leaves were incubated in chlorazole black E (CBE) staining solution at 60°C overnight. The CBE solution was appropriately discarded and the samples were destained in 50% glycerol overnight or several days (longer destaining leads to better contrast). Samples were carefully placed on glass slides and visualised by microscopy using the DIC objectives.

CBE staining

0.03 % (w/v)	CBE
1 Vol	H_2O

1 Vol	Lactic acid
1 Vol	Glycerol

4.7.6 WGA-Alexa Fluor 488 and Propidium Iodide Staining

In order to visualize fungal hyphae in planta WGA-Alexa Fluor 488 (WGA-AF; Molecular Probes, Invitrogen, Karlsruhe), which has affinity to fungal chitin and fluorescently labeled, was used in combination with propedium iodide, which stains plant cell wall as well as dead plant cells. Infected leaf was cut into 2 cm segments and infected nodes and ears were manually sectioned, and submerged in ethanol 96% overnight. The tissues were placed in 10% KOH for overnight at room temperature or 3-4 h at 95°C and then washed once with 1X PBS, pH 7.4. WGA-AF propidium iodide staining solution was added to cover the plant sample. The samples were incubated for 30 min, and during incubation vacuum infiltration was applied 3 times for 1 min. The samples were destained with 1X PBS Tween 20. Samples were directly microscoped or incubated in the dark at 4°C.

10X Phosphate Buffered Saline (PBS)

80 g/l	NaCl
2 g/l	KCl
14.4 g/l	Na_2HPO_4
2.4 g/l	KH_2PO_4

WGA-AF Propidium Iodide Staining Solution

Stock solutions (store in dark at -20°C)

1 mg/ml	WGA/AF-488 in H2O; store in dark at 4°C
10 mg/ml	Propidium Iodide in PBS (pH 7.4); store in dark at 4°C

Working solution (store in dark)

10 µg/ml	WGA/AF-488
20 µg/ml	Propidium-Iodide
0.02%	Tween 20
1X	PBS, pH 7.4

4.7.7 FM4-64 Staining

For staining plant and fungal cell membranes FM4-64 (Molecular Probes, Invitrogen, Karlsruhe) was used. The infected ears were manually thin-sectioned and dipped in FM4-64 staining solution (17 µM FM4-64 in water) and incubated in the dark and on ice for 30 min then investigated with confocal microscope.

4.7.8 3,3'-Diaminobenzidine Staining

To test ROS production in ears in response to *S. reilianum* proliferation 3,3'-Diaminobenzidine (DAB) staining was used. Four week-old ears were manually thin sectioned and immediately immersed in freshly prepared DAB staining solution (1 mg/ml in water). The samples were incubated in the dark at room temperature for 3 h. Ear sections were destained in ethanol: chloroform (4:1), and then kept in the dark in 60% glycerin until microscopic analysis.

4.8 Biochemical Analysis

4.8.1 ROS Measurement

Measuring ROS production in ears in response to *S. reilianum* proliferation was performed according to (Herzog and Fahimi, 1973). Four week-old ears were manually thin sectioned, weighed (50-80 mg) and immediately 10 volumes of freshly prepared DAB staining solution (1 mg/ml in water) were added. The samples were incubated in the dark at room temperature for 5 h. A control DAB staining solution without ear sections were incubated under the same conditions and used as blank. The ear sections were removed and the DAB solutions were measured photometrically at 465 nm.

4.8.2 Hormone Measurements

To measure auxin and giberellin concentrations plant material was extracted as previously described with some modifications (Matyash et al., 2008). Plant material (100 mg) was extracted with 0.75 mL of methanol containing 20 ng D_5-IAA (Eurisotop, Freising, Germany), 10 ng D_3-GA3 (OlChemIm Ltd, Olomouc, Czech Republic) each as internal standard. After vortexing, 2.5 mL of methyl-*tert*-butyl ether (MTBE) were added and the extract was shaken for 1 h at 4°C. For phase separation, 0.6 mL water was added. The mixture was incubated for 10 min at room

temperature and centrifuged at 450 x *g* for 15 min. The upper phase was collected and the lower phase was reextracted with 0.7 mL methanol/water (3:2,5 v/v) and 1.3 mL MTBE as described above. The combined upper phases were dried under streaming nitrogen and resuspended in 100 µl of acetonitrile/water/acetic acid (20:80:0.1, v/v/v).

The analysis of constituents was performed using an Agilent 1100 HPLC system (Agilent, Waldbronn, Germany) coupled to an Applied Biosystems 3200 hybrid triple quadrupole/linear ion trap mass spectrometer (MDS Sciex, Ontario, Canada). Nanoelectrospray (nanoESI) analysis was achieved using a chip ion source (TriVersa NanoMate; Advion BioSciences, Ithaca, NY, USA). Reversed-phase HPLC separation was performed on an EC 50/2 Nucleodure C18 gravity 1.8 µm column (50 x 2.1 mm, 1.8 µm particle size; Macherey and Nagel, Düren, Germany) applying a column temperature of 30°C. For analysis 10 µl extract were injected. The binary gradient system consisted of solvent A, water/acetic acid (100:0.1, v/v) and solvent B, acetonitrile/acetic acid (100:0.1, v/v) with the following gradient program: 5 % solvent B for 1 min, followed by a linear increase of solvent B up to 95 % within 10 min and an isocratic run at 95 % solvent B for 4 min. To re-establish starting conditions a linear decrease to 5% B within 2 min was performed, followed by 10 min isocratic equilibration at 5% B. The flow rate was 0.3 ml min^{-1}. For stable nanoESI, 130 µl min^{-1} of 2-propanol/acetonitrile/water/acetic acid (70:20:10:0.1, v/v/v/v) delivered by a 2150 HPLC pump (LKB, Bromma, Sweden) were added just after the column via a mixing tee valve. By using another post column splitter 790 nl min^{-1} of the eluent were directed to the nanoESI chip. Ionization voltage was set to -1.7 kV. Phytohormones were negatively ionized and detected in a scheduled multiple reaction monitoring mode.

For the scheduled mode the MRM detection window was 72 sec and a target scan time of 1.2 sec was applied. Mass transitions were as follows: 179/135 [declustering potential (DP) -40 V, entrance potential (EP) -6.5 V, collision energy (CE) -22 V] for D_5-IAA, 174/130 (DP -40 V, EP -6.5 V, CE -22 V) for IAA, (DP -55 V, EP -10 V, CE -40 V) for D_2-GA_3, 345/143 (DP -85 V, EP -10 V, CE -38 V) for GA_3, 347/273 (DP -115 V, EP -10 V, CE -30 V) for GA_1, 331/213 (DP -105 V, EP -10 V, CE -40 V) for GA_4, 329/145 (DP -120 V, EP -10 V, CE -34 V) for GA_5, 363/275 (DP -160 V, EP -10 V, CE -24 V) for GA_8, 315/271 (DP -95 V, EP -10 V, CE -28 V) for GA_9, 331/287 (DP -95 V, EP -10 V, CE -30 V) for GA_{20}, 347/259 (DP -240 V, EP -10 V, CE -24 V) for GA_{34}. The mass analyzers were adjusted to a resolution of 0.7 amu full width at half-

height. The ion source temperature was 40 °C, and the curtain gas was set at 10 (given in arbitrary units). Quantification was carried out using a calibration curve of intensity (*m/z*) ratios of [unlabeled]/[deuterium-labelled] *vs.* molar amounts of unlabeled (0.3-1000 pmol).

4.8.3 GFP Fluorescence Measurements

To measure the silencing effect on GFP expression fluorometric measurement for the GFP-expressing strains was performed. *S. reilianum* was grown in 2 ml YEPSL and incubated at 28°C with 200 rpm shaking for 8-12 h. This culture was used to inoculate 10 ml CM liquid medium at 28°C with 200 rpm shaking overnight until OD_{600nm}= 0.5 was reached. From each culture 1 ml was centrifuged at 13000 rpm for 2 min, the pellet was resuspended in 1 ml water and then the fluorescence was measured by Safire-Photometer (Tecan, Switzerland) for all strains in triplicates in the same microtiter plate. In addition, the OD_{600nm} was measured and used to normalize the fluorescence values.

4.9 Bioinformatic Analysis

4.9.1 DNA Sequencing and Analysis

All sequencing reactions were done through the services of ADIS at the Max Planck Institute for Plant Breeding, Cologne. Purified PCR products or plasmid DNA and the respective primers were sent in the required concentrations. The electropherograms obtained were manually analized using the software Chromas Lite V2.0 (Technelysium Pty Ltd, Australia). DNA editing, comparisons and construction were simulated in Clone Manager 9 (Scientific and Educational Software, USA). Sequence alignments were performed using Clustal X software (Thompson et al., 1997).

4.9.2 Sequence Annotation and Prediction

Signal peptide prediction (Emanuelsson et al., 2007)

SignalIP 3.0 sever: http://www.cbs.dtu.dk/services/SignalP

N-myristoylation and phosphorylation sites, and nuclear localization signal predictions (Sigrist et al., 2010)

PROSITE: http://myhits.isb-sib.ch/cgi-bin/motif_scan

Ubiquitination prediction (Li et al., 2009)

BDM-PUB: http://bdmpub.biocuckoo.org/prediction.php

Sequence alignment

ClustalX software (Thompson et al., 1997) was used to align the DNA or protein sequences to analyze sequence similarities.

5. REFERENCES

Agrios GN (1997) Plant diseases caused by fungi, Vol 4. Academic Press, San Diego, California, USA

Altschul SF, Gish W, Miller W, Myers EW, Lipman DJ (1990) Basic local alignment search tool. J. Mol. Biol. **215:** 403-410

Ambrose BA, Lerner DR, Ciceri P, Padilla CM, Yanofsky MF, Schmidt RJ (2000) Molecular and genetic analyses of the *silky1* gene reveal conservation in floral organ specification between eudicots and monocots. Mol. Cell **5:** 569-579

Banuett F, Herskowitz I (1989) Different a alleles of *Ustilago maydis* are necessary for maintenance of filamentous growth but not for meiosis. Proc. Natl. Acad. Sci. USA **86:** 5878-5882

Banuett F, Herskowitz. I (1994) Morphological transitions in the life cycle of *Ustilago maydis* and their genetic control by the *a* and *b* loci. Exp. Mycol. **18:** 247–266

Barazesh S, McSteen P (2008) Hormonal control of grass inflorescence development. Trends Plant Sci. **13:** 656-662

Bauer R, Begerow D, Oberwinkler F, Piepenbring M, Berbee ML (2001) Ustilaginomycetes, Vol 7. Springer Verlag, Berlin

Begerow D, Stoll M, Bauer R (2006) A phylogenetic hypothesis of Ustilaginomycotina based on multiple gene analyses and morphological data. Mycologia **98:** 906-1016

Bennetzen JL, Hake SC (2009) Handbook of maize: its biology. Springer, New York

Bernardo R, Bourrier M, Olivier JL (1992) Generation means analysis of resistance to head smut (*Sporisorium reiliana*) in maize. Agronomie **12:** 303-306

Bernardo R, Bourrier M, Olivier JL (1992) Generation means analysis of resistance to head smut in maize. Agronomie **12:** 303-306

Bhaskaran S, Smith RH (1993) Carbohydrates, invertase activity, growth and dimorphism in *Sporisorium reilianum*. Mycopathologia **122:** 35-41

Bhaskaran S, Smith RH, Frederiksen RA (1990) Gibberellin A_3 reverts floral primordia to vegetative growth in sorghum. Plant Sci. **71:** 113-118

Bhaskaran S, Smith RH, Frederiksen RA (1991) A factor that promotes mycelial development in Sporisorium reilianum *in vitro*. Bot. Gaz. **152:** 453-459

Block A, Li G, Fu ZQ, Alfano JR (2008) Phytopathogen type III effector weaponry and their plant targets. Curr. Opin. Plant Biol. **11:** 396-403

Bortiri E, Chuck G, Vollbrecht E, Rocheford T, Martienssen R, Hake S (2006) *Ramosa2* encodes a LATERAL ORGAN BOUNDARY domain protein that determines the fate of stem cells in branch meristems of maize. Plant Cell **18:** 574-585

Bortiri E, Hake S (2007) Flowering and determinacy in maize. J. Exp. Bot. **58:** 909-916

Bos JIB, Armstrong MR, Gilroy EM, Boevink PC, Hein I, Taylor RM, Zhendong T, Engelhardt S, Vetukuri RR, Harrower B (2010) *Phytophthora infestans* effector AVR3a is essential for virulence and manipulates plant immunity by stabilizing host E3 ligase CMPG1. Proc. Natl. Acad. Sci. USA **107:** 9909-9914

Brachmann A, König J, Julius C, Feldbrügge M (2004) A reverse genetic approach for generating gene replacement mutants in *Ustilago maydis*. Mol. Genet. Genomics **272:** 216-226

Brefort T, Doehlemann G, Mendoza-Mendoza A, Reissmann S, Djamei A, Kahmann R (2009) *Ustilago maydis* as a pathogen. Annu. Rev. Phytopathol. **47:** 423-445

Bressman EN, Barss HP (1933) Experiments with head smut of corn in western Oregon. Phytopathology **23:** 396-403

Casady AJ (1969) Propagation from proliferated sorghum spikelets caused by head smut infection. Crop Sci. **9:** 381-382

Chen Y, Chao Q, Tan G, Zhao J, Zhang M, Ji Q, Xu M (2008) Identification and fine-mapping of a major QTL conferring resistance against head smut in maize. Theor. Appl. Genet. **117:** 1241-1252

Chuck G, Meeley R, Hake S (2008) Floral meristem initiation and meristem cell fate are regulated by the maize *AP2* genes *ids1* and *sid1*. Development **135:** 3013-3019

Chuck G, Meeley RB, Hake S (1998) The control of maize spikelet meristem fate by the *APETALA2*-like gene *indeterminate spikelet1*. Genes Dev. **12:** 1145-1153

Chuck G, Muszynski M, Kellogg E, Hake S, Schmidt RJ (2002) The control of spikelet meristem identity by the *branched silkless1* gene in maize. Science **298:** 1238-1241

Clark SE, Williams RW, Meyerowitz EM (1997) The *CLAVATA1* gene encodes a putative receptor kinase that controls shoot and floral meristem size in Arabidopsis. Cell **89:** 575-585

Cline M, Wesse T, Iwamura H (1997) Cytokinin/auxin control of apical dominance in Ipomoea nil. Plant Cell Physiol. **38:** 659-667

Coe EH, Neuffer MG, Hoisington DA (1988) The genetics of com. American Society of Agronomy, Madison

Coen ES, Meyerowitz EM (1991) The war of the whorls: genetic interactions controlling flower development. Nature **353:** 31-37

Cohen SN, Chang ACY, Hsu L (1972) Nonchromosomal antibiotic resistance in bacteria: genetic transformation of *Escherichia coli* by R-factor DNA. Proc. Natl. Acad. Sci. USA **69:** 2110

Colasanti J, Yuan Z, Sundaresan V (1998) The *indeterminate* gene encodes a zinc finger protein and regulates a leaf-generated signal required for the transition to flowering in maize. Cell **93:** 593-603

Colombo L, Franken J, Koetje E, Van Went J, Dons HJM, Angenent GC, Van Tunen AJ (1995) The petunia MADS box gene *FBP11* determines ovule identity. Plant Cell **7:** 1859-1868

Colombo L, Marziani G, Masiero S, Wittich PE, Schmidt RJ, Gorla MS, Pè ME (1998) *BRANCHED SILKLESS* mediates the transition from spikelet to floral meristem during *Zea mays* ear development. Plant J. **16:** 355-363

Crawford S, Shinohara N, Sieberer T, Williamson L, George G, Hepworth J, Müller D, Domagalska MA, Leyser O (2010) Strigolactones enhance competition between shoot branches by dampening auxin transport. Development **137:** 2905-2913

Dangl JL, Jones JDG (2001) Plant pathogens and integrated defence responses to infection. Nature **411:** 826-833

Davies CR, Seth AK, Wareing PF (1966) Auxin and kinetin interaction in apical dominance. Science **151:** 468-469

De Wit PJGM (1997) Pathogen avirulence and plant resistance: a key role for recognition. Trends Plant Sci. **2:** 452-458

Dellaporta SL, Moreno MA, Delong A (1991) Cell lineage analysis of the gynoecium of maize using the transposable element *Ac*. Development **113:** 141-147

Ditta G, Pinyopich A, Robles P, Pelaz S, Yanofsky MF (2004) The *SEP4* gene of *Arabidopsis thaliana* functions in floral organ and meristem identity. Curr. Biol. **14:** 1935-1940

Domagalska MA, Leyser O (2011) Signal integration in the control of shoot branching. Nat. Rev. Mol. Cell Biol. **12:** 211-221

Dreni L, Jacchia S, Fornara F, Fornari M, Ouwerkerk PBF, An G, Colombo L, Kater MM (2007) The D-lineage MADS-box gene *OsMADS13* controls ovule identity in rice. Plant J. **52:** 690-699

Dutzmann S, Duben J (1993) Maiskopfbrand zukuenftig auch in Deutschland von Bedeutung? Vorbeugende Maßnahmen sind empfehlen. Mais Fach. For. Prod. Ver. Oek. **21:** 140–142

Eaton CJ, Cox MP, Ambrose B, Becker M, Hesse U, Schardl CL, Scott B (2010) Disruption of signaling in a fungal-grass symbiosis leads to pathogenesis. Plant Physiol. **153:** 1780-1794

Edw L (1931) A check list of plant diseases and fungi occurring in Egypt. Transact. Kansas Academy Sci. **34:** 41-106

Ellis JG, Dodds PN, Lawrence GJ (2007) Flax rust resistance gene specificity is based on direct resistance-avirulence protein interactions. Annu. Rev. Phytopathol. **45:** 289-306

Emanuelsson O, Brunak S, von Heijne G, Nielsen H (2007) Locating proteins in the cell using TargetP, SignalP and related tools. Nat. Prot. **2:** 953-971

Feldbrügge M, Kämper J, Steinberg G, Kahmann R (2004) Regulation of mating and pathogenic development in *Ustilago maydis*. Curr. Opin. Microbiol. **7:** 666–672

Fletcher JC, Brand U, Running MP, Simon R, Meyerowitz EM (1999) Signaling of cell fate decisions by *CLAVATA3* in Arabidopsis shoot meristems. Science **283:** 1911-19114

Fuyao Z, Junai P, Zhihong D, Qingjun C, Huang Y (2010) Identification of a new race of *Sporisorium reilianum* and characterization of the reaction of sorghum Lines to four races of the head smut pathogen. J. Phytopathol. **159:** 342-346

Gallavotti A, Yang Y, Schmidt RJ, Jackson D (2008) The relationship between auxin transport and maize branching. Plant Physiol. **147:** 1913-1923

Gallavotti A, Zhao Q, Kyozuka J, Meeley RB, Ritter MK, Doebley JF, Pè ME, Schmidt RJ (2004) The role of *barren stalk1* in the architecture of maize. Nature **432:** 630-635

Gapper C, Dolan L (2006) Control of plant development by reactive oxygen species. Plant Physiol. **141:** 341-345

Ghareeb H, Bozsó Z, Ott PG, Repenning C, Stahl F, Wydra K (2011) Transcriptome of silicon-induced resistance against *Ralstonia solanacearum* in the silicon non-accumulator tomato implicates priming effect. Physiol. Mol. Plant Pathol. **75:** 83-89

Gietz RD, Schiestl RH (2007) Microtiter plate transformation using the LiAc/SS carrier DNA/PEG method. Nat. Prot. **2:** 5-8

Gillissen B, Bergemann J, Sandmann C, Schroeer B, Bölker M, Kahmann R (1992) A two-component regulatory system for self/non-self recognition in *Ustilago maydis*. Cell **68:** 647-657

Heckman KL, Pease LR (2007) Gene splicing and mutagenesis by PCR-driven overlap extension. Nat. Prot. **2:** 924-932

Herzog V, Fahimi HD (1973) A new sensitive colorimetric assay for peroxidase using 3, 3'-diaminobenzidine as hydrogen donor. Anal. Biochem. **55:** 554-562

Hoffman CS, Winston F (1987) A ten-minute DNA preparation from yeast efficiently releases autonomous plasmids for transformaion of *Escherichia coli*. Gene **57:** 267-272

Holliday R (1974) *Ustilago maydis*. New York, Plenum Press

Hoshi A, Oshima K, Kakizawa S, Ishii Y, Ozeki J, Hashimoto M, Komatsu K, Kagiwada S, Yamaji Y, Namba S (2009) A unique virulence factor for proliferation and dwarfism in plants identified from a phytopathogenic bacterium. Proc. Natl. Acad. Sci. USA **106:** 6416-6421

Hu L, Liang W, Yin C, Cui X, Zong J, Wang X, Hu J, Zhang D (2011) Rice MADS3 regulates ROS homeostasis during late anther development. Plant Cell **23:** 515-533

Hubbard L, McSteen P, Doebley J, Hake S (2002) Expression patterns and mutant phenotype of *teosinte branched1* correlate with growth suppression in maize and teosinte. Genetics **162:** 1927-1935

Huijser P, Klein J, Lönnig WE, Meijer H, Saedler H, Sommer H (1992) Bracteomania, an inflorescence anomaly, is caused by the loss of function of the MADS-box gene *squamosa* in *Antirrhinum majus*. EMBO J. **11:** 1239

Isbell VR, Morgan PW (1982) Manipulation of apical dominance in sorghum with growth regulators. Crop Sci. **22:** 30-35

Jeong S, Trotochaud AE, Clark SE (1999) The Arabidopsis *CLAVATA2* gene encodes a receptor-like protein required for the stability of the CLAVATA1 receptor-like kinase. Plant Cell **11:** 1925-1933

Jofuku KD, Boer BGW, Montagu MV, Okamuro JK (1994) Control of Arabidopsis flower and seed development by the homeotic gene *APETALA2*. Plant Cell **6:** 1211-1225

Kadotani N, Nakayashiki H, Tosa Y, Mayama S (2004) One of the two Dicer-like proteins in the filamentous fungi Magnaporthe oryzae genome is responsible for hairpin RNA-triggered RNA silencing and related small interfering RNA accumulation. J. Biol. Chem. **279:** 44467-44474

Kämper J (2004) A PCR-based system for highly efficient generation of gene replacement mutants in *Ustilago maydis*. Mol. Genet. Genomics **271:** 103-110

Kämper J, Kahmann R, Bölker M, Ma LJ, Brefort T, Saville BJ, Banuett F, Kronstad JW, Gold SE, Müller O, Perlin MH, Wösten HAB, de Vries R, Ruiz-Herrera J, Reynaga-Pena CG, Snetselaar K, McCann M, Perez-Martin J, Feldbrugge M, Basse CW, Steinberg G, Ibeas JI, Holloman W, Guzman P, Farman M, Stajich JE, Sentandreu R, Gonzalez-Prieto JM, Kennell JC, Molina L, Schirawski J, Mendoza-Mendoza A, Greilinger D, Munch K, Rossel N, Scherer M, Vranes M, Ladendorf O, Vincon V, Fuchs U, Sandrock B, Meng S, Ho ECH, Cahill MJ, Boyce KJ, Klose J, Klosterman SJ, Deelstra HJ, Ortiz-Castellanos L, Li WX, Sanchez-Alonso P, Schreier PH, Hauser-Hahn I, Vaupel M, Koopmann E, Friedrich G, Voss H, Schluter T, Margolis J, Platt D, Swimmer C, Gnirke A, Chen F, Vysotskaia V, Mannhaupt G, Guldener U, Munsterkotter M, Haase D, Oesterheld M, Mewes HW, Mauceli EW, DeCaprio D, Wade CM, Butler J, Young S, Jaffe DB, Calvo S, Nusbaum C, Galagan J, Birren BW (2006) Insights from the genome of the biotrophic fungal plant pathogen *Ustilago maydis*. Nature **444:** 97-101

Kim JG, Taylor KW, Hotson A, Keegan M, Schmelz EA, Mudgett MB (2008) XopD SUMO protease affects host transcription, promotes pathogen growth, and delays symptom development in *Xanthomonas*-infected tomato leaves. Plant Cell **20:** 1915-1929

Laudencia-Chingcuanco D, Hake S (2002) The *indeterminate floral apex1* gene regulates meristem determinacy and identity in the maize inflorescence. Development **129:** 2629-2638

Leibfried A, To JPC, Busch W, Stehling S, Kehle A, Demar M, Kieber JJ, Lohmann JU (2005) WUSCHEL controls meristem function by direct regulation of cytokinin-inducible response regulators. Nature **438:** 1172-1175

Leslie JF (2003) Sorghum and millets diseases. Wiley-Blackwell

Li A, Gao X, Ren J, Jin C, Xue Y (2009) BDM-PUB: Computational prediction of protein ubiquitination sites with a bayesian discriminant method. **Submitted**

Li S, Lauri A, Ziemann M, Busch A, Bhave M, Zachgo S (2009) Nuclear activity of ROXY1, a glutaredoxin interacting with TGA factors, is required for petal development in *Arabidopsis thaliana*. Plant Cell **21:** 429-441

Li S, Zachgo S, Jean-Pierre J (2009) Glutaredoxins in development and stress responses of plants. Adv. Bot. Res. **52:** 333-361

Li XH, Wang ZH, Gao SR, Shi HL, Zhang SH, George MLC, Li MS, Xie CX (2008) Analysis of QTL for resistance to head smut (*Sporisorium reiliana*) in maize. Field Crops Res. **106:** 148–155

Lim PO, Kim HJ, Gil Nam H (2007) Leaf senescence. Annu. Rev. Plant Biol. **58:** 115-136

Loubradou G, Brachmann A, Feldbrügge M, Kahmann R (2001) A homologue of the transcriptional repressor Ssn6p antagonizes cAMP signalling in *Ustilago maydis*. Mol. Microbiol. **40:** 719-730

Lübberstedt T, Xia XC, Tan G, Liu X, Melchinger AE (1999) QTL mapping of resistance to *Sporisorium reiliana* in maize. Theor. Appl. Genet. **99:** 593-598

Maeo K, Tokuda T, Ayame A, Mitsui N, Kawai T, Tsukagoshi H, Ishiguro S, Nakamura K (2009) An AP2 type transcription factor, WRINKLED1, of *Arabidopsis thaliana* binds to the AW box sequence conserved among proximal upstream regions of genes involved in fatty acid synthesis. Plant J. **60:** 476-487

Magill C, Jin Z, Erattaimuthu SR, Prom LK, Greenwald C, Erpelding JE, Montes N, Perumal R, Odvody G, Frederiksen R (2011) Virulence and molecular genotyping studies of *Sporisorium reilianum* isolates in sorghum. Plant Dis. **95:** 523-529

Malcomber ST, Kellogg EA (2004) Heterogeneous expression patterns and separate roles of the *SEPALLATA* gene *LEAFY HULL STERILE1* in grasses. Plant Cell **16:** 1692-1706

Martinez C, Jauneau A, Roux C, Savy C, Dargent R (2000) Early infection of maize roots by *Sporisorium reilianum* f. sp. *zeae*. Protoplasma **213:** 83-92

Martinez C, Roux C (2002) The biological cycle of *Sporisorium reilianum* f.sp. zeae: an overview using microscopy Mycologia **94:** 505-514

Martinez C, Roux C, Dargent R (1999) Biotrophic development of *Sporisorium reilianum* f. sp. zeae in vegetative shoot apex of maize. Phytopathology **89:** 247-253

Martinez C, Roux C, Jauneau A, B´ecard G, Dargent R (2003) Effect of water potential on the development of an haploid strain of *Sporisorium reilianum* f.sp. zeae. Plant Soil **251:** 65–71

Matheussen AM, Morgan PW, Frederiksen RA (1991) Implication of gibberellins in head smut (*Sporisorium reilianum*) of *Sorghum bicolor*. Plant Physiol. **96:** 537-544

Matyac CA (1985) Histological development of *Sphacelotheca reiliana* on Zea mays. Plant Dis. **75:** 924-929

Matyac CA, Kommedahl T (1985) Factors affecting the development of Head Smut caused by *Sphacelotheca reiliana* on corn. Phytopathology **75:** 577-581

Matyash V, Liebisch G, Kurzchalia TV, Shevchenko A, Schwudke D (2008) Lipid extraction by methyl-tert-butyl ether for high-throughput lipidomics. J. Lipid Res. **49:** 1137-1146

Mayer KFX, Schoof H, Haecker A, Lenhard M, Jürgens G, Laux T (1998) Role of WUSCHEL in regulating stem cell fate in the Arabidopsis shoot meristem. Cell **95:** 805-815

McSteen P (2009) Hormonal regulation of branching in grasses. Plant Physiol. **149:** 46-55

McSteen P, Hake S (2001) *barren inflorescence2* regulates axillary meristem development in the maize inflorescence. Development **128:** 2881-2891

McSteen P, Malcomber S, Skirpan A, Lunde C, Wu X, Kellogg E, Hake S (2007) *barren inflorescence2* encodes a co-ortholog of the *PINOID* serine/threonine kinase and is required for organogenesis during inflorescence and vegetative development in maize. Plant Physiol. **144:** 1000-1011

Meinert G (1997) Bekämpfung des Maiskopfbrandes zulassung von Atout 10 in Aussicht. *In*, Vol 25, p 56

Mena M, Ambrose BA, Meeley RB, Briggs SP, Yanofsky MF, Schmidt RJ (1996) Diversification of C-function activity in maize flower development. Science **274:** 1537-1540

Meyer VG (1966) Flower abnormalities. Bot. Rev. **32:** 165-218

Møller IM, Sweetlove LJ (2010) ROS signalling - specificity is required. Trends Plant Sci. **15:** 370-374

Morgan PW, Miller FR, Quinby JR (1977) Manipulation of sorghum growth and development with gibberellic acid. Agron. J. **69:** 789-793

Munkacsi AB, Stoxen S, May G (2007) Domestication of maize, sorghum, and sugarcane did not drive the divergence of their smut pathogens. Evolution **61:** 388-403

Munné-Bosch S, Alegre L (2004) Die and let live: leaf senescence contributes to plant survival under drought stress. Funct. Plant Biol. **31:** 203-216

Münster T, Ursula Wingen L, Faigl W, Werth S, Saedler H, Theißen G (2001) Characterization of three *GLOBOSA*-like *MADS-box* genes from maize: evidence for ancient paralogy in one class of floral homeotic B-function genes of grasses. Gene **262:** 1-13

Ng M, Yanofsky MF (2001) Function and evolution of the plant MADS-box gene family. Nat. Rev. Genet. **2:** 186-195

Nickerson NH (1954) Morphological analysis of the maize ear. Am. J. Bot. **41:** 87-92

Njuguna JGM (2001) Combating head smut of maize caused by *sphacelotheca reiliana* through resistance breeding. *In* Seventh Esterrn and Southern Africa Regional Maize Conference, pp 110-112

Nordström A, Tarkowski P, Tarkowska D, Norbaek R, Åstot C, Dolezal K, Sandberg G (2004) Auxin regulation of cytokinin biosynthesis in *Arabidopsis thaliana*: a factor of potential importance for auxin-ytokinin-regulated development. Proc. Natl. Acad. Sci. USA **101:** 8039-8044

Oh BJ, Frederiksen RA, Smith RH (1994) Glycoprotein changes in vegetative to floral meristems of sorghum detected by biotinylated lectins. Plant Sci. **101:** 181-187

Ohmori S, Kimizu M, Sugita M, Miyao A, Hirochika H, Uchida E, Nagato Y, Yoshida H (2009) *MOSAIC FLORAL ORGANS1*, an *AGL6*-like mads box gene, regulates floral organ identity and meristem fate in rice. Plant Cell **21:** 3008-3025

Pastori GM, Trippi VS (1993) Antioxidative protection in a drought resistant maize strain during leaf senescence. Physiol. Plant. **87:** 227-231

Phillips KA, Skirpan AL, Liu X, Christensen A, Slewinski TL, Hudson C, Barazesh S, Cohen JD, Malcomber S, McSteen P (2011) *vanishing tassel2* encodes a grass-specific tryptophan aminotransferase required for vegetative and reproductive development in maize. Plant Cell **23:** 550-566

Pieterse CMJ, Leon-Reyes A, Van der Ent S, Van Wees SCM (2009) Networking by small-molecule hormones in plant immunity. Nat. Chem. Biol. **5:** 308-316

Prusinkiewicz P, Crawford S, Smith RS, Ljung K, Bennett T, Ongaro V, Leyser O (2009) Control of bud activation by an auxin transport switch. Proc. Natl. Acad. Sci. USA **106:** 17431-17436

Raghavendra S, Safeeulla KM (1979) Histopathologicai studies on ragi (*Eleusine coracana* (L.) Gaertn.) infected by *Sclerophthora macrospora* (Sacc.) Thirum. Shaw and Naras. Proc. Indian Natl. Sci. Acad. (B Biol. Sci.) **88:** 19-24

Reed GM, Swabey M, Kolk LA (1927) Experimental studies on head smut of corn and sorghum. Bull. Torrey Bot. Club **54:** 295-310

Robzyk K, Kassir Y (1992) A simple and highly efficient procedure for rescuing autonomous plasmids from yeast. Nucleic Acids Res. **20:** 3790

Römer P, Hahn S, Jordan T, Strauß T, Bonas U, Lahaye T (2007) Plant pathogen recognition mediated by promoter activation of the pepper *Bs3* resistance gene. Science **318:** 645-648

Rooney HCE, van't Klooster JW, van der Hoorn RAL, Joosten MHAJ, Jones JDG, de Wit PJGM (2005) Cladosporium Avr2 inhibits tomato Rcr3 protease required for *Cf-2*-dependent disease resistance. Science **308:** 1783-1786

Sachs T (1981) The control of the patterned differentiation of vascular tissues. Adv. Bot. Res. **9:** 151-262

Sachs T, Thimann KV (1967) The role of auxins and cytokinins in the release of buds from dominance. Am. J. Bot. **54:** 136-144

Sambrook J, Russell DW (2001) Molecular cloning. CSHL Press

Satoh-Nagasawa N, Nagasawa N, Malcomber S, Sakai H, Jackson D (2006) A trehalose metabolic enzyme controls inflorescence architecture in maize. Nature **441:** 227-230

Schirawski J, Heinze B, Wagenknecht M, Kahmann R (2005) Mating type loci of *Sporisorium reilianum*: novel pattern with three *a* and multiple *b* specificities. Eukaryot. Cell **4:** 1317-1327

Schirawski J, Mannhaupt G, Münch K, Brefort T, Schipper K, Doehlemann G, Di Stasio M, Rössel N, Mendoza-Mendoza A, Pester D, Müller O, Winterberg B, Meyer E, Ghareeb H, Wollenberg T, Münsterkötter M, Wong P, Walter M, Stukenbrock E, Güldener U, Kahmann R (2010) Pathogenicity determinants in smut fungi revealed by genome comparison. Science **330:** 1546-1548

Schmidt RJ, Veit B, Mandel MA, Mena M, Hake S, Yanofsky MF (1993) Identification and molecular characterization of *ZAG1*, the maize homolog of the Arabidopsis floral homeotic gene *AGAMOUS*. Plant Cell **5:** 729-737

Schoof H, Lenhard M, Haecker A, Mayer KFX, Jürgens G, Laux T (2000) The stem cell population of Arabidopsis shoot meristems is maintained by a regulatory loop between the *CLAVATA* and *WUSCHEL* genes. Cell **100:** 635-644

Schulz B, Banuett F, Dahl M, Schlesinger R, Schäfer W, Martin T, Herskowitz I, Kahmann R (1990) The *b* alleles of *U. maydis*, whose combinations program pathogenic development, code for polypeptides containing a homeodomain-related motif. Cell **60:** 295-306

Segers GC, Zhang X, Deng F, Sun Q, Nuss DL (2007) Evidence that RNA silencing functions as an antiviral defense mechanism in fungi. Proc. Natl. Acad. Sci. USA **104:** 12902-12906

Semisi ST, Ball SFL (1989) Infection of the pearl millet (*Pennisetum americanum*) inflorescence by the downy mildew fungus (*Sclerospora graminicola*). Plant Pathol. **38:** 571-576

Shani E, Yanai O, Ori N (2006) The role of hormones in shoot apical meristem function. Curr. Opin. Plant Biol. **9:** 484-489

Sheridan WF (1988) Maize developmental genetics: genes of morphogenesis. Annu. Rev. Genet. **22:** 353-385

Sigrist CJA, Cerutti L, De Castro E, Langendijk-Genevaux PS, Bulliard V, Bairoch A, Hulo N (2010) PROSITE, a protein domain database for functional characterization and annotation. Nucleic Acids Res. **38:** D161-D166

Singh D, Mathur SB (2004) Histopathology of seed-borne infections. CRC

Skibbe DS, Doehlemann G, Fernandes J, Walbot V (2010) Maize tumors caused by *Ustilago maydis* require organ-specific genes in Host and pathogen. Science **328:** 89-92

Skirpan A, Wu X, McSteen P (2008) Genetic and physical interaction suggest that BARREN STALK1 is a target of BARREN INFLORESCENCE2 in maize inflorescence development. Plant J. **55:** 787-797

Snetselaar KM, Mims CW (1992) Sporidial fusion and infection of maize seedlings by the smut fungus *Ustilago maydis*. Mycologia **84:** 193-203

Southern EM (1975) Detection of specific sequences among DNA fragments separated by gel electrophoresis. J. Mol. Biol. **98:** 503-517

Stromberg EL, Stienstra WC, Kommedahl T, Matyac CA, Windels CE, Geadelmann JL (1984) Smut expression and resistance of corn to *Sphacelotheca reiliana* in Minnesota. Plant Dis. **68:** 880-884

Tanaka M, Takei K, Kojima M, Sakakibara H, Mori H (2006) Auxin controls local cytokinin biosynthesis in the nodal stem in apical dominance. Plant J. **45:** 1028-1036

Tang M, Li G, Chen M (2007) The phylogeny and expression pattern of *APETALA2*-like genes in rice. J. Genet. Genom. **34:** 930-938

Theissen G, Strater T, Fischer A, Saedler H (1995) Structural characterization, chromosomal localization and phylogenetic evaluation of two pairs of *AGAMOUS*-like *MADS-box* genes from maize. Gene **156:** 155-166

Thompson BE, Bartling L, Whipple C, Hall DH, Sakai H, Schmidt R, Hake S (2009) *bearded-ear* encodes a MADS box transcription factor critical for maize floral development. Plant Cell **21:** 2578-2590

Thompson BE, Hake S (2009) Translational biology: from Arabidopsis flowers to grass inflorescence architecture. Plant Physiol. **149:** 38-45

Thompson JD, Gibson TJ, Plewniak F, Jeanmougin F, Higgins DG (1997) The CLUSTALX windows interface: flexible strategies for multiple sequence alignment aided by quality analysis tools. Nucleic Acids Res. **25:** 4876-4882

Thompson JD, Gibson TJ, Plewniak F, Jeanmougin F, Higgins DG (1997) The CLUSTALX windows interface: flexible strategies for multiple sequence alignment aided by quality analysis tools. Nucleic Acids Res. **25:** 4876

Touraud G, Bill L, Piollat MT (1997) Phyllodied panicles caused by head smut of maize and vegetative multiplication of maize. Plant Cell Tiss. Org. Cult. **50:** 19–26

Tsukuda T, Carleton S, Fotheringham S, Holloman WK (1988) Isolation and characterization of an autonomously replicating sequence from *Ustilago maydis*. Mol. Cell. Biol. **8:** 3703-3709

van der Biezen EA, Jones JD (1998) Plant disease-resistance proteins and the gene-for-gene concept. Trends Biochem. Sci. **23:** 454-456

van der Hoorn RAL, Kamoun S (2008) From guard to decoy: a new model for perception of plant pathogen effectors. Plant Cell **20:** 2009-2017

Van Doorn WG (2008) Is the onset of senescence in leaf cells of intact plants due to low or high sugar levels? J. Exp. Bot. **59:** 1963-1972

Veit B, Greene B, Lowe B, Mathern J, Sinha N, Vollbrecht E, Walko R, Hake S (1991) Genetic approaches to inflorescence and leaf development in maize. Development **113:** 105-111

Veit B, Schmidt RJ, Hake S, Yanofsky MF (1993) Maize floral development: new genes and old mutants. Plant Cell **5:** 1205-1215

Vollbrecht E, Springer PS, Goh L, Buckler Iv ES, Martienssen R (2005) Architecture of floral branch systems in maize and related grasses. Nature **436:** 1119-1126

Voth PD, Mairura L, Lockhart BE, May G (2006) Phylogeography of *Ustilago maydis virus H1* in the USA and Mexico. J. Gen. Virol. **87:** 3433-3441

Weigel D, Meyerowitz EM (1994) The ABCS of floral homeotic genes. Cell **78:** 203-209

Wheeler DL, Barrett T, Benson DA, Bryant SH, Canese K, Chetvernin V, Church DM, DiCuccio M, Edgar R, Federhen S, Geer LY, Kapustin Y, Khovayko O, Landsman D, Lipman DJ, Madden TL, Maglott DR, Ostell J, Miller V, Pruitt KD, Schuler GD, Sequeira E, Sherry ST, Sirotkin K, Souvorov A, Starchenko G, Tatusov RL, Tatusova TA, Wagner L, Yaschenko E (2006) Database resources of the National Center for Biotechnology Information. Nucleic Acids Res. **35:** D5-D12

Whipple CJ, Ciceri P, Padilla CM, Ambrose BA, Bandong SL, Schmidt RJ (2004) Conservation of B-class floral homeotic gene function between maize and Arabidopsis. Development **131:** 6083-6091

Wisser RJ, Balint-Kurti PJ, Nelson RJ (2006) The genetic architecture of disease resistance in maize: a synthesis of published studies. Phytopathology **96:** 120-129

Wu X, McSteen P (2007) The role of auxin transport during inflorescence development in maize (*Zea mays*, Poaceae). Am. J. Bot. **94:** 1745-1755

Xiang T, Zong N, Zou Y, Wu Y, Zhang J, Xing W, Li Y, Tang X, Zhu L, Chai J (2008) *Pseudomonas syringae* effector AvrPto blocks innate immunity by targeting receptor kinases. Curr. Biol. **18:** 74-80

Xing S, Zachgo S (2008) *ROXY1* and *ROXY2*, two Arabidopsis glutaredoxin genes, are required for anther development. Plant J. **53:** 790-801

Yanofsky MF, Ma H, Bowman JL, Drews GN, Feldmann KA, Meyerowitz EM (1990) The protein encoded by the *Arabidopsis* homeotic gene *agamous* resembles transcription factors. Nature **346:** 35-39

Yoo SD, Cho YH, Sheen J (2007) Arabidopsis mesophyll protoplasts: a versatile cell system for transient gene expression analysis. Nat. Prot. **2:** 1565-1572

ACKNOWLEDGEMENTS

I sincerely express my deep sense of gratitude to Prof. Dr. Jan Schirawski for supervision, precious support, providing me with all sources of knowledge, and his friendly attitude in approaching valuable discussions and advices. I thank and express my respect to Prof. Dr. Jan Schirawski and Prof. Dr. Regine Kahmann, who taught me how to be a critical minded and served as referees and examiners of my dissertation. I am grateful to Prof. Dr. Regine Kahmann, Prof. Dr. Alfred Batschauer and Dr. Stuart Huntley, Prof. Dr. Annette Becker, Prof. Dr. Sabine Zachgo for invaluable support, constructive criticisms and fruitful discussions. I would like to specially thank the following people:

Prof. Dr. Alfred Batschauer and Prof. Dr. Michael Bölker for serving as examiners.

Elmar Meyer, Dr. Katja Zuther, Frank Drechsler, Yulei Zhao, Yufei Wang, Mohammad Tanbir Habib, Sebastian Ziemann, Jennifer Krüger, Alana Poloni, Theresa Wollenberg, Dr. Britta Winterberg, Nikolas Rakebrandt, Christian Nolte, Lorena Stannek, Julia Imkampe, Jannik Donner, Simon Uhse, Helga Fernández Llamosas, Mascha Valevich, Stephan Poppe, Stefanie Uhlmann, Christine Platzer for the family and motivating atmosphere they created in the lab.

Elmar Meyer, Yufei Wang, Frank Drechsler, Sebastian Ziemann and Nikolas Rakebrandt for technical assistance.

Prof. Dr. Ivo Feussner, Dr. Tim Iven and Dr. Cornelia Herrfurth for their support with the establishment of the hormone measurements.

The group's members of Prof. Dr. Regine Kahmann, Prof. Dr. Michael Feldbrügge, Prof. Dr. Volker Lipka, Prof. Dr. Christiane Gatz and Prof. Dr. Jörg Kämper for discussions, advices and nice cooperation.

I would like also to thank my home institute, the National Research Center in Egypt, for giving me the permission to accomplish my PhD in Germany, and the International Max Planck Research School in Marburg, the Göttingen Graduate School for Neurosciences and Molecular Biosciences (GGNB; DFG grant GSC 226/1), FAZIT foundation, the German Initiative of Excellence (DFG ZUK45/1) for funding.

I would like to extend my sincere gratitude to my mother, father, wife, sisters and brother for their precious support and inspiration during my PhD.

CURRICULUM VITAE

Hassan Ghareeb

Born 15 November 1979 in Giza, Egypt

School Education

9/1986 – 6/1991	Warak Alhadr Primery School
9/1991 – 6/1994	Abduallah Abn Rawaha Preparatory School
9/1994 – 6/1997	Yousef Alsbay Secondary School

University Education and Academic Activities

9/1997 – 7/2001	Bachelor in Biotechnology, Faculty of Agriculture, Cairo University, Egypt
8/2001 – 8/2002	Research assistant in Cell Manipulation Lab, Institute of Plant Pathology, Agriculture Research Center, Giza, Egypt
9/2002 – Now	Research permanent position in Plant Biotechnology Department, National Research Center, Giza, Egypt
3/2004 – 10/2004	Vocational Training at Molecular Cell Biology Lab, BioZetrum, Martin Luther University of Halle-Wittenberg, Germany. Carried out project "Silencing *Ribonuclease LX* gene in tomato using RNA interference".
10/2005 – 9/2007	Master in Plant Biotechnology, Faculty of Natural science, Leibniz University of Hannover, Germany. Thesis topic "Transcriptome profiling of silicon-induced resistance in tomato against *Ralstonia solanacearum*".

Dissertation

10/2007 – 5/2011	PhD from the International Max Planck Research School, carried out at Department of Organismic Interactions, Max Planck Institute for Terrestrial Microbiology, and Department of Molecular Biology of Plant-Microbe Interactions, Georg August University of Göttingen, Germany. Dissertation title: "Molecular Dissection of Maize-*Sporisorium reilianum* Interactions: Host Developmental Changes and Pathogen Effectors" under supervisopn of Prof. Dr. Jan Schirawski.